MODEL TESTING OF GEOGRIDS IN UNPAVED ROADS

by

Jeremy Pennard Love

A Thesis submitted for the Degree

of Doctor of Philosophy

at the

University of Oxford.

New College

Trinity term, 1984.

ABSTRACT

Model Testing of Geogrids in Unpaved Roads

J.P.Love
New College, University of Oxford

A Thesis submitted for the Degree of Doctor of Philosophy

Trinity Term, 1984

Simple unpaved roads consist of a layer of coarse granular material placed directly onto the surface of weak or compressible ground. It is thought that the construction of such roads can be considerably improved by the incorporation of a geogrid at the base of the granular fill layer.

Geogrids are a type of geotextile, distinguished by their relatively large aperture size. Laying out a geogrid on the surface of the ground before placing the fill layer may in many cases allow a reduced thickness of fill material to be used, and may also substantially increase the load required to cause a complete failure of the system. No generally accepted design method exists for the construction of reinforced unpaved roads, due to the complex mechanisms which govern deformations in the system. The primary aim of this dissertation was to investigate the performance, in such a construction, of a particular geogrid, namely Tensar, manufactured by Netlon Ltd.

A detailed model study into failure mechanisms was undertaken using laboratory apparatus constructed to conduct work at 1/4 full scale. Simple plane-strain, monotonic footing tests were carried out on systems consisting of a fill layer compacted onto a consolidated clay subgrade, both with and without the incorporation of a model grid at their interface. The testing technique included a comprehensive study of photographs taken of marker movements in the clay through the transparent sides of the test-box during tests.

The relevant failure mechanisms associated with reinforced and unreinforced systems were established. In addition the significance of shear stresses acting at the subgrade surface was recognised and a concept whereby the appropriate subgrade bearing capacity factor is related to these shear stresses was developed. The modelling techniques adopted in this work obviated the need for a centrifuge.

PREFACE

I have very much enjoyed being a member of the Oxford Soil Mechanics Group. Under the management of Professor Peter Wroth, it has been a most friendly and stimulating place to work. Despite many other responsibilities as Head of Department, Professor Wroth himself has always made time to discuss and challenge my ideas for which I am most grateful.

I would particularly like to thank Dr George Milligan for his help. He has been an extremely able and understanding supervisor of my work here, and has continually helped me forward over many hurdles. His advice has always been sound and given kindly.

I would also like to thank all other members of the group for their help, but especially Dr Guy Houlsby, whose computer programs have been vital for the analysis of my work, and whose clear thinking and good advice has been invaluable throughout my work. I must also especially thank my Malaysian friend S. S. Gue with whom I shared a laboratory, and whose tidiness and organization were a great lesson.

I am indebted to Bob Earl for his most capable work in the Lab, for building the rig in the first place and for making continual improvements to it. In addition, I am most grateful to Stuart Oldham for his untiring explanations of electronic equipment and to Steve Hoare for his advice and help on soil testing.

Finally, I would like to express my thanks to Netlon Ltd and to all the members of the Tensar Steering Committee for the many useful discussions and comments from which my work benefitted.

To Lois

CONTENTS

CHAPTER 1

INTRODUCTION

1.1 Unpaved Roads

Simple unpaved roads consist of an unbound aggregate subbase overlaying an existing, typically weak, subgrade. The quality of fill-types used for the subbase layer vary from poor locally available materials or cheap minewaste to good quality crushed stone. The subgrade generally has a poor bearing capacity, to necessitate a road base in the first place, and may range from a medium strength clay to a very soft clay, peat or swamp.

The structure may not be paved for many reasons. The road may only have a very brief design life, such as would be the case for a temporary access road. Large deformations may be tolerable, such as for site construction haulage roads. Cost or technology may be a limiting factor such as in developing countries. In most cases the unpaved road is a structure which lends itself to the application of geotextile reinforcement.

1.2 Geotextiles and Geogrids

The term 'geotextile' refers to any synthetic permeable material which is used in conjunction with soil materials as an integral part of civil engineering construction. The term 'geogrid' refers to one

particular sort of the many types of geotextile which exist today.

The type of geotextile which can be referred to as a geogrid includes any kind of mesh and any kind of grid used in geotechnical engineering, as distinct from the types of geotextile which are 'fabrics' or 'cloths'. A range of polymer geogrids, marketed under the name of Tensar, have recently been developed by the company Netlon Ltd. This material relies on a stretching process during its manufacture to orientate the polymer plastic, thereby increasing strength and stiffness.

Unpaved road design can benefit in many ways from the inclusion of a horizontal layer of most types of geotextile placed at the subgrade-subbase interface. Additional horizontal layers may also be beneficially included in the subbase itself at various spacings (Gourc, Perrier and Riondy, 1983), although only the former case is considered in this dissertation. The way in which a geotextile can improve the performance of an unpaved road has been quantified by many researchers over the last 10 years, with the primary beneficial functions falling into the main categories of drainage, filtration, separation, reinforcement and membrane action. A full description of each of these headings has appeared in many publications to date (Bender and Barenberg, 1978, Robnett and Lai, 1982, and Ingold and Crowcroft, 1984) but it is worthwhile for completeness to include a short paragraph on each here.

Drainage: Drainage can take place across a geotextile as well as along its length. The subgrade may drain under load and thereby increase its bearing capacity.

Filtration: A geotextile will act as a filter against the migration of fine particles from subgrade to subbase driven by the pumping action of traffic loading. However, a geotextile which acts well as a filter may

become too clogged to act as an effective drainage medium with time.

Separation: A geotextile will prevent the loss of subbase material into the subgrade on a macro scale, thereby ensuring retention of the full design thickness of the subbase even at large deformations. Local punching bearing failure is prevented at the interface of the two materials. This separation effect can be more important than the effects of filtration and drainage for a road with a short working life which is also designed for large deformations.

Reinforcement: A geotextile provides tensile strength to a system which otherwise has none. By introducing a tensile load carrying member at the base of the aggregate layer lateral movements are restrained and the stiffness of the system increases.

Membrane action: The geotextile will additionally , at large out of plane deformations, develop significant membrane forces. A membrane force is merely the resolution of the geotextile tension vertically. By reducing pressure on the subgrade directly beneath the load and increasing pressure out to the sides, membrane action helps to re-distribute load more evenly onto the subgrade.

These categories represent the areas in which a geotextile can contribute to a direct saving in subbase thickness, and thereby an overall lowering of costs if savings outweigh the price of the geotextile. There are also other fringe areas in which a geotextile can be of benefit in an unpaved road design, without directly resulting in a fill thickness saving: for instance a geotextile may allow better compaction of the subbase by virtue of its horizontal restraint and its separation effect. It may also allow a road to be built across particularly difficult terrain where a simple road would otherwise be impossible.

Much research work to date has been aimed at quantifying these effects and in developing design methods, but this has been found difficult to do since the problem is very complex. Design methods tend to be based on empirical results, only applying to a particular geotextile, and the analytical models which do have general application rely on major assumptions concerning such areas as geotextile strain distributions, deflected shapes, load spread angles and subgrade bearing capacity factors.

There has been no comprehensive research to date, however, specifically concerned with the use of geogrids in unpaved road design. It seems possible that many functions of a geotextile mentioned earlier might be performed better by Tensar geogrids which are stiffer than other geotextiles and interact with the surrounding soil in a different manner. Most geotextiles rely on a soil-fabric friction for interaction with the surounding soil. The large apertures of a geogrid, which allow the surrounding soil particles to interlock through the grid, give rise to a very different type of bond. The following section briefly describes the main work on geotextiles to date.

1.3 **Work To Date**

1.3.1 Early Field Trials

Webster and Watkins (1976), and subsequently Webster and Alford (1977), of the US Corps of Engineers conducted a well documented series of field tests during the years 1975 - 1977 involving trafficking sections of 350mm subbase laid on a soft clay subgrade, employing a selection of reinforcing techniques . One of these techniques consisted of a single layer of the geotextile Bidim, and a second incorporated a

single layer of the much stiffer impervious membrane T16. The rut depths in both sections throughout the trial were significantly less than in the control section, and in the T16 section significantly less again than in the less-stiff Bidim section. These tests unequivocably demonstrated the benefits of using geotextiles and the effects of fabric stiffness.

It is significant that trafficking was always limited to the same wheel path in the above trials. Other field trials which have allowed traffic-wander across the road (Steward, Williamson and Mahoney, 1977, and Morel, Quibel, Puiatti and Puig, 1977) show less dramatic improvements.

1.3.2 Laboratory Work and More Recent Field Trials

A number of programmes of research have been conducted in the last 10 years. In 1977 the first major conference covering this topic took place at Paris and the papers presented in the conference proceedings form a good starting point for this review. A contribution was made by Andersson (1977) who conducted cyclic plate bearing tests on a subgrade/subbase system incorporating the geotextile Terram. He also explored the effect of subgrade water content. He concluded that although the influence of the geotextile on elastic deformations is negligible its influence is considerable by the time failure occurs.

Jessberger (1977) also did tests on Terram, this time in large test pits. After conducting plate bearing tests on a range of subgrade strengths and subbase thicknesses he also showed that the geotextile did improve the bearing behaviour of the system. He went on to develop a numerical analysis which had mixed success in modelling the mechanical behaviour of the materials.

Sørlie (1977) did plate bearing tests on similar systems including several subgrade materials, incorporating the geotextile Fibertex, but with less conclusive results. He suggested that the advantages of including a geotextile were minimal.

Petrik (1977) did footing tests on a pin model and was able to draw up contours of horizontal and vertical stresses in the subgrade foundation. He demonstrated a marked reduction in horizontal stresses in the system due to reinforcement.

Jarrett, Lee and Ridell (1977), having conducted an extensive series of plate bearing tests on a peat subgrade incorporating geotextiles of four different stiffnesses, made the important point that the stiffer a geotextile is the better it performs.

McGown and Andrawes (1977) looked at a more fundamental aspect of soil reinforcement, conducting plane strain tests on unit cells of reinforced sand.

Barvashov et al (1977), with more plate bearing tests, this time on fine sand, discussed the advantages of geotextile pre-tensioning.

Two years before this conference, however, two interesting pieces of research both conducted in the USA, had already been published, namely Barenberg, Dowland and Hales (1975) and Binquet and Lee (1975). Barenberg et al conducted tests on a soft clay/coarse crushed stone with a cyclic pneumatic piston (a precursor to the work presented by Bender and Barenberg, 1978). They reported significant improvement in permanent deformations from the inclusion of the geotextile Mirafi, and developed a useful design method discussed further below. Binquet and Lee conducted model strip footing tests on a soil mass incorporating metal strip

reinforcement. They noted that stress states in the soil, and hence failure modes changed with reinforcement, and developed a limit equilibrium method for analysis. Since the Paris conference in 1977 there has been continuing work in this field. In 1978 Bender and Barenberg of Illinois University published a paper on static and cyclic plate loading tests that were carried out on their pavement test track. These pavements however were not subjected to sufficient load to cause plastic failure in the subgrade, and are not so useful as a second set of tests also reported in the paper. In a long thin test-box with transparent sides, a hand-compacted layer of clay overlain by a crushed-stone subbase was subjected to repeated 2-D loading from a 200mm wide footing. The geotextile Mirafi was used at the interface. A method for design was developed and is discussed further below. This work led straight on to that conducted by Kinney for his PhD thesis (Kinney, 1979), also at Illinois University: Kinney did extensive monotonic (load controlled) and cyclic 2-D tests using the box described above. Using 3/4" nail markers he looked briefly at movements in the clay, but did not report this in great depth. His main contribution is the Fabric Tension Model which he proposes as a method of design which is also discussed in further detail below. In 1981 Robnett and Lai of the Georgia Institute of Technology conducted a series of cyclic load plate tests in large circular test pits to compare the use of a number of different geotextile types. They concentrate on the effect of 'initial fabric modulus' and show that savings of aggregate thickness attributable to each geotextile increases with this property.

During this time work similar to that conducted at Illinois University was being conducted at the University of Grenoble in France by Gourc, Perrier and Riondy. This work is presented in the form of two

papers in the proceedings of the second major conference in this area of research held at Las Vegas in 1982 . The papers (Gourc, Perrier et al, 1982, and Gourc, Matichard et al, 1982) are in French but an English version (Gourc, Perrier and Riondy, 1983) may be found in the proceedings of the VIII ECSMFE held at Helsinki in the following year. Testing consisted of 2-D loading of a soft clay, built from unfired clay bricks, overlain by an aggregate layer loaded by a 150mm footing. The loading was both monotonic at a very slow rate of displacement, and cyclic. The researchers looked at the effect of including a single layer of the geotextile Bidim at the interface, both with its ends free and with its ends restrained. They also considered various arrangements of the geotextile in the subbase layer. The sides of the box being transparent movement of markers in the subgrade were again followed, but apart from noting general trends of these movements no explanations were offered. A method of pavement analysis was devised which is described further below.

The Las Vegas proceedings include much important work conducted in the laboratory, in the field and analytically. Sowers, Collins and Miller (1982) report on full scale tests conducted in 1977 and comment on the very effective repair of a well rutted geotextile-reinforced road by simple infilling, taking advantage of an already pretensioned fabric. The researchers also noted that the width of the depressed region of geotextile increased with surface deflection. A fully instrumented field trial reported by Ramalho-Ortigao and Palmeira (1982) suggests that design methods should not necessarily assume a good stiff aggregate type for the subbase layer because locally available sub-standard material is often more attractive to use. The trial looked at various boundary conditions for the geotextile, including wooden stakes and folded-back ends, and an interesting cost breakdown is presented in the paper. A

further paper submitted by Kinney (1982) looks at the minimum effective widths of geotextiles.

1.3.3 Design Methods

The main design methods proposed to date are summarised below:

Barenberg, Dowland and Hales (1975) - the design method stipulates that the subgrade stress under the centre line of a wheel load (as found by the Boussinesq analysis for a uniform circular load on a semi-infinite elastic halfspace) should not exceed 6.0 C_u for a system with a geotextile present, and 3.3 C_u for one without. No further account of the presence of the geotextile is taken.

Bakker (1977) - the design method is based on bearing capacity factors. An angle of 45^0 is taken for load distribution in the subbase and the bearing capacity of the unreinforced subgrade is calculated according to Equation 1.1, Figure 1.1 , where n is a shape factor taken to be 1.3 and N_q , N_c , N_γ are bearing capacity factors associated with the subgrade . In the reinforced case, the deformed shape of the geotextile is represented very simply by two straight lines inclined at an angle α, as shown in Figure 1.1 . The strain in the geotextile is assumed uniform throughout at $\sec\alpha - 1$, and the vertical component of the stress in the membrane, $\sigma_m \sin\alpha$, is used to modify the formula as shown in Equation 1.2 .

Kinney (1979) - through an iterative procedure known as the Fabric Tension Model, Kinney calculates the effective surface load reduction due to both the fabric induced normal stresses (membrane effect) and the strain energy stored in the fabric. This is based on the assumed deformed shape of the fabric shown by the circular arcs in Figure 1.2 .

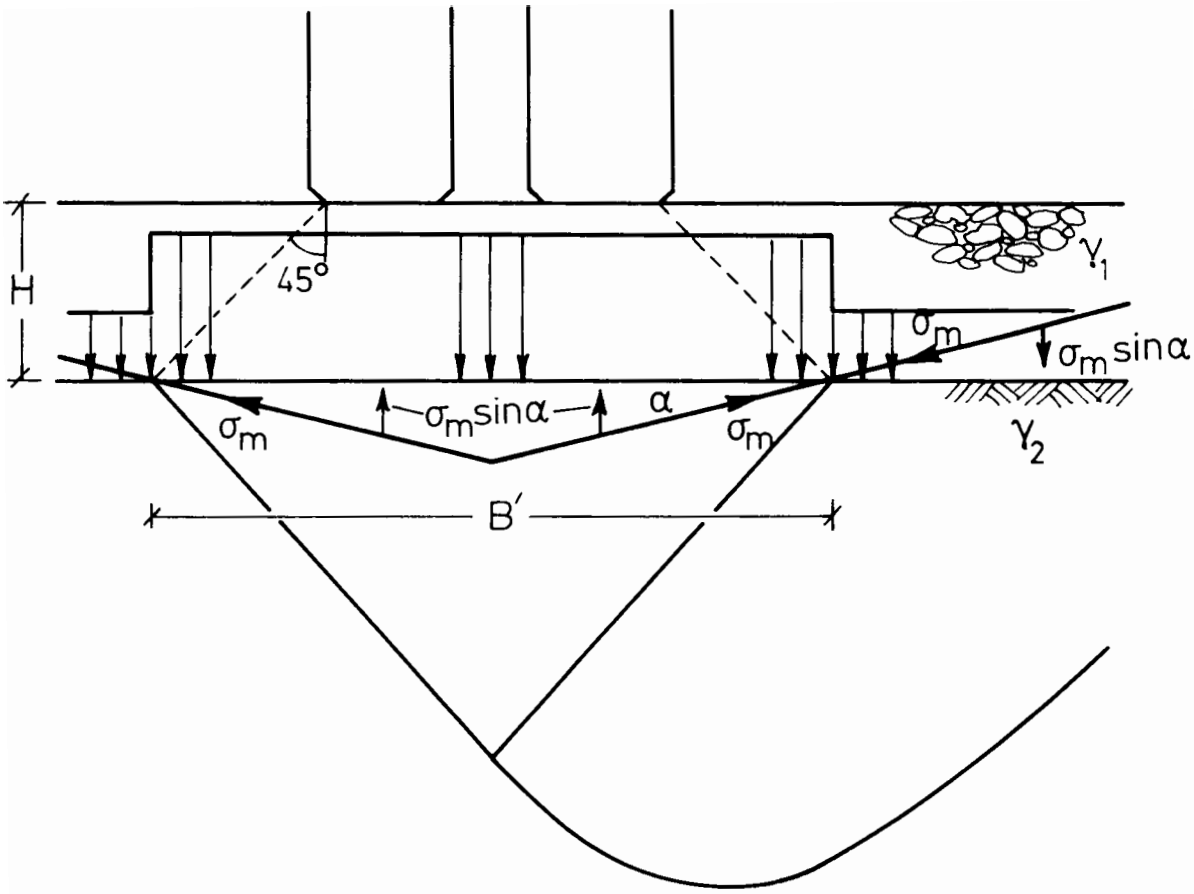

$$p = n[N_q \gamma_1 H + N_c C_u + N_\gamma \gamma_2 B'/2] \quad ...1.1$$

$$p - \sigma_m \sin\alpha = n[N_q(\gamma_1 H + \sigma_m \sin\alpha) + N_c C_u + N_\gamma \gamma_2 B'/2] \quad ...1.2$$

Figure 1.1 Model for calculation of subgrade bearing capacity (after Bakker, 1977)

The maximum subgrade stress under the centreline of a wheel-load is then predicted by the Boussinesq analysis, but taking into account this load reduction. It is concluded that there should be adequate aggregate thickness for this maximum subgrade stress not to exceed 3.0 C_u .

Giroud and Noiray (1981) - a pyramidal distribution of load through the aggregate layer is adopted and a value of $\tan^{-1}$ 0.6 taken for the angle of distribution irrespective of whether the system is reinforced with a geotextile or not. A deformed shape for the subgrade/subbase interface is assumed according to sections of parabolas as in Figure 1.3 which will depend on the ratio of wheel width to distance between wheel sets. If a geotextile is present the reduction of pressure on the subgrade due to the tension in the geotextile is calculated and subtracted from the previously calculated pyramidal load distribution. It is then suggested that the net load on the subgrade must not exceed $\pi \times C_u$ if the system is unreinforced, or $(\pi + 2)C_u$ if it is. This is then upgraded from a quasi-static model to a design which accomodates live traffic loads by using the data from the test program conducted by the US Corps of Engineers (Section 1.3.1), and making some reasonable assumptions. This method in essence incorporates the best of both of the two preceeding design methods by combining the distinction between elastic limit and plastic limit of the subgrade soil for unreinforced and reinforced systems respectively, and the effect of membrane action. Giroud, Ah-line and Bonaparte (1984) have further developed this design method by taking into account progressive deterioration of the base layer and by doing away with calculations of membrane action, but including a different load distribution angle for reinforced and unreinforced bases. This is perhaps the most useful and most simply used design method available to date.

Goure, Perrier and Riondy (1983) - in this paper the additional load

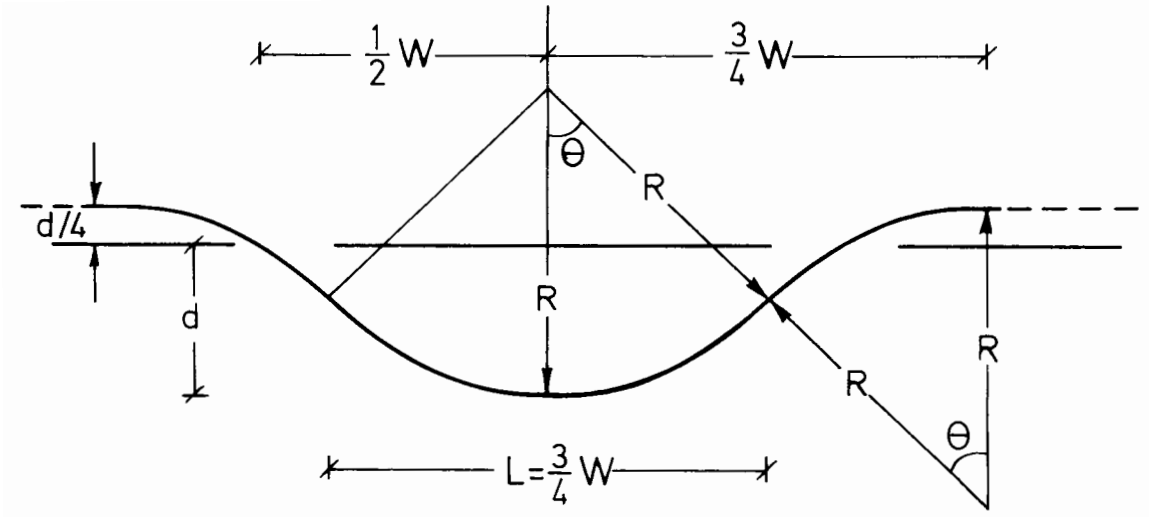

$$R = \frac{9}{80}\frac{W^2}{d} + \frac{5}{16}d$$

$$\theta = \tan^{-1}\left(\frac{10}{6}\frac{d}{W}\right)$$

Figure 1.2 Approximate deformed shape of Base-Subgrade interface (after

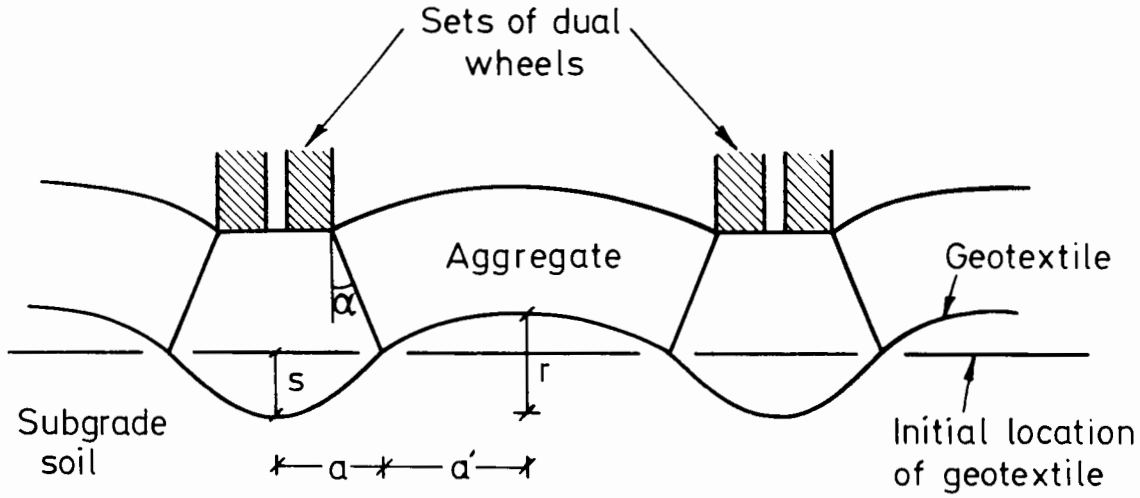

Figure 1.3 Shape of deformed geotextile (after Giroud and Noiray, 1981)

carrying capacity of a system which includes a geotextile, Δp , is quantified in two parts - that due to membrane action, Δp_M , and that due to a better load distribution angle in the aggregate, Δp_R . Again circular arcs are used, this time with no heaved portion (Figure 1.4). There is no mention of elastic or plastic ultimate loads for the subgrade.

Sellmeijer, Kenter and Van den Berg (1982) - this paper sets up equilibrium equations for both the geotextile and the subgrade and solves them simultaneously. In this way the deformed shape of the geotextile can be obtained. A zone of plastic subgrade soil is considered to extend between the two crests on the derived geotextile profile. A vertical equilibrium calculation is then carried out across this assumed failure width. This work effectively extends the work done by Nieuwenhuis (1977)

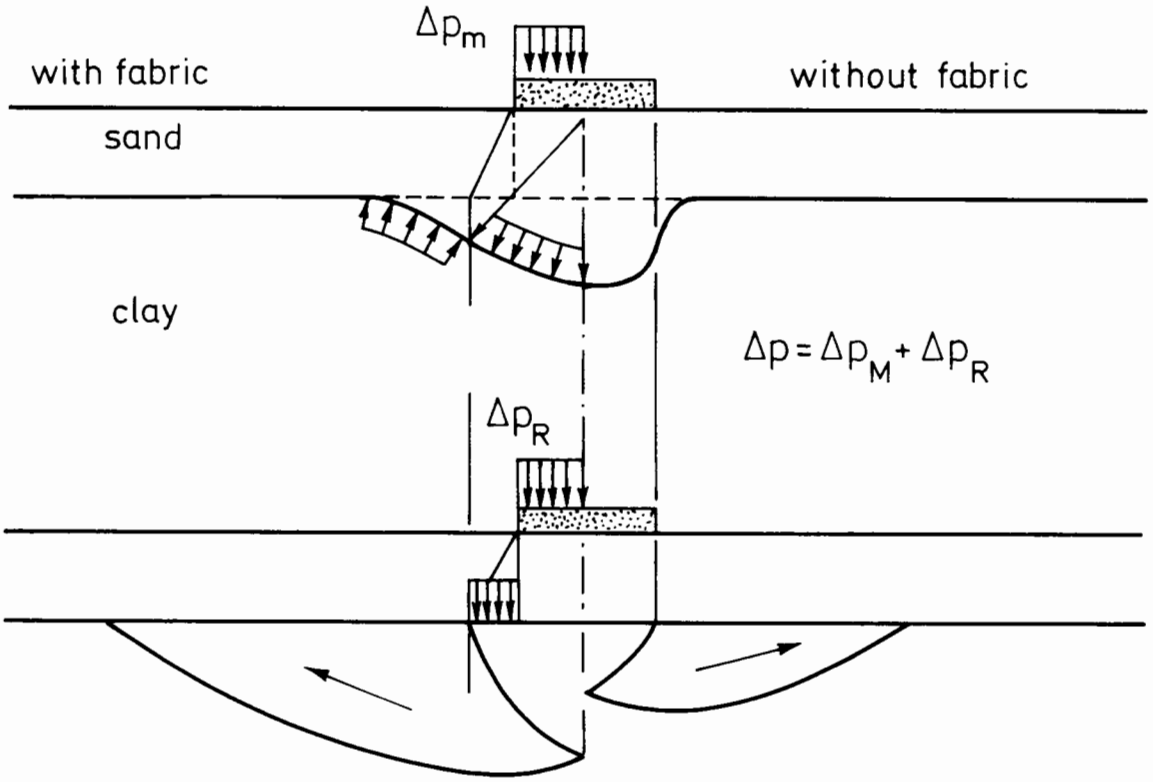

Figure 1.4 Reinforcement mechanism (after Gourc et al, 1982)

for a purely elastic subgrade, to the more realistic situation of an elasto-plastic subgrade.

1.3.4 Summary

It is apparent from the design methods above that despite most papers' stated aims of establishing the different mechanisms at work in the reinforced and unreinforced system, not one specifically identifies and accordingly quantifies these separate mechanisms. Instead each employs a method of ingeniously sidestepping this main issue. It will also be noted that in none of the above mentioned experimental work has there been the following:

- an attempt to scale material properties accurately when a problem is modelled at reduced geometrical scale
- comprehensive information concerning the strains developed in the subgrade body
- preparation of a clay subgrade foundation for lab tests by a consolidation process to produce a fully saturated clay with a realistic strength with depth profile
- pore pressure monitoring during 2-D plane strain lab tests on a problem of this kind.

This laboratory testing programme attempted to cover these points and to provide the joint sponsors, Netlon Ltd and the Science and Engineering Research Council, with a better understanding of the mechanisms by which geogrids enhance the performance of unpaved roads.

CHAPTER 2

DESIGN OF APPARATUS

2.1 Introduction

In order to tackle the main issue of identifying the basic mechanisms of failure in unreinforced and reinforced unpaved road systems, a deliberately simple approach was taken. The complexity of traffic loading combined with non-homogeneity in ground conditions make the full scale real-life situation an extremely difficult problem to analyse. It was decided that a set of monotonic, constant rate of penetration, plane strain footing tests conducted at reduced scale would be a sufficiently simplified version of the real situation to be able to discover these basic mechanisms.

2.2 Modelling at Reduced Scale

When conducting model tests at reduced scale it is necessary to reduce the geometrical dimensions of each component by the scale factor. Since a scale factor of 4 was used for this model study, the 75mm model footing width corresponded to a single-tyre width of 300mm in the field. Typical field subbase thicknesses for an unpaved road lie in the range 0 - 400mm , and so the fill thickness range for the model was taken as 0 - 100mm . In addition, the fill material was itself scaled. Combinations of appropriate fractions of sand and gravel were made up to give a scaled equivalent of Type 1 material, as specified in the

Department of Transport Specification for Road and Bridge works (Figure 2.1). Despite being unneccessarily restrictive for many real applications, this grading has the advantage of being well defined and widely familiar. Very fine particle sizes were omitted as they tend to cause problems in testing.

The grid used was a scaled version of Tensar SS1, produced similarly to the full scale material from a fully orientated polymer. The very same polymer could not be used for reasons outlined further below, but the aperture size of the grid was reduced by the scale factor in order to correctly model the very important particle/grid interlock effect. A comparison of full-scale and model grid dimensions is laid out in Table 2.1 .

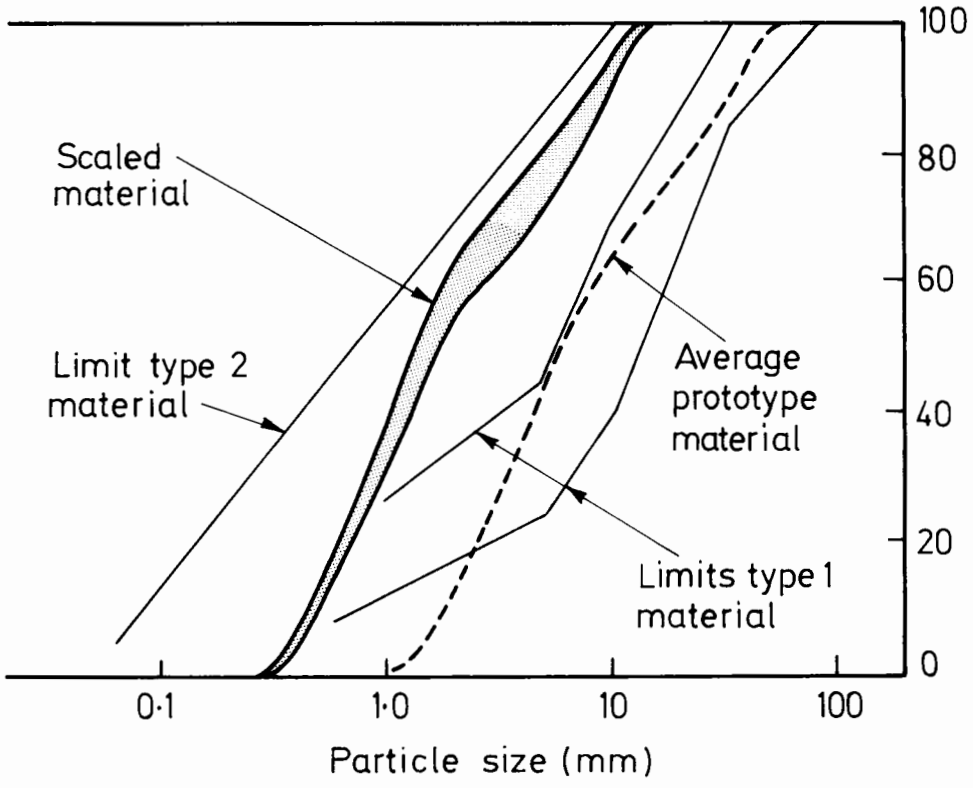

Figure 2.1 Grading of fill material

It is not enough, however, simply to reduce geometrical dimensions in the model: it is necessary in addition to reduce appropriately material properties in the system, such as strengths and stiffnesses. The extent to which each property should be scaled is given by dimensional analysis, in which all relevant parameters should be considered. The load bearing ability of the system will depend on the following:

$$q = f_1(\delta , B , H , C_u , s , G_1 , G_2 , \gamma_1 , \gamma_2 , \phi')$$

where:

- δ - penetration of footing
- B - width of footing
- H - depth of fill layer
- C_u - undrained shear strength of subgrade
- s - stiffness of grid per unit width (kN/m)
- G_1 - elastic shear modulus of fill material
- G_2 - elastic shear modulus of subgrade
- γ_1 - unit weight of fill material
- γ_2 - unit weight of subgrade
- ϕ' - angle of internal friction for fill material

The above parameters are each well defined quantities apart from s, the 'stiffness' of the grid. The stiffness of a grid is a term which is often used loosely, so that it is important to define its meaning here fully. The quantity s is a stiffness per unit width, whose units are kN/m, and is defined as the 5% strain secant modulus from a plot of load per unit width against strain. Furthermore s is of the form

$$s = E't$$

where E' is an effective Young's Modulus which takes into account the

TABLE 2.1 COMPARISON OF FULL SCALE AND MODEL GRID DIMENSIONS

	Aperture size		ribs		nodes
	length	width	width	thickness	thickness
SSI	38	28	3.3	0.5-0.8	2.9
Model grid	9.0-10.0	8.0-9.0	0.3-0.5	0.15-0.25	0.8-1.0
Full scale equivalent of model grid	36-40	32-36	1.2-2.0	0.6-1.0	3.2-4.0

Dimensions in mm

apertures between ribs of material in the grid, and t is the thickness of the grid. It should be noted that if the dimensions of a grid are reduced by a scale factor, t will reduce by the scale factor, but E' will remain unchanged since the geometry of the grid is kept the same and the grid is made from the same material.

Proceeding with the dimensional analysis, the set of parameters above may be arranged into dimensionless groups in the usual way as below.

$$q/C_u = f_2(\delta/B , H/B , \gamma_1 B/C_u , s/C_u B , G_2/C_u , G_1/G_2 , \gamma_1/\gamma_2 , \phi')$$

For justifiable extrapolation between model and full-scale the numerical value of each dimensionless group should be the same in the model and at full scale. If γ_1 and γ_2 cannot be scaled without a centrifuge, then the material properties C_u , G_2 and G_1 must be reduced by the scale factor, and s by the scale factor squared (hence E' by the scale factor). The problems arising from this are that:

- very low shear strength clays are difficult to work with

- the grid's stiffness, s , is only reduced by a factor of 4 by using a model grid of 1/4 thickness. The additional factor of 4 reduction in s must come from a reduction in the effective Young's Modulus of the grid, E' . However the effective Young's modulus of a full scale polymer grid is not altered by the simple scaling of its geometry as mentioned earlier. The only way a change in modulus can be achieved is by either using a different polymer, a reduced rate of testing, elevated temperatures or a combination of these (see Section 5.2.2).

Since interest lay in a range of subgrade undrained shear-strengths 20 - 60 kPa in the field, a range of 5 - 15 kPa was looked at in the model. A typical strength-with-depth profile was simulated by allowing swelling at only the top surface of the clay sample after its consolidation. The scaling of the Shear Modulus of the fill, G_1 , and yet the conservation of its internal angle of friction, ϕ' , were found to be compatible. G_1 is affected mainly by the mean normal stress, p' , and the void ratio of the fill, with the relationship between G_1 and p' being

$$G_1/p_a = A(p'/p_a)^{0.5}$$ where: p_a - atmospheric pressure

A - constant

(Wroth, Randolph, Houlsby and Fahey, 1979)

In the model p' is reduced by the scale factor of 4 , causing G_1 to reduce by a factor of only 2 . The additional reduction factor of 2 was achieved by a small increase in voids ratio, which also acted to decrease the value of ϕ' . This effect on ϕ' was found to be offset, however, by its tendency to increase with the decrease in mean stress level, p' .

The shear modulus of the clay is proportional to its undrained shear strength, C_u, for overconsolidated clays, so presents little scaling problem (see Section 6.1.1).

Compactive effort per unit area used on the fill layer should also be reduced - by the scale factor squared, the relevant dimensionless group being:

$$\text{Compactive Effort per unit Area} / C_u B$$

but whether this was achieved or not is difficult to ascertain.

2.3 **Apparatus**

2.3.1 General Requirements

The apparatus had to meet the following general requirements:

- clay samples, with a range of strengths, had to be prepared by normal consolidation from slurry form
- clay samples had to undergo bearing capacity tests under plane-strain conditions with and without an overlying layer of granular fill (varying depth), with and without a horizontal layer of grid reinforcement between the clay and granular fill
- two sides of the clay box had to be transparent, allowing strains on the front face of the clay sample to be measured by photographic means.

An 18 ton press Figure 2.3 and a perspex sided aluminium box Figure 2.4 , which fitted inside the press, constituted the main pieces of equipment. Both items were one-off, being designed specifically for the work, and were built in the Oxford University Engineering Department workshops. The size of the sample (300mm by 1000mm in plan, by 400mm in depth) was such that 1/4 full scale tests could be carried out without significant effects from boundary conditions, the reasoning being as follows.

The depth and breadth over which a footing, or wheel, of width B is likely to have effect (the 'affected zone') are represented by D and W respectively in Figure 2.2. Taking an upperbound value for $\tan\alpha$ of 0.7 for load spread through the fill layer, the dimensions of a clay sample for tests at 1/4 scale had therefore to be at least D/4 (177mm) by W/4 (925mm), the working as below:

$B' = B + 2H\tan\alpha$ where $B = 300mm$ Field Value

$H_{max} = 500mm$ " "

$\tan\alpha = 0.7$

$B' = 1000mm$

$D = B'/\sqrt{2} = 707mm$

$W = 3B' + 2Ht\tan\alpha = 3.70m$

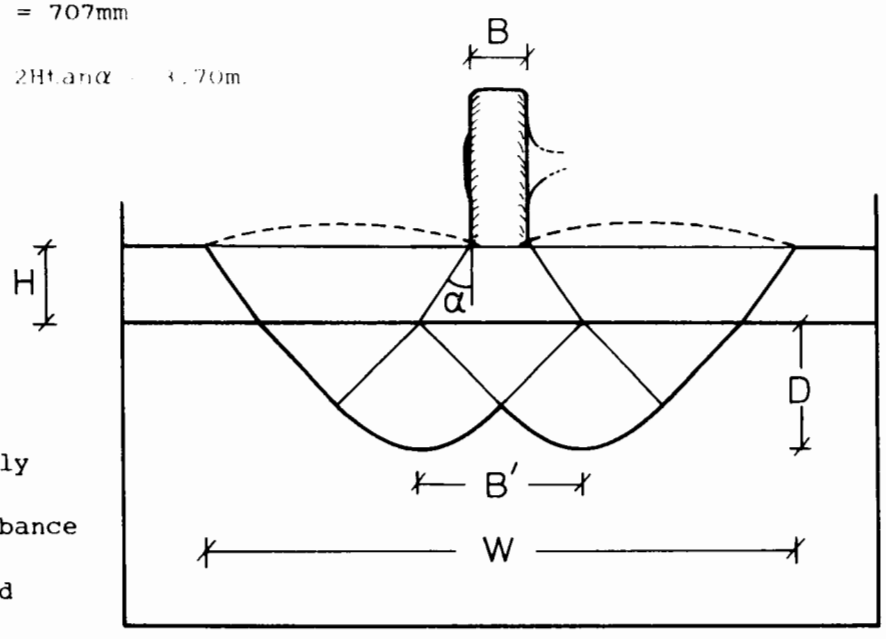

Figure 2.2 Likely extent of disturbance due to wheel load

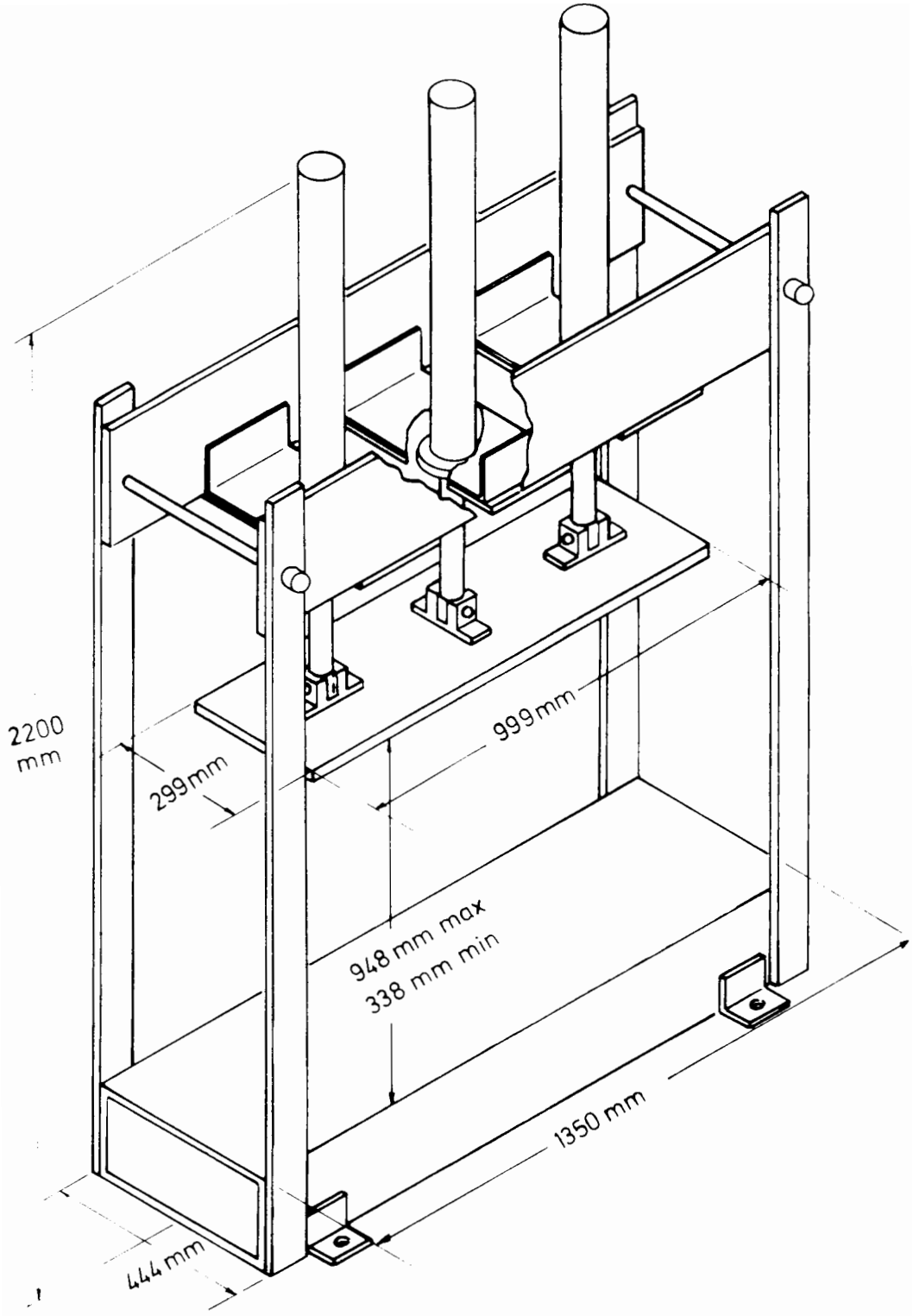

Figure 2.3 Load-press, with consolidation platen attached

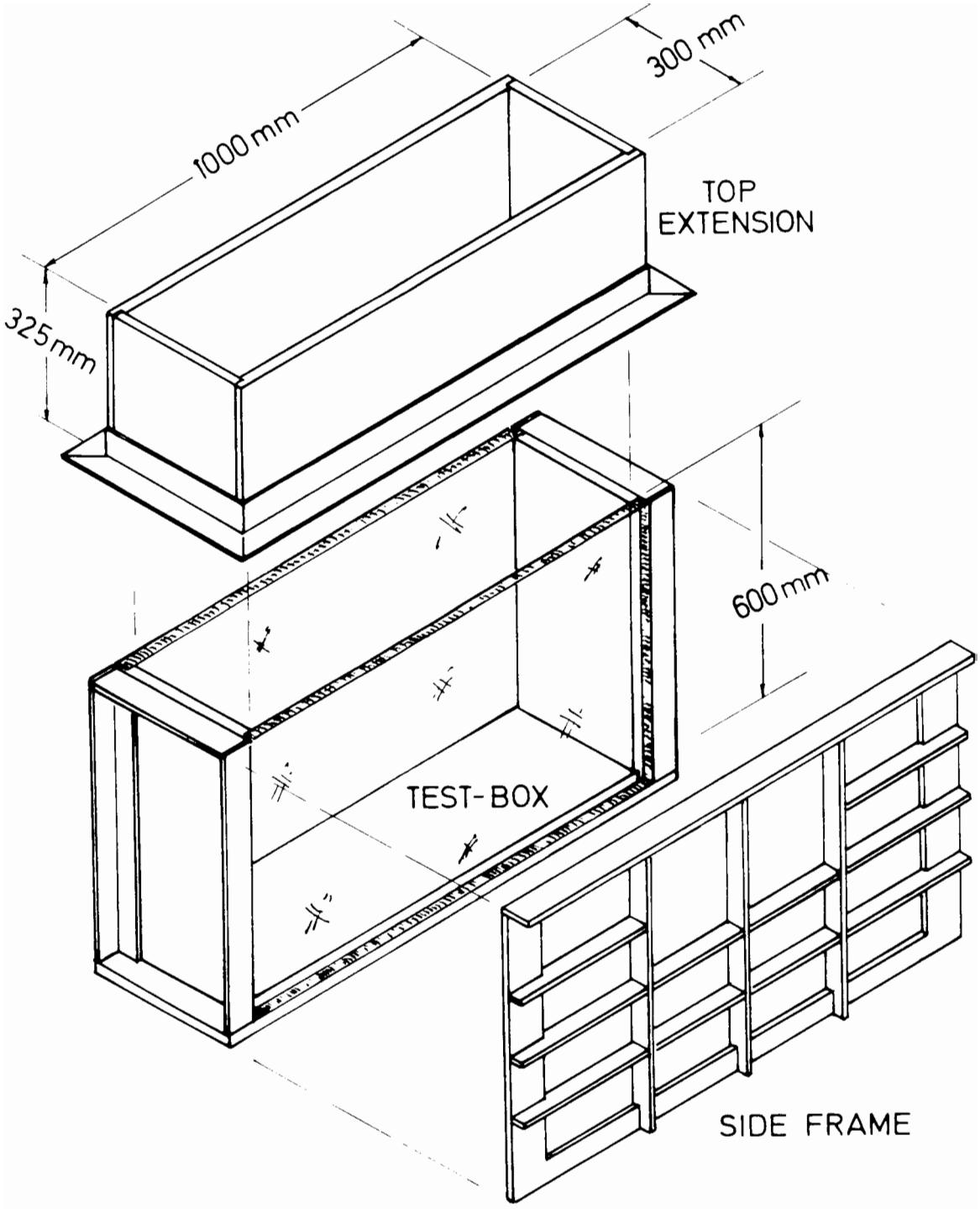

Figure 2.4 Test-box, with side frame and top-extension

It was recognised that the affected zone would deepen as the footing descended under its load, especially in a reinforced test: taking into account experience from the preliminary tests by Milligan (1981) and as a reasonable compromise between practicality and ideally infinitely-distant boundaries, the dimensions of 400mm by 1000mm were chosen. The third dimension, the width of the sample, had to be sufficiently large for edge effects (wall friction) not to affect results significantly, and yet not be any larger than necessary in view of the consolidation forces which increase in proportion to the plan area of the sample: a width of 300mm was chosen. This width prohibited the use of X-ray techniques for determining internal strains, but such techniques would have been in any case too slow for the rate of testing. Both the consolidation and testing stages were conducted with the test-box in the press. A 'top-extension' piece, Figure 2.4 , fitted to the test box for consolidation, was removed before testing. The press provided the load necessary both for consolidation and testing by suitable arrangement (Plate 2.1).

2.3.2 The Test Box

The test-box had to have a side through which photographs could be taken, while at the same time being able to withstand the large pressures associated with the consolidation process. It was therefore decided that it should have two sides made of perspex supported by two metal frames (Figure 2.4) which would obscure as little of the face as possible during tests, and a removable top-extension piece to be used only during consolidation. Two separate strengthening pillars were also necessary to brace the whole assembly during consolidation (as in Plate 2.1). The steel frames were designed to hold the front and back faces of 25mm

Plate 2.1 Set up for consolidation

perspex in position against an 'O-ring' seat as well as to provide extra stiffness, obviating the need to bolt through the perspex. The rig was designed to restrain lateral movement at the centre of the perspex faces to less than 0.25mm at a maximum consolidation pressure of 600 kPa. (In fact the maximum consolidation pressure actually used for sample preparation was only 450 kPa). The initial depth of slurry required mixed at twice the liquid limit to a water content of approximately 120%, to produce a 400mm thick block of clay under 450 kPa was estimated at 810mm . This estimation was based on the consolidation work of Freeman (1982), who had used the same type of Speswhite Kaolin under similar conditions. After consolidation, once the loading platen and the top extension to the box had been removed, the clay sample had to be trimmed

to an exact size. For this reason more slurry was allowed for in the first place to produce a clay block slightly in excess of 400mm . The box was therefore designed for a maximum slurry depth of 850mm, which allowed sufficient extra height above the slurry for the loading platen to be lowered onto the slurry and to ensure that it was descending true at the start of consolidation. The base of the box had a drainage channel (6mm wide) cut centrally along its length. Drainage holes (6mm diameter) with taps on the underneath were placed at either end. A 3mm thick piece of porous Vyon sheet, cut exactly to size, was inlaid into the base to act as a drainage layer and filter. Flexible plastic hose (6mm internal diameter) attached to the taps took drainage water to the same level as that above the sample to maintain a constant head of water at both drainage faces.

As previously mentioned, the front and back faces of the test-box were both made from perspex, so that friction was the same on both boundaries. But these two faces were not identical due to the necessity of being able to expose temporarily the front face of the clay in order to prepare it with a grid of visible markers. By deforming with the clay, these markers allowed displacement patterns in the clay during a test to be recorded from photographs. The front face through which photographs were taken therefore consisted of two sheets of perspex, one 19mm thick sheet and one 6mm thick sheet, cut to the same dimensions. This was so that the extra pliability of a thinner face in contact with the clay could greatly ease exposing the clay face by a peeling action when it came to positioning photographic markers. The back face consisted of one 25mm thick perspex sheet, in which a number of holes were drilled and tapped for pore pressure and total pressure transducer mounting. The back frame was originally made in two pieces with the join

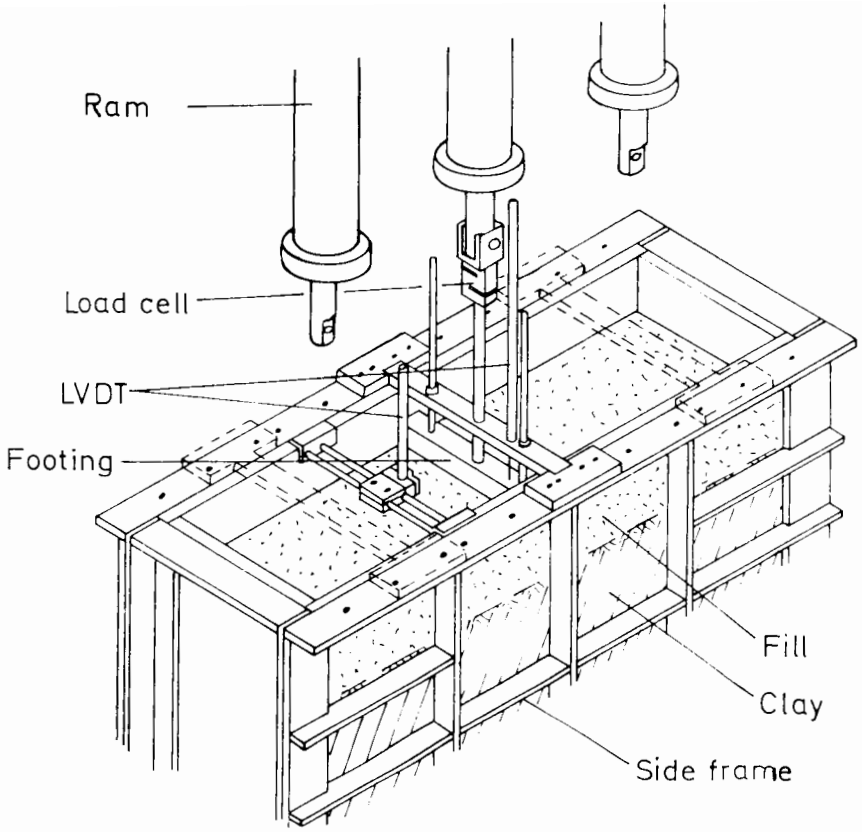

Figure 2.5 Set up for testing

at the clay-aggregate interface since it was thought this might aid trimming of the sample: this idea was subsequently abandoned and the two halves were fixed firmly together.

The range of field aggregate thicknesses to be considered was originally fixed at 0 - 0.5m , so that the maximum model depth had to be 125mm . The top of the test box was then set at 75mm above this level, which allowed the footing some 30mm travel before coming into contact with the surface of the fill layer.

The top surface of the metal support frames provided a firm platform across which a 'bridge' could be fixed during tests (see Figure 2.5). The bridge housed bushing collars for the footing guides to run in, to ensure that the footing descended vertically: it also carried an LVDT which monitored the descent of the footing. It could be fixed in three

positions - one under each ram - and bolted into already existing holes. To obtain a profile of the aggregate surface two 'jockeys' (Figure 2.5) holding one LVDT each slid the entire length of the test box supported on the top surface of the perspex sheets. The LVDT's also had freedom to move across the width of the test box on the jockeys.

The front and back faces were made completely removable to enable cleaning out of the box at the end of tests.

2.3.3 The Load-Press

The press (Figure 2.3) was designed to provide a maximum force of 18T, which for the consolidation phase, had to be applied as evenly as possible over a rectangular area (1000mm by 300mm). For the testing stage a much smaller force, estimated at a maximum 1.5T, had to be applied to a thin footing 75mm by 300mm. The more sites that the footing could be mounted the better so that as many tests as possible could be conducted on each sample of clay. It was therefore decided that the press should have three 6T rams, all of which could act on the platen during consolidation, and any one of which could be used for tests. This requirement excluded all commercially available industrial presses.

The press consisted of a firm bottom table on which the box sat, an overhead 'top assembly' on which the three rams were mounted, and four corner struts to support the top assembly. The combination of a box and separate press was adopted instead of a Rowe cell apparatus because the latter required tensile forces to be transmitted through the walls of the cell during consolidation: in the case of the former these forces could be carried in the press. It would be less easy to provide for these tensile forces in a Rowe cell which had two of its four sides made of

perspex. Secondly a separate apparatus for conducting tests would have had to have been designed and built in addition to the apparatus required for consolidation.

Ideally the positioning of the rams on the loading platen should have been such as to produce a uniform pressure on the clay during consolidation for a minimum thickness and weight of platen. The requirement that each of the rams was to be used for load-testing was an additional constraint. As a compromise, the rams were spaced apart by L/3 , L being the length of the platen. The platen was made 25mm thick, and its worst deflection at maximum load was estimated at approximately 0.5mm .

The bottom table of the press was of box section and was designed not to deflect centrally by more than 0.2mm at full load. The top assembly of the press, being less critical, was similarly designed not to deflect more than 0.5mm. Two 25mm diameter shear pins held the top assembly in position: by simply removing one of these pins the whole assembly could be rotated upside-down through 180^{o}. This allowed vertical access to the box by overhead crane and general maintenance of the rams. The pins were designed to be the weak point in the rig, so as to act as 'fuses' in the event of excess loading. The factor of safety was 2 . The bolts used throughout the press and test box were all high tensile and had a factor of safety against failure of at least 5 . The platen was also fixed onto the rams with shear pins, fitting through mounting blocks on the top surface of the platen. The arrangement of the blocks (see Figure 2.3) was such that tilting of the piston about any horizontal axis was resisted, ensuring the platen descended as levelly as possible. This design obviated the need for guide collars that might have been fitted across the top of the extension box to prevent

platen-tilt. The platen was made of stainless steel (25mm thickness) since it was in constant contact with water; all other steel used for the press and test box was mild steel.

Clearance between the platen and the inside walls of the box was 0.5mm . Sealing around the platen was found to be adequately provided by cutting a piece of Vyon porous sheet, necessary as a filter in the first place, slightly oversize (100lmm by 30lmm) and bevelling its edges, as in Figure 2.6 . This allowed up to 40 kPa to be placed on the slurry as an initial consolidation increment. Two holes, diameter 6mm, were drilled into the platen either end for drainage.

The rams were pressurised from a nitrogen supply kept at a maximum of 2,000 psi. A simple pneumatic system stepped this pressure down and held it constant at any required value in the range 0 - 2000 psi ±2 psi,

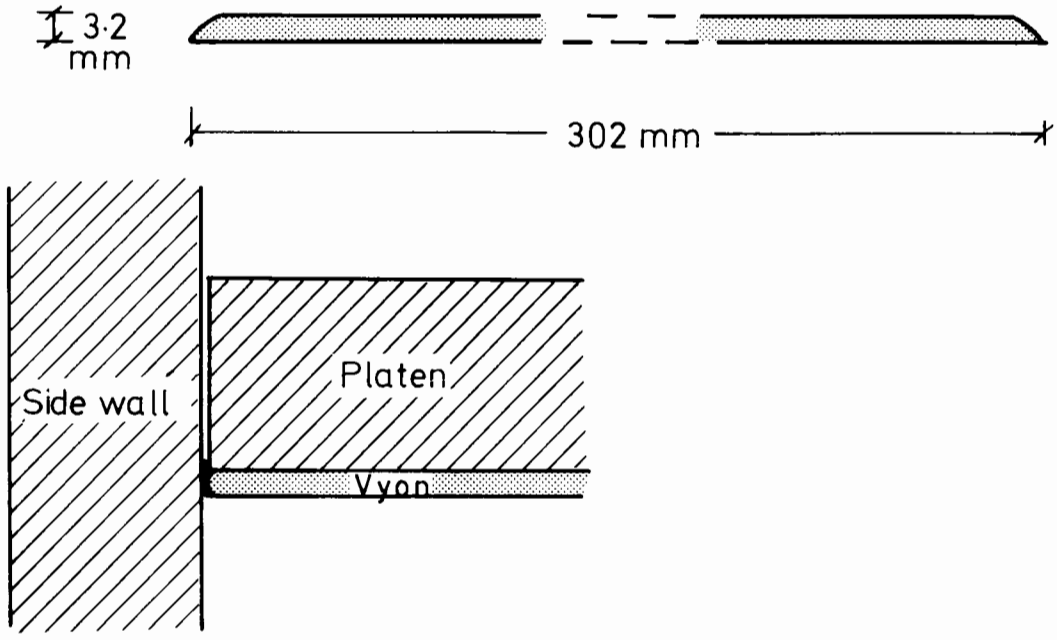

Figure 2.6 Porous Vyon seal

2000 psi in the rams being enough to provide 18t on the load platen. The pneumatic line included a pressure gauge which could be read to an accuracy of ±2 psi, a non-bleed type gas regulator which could be set to the same accuracy, 3 on/off valves which enabled rams to be used in any combination, and three 6m lengths of flexible double-braided stainless steel hose taking the pressure to the rams (see Plate 2.2 for control board). A pneumatic system was chosen to power the rams, over a hydraulic system, because it was silent and considered simpler. To raise the rams after consolidation, however, a hydraulic system was used (Figure 2.7). Thus the rams had compressed nitrogen on one side and hydraulic oil on the other. Sealing was not considered a problem at the time of design, but some difficulties were experienced due to this. The reason for the choice of hydraulics over pneumatics for the low pressure side of the rams lay in the need to do constant rate of penetration tests: by fitting a pressure compensating flow control device into the

Plate 2.2 Control board

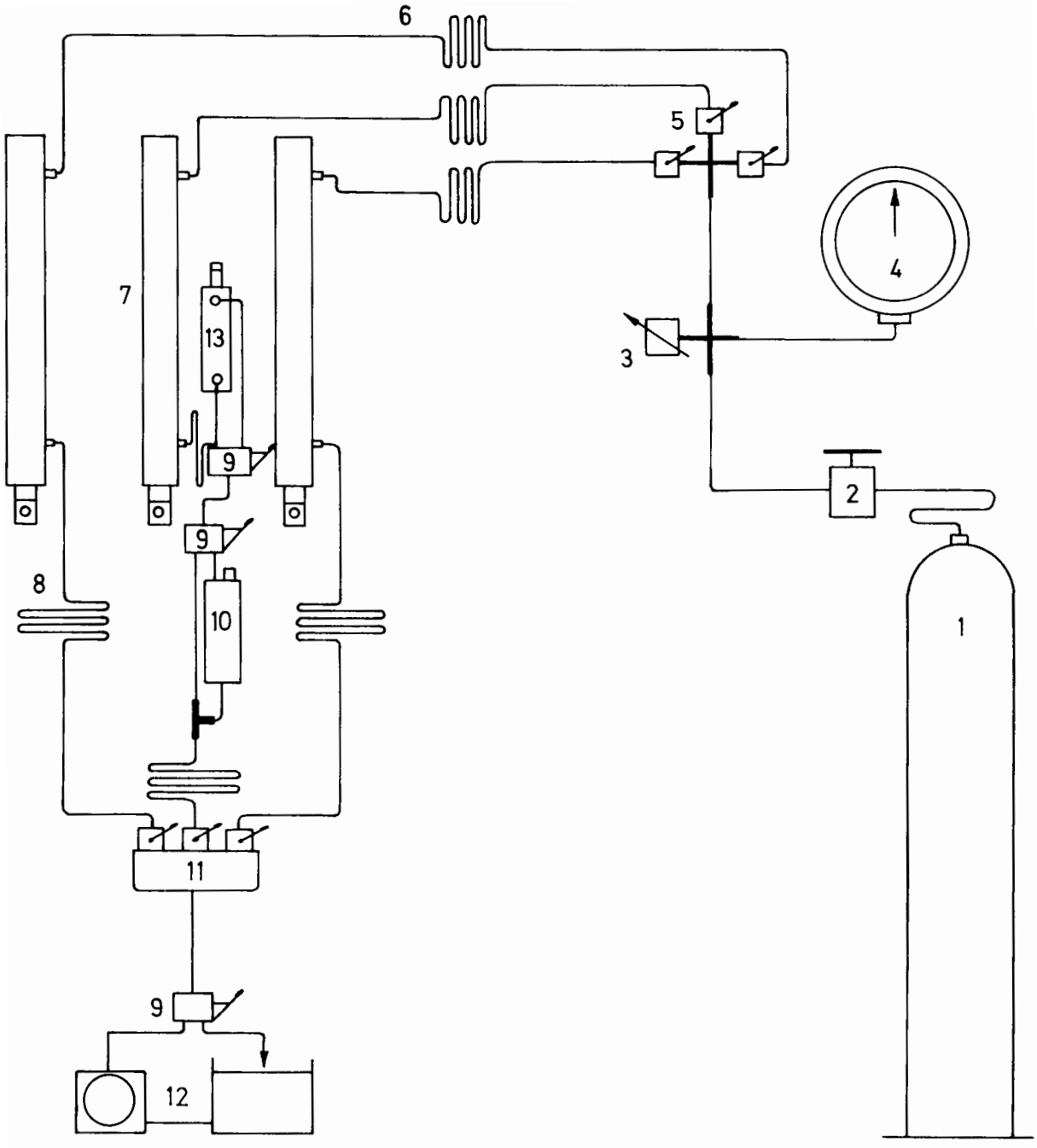

1 Nitrogen cylinder
2 Pressure regulator
3 Pressure relief valve
4 Pressure gauge
5 Isolator valves
6 Flexible pneumatic hose
7 Rams
8 Flexible hydraulic hose
9 Diverter valve
10 Constant flow device
11 Junction with isolator valves
12 Pump and oil reservoir
13 Limit piston

Figure 2.7 The pneumatic/hydraulic control system

hydraulic line, the flow-rate of oil out of a ram could be held constant no matter what the pressure, which ensured a constant rate of descent for the footing during tests. The hydraulic system comprised a simple oil pump run off the laboratory air line, on/off valves to each ram, and a diverter valve which either incorporated the pressure compensating flow control device or bypassed it. In addition, a fourth much smaller hydraulic two-way piston was incorporated in the line as a limiter to footing travel during tests, which was switched out during consolidation. Flexible rubber hoses were used, and all hose ends were re-usable so modifications could be made relatively simply.

During tests, load was transferred from the ram (75mm internal diameter) to a slender shaft (25mm diameter) which passed through the bridge to the footing. The 25mm shaft had to be slender so that the width of the bridge could be kept to that of the footing. This allowed the LVDTs on the jockeys maximum travel (see Figure 2.5).

2.4 **Instrumentation**

The three pore pressure transducers used were the Druck PDCR 81/S special miniature transducer which, unlike the PDCR 81 , had a securing flange (Figure 2.8). Overall dimensions were 6.4mm in diameter by 11.4mm in length. Powered by a 5V DC signal, positive supply earthed according to the manufacturers recommendation, their output lay in the range 0 - 40mV , full-scale deflection 350 kPa . The total pressure transducers were both Druck PDCR 53 , which also had a securing flange (Figure 2.8). These devices, much bigger than the pore pressure transducers, had a diameter of 11.8mm and length of 41mm. Powered by a 10V DC supply, these gave an output in the range 0 - 35mV , full-scale deflection

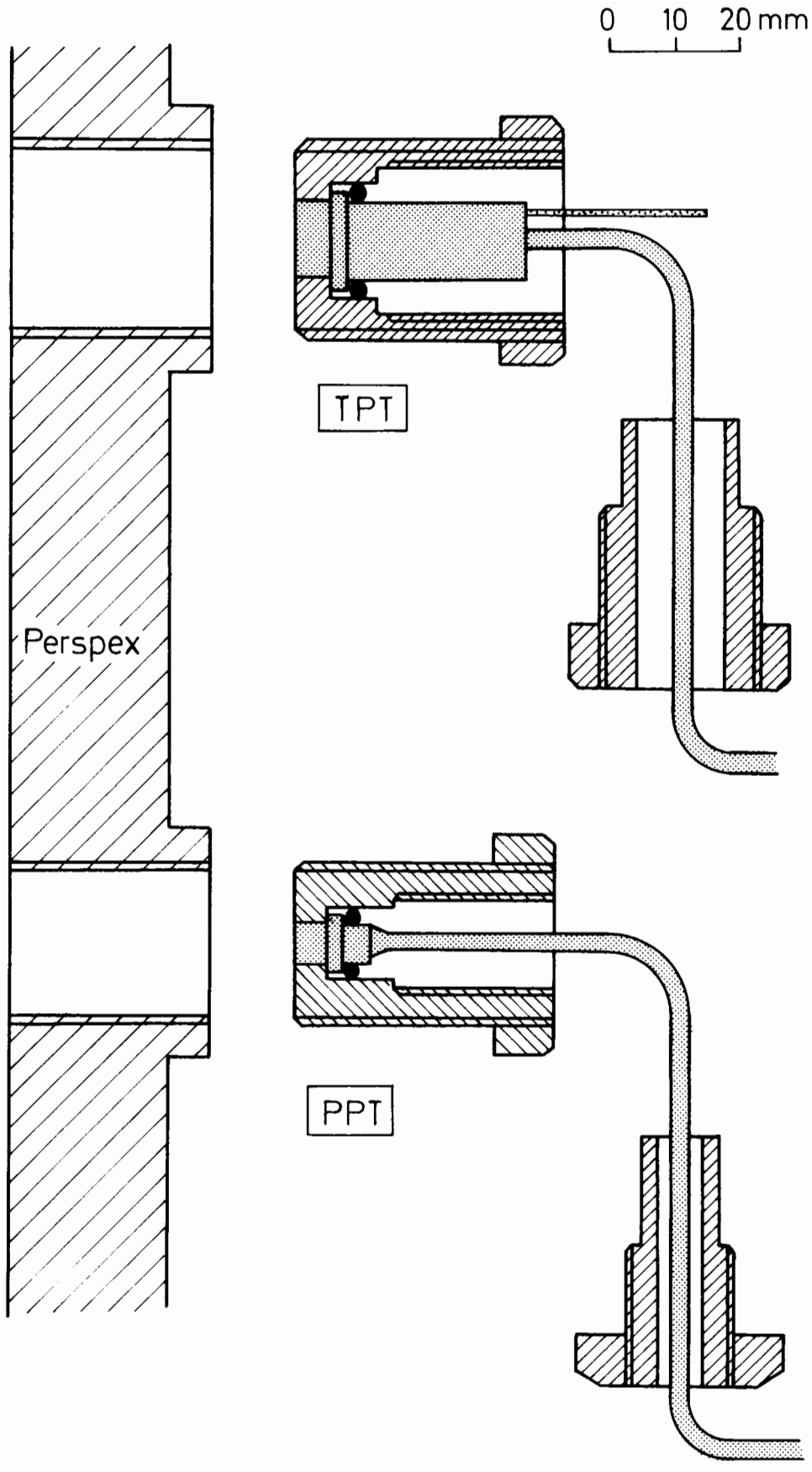

Figure 2.8 Mounting arrangement for Pore Pressure and Total Pressure Transducers

500kPa . The pore pressure and total pressure transducers were mounted into ports in the back face of the test box. Special brass plugs were made up to screw in behind the transducer, to push them up against an 'O-ring' . This gave a good seal and ensured that the front of the transducer always sat flush with the inside wall of the box.

Four LVDT's were used, all of the AC type. A 500mm stroke AC250 , manufactured by Sangamo Transducers, was used during consolidation to monitor the descent of the platen. A 200mm stroke D5/4000C ,

A Pore Pressure Transducer
B Total Pressure Transducer
C 500mm stroke LVDT
D 200mm stroke LVDT
E 100mm stroke LVDT
F 1.5t Load Cell
G 75mm width Footing
H Bridge
J Jockey
K Surface Levelling Tool

Plate 2.3 Apparatus and Instrumentation

manufactured by RDP Electronics, was used during tests to monitor footing descent. Two 100mm stroke D5/2000 , also from RDP, were used during testing to monitor surface heave either side of the footing and used during surveying. These LVDT's were not placed directly onto the fill surface, but onto small metal tins which prevented the armatures digging into the surface. The diameter of these tins was 64mm.

Four conditioning modules were used in conjunction with these AC LVDT's in order to supply AC to the LVDT , and to convert the signal from the LVDT back into DC . The Sangamo conditioning card was supplied with a 30V DC supply, with an output in the range 0 - 10V . The three RDP conditioning modules were also supplied with 30V and had outputs in the range ±200mV .

The Load cell used was a D95/15,000 hermetically sealed, strain-gauged 'Z'-device, manufactured by Sangamo. This was supplied with 15V DC , and had a sensitivity of 32kg/mV, and 1.5t full scale deflection.

The instrumentation was powered from an HTC 1 triple output DC power supply, the voltage on each rail being +15V , -15V and +5V . This power

TABLE 2.2 COST OF INSTRUMENTATION

Pore Pressure Transducers		3 @ £200
Total Pressure Transducers		2 @ £120
LVDT	500mm Stroke	£160
	200mm Stroke	£95
	100mm Stroke	2 @ £64

Conditioning Modules	3 @ £50 1 @ £86
Load Cell	£195
Power Supply	£78
Multimeter	£135

(1982 prices)

supply was appropriately screened and housed in a single box with the four conditioning modules. This box had a multi-way switch on it to check each instrument locally, using a Bach-Simpson model 461 multimeter. It also had a multi-channel connector, which linked it to the data-logger via a multi-core screened cable.

The Data-scanner used was a 16-channel 7010 Solartron Minate, coupled to a 7060 Solartron Systems Voltmeter, both run from a 380Z Research Machines micro-computer. During each test the scanning program, written in BASIC , took a time-reading and scanned all 9 pieces of instrumentation continuously, with a period of 0.6 seconds. During a test taking typically 20s , with a footing descent rate of 2.5mm/s , 30 - 35 sets of readings were taken at approximately 1.5mm increments of footing penetration. The signals were read to 'five nines' accuracy, on the voltmeter's 100mV range. Readings were taken, in mV , to 3 decimal places, a very adequate level of accuracy for this research. If faster sets of readings were attempted by specifying a lesser degree of accuracy, spurious mains-related 'noise' caused corruption of the signal starting from the first decimal place. This is because readings were being taken too fast for the integration-time spent on the signal by the voltmeter to cover one complete cycle of mains-related background noise, so that the 'noise' effect was not averaged out. For any further speed, therefore, the signals would have had to have been amplified from the mV range to avoid this problem.

During consolidation, a JJ Instruments CR 450 chart recorder was used to monitor continuously the output from the long-stroke AC250 LVDT , to obtain a record of the platen descent with time.

A 10" Budenberg pressure gauge (215 GP , 0 - 3000 psi) was used to

record the gas pressure in the rams during consolidation, supplied via the XX87 BOC high pressure gas regulator from the Oxygen-Free Nitrogen gas cylinders (Plate 2.2).

A Pilcon Hand Shear Vane (Plate 2.4) was used for obtaining values of undrained shear strength from the clay. The larger of the two vanes supplied (H = 50mm , D = 33mm) was used throughout. The vane was always inserted vertically to a mid-vane depth of 55mm below the clay surface, and rotated by hand at 1 rpm. The relationship between Torque (Nm), T , and shear strength (kPa), C_u , is taken in BS1377 to be

$$T/C_u = \pi D^2[H/2 + D/6] = 0.104\ m^3$$

The manufacturers, Pilcon, base their calibration on the empirical results obtained from work done by Serota and Jangle in 1972 , which gives a value 14% higher than this (see Ground Engineering, Vol 15, No 5, p49, July 1982). Calibration work carried out on the vane used in this test programme, involving hanging standard weights over a pulley in order to prevent bending of the shaft when torque was applied, indicated that a value 19% in excess of the BS1377 value was appropriate.

Plate 2.4 Shear Vane (with extension) and Augur

CHAPTER 3

EXPERIMENTAL PROCEDURE

3.1 Consolidation

3.1.1 Building the Rig

The test-box was dismantled after each sample and cleaned out before reassembly. The complete reassembly procedure is described here.

The bottom drainage lines were checked for blockages, then filled with water and the taps closed. The pore pressure and total pressure mountings described in the last chapter were screwed into the perspex back face at the relevant ports, and plugs were put into the remaining port positions. PTFE tape was used for a good seal. The back face was tried in position and checked for height, to ensure it was level with the dural end pieces. It was found that the perspex sheets changed shape with time and that either packing underneath or shaving of the top surface was necessary periodically. The perspex face was then fixed permanently in place by lining the inside of the 'O-ring' seat with transparent Superflex silicone sealant, and by bolting on the metal side frame. This squeezed out a lot of the sealant, and a smooth finish was obtained by running a finger along the inside joint and removing any excess. The two front face sheets of perspex were then tried in position, and again any top surface variation in the two pieces was cured by either appropriate packing or shaving. The inside 6mm thick sheet was pressed against the O-ring lined with silicone sealant as before. The

19mm sheet was fixed to it using screws flush with the inside surface, taking care to clean any trapped dirt between the two sheets attracted by static. The metal side frame was bolted on, clamping the perspex in place. Again, excess silicone sealant was smoothed off. The recesses around the screws fixing the two perspex sheets together, were also smoothed over with the silicone sealant. The internal walls of the box were coated with silicone grease, but taking care to minimise the amount in the vicinity of and directly above each pore pressure transducer position in order to avoid clogging of the stones. It was found useful to also include a thin (0.1mm) polythene sheet on the inside of the front face, for further ease of separation when it came to exposing the clay for marking. This was cut to size and smoothed into position with more grease. The end of the sheet draped over the top of the box, to be held in place by the top-extension piece which was fitted next. The top surface of the test-box was lined with sealant and the top-extension, also coated on the inside with grease, was lowered onto it using the overhead crane. It was bolted down by tightening screws in an even sequence, clamping the polythene sheet. The position of the extension was checked with the load platen, mounted on the three rams, before finally tightening the screws. Lastly, the outside bracing-pillars were moved into position and connected: the reaction pieces, in contact with the centre of the side frames, were screwed up hand tight. When the slurry was ready to be pumped in, a saturated piece of 3mm thick porous Vyon sheeting was put in at the bottom of the box.

3.1.2 Mixing the Slurry

Speswhite Kaolin was mixed under vacuum with water to approximately twice its liquid limit, at a water content of 120% . The mixer used was made by Winkworth Machinery Ltd , model No. 2056 , and of the type described by Gue (1984), Plate 3.1 . It was found that two 25kg bags of kaolin and 60 litres of water could be mixed at a time, and that it took 3 or 4 mixer loads during the day to fill up the box with slurry. Each mix was hand stirred before the motor was started, to prevent dry powder caking to the sides of the mixer. Each load was mixed for 2 hours under a vacuum in the range 10 - 16 kPa absolute pressure. It was found that any greater vacuum caused excessive cavitation to occur, giving rise to

Plate 3.1 The Mixer

many small bubbles in the slurry. Pressure was restored slowly over a 5 minute period after the two hours. This resulted in a smooth homogeneous fully saturated slurry.

After mixing, the slurry was transferred to the box using a Warren Rupp Co. 'Sandpiper' diaphragm slurry pump attached to the base of the mixer and operated by compressed air at 100psi . The delivery hose from the pump was used to 'tremie' the slurry for best results. Once the slurry reached and just covered each pore pressure position in turn, pumping was stopped briefly to insert the transducer and then resumed. In this way the transducers were exposed to air for a minimum amount of time (about 5 seconds) during transfer from a bowl of deaired water. They had previously been under vacuum, cycled several times, since the day before. When the desired level of slurry in the box was reached, a second piece of porous Vyon sheet was laid on top as described in the last chapter and the load platen lowered.

3.1.3 Consolidation of the Clay

During consolidation the platen descent was continuously monitored by a 0.5m stroke LVDT connected to a chart recorder. In addition readings by hand were taken of consolidation load, pore pressures and total pressures, and a check on the tilt of the load-platen was made with a metre rule. The load on the platen was, as a general rule, doubled every other day from an initial pressure of 30 kPa , until the final increment which was left on for 4 days. Typical consolidation summaries for each of the three types of sample are presented in Figures 3.1 to 3.3 , the maximum load on a sample being 110 kPa , 220 kPa or 450 kPa depending on the strength required. After this final increment, the

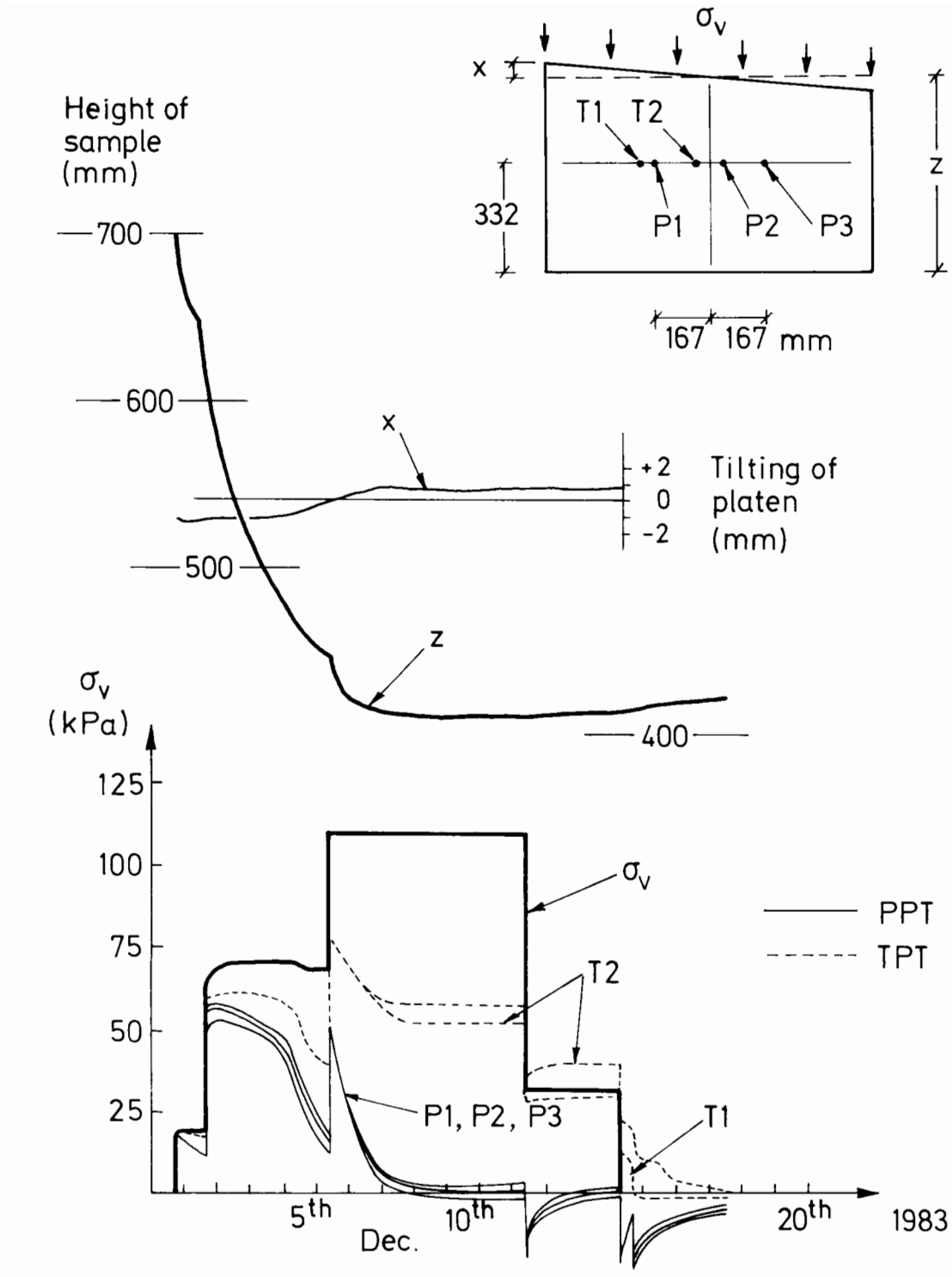

Figure 3.1 Consolidation Summary for Sample X (Nominal C_u = 6kPa)

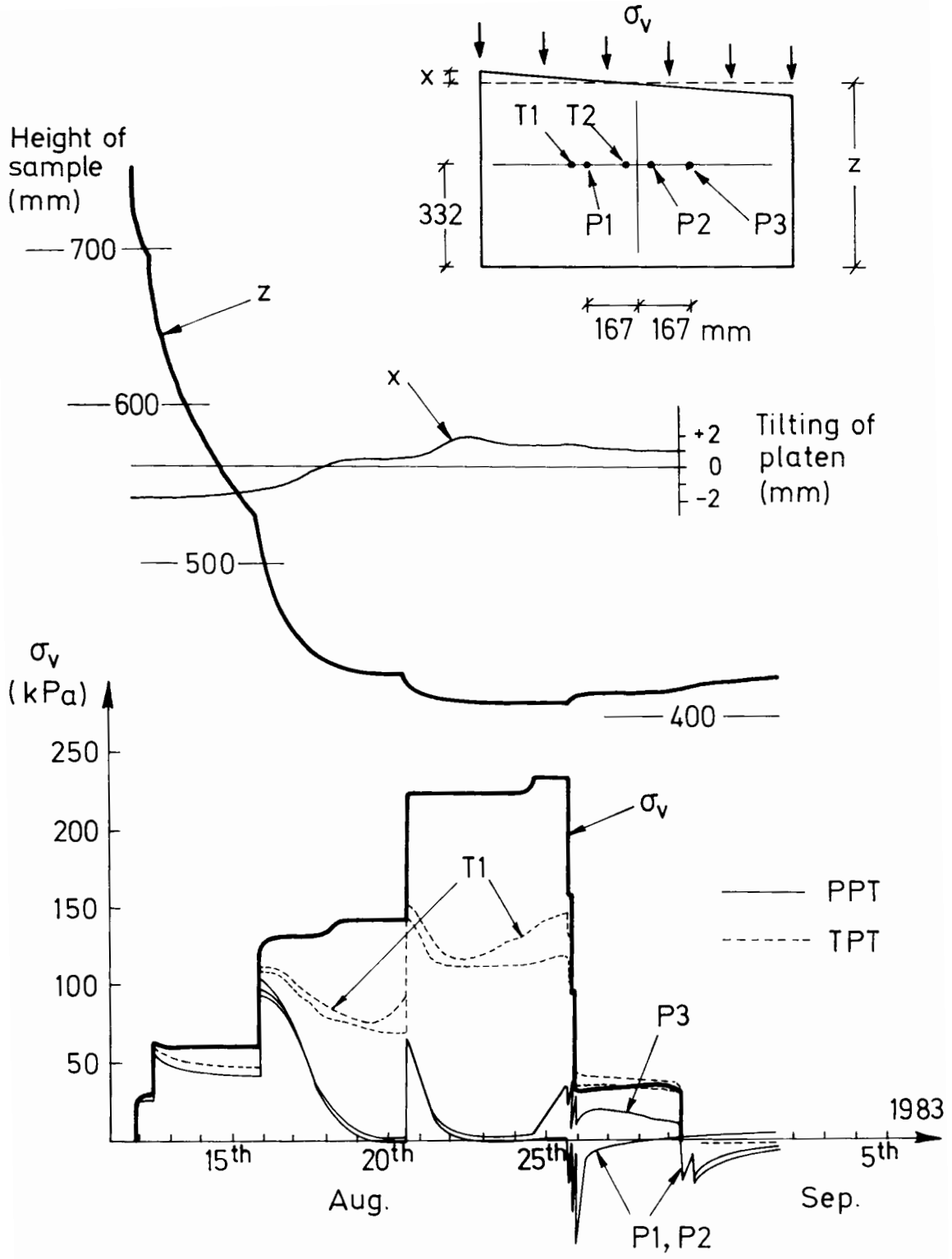

Figure 3.2 Consolidation Summary for Sample J (Nominal C_u = 9kPa)

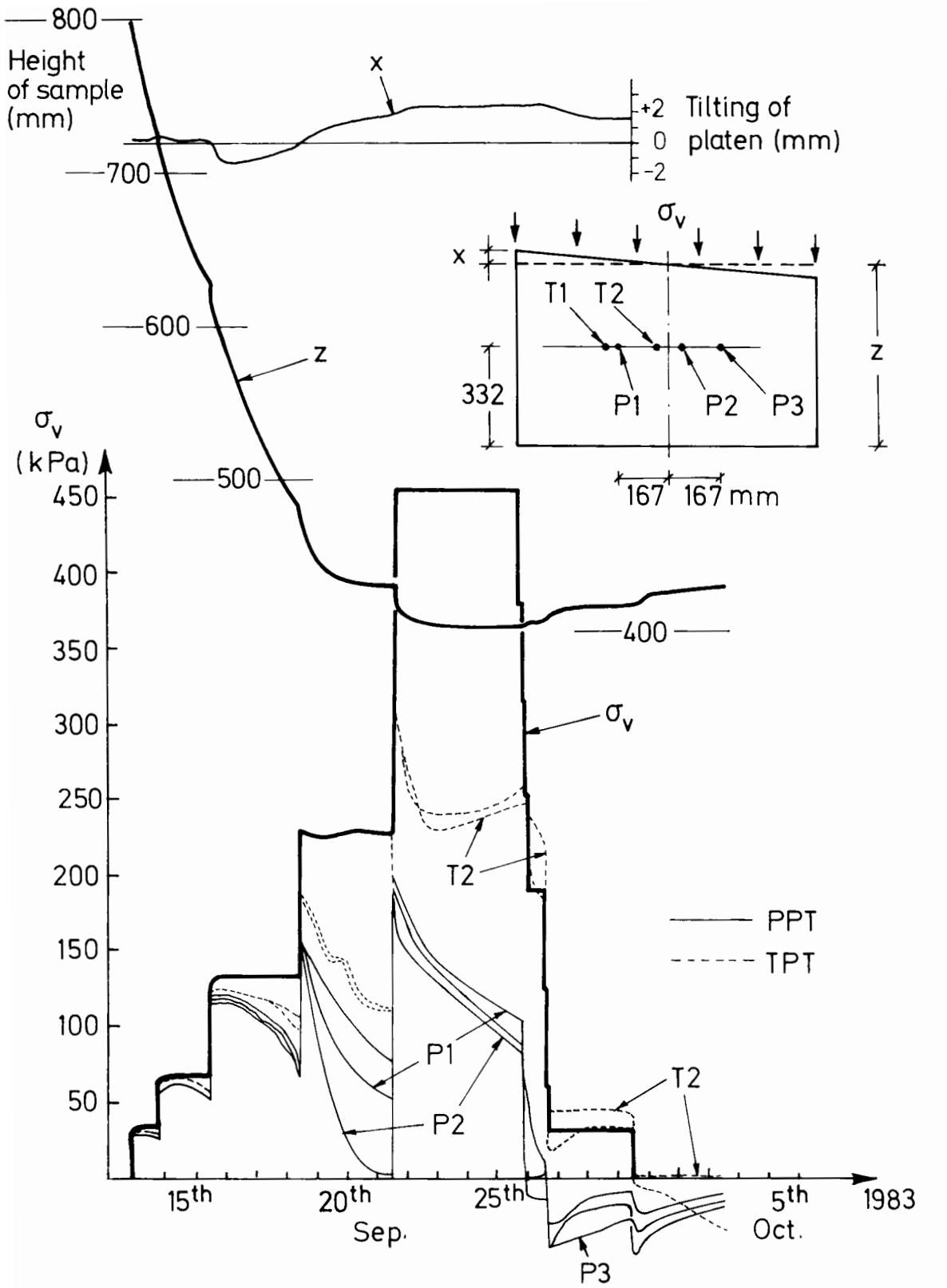

Figure 3.3 Consolidation Summary for Sample F (Nominal C_u = 14kPa)

would exist. A typical example of a contour plot is shown in Figure 3.4.

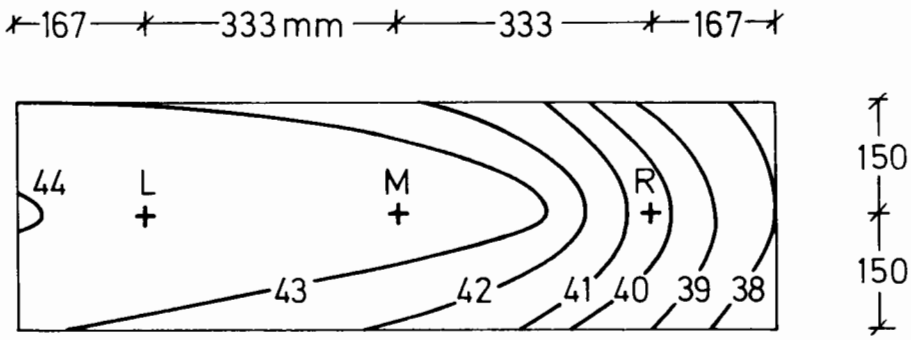

Figure 3.4 Contour plot for surface of Sample C (Contours in mm)

3.1.4 Marking the Front Face

The front-face was then removed in order to mark the clay. The metal side frame was unbolted, and the 19mm perspex sheet was detached from the inner 6mm sheet. The inner 6mm sheet was carefully removed by breaking the silicone seal at one side and peeling the sheet off slowly, and the inside piece of polythene facilitated this. Once the clay face was completely exposed the polythene was thrown away. Previously a comprehensive 15mm grid of approximately 1000 lead-shot markers, had been stuck onto a large sheet of graph paper. The paper was marked with the appropriate positions and was liberally greased: the shot markers were held in position by the grease when the sheet was lifted and positioned on the inside of the 6mm perspex face. The face was replaced and pressure applied to push the markers into the clay. The perspex was lowered once more to remove the empty piece of graph paper and then finally repositioned after being cleaned up and regreased. It was not necessary to put in a new silicone seal.

This operation took typically 15 minutes and worked well. The 19mm perspex sheet was replaced and the metal frame refixed. The surface of the clay was kept wet throughout. The following day the sample was tested.

3.2 **Testing**

3.2.1 First Layer - Central Tests

Local variations in clay strength play an important part in the scatter of test results. It was considered important to take one shear vane reading centrally under each ram before testing to get an independent strength reading for each position. It is true that this disturbed the subgrade before testing took place, but a similar reading was taken before each and every test in the same relative position, thus the effect is not seen in test results.

In order to have a perfectly flat clay subgrade the top surface of the sample had to be levelled. This was done by trimming it with a special tool which ran along the top of the perspex (see Figure 3.5), levelling the clay sample at a height of 407mm . The inside of the perspex was wiped and cleaned to give a good straight-line definition of the subgrade surface. It is important to note that the new strength with-depth profile for each subgrade depended on the amount of clay removed by this trimming operation. Innacuracies in the initial height of slurry put in the box at the start of consolidation, variations in initial water content, and small variations in maximum consolidation pressure meant that the amount of clay that had to be trimmed was not the same for each sample: consideration of this fact had subsequently to be taken into account (Section 5.1.4). The clay surface was not

re-moistened after this operation.

In a reinforced test, a layer of grid was placed next. In later tests the grid had 10mm diameter fluorescent markers glued along its front edge (Section 5.2.2) and it was important to ensure that these discs seated into the clay and that they were in direct contact with the perspex. They were liberally coated in silicone grease to help achieve this. In earlier tests, when the grid had no markers, thin inclinometer sticks cut from stiff wire, 250mm in length, were inserted through the last aperture of the grid at the ends of the box. This was to see if, and at what point, during a test the grid started to pull away from the sides of the box. The sticks were pushed 50mm into the clay, standing out 100mm above a fill layer that was 100mm thick. These sticks could only be positioned at the sides of the box, so as not to hinder

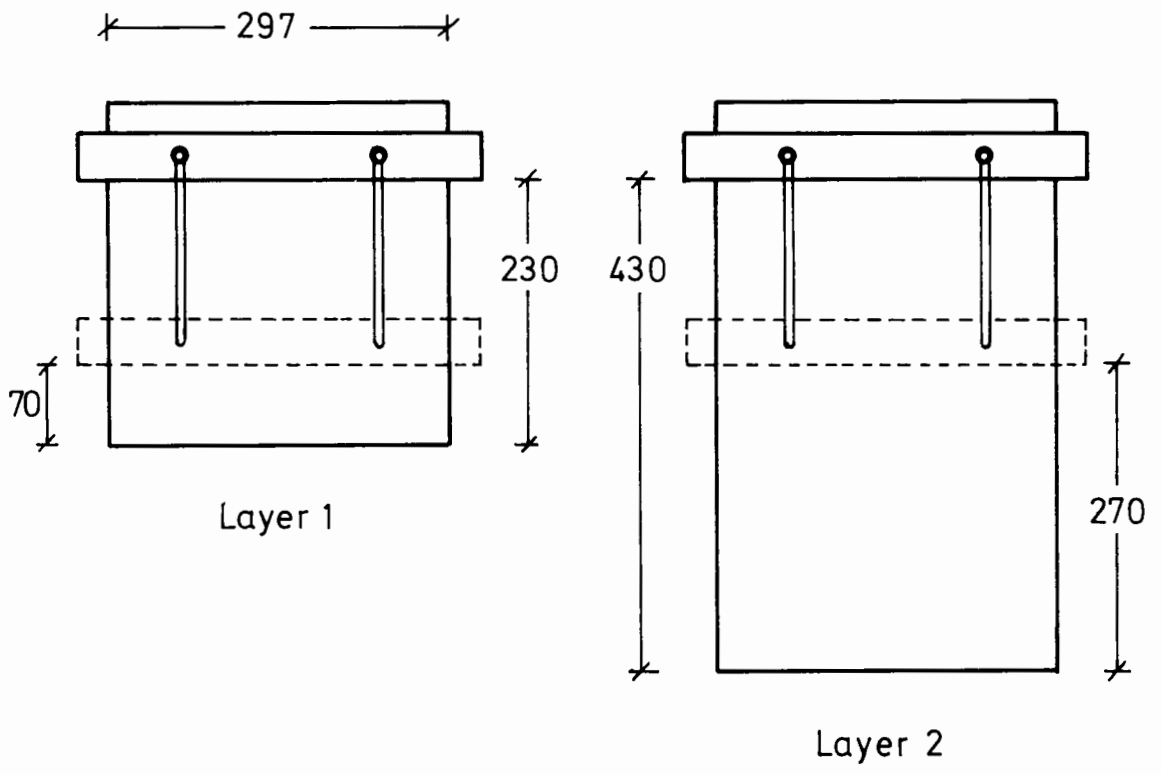

Figure 3.5 Adjustable surface levelling tools

compaction of the fill layer. In all reinforced tests the grid was smoothed out over the subgrade and made to lie flat.

Placing of the fill was carried out by hand scoop. The fill, mixed to a water content of 10% , was placed in lifts approximately 25mm thick and compacted. Compaction was carried out by first lightly tamping with a wood board (250mm by 150mm), until the layer was level; then more firmly with a 1 kg nylon hammer on the same wood board. The final lift was levelled as accurately as possible using the adjustable levelling tool described earlier (Figure 3.5). This was a time-consuming process which resulted in a surface which was level to within ±0.5mm of the mean. This was carefully surveyed with the LVDT/jockey arrangement for local variations. A photo of the front face of the box was taken with the OM1 SLR camera set up on its tripod, using a 50mm lens. This lens was then switched for a 135mm lens which gave a close up of the area to be tested.

The load cell and footing were fixed onto the central ram and the bridge bolted in place. An LVDT either side of the footing was placed to measure surface heave at the estimated maximum points. After a dry run with the data scanner, and with the limit piston ready to stop footing travel at the desired point the test was started. The simple footing was driven 50mm into the system at a constant rate of descent, approximately 2.5mm/s . Photos were taken throughout, using the power drive facility on the OM1 (Plate 3.2) . A video recording was also made of the later tests. The tests lasted typically 20 seconds, at the end of which the OM1 lens was changed back to 50mm and a comprehensive set of pictures taken from various angles.

It was possible after a test to see discrete slip lines in the clay, highlighted by the pink silicone grease. These were traced with a felt

Plate 3.2 Central test in progress (J2M)

pen onto the perspex and photographed. The fill surface was re-surveyed, and moisture content samples taken for drying. The fill was taken out and set aside for possible re-use. The grid was closely inspected, and any cutting in of the grid into the clay was measured. It was then removed and a site investigation conducted on the clay. Moisture content samples and shear vane readings were taken across the sample (Figure 3.6). The clay surface was then completely cleared of all bits of sand and gravel and relevelled, filling in the central trench, at 20mm lower than before ready for further testing.

3.2.2 First Layer - Side Tests

The next test to be conducted was a control test. This was carried out in one of the side positions, directly onto the clay. The footing and bridge assembly was secured under the ram on whichever side most closely resembled the central position in terms of clay strength, as determined from the initial shear vane readings, and the test conducted

at the same speed as before. Only footing travel and the load on the footing were recorded by the data scanner during these tests. No comprehensive set of photos were taken, nor any pore pressure measurement or surveying of the clay surface done. The 20mm difference in clay surface levels had to be taken into account when comparing central and side test results (Section 5.1.4) .

Finally, a third test could be conducted under the remaining ram, on the other side of the box. Similar conditions to the central test were usually set up in order to do a useful check on repeatibility. The proximity of the side-wall clearly influenced the test, causing an asymmetric failure mode and, in general, slightly higher bearing capacity than for the corresponding central test. If the side tests involved reinforcement, the grid was pinned at the side-wall with a special

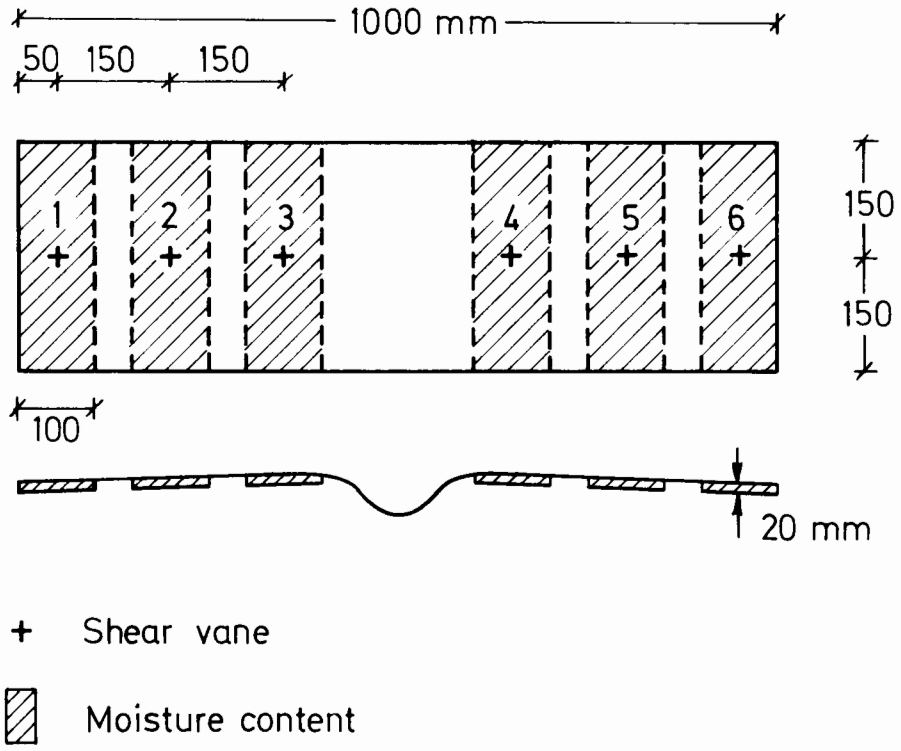

Figure 3.6 Shear Vane and Moisture Content determination sites after each central test

comb (Figure 3.7) attempting to model one half of the real two-wheel situation.

In the later samples this third side test was sacrificed in favour of doing a more complete site investigation after the central test. Triaxial samples were extracted and a set of additional shear vane readings were taken at a greater depth instead (Section 5.1.1) .

These three tests were always conducted during a single day, at the end of which the complete top half of the clay block was removed. This left a sample of height 227mm for the next stage of testing. It was considered that this bottom half of the sample, unaffected by the first day's testing, could be used for a further 3 tests (see Section 7.3.3) .

3.2.3 Second Layer

The 227mm clay block was allowed to swell, under water, for a further 2 complete days. This was in order to allow any effects from the

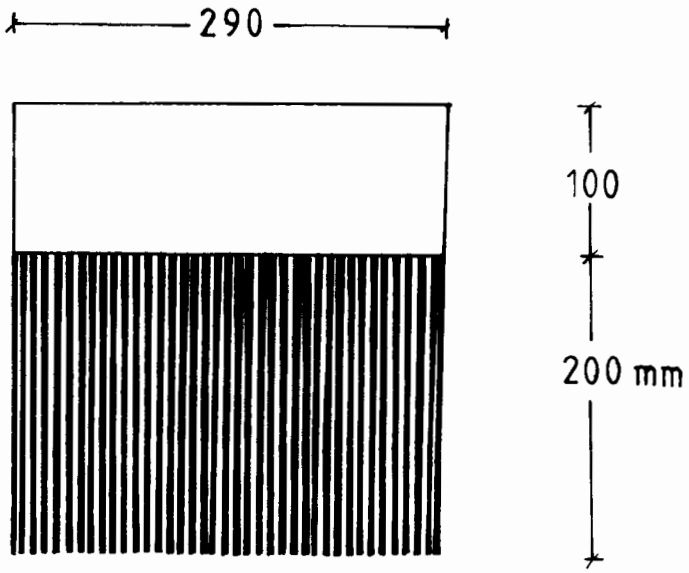

Figure 3.7 Grid restraint comb

first day's testing, and the effects of removing 180mm overburden to stabilize. Testing Day 2 was usually a direct repeat of Day 1, except that if the earlier central test had been unreinforced then this time it would be reinforced, and vice versa. Three initial shear vane readings were taken once more, and the sample trimmed to a height of 207mm to remove its very soft surface, as before.

After these final three tests had been completed the test-box was dismantled and the clay block disposed of. The perspex sheets were cleaned thoroughly, and the remains of the silicone seal removed in readiness for the next sample preparation.

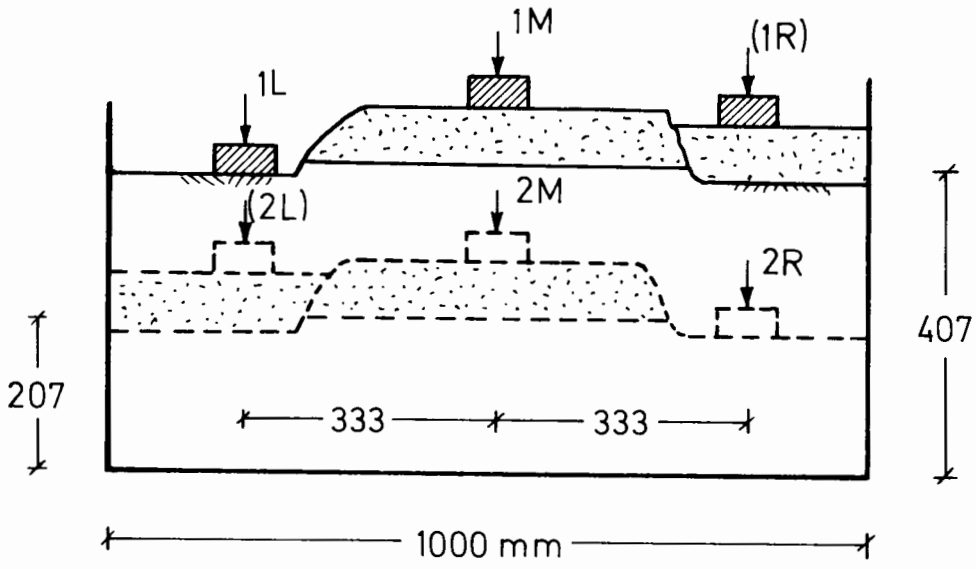

Figure 3.8 First and Second Layer test positions

3.2.4 Test References

The way in which a set of up to 6 tests could be conducted on each clay sample has just been described. Each test then had a reference as follows:

1. Clay block letter (A - Z)

2. Layer 1 or 2

3. Test position (M - middle , L - left , R - right)

Thus C1M would be the central test on the first layer of Sample C , and G2R would be the right hand test on the second layer of Sample G (Figure 3.8) . The details of each central test can be found quickly from Table 4.1 , while details of each side test can be found from Table 4.3 .

CHAPTER 4

RESULTS OF TESTS

4.1 Main Test Programme

4.1.1 Introduction

The testing programme was designed to look at geogrid inclusion in unpaved roads over a typical range of road thicknesses and subgrade strengths. A comprehensive set of 9 combinations was covered. Fill thicknesses of 50mm, 75mm and 100mm were each tested on clay subgrades of nominal undrained strength 6 , 9 and 14 kPa . For the equivalent field values, these figures should be multiplied by 4 (Chapter 2).

A separate clay sample was used for each of these 9 combinations, while on each clay sample both a test with and without the grid were performed for comparison. This was done by removing the affected area of clay and relevelling the surface for the second test, as has been described in the last Chapter. Table 4.1 shows the details of each of these main tests. Ten samples of clay, A - K , were used to cover the nine combinations with H and J providing an exercise in repeatibility. The postscript of 1 or 2 denotes whether the test was conducted on the first clay layer or the second (Section 3.2.4). Tests on Samples A - K followed an identical procedure, a complete description of which is made in Chapter 3 . Briefly, a simple footing was driven 50mm into the system at a constant rate of descent (approximately 2.5 mm/s). During the test photographs were taken of the deforming system. The load on the footing,

TABLE 4.1 DETAILS OF TESTS

		Strength of Clay (kPa)						
		6	9	14		6	9	14
Depth of Fill (mm)	50	A1M	B2M	C2M	50	A2M	B1M	C1M
	75	D1M	E2M	F1M	75	D2M	E1M	F2M
	100	G1M	H2M J2M	K1M	100	G2M	H1M J1M	K2M
		UNREINFORCED TESTS				REINFORCED TESTS		

the heave of the surrounding fill surface and pore pressure and total pressure responses were continuously scanned with respect to the footing penetration. A full description of the type of fill material and the characteristics of the model grid used in these tests can be found in Section 5.2 .

4.1.2 Load - Penetration

A summary of the Load-Penetration data for each of these main tests is presented in Figure 4.1 . The curves are equally well grouped in subgrade strengths, or according to fill thickness, as is shown in this figure . From these results clear trends emerge. Figure 4.1b shows the increase in bearing capacity and initial system stiffness, which result from increasing clay strength. Figure 4.1a shows that although the bearing capacity increases with fill thickness for a given subgrade strength it does so less rapidly than might be expected. Both figures demonstrate that the systems with a grid show a marked improvement in performance over those without by the end of the test. In the early stages of the test, after only a few mm footing penetration the grid is seen from Figure 4.1a to stiffen the initial response of the system for tests on the two stronger categories of clay,

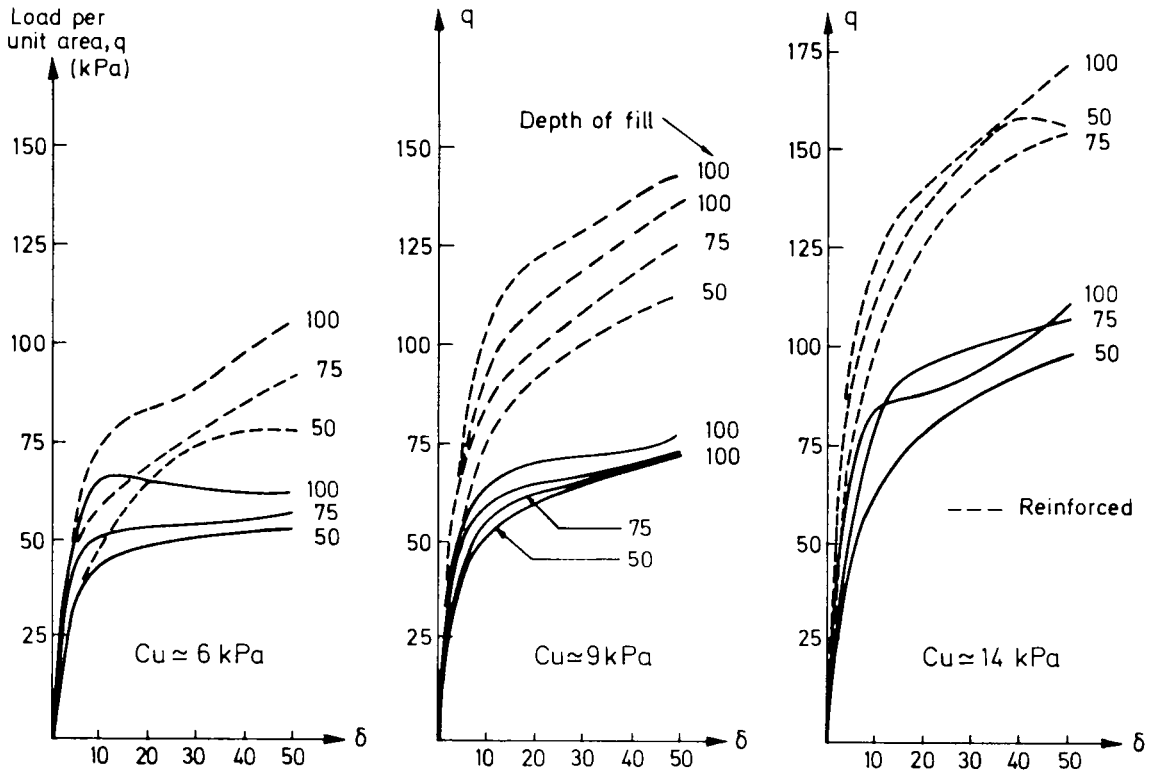

a) Grouped according to strength of clay

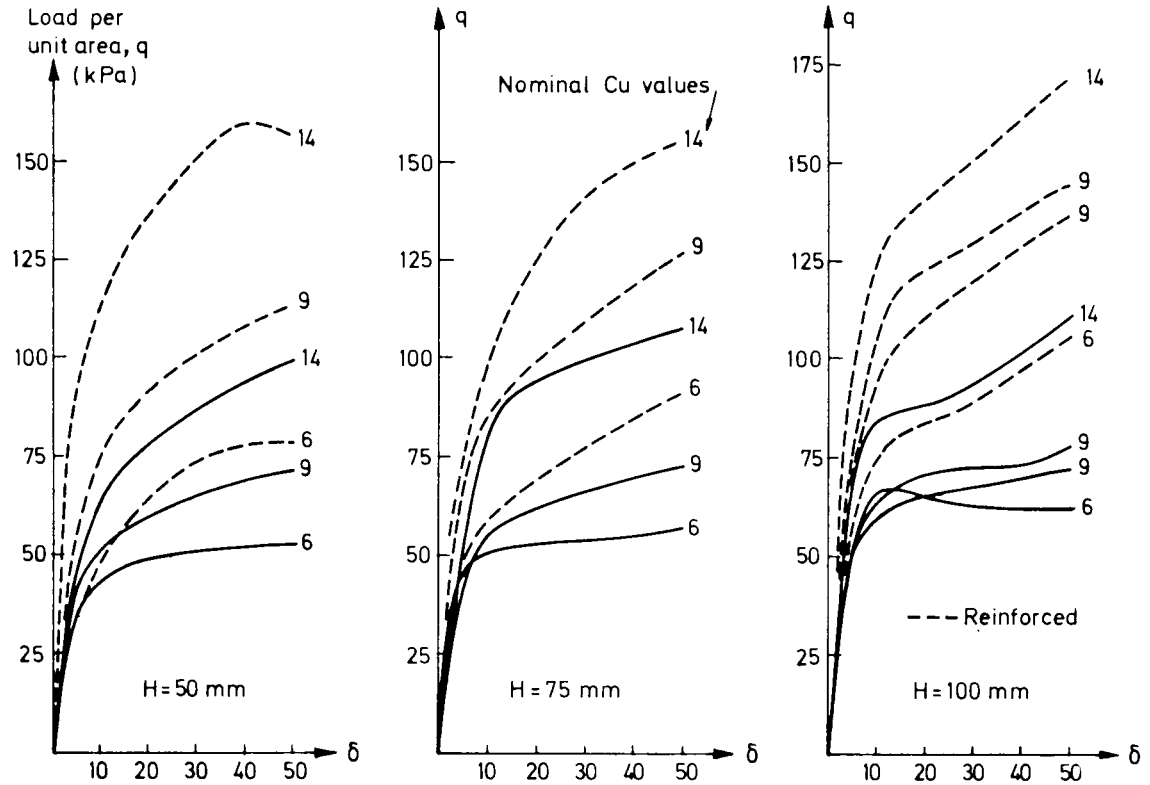

b) Grouped according to thickness of fill layer

Figure 4.1 Summary of Load-Penetration data for central tests

but not on the weakest.

The results in Figure 4.1a and b cover the main tests which were conducted centrally in the box. They should be taken in context, however, because variations in subgrade strength existed between samples of the same nominal strength to the order of ±10% , due to the following effects:

- small variations in maximum consolidation pressure
- different amounts of trimming (up to 20mm) at the end of consolidation, necessary to produce the required sample height of 407mm
- effects of tilting of the platen.

Control tests were conducted on most samples at one side of the box after the corresponding central test, in order to complement the main tests. But the last two points above also affect clay strengths locally within a particular sample. For this reason all tests, including these control tests, should be corrected for their respective subgrade strength values if they are to be compared truly with any other test. The method by which these individual values of C_u are assigned is described in Section 5.1.4 . The complete set of values appears in Table 4.2 , while confirmation of the relevance of these individual strength values, C_u , comes from a comparison between the predicted failure load of $(\pi + 2)C_u$ and what is observed in these 'subgrade-alone' control tests. The load at which displacements start to increase rapidly is approximately equal to $5C_u$ in each case (Figure 4.2).

In most earlier samples, tests were conducted on the remaining side of the box in addition, to get the most out of each clay block (Plate 4.1). These tests were useful for establishing the effect of some secondary variables such as proximity of the fixed boundary wall, and as a check on the results from the central test. Details of these extra tests can be found in Table 4.3 .

TABLE 4.2 INDIVIDUAL VALUES OF C_u FOR EACH TEST

A1M 6.0	**B1M 8.9**	**C1M 15.2**
A1R 6.6	(B1L 11.1)	C1L 17.2
A2M 5.9	**B2M 8.8**	**C2M 12.7**
A2R 6.2	B2R 9.4	C2L 13.5
	(B2L 9.4)	
D1M 5.6	**E1M 8.5**	**F1M 13.3**
(D1R 5.7)	E1R 9.6	F1R 14.4
(D1L 6.6)	**E2M 8.2**	**F2M 13.0**
D2M 5.6	E2R 8.7	F2L 13.7
D2L 6.1		
(D2R 5.9)		
G1M 5.9	**H1M 8.8**	**J1M 8.7**
G1R 5.9	H1L 10.5	J1L 10.3
(G1L 6.5)	(H1R 9.8)	**J2M 8.0**
G2M 5.8	**H2M 8.5**	J2R 9.1
G2R 5.9	H2L 9.0	
(G2L 5.5)	(H2R 8.4)	
K1M 14.8	**L1M 8.8**	**M1M 6.4**
K1R 15.7	(L1R 8.8)	M1R 6.5
(K1L 17.9)	**L2M 9.0**	**M2M 6.1**
K2M 13.5	(L2R 8.9)	M2R 6.3
K2R 14.2	(L2L 9.1)	
(K2L 14.4)		

Notes
1. Heavy type refers to tests conducted in middle of test-box
2. Unbracketed values refer to control tests conducted on the clay alone, at side of test-box
3. Brackets refer to extra tests employing a fill layer, conducted at side of test-box
4. All values in kPa

The complete set of Load-Penetration plots for the tests conducted on each sample appear in Figures 4.3 to 4.5 . Typically, when tested under identical conditions, the extra side tests showed greater load carrying capacity than the central tests, after the effect of relevelling at 20mm deeper into the subgrade had been taken into account. The effect is not so obvious, however, in reinforced tests. A possible explanation is that the proximity of the side wall serves to confine the subbase material, increasing its stiffness on that side. In the case of a reinforced test the result is less marked since the grid serves to confine the fill material in that manner anyway.

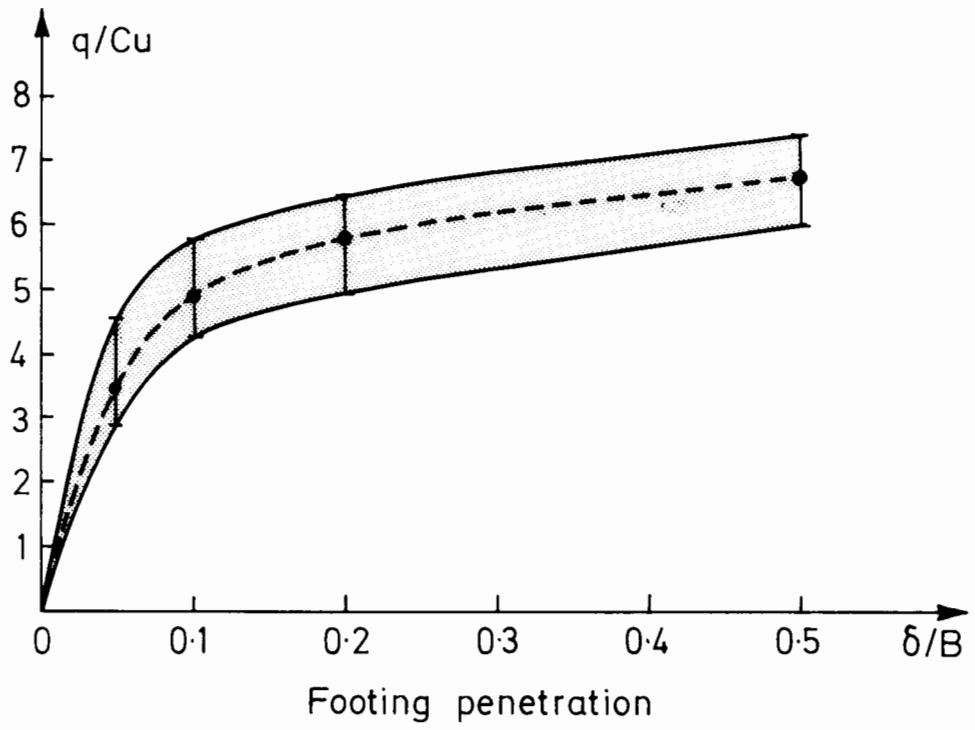

Figure 4.2 Normalised Load-Penetration data for 18 tests on clay alone

TABLE 4.3 DETAILS OF EXTRA SIDE TESTS

	Depth of Fill	Strength of clay	Notes	
B1L	50	9	Grid pinned on LHS only	
B2L	50	9	(Unreinforced)	
D1R	75	6	(Unreinforced)	CBR tests conducted - not reported here
D1L	75	6	(Unreinforced) 25mm penetration only	
D2R	-	6	Grid pinned both ends - no fill layer	
G1L	100	6	(Unreinforced)	
G2L	100	6	Grid unpinned	
H1R	100	9	Grid unpinned	
H2R	100	9	(Unreinforced)	
K1L	100	14	(Unreinforced)	
K2L	100	14	Grid unpinned	
L1R	75	9	(Unreinforced)	
L2L	75	9	(Unreinforced)	
L2R	75	9	(Unreinforced) 150mm Footing width	

Note
All other side tests were control tests conducted directly onto the surface of the clay

Plate 4.1 Test conducted at side of box

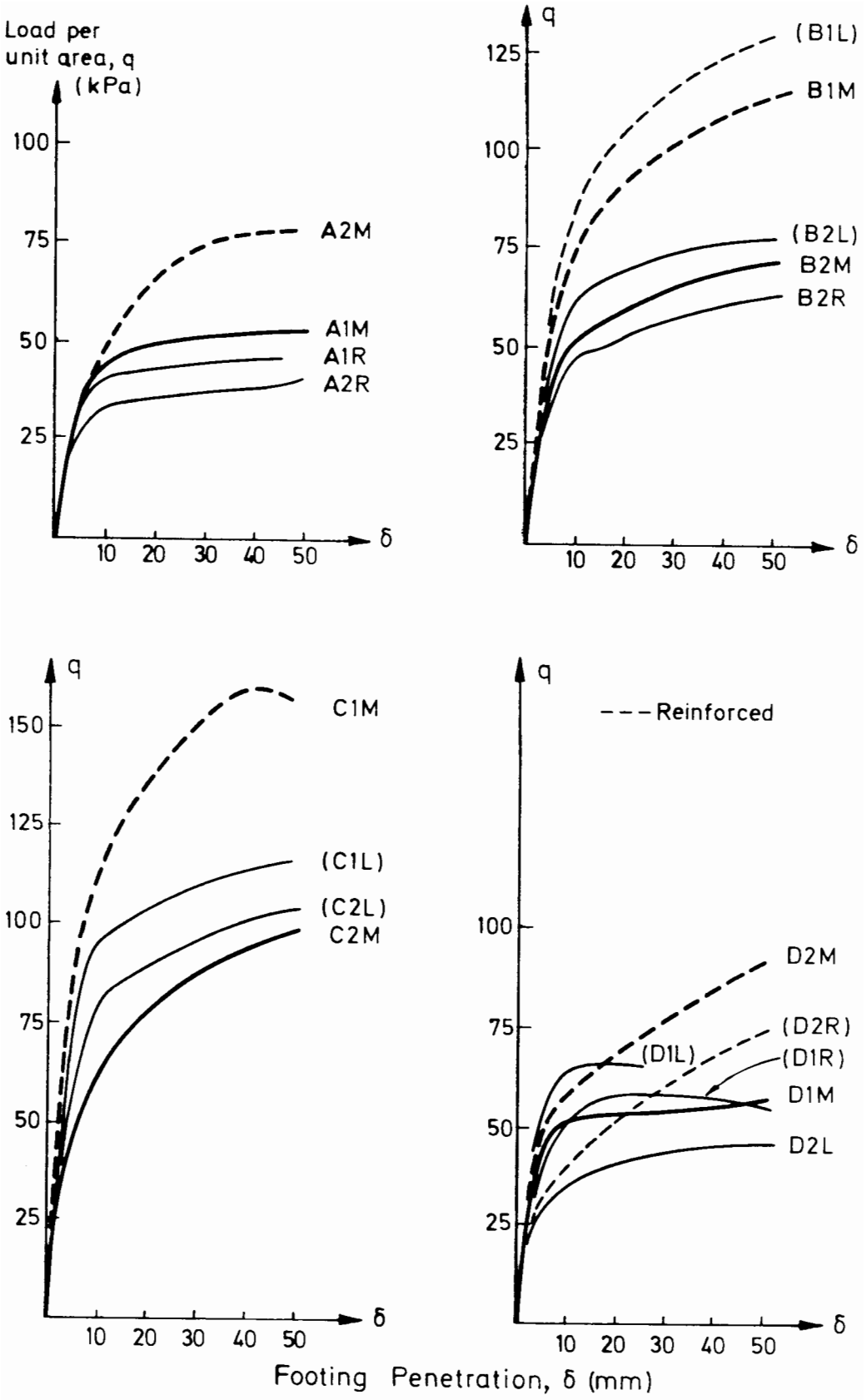

Figure 4.3 Load-Penetration data for tests on Samples A - D

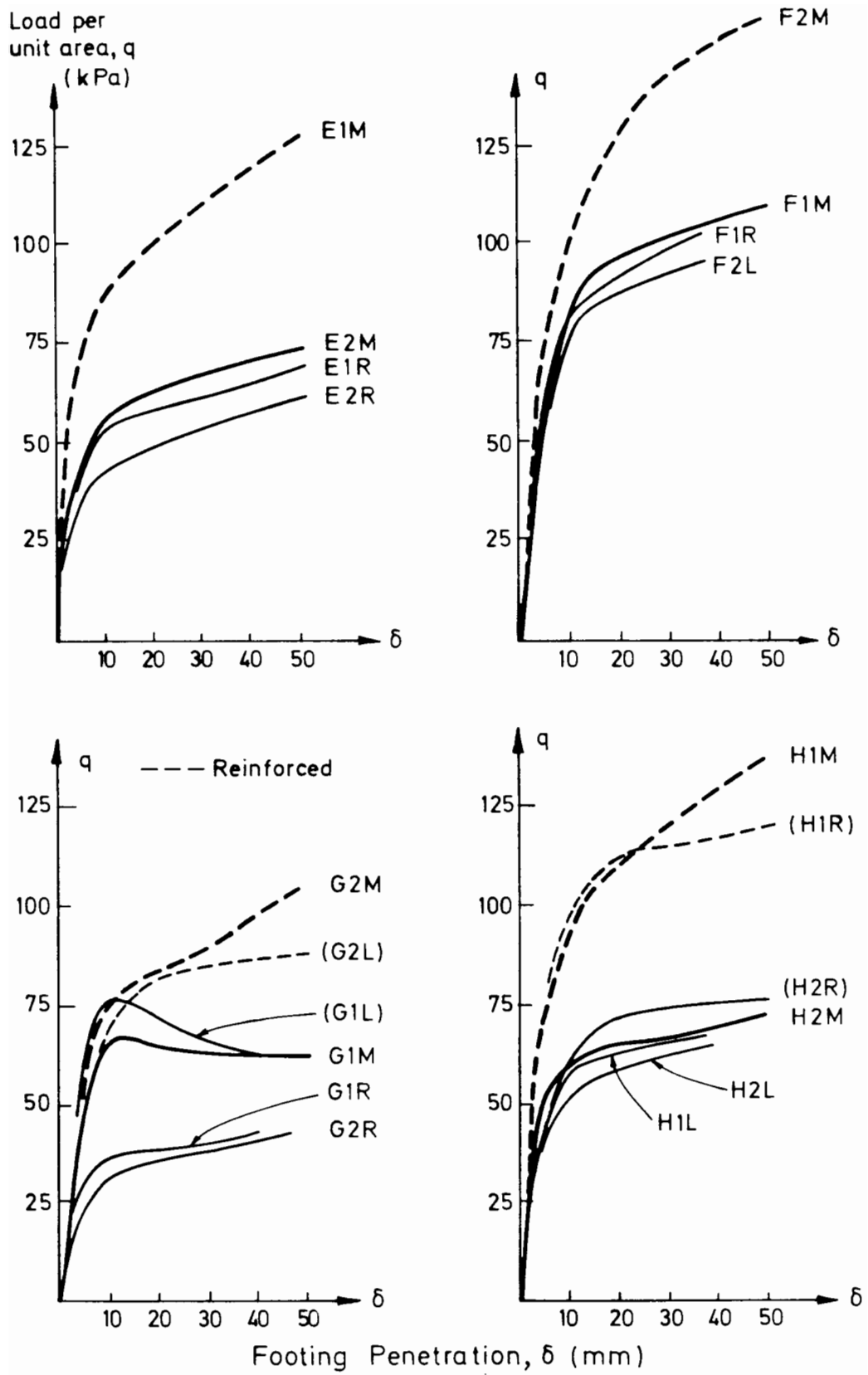

Figure 4.4 Load-Penetration data for tests on Samples E - H

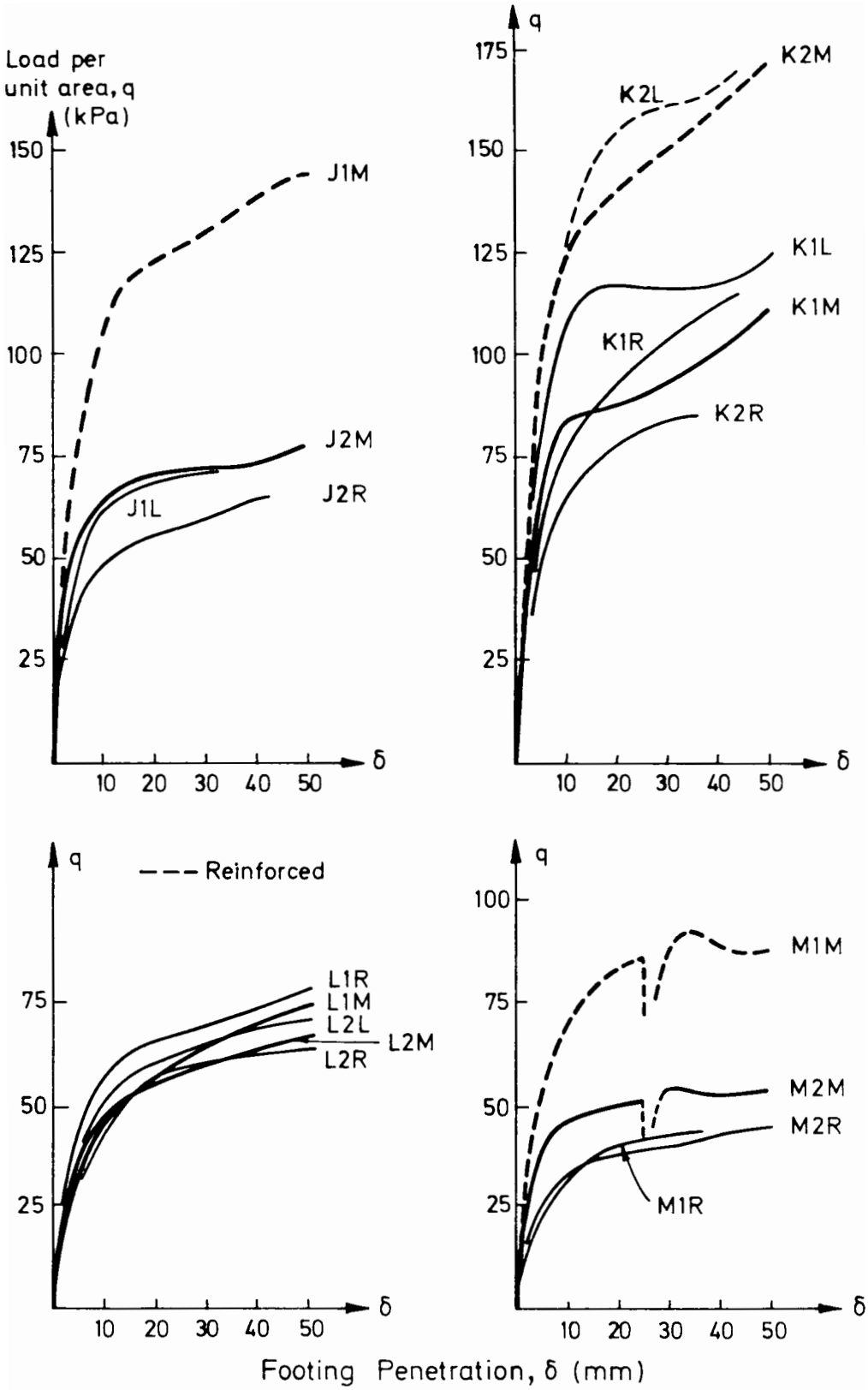

Figure 4.5 Load-Penetration data for tests on Samples J - M

4.1.3 Surface Heave

Useful information comes from the two surface heave LVDTs. These instruments record heave at a particular point on the fill surface throughout a test. They were positioned at the estimated maximum points, generally on the centreline of the box, one on either side of the footing (Plate 4.2). Typical plots of Heave, h , versus Footing Penetration, δ , are presented for both reinforced and unreinforced tests on Samples H and J (Figure 4.6). The results from these and all other tests show that:

- the development of heave is instantaneous and increases linearly with footing penetration
- the amount of heave in reinforced tests is less, the ratio of h : δ being approximately 1/4 for reinforced tests, 1/3 for unreinforced tests
- the failure mode is not always symmetrical.

In some tests, both LVDTs were mounted on the same jockey (i.e. on the same side of the footing and at the same distance from it), one measuring heave at the centre of the box, the other at the front face. The result, as shown in Figure 4.7 shows less heave at the sides of the box than in the middle, indicating a definite boundary effect. This effect is reduced in the reinforced test: a significant fact which suggests that the mechanism of failure in a reinforced test, being relatively unaffected by sidewall friction on the fill material, must therefore be more deep-seated in the clay layer where side wall friction will not be so great.

Plate 4.2 View of LVDT

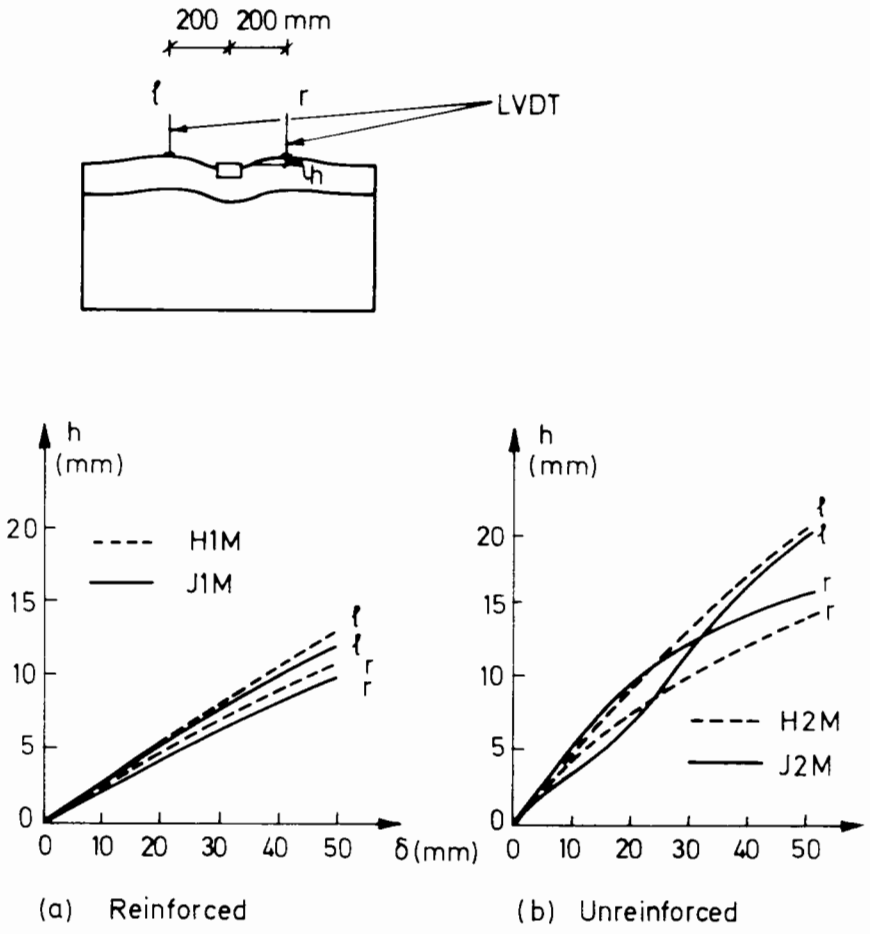

Figure 4.6 Heave versus Footing Penetration for reinforced and unreinforced tests on Samples H and J

A better picture of surface heave is obtained from a complete before-and-after survey of the fill. When photographic information is added to the before-and-after profile of the fill/clay interface together with positions of observed slip planes, the differences between reinforced and unreinforced tests become very clear. Before-and-after profiles are shown for each of the main tests in Figures 4.8 to 4.10 . The following main points emerge for a reinforced test:

- the failure planes extend more deeply into the subgrade, indicating a greater zone of deforming clay
- the trough beneath the footing is always deeper
- the surface heave profile is smooth, with material spread more thinly and over a greater distance. In comparison, the unreinforced test profile is more severe.

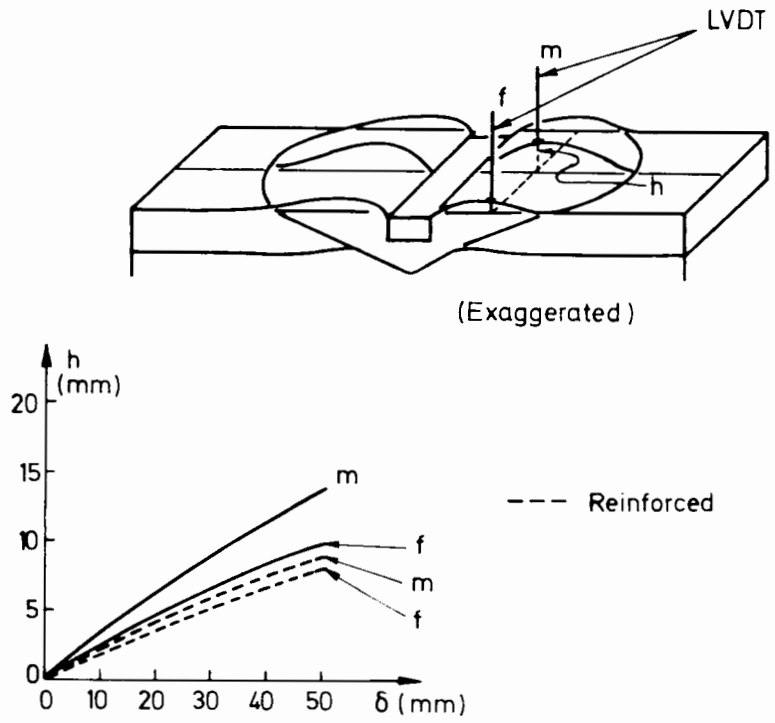

Figure 4.7 Surface Heave, h , versus Footing Penetration, δ , at middle and at front of Test-box for Sample F

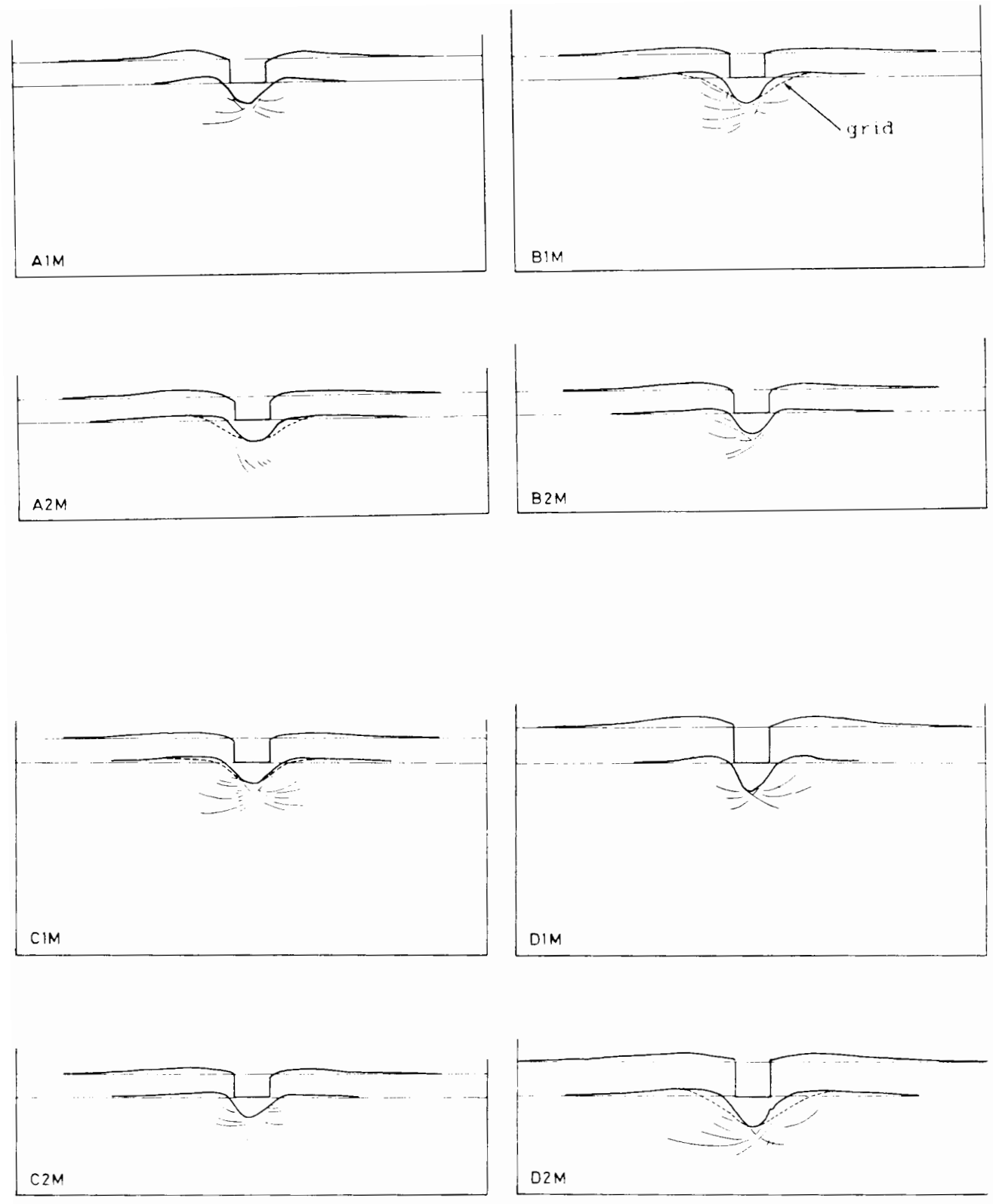

Figure 4.8 Before-and-after profiles for central tests on Samples A - D

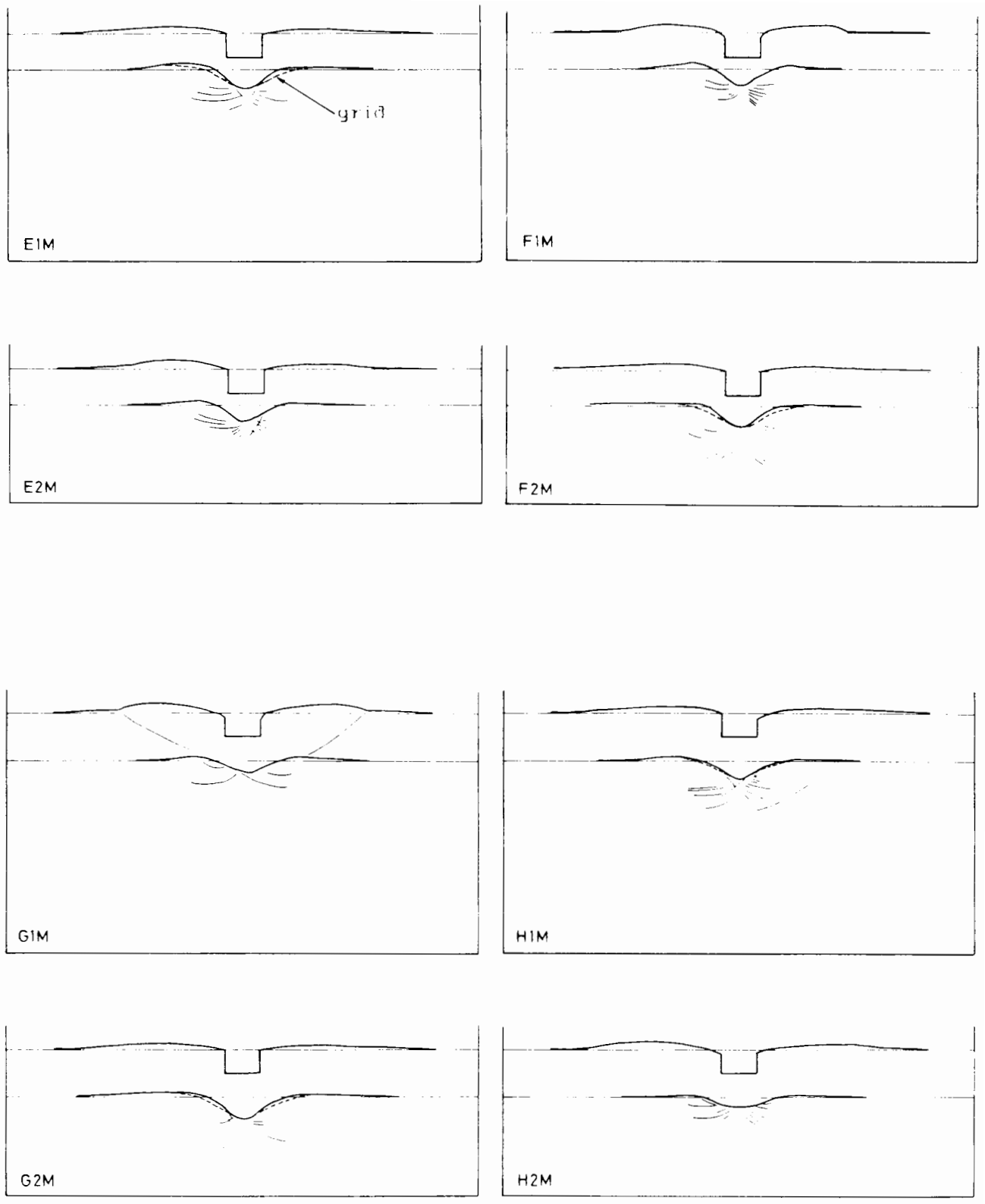

Figure 4.9 Before-and-after profiles for central tests on Samples E - H

These points are further developed in Chapter 7 , in conjunction with the evidence from photographic measurement of marker movements in the clay. But it is important to appreciate that the points above are made for systems which have been subjected to an equal amount of footing penetration. The reinforced tests show greater deformation of the subgrade, but also carry correspondingly greater footing loads as a result.

A more dramatic way of presenting the effect of grid reinforcement is to compare before-and-after profiles for reinforced and unreinforced systems subjected to the same load. Compare the profiles in Figure 7.24. The first shows a reinforced test under a footing load which has caused minimal footing penetration. The second shows the corresponding unreinforced test under the same load and at complete failure (see Section 7.3.2).

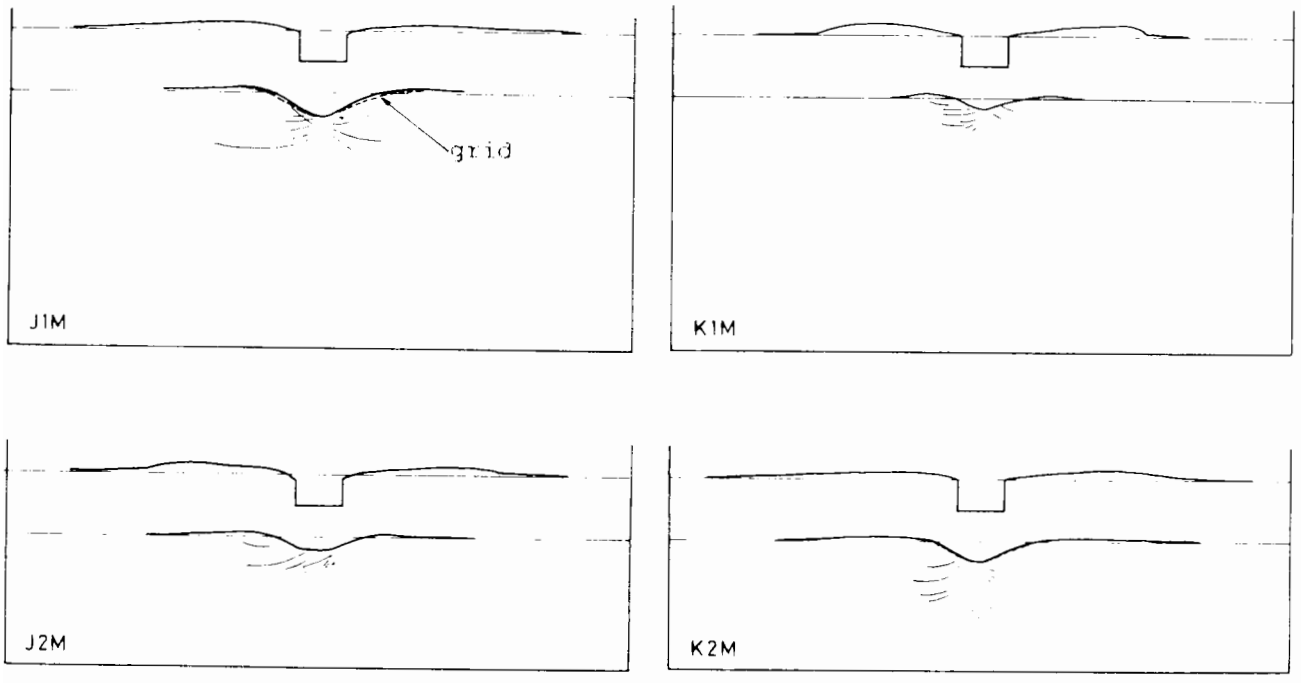

Figure 4.10 Before-and-after profiles for central tests on Samples J , K

4.1.4 Pore Pressure Transducers

Despite the great care taken over deairing, and the manufacture of elaborate ports (Figure 2.8), the read-outs obtained during tests from the pore pressure transducers (PPTs) are of limited use in determining precise failure mechanisms of the subbase-subgrade system.

Samples H and J were tested identically and in most respects performed remarkably similarly (Section 4.1.6 below). The PPT responses are shown in Figure 4.11 . Although similar trends are seen, on the whole repeatibility is bad, throwing doubt on the usefulness of this data. This having been said, it is perhaps asking too much of the transducers to do any more than to give information about general performance in qualitative terms. It was decided to insert the transducers horizontally, flush with the inside face of the box right at the start of consolidation, after several unsatisfactory attempts were made at inserting the transducers into the clay body nearer the testing date. It is therefore possible that smearing of the stones with side-wall grease may have caused the transducer response to have slowed up by the time tests were conducted, and by different amounts for each sample. Local arching effects across the transducer face itself, and shear stresses developed by the stone/clay friction, may have had significant effects. The PPT read-outs for all tests, for which data is available are shown grouped in Figures 4.12 and 4.13 . The following points regarding these figures should be noted:

1. In each test three PPT responses were taken - one approximately on the centreline of the footing, and two others, one on either side, at a distance of 167mm from the footing (Figure 4.14).

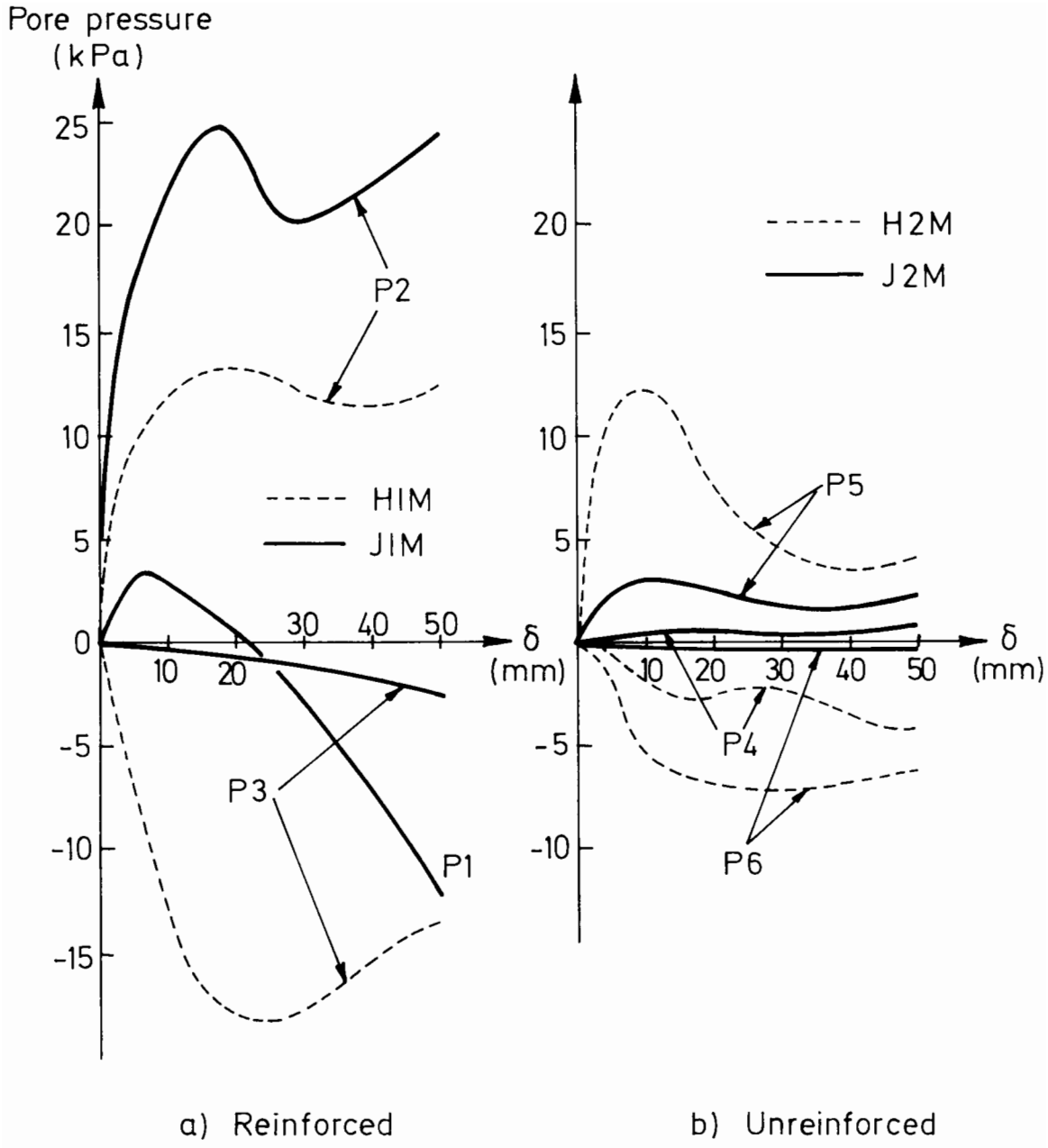

Figure 4.11 Pore Pressure response versus Footing Penetration for reinforced and unreinforced tests on Samples H and J (Transducer positions in Figure 4.14)

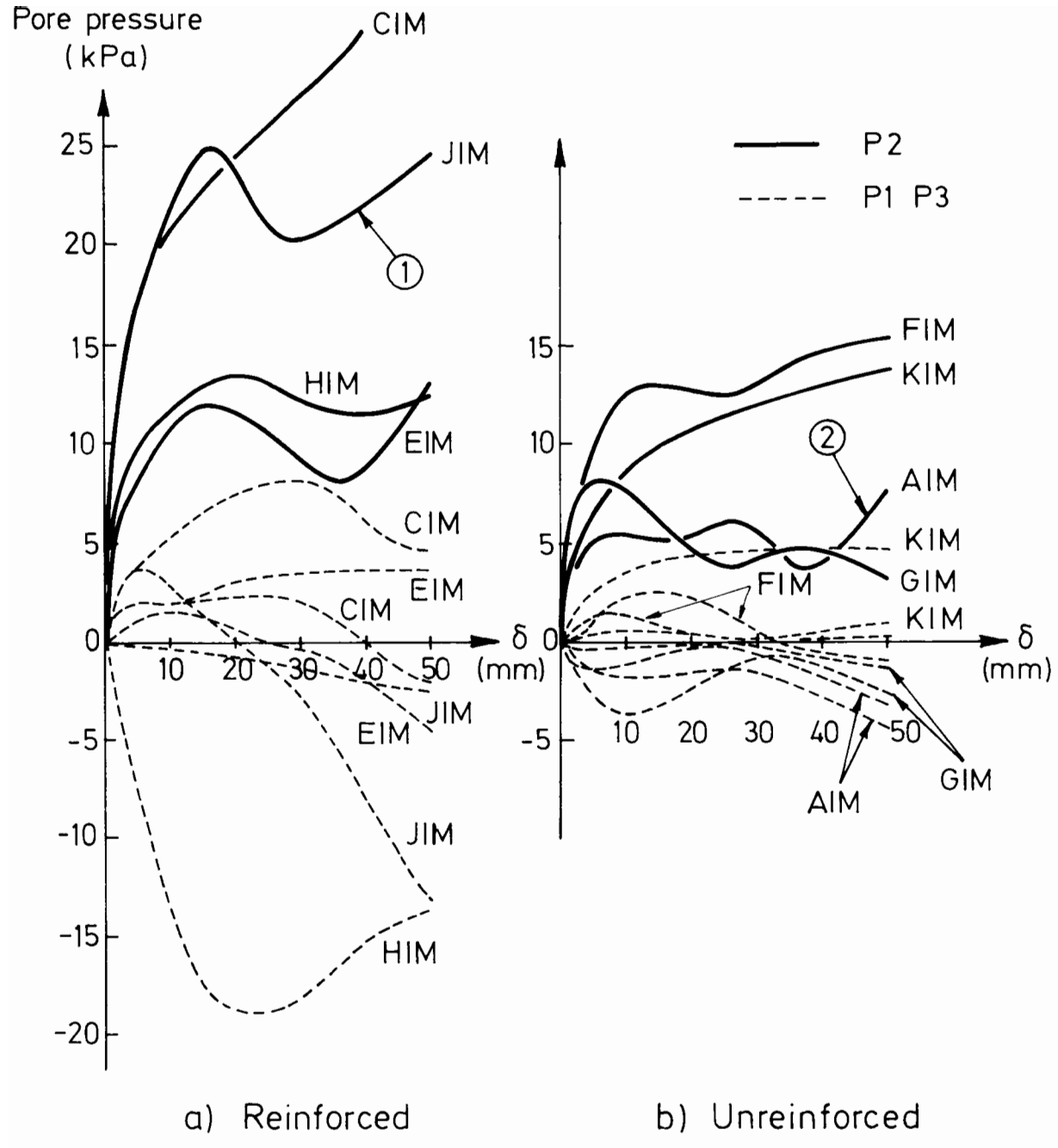

Figure 4.12 Pore Pressure response versus Footing Penetration for reinforced and unreinforced tests on Layer 1 (Transducer positions in Figure 4.14)

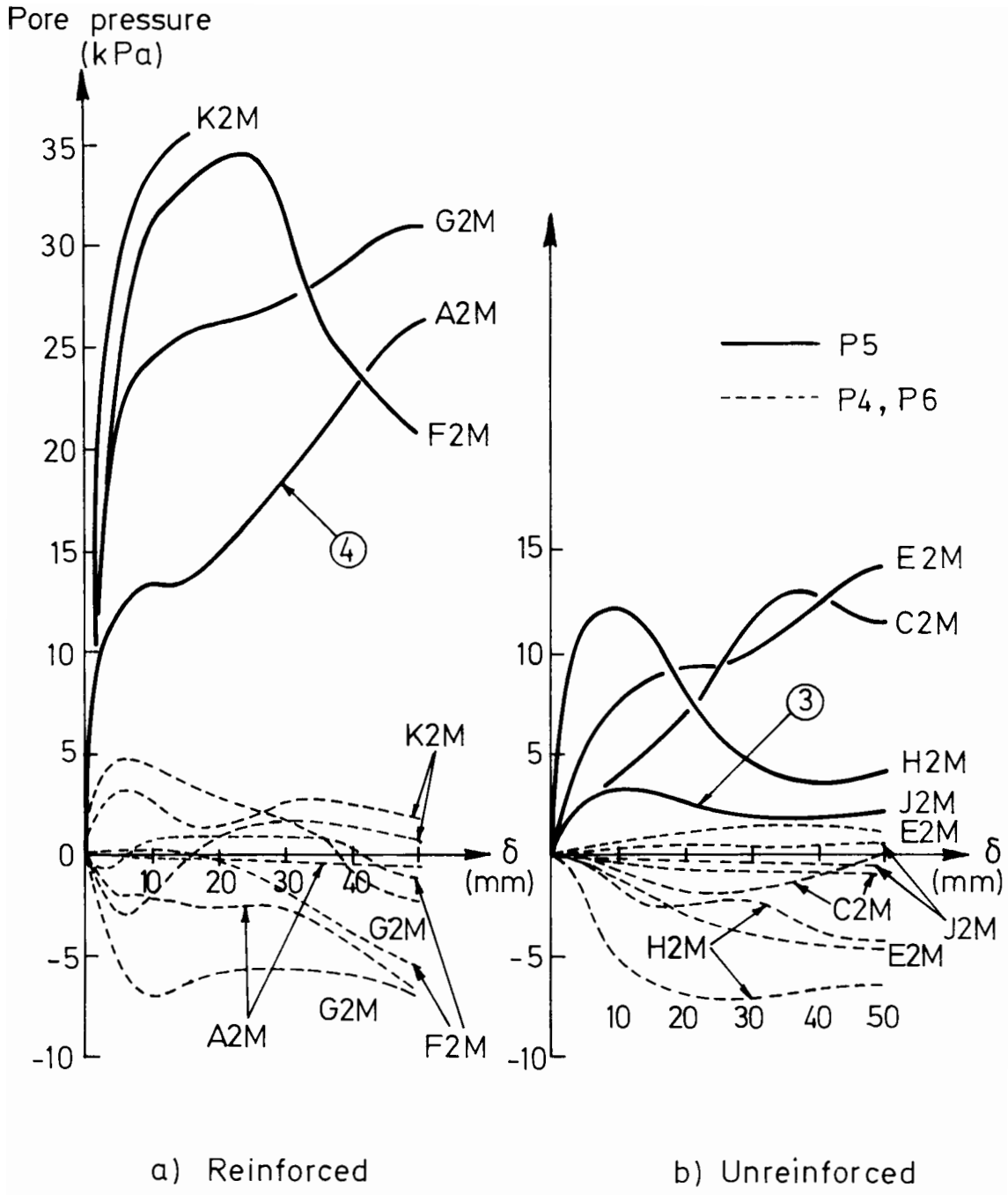

Figure 4.13 Pore Pressure response versus Footing Penetration for reinforced and unreinforced tests on Layer 2

(Transducer positions in Figure 4.14)

2. In Layer 1 tests, the transducers are at a depth of 75mm in the clay, while in Layer 2 tests the depth is only 38mm. This was due to restrictions imposed by the metal side frame.

The consequence of the second note above is that a direct comparison between the reinforced and unreinforced tests on a particular sample cannot be made. However, of the ten tests performed on Layer 1, five were reinforced (B,C,E,H,J) and five unreinforced (A,D,F,G,K), the same being true for Layer 2. Turning to Figure 4.12 all the responses for tests conducted on Layer 1 will be seen separated into reinforced tests and unreinforced tests. Two trends are apparent:

- in all tests the response of the transducer in the middle, P2 , is greater than for those at the side, P1 and P3 , the latter sometimes going negative

- the magnitude of transducer responses is generally greater in tests which include a grid.

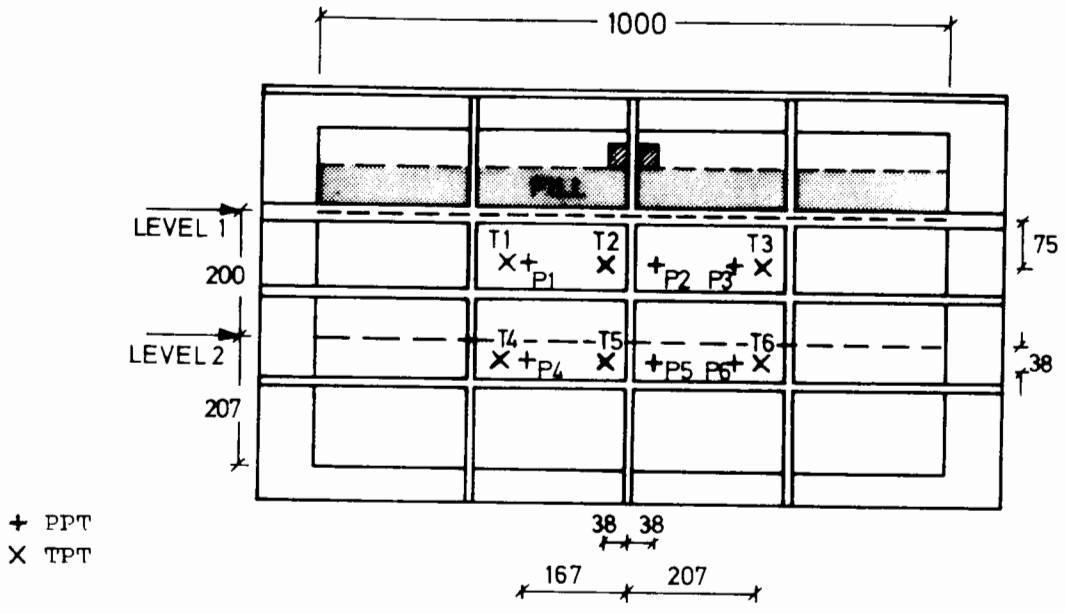

Figure 4.14 Positions of Pore Pressure and Total Pressure Transducers on back face of Test-box

The first result is as expected, except for the negative pore water pressures. The second result is not conclusive evidence on its own that the higher PPT responses for a given footing penetration are directly attributable to the presence of the grid, since different test conditions applied to the reinforced and unreinforced tests. For instance the fact that curve (1) shows a greater response than curve (2) may simply be due to the fact that curve (1) corresponds to a test conducted on a thicker fill layer and stronger clay than curve (2). On studying Figure 4.13 , however, confirmation of the result comes from the fact that the reinforced tests still show the greater pore pressure response despite test conditions being reversed. For instance curve (4) now shows a greater response than curve (3). This result of higher pore pressure responses being developed during the reinforced tests is one that might be expected, for the reason that greater loads are being dealt with generally. If the PPT responses are normalised with respect to footing load, the sets of responses for reinforced and unreinforced tests become relatively indistinguishable. Again, in both Figures 4.12 and 4.13 , the stronger clays and thicker fills would generally appear to cause greater pore pressure responses, although this is not always the case.

The occasional occurrence of negative PPT responses is in keeping with an overconsolidated clay subjected to large shear stresses. But the TPT responses (Figures 4.16 and 4.17) are also seen on occasion to go negative. This behaviour is therefore more likely to be due to the ports at some distance from the centreline of loading being affected by deflection of the perspex wall itself.

The PPTs were used to more satisfactory effect during the consolidation process. The decay of excess pore pressures after each increment was a useful check on the rate at which load could be

increased/decreased, and as indication as to if and when equilibrium had been reached. Typical responses are shown in the consolidation summaries of Figures 3.1 to 3.3 . It is noted that in the case of the strongest clay sample (Figure 3.3) a complete dissipation of pore pressures was not seen to occur over the 4 days after the final increment. This was a consistent result with each of the strongest clay samples for which pore pressures were monitored, seemingly indicating that equilibrium was not completely reached before the unloading stage. Plotted in Figure 4.15 is the Log(Time) Settlement curve for this final increment which suggests conversely that equilibrium was reached. Whether equilibrium was reached at this stage or not is of no serious consequence, however, but could perhaps account for the relatively high level of specific volume, v , seen in the strongest clay samples at the end of consolidation in Figure 5.15 . It is only important that a consistent preparation method was maintained for all samples during the test programme. It is also noted that the instantaneous increase or decrease in pore pressures at each increment or decrement was seen to match well the changes in magnitude of vertical pressure applied, indicating that there was little friction loss in the rams or around the platen.

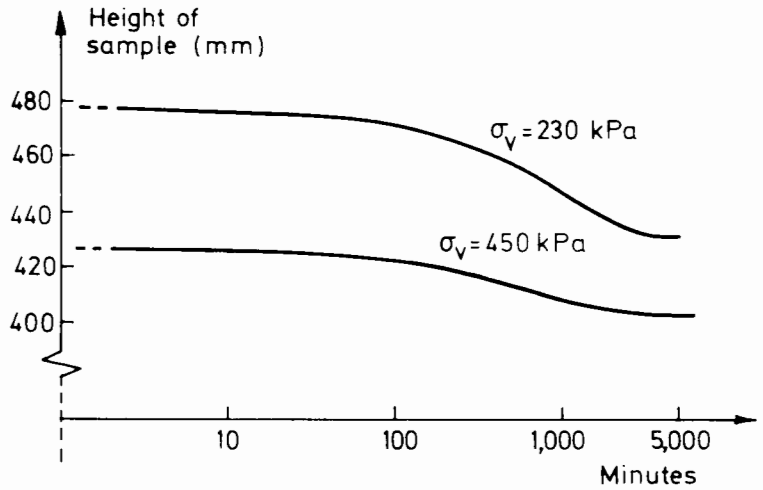

Figure 4.15 Log(Time)-Settlement curves for last two increments during consolidation of Sample F

4.1.5 Total Pressure Transducers

The total pressure transducers (TPTs) were also mounted horizontally into the back face of the box in specially manufactured ports (Figure 2.8 and 4.14), and were useful for monitoring the progress of consolidation. In conjunction with the PPT readings, the TPT read-outs enabled calculations to be made of K_o, the ratio of horizontal to vertical effective stress.

TPTs do not suffer from the same drawbacks as PPTs : they have no stone that can get clogged with grease, and there is no deairing problem. During tests it was hoped therefore that a less scattered, more consistent set of results could be expected. The complete set of TPT data is presented in Figures 4.16 and 4.17 in a similar manner to that for the PPT data. Again, transducers are at a depth of 75mm in the clay for Layer 1 tests, and at 38mm for Layer 2 (Figure 4.14). In each test two TPTs were used. For the earlier samples both transducers were put at 207mm either side of the footing centreline (T1, T3); for later samples one of the transducers was moved to a new port position, approximately on the centreline of the footing (T2). As in the PPT response, the response of the central TPT is much greater than out to the side. Disappointingly, scatter would seem to be much the same as for the PPTs . In contrast to the result for pore pressure shown in Figures 4.12 and 4.13 , however, both Figures 4.16 and 4.17 appear to indicate that the presence of a grid has no discernible effect on the total pressure response.

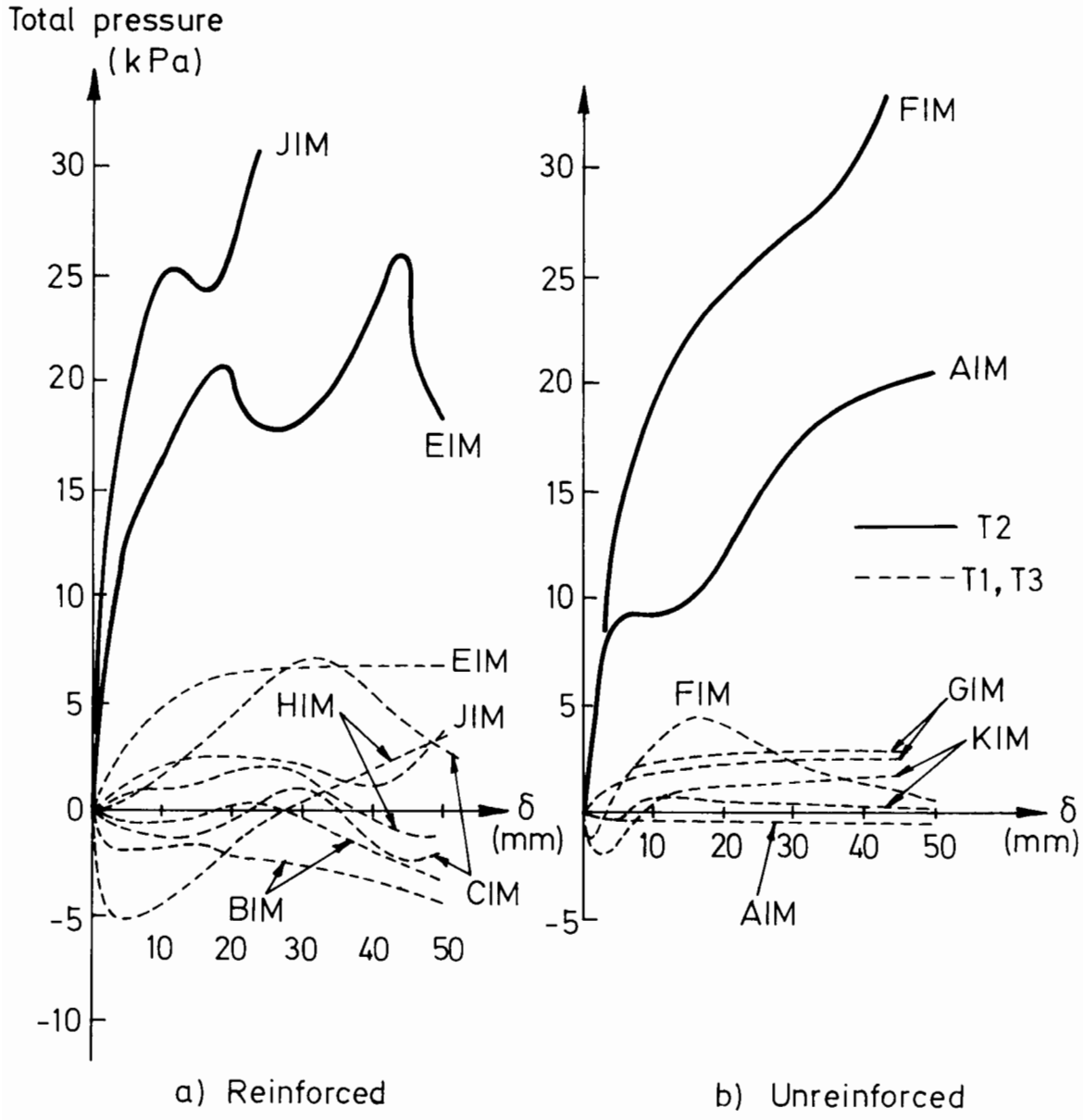

Figure 4.16 Total Pressure response versus Footing Penetration for reinforced and unreinforced tests on Layer 1

(Transducer positions in Figure 4.14)

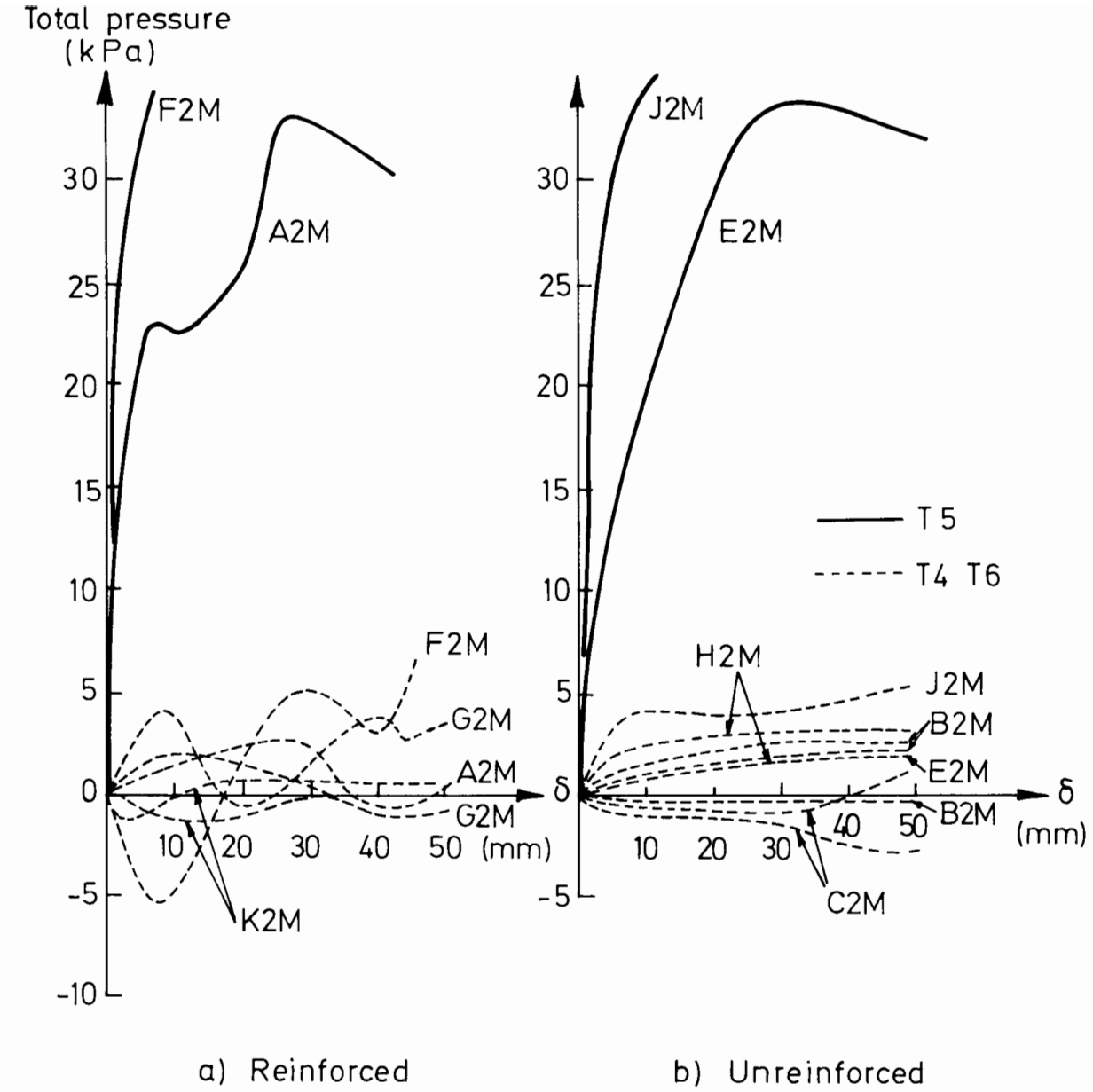

Figure 4.17 Total Pressure response versus Footing Penetration for reinforced and unreinforced tests on Layer 2

(Transducer positions in Figure 4.14)

4.1.6 Repeatibility

Repeatibility is a major concern in this type of testing. If a series of tests is conducted in which the effect of a changing parameter is being studied, it is imperative to establish the amount of agreement that is obtainable between results of two tests for which the parameter was not varied. It is easy to attribute apparent trends in data to the variables being changed, and draw involved conclusions from the result, when very often the observed variations in test results are smaller in magnitude than the accuracy of experimental repeatibility. For this reason two supposedly identical samples H and J were tested as similarly as possible, in order to ascertain the repeatibility of the testing procedure. In fact, for Sample J the third test on each Layer was not conducted, in favour of a more complete site investigation. But this is irrelevant since it is the central tests which are being compared and, to a lesser extent, the subgrade-alone plots only. The Load - Penetration plots for tests on each sample may be compared from Figures 4.4 and 4.5 , and the before-and-after system profiles can be compared from Figures 4.9 and 4.10 . In the case of the former, it is fortunate that the independent strength values as tabulated in Table 4.2 for the central tests on each sample are similar enough to be able to make true comparisons between Figures 4.4 and 4.5 possible without need of adjustment. But it is unfortunate that the fill types used in both sets of tests were slightly different (Section 5.2.1) due to the original supply-quarry having to close down, and a new one having to be used instead. As a result, the values of dry unit weight obtained in the fill layer after compaction with the new material were slightly higher than before (see Table 4.4). This increase in dry density is of the order of 4% and helps account for the higher load carrying capacity of tests on

TABLE 4.4 DRY UNIT WEIGHT, γ_D , OF FILL MATERIAL

Sample	Reinforced	Unreinforced
C	17.2	–
E	17.2	17.1
J	17.9	17.7
F	17.7	17.8

(Values in kNm^{-3})

Sample J over Sample H . In passing, it can be noted from Table 4.4 that the presence of a grid does not measurably affect the dry unit weight of the fill layer for a given compactive effort.

The difference between tests H1M , J1M and H2M, J2M in terms of load at a given footing penetration is of the order of ±4% from a common mean. If this can be taken as a representative error it can account for anomalies such as the apparent contradiction in test results for F1M and K1M : both tests are conducted on a clay of similar strength, but test F1M on 75mm of fill shows a higher bearing capacity than K1M on 100mm . The result was made even stranger when the independent strength values for each test of 13.3 and 14.8 respectively were taken into account. The apparent anomaly in the results of tests C1M and F2M , on the other hand (see 50mm and 75mm curves for a reinforced test on C_u = 14kPa , Figure 4.1a), can be explained by the difference in the individual clay strength values 15.2 and 13.0 respectively. It should be noted that Figures 4.1a and b are somewhat misleading, since the curves do not incorporate the effect of individual clay strength values for each test, and have not been normalised. This is carried out in Chapter 6 .

The before-and-after test profiles for tests on Samples H and J in Figures 4.9 and 4.10 compare extremely well. Even the shear planes look

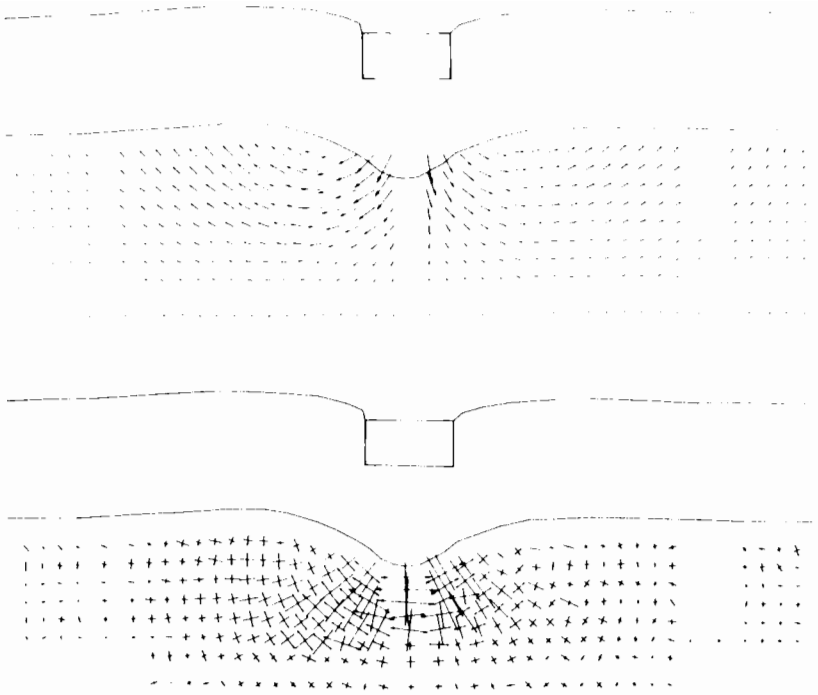

a) H1M (Reinforced test)

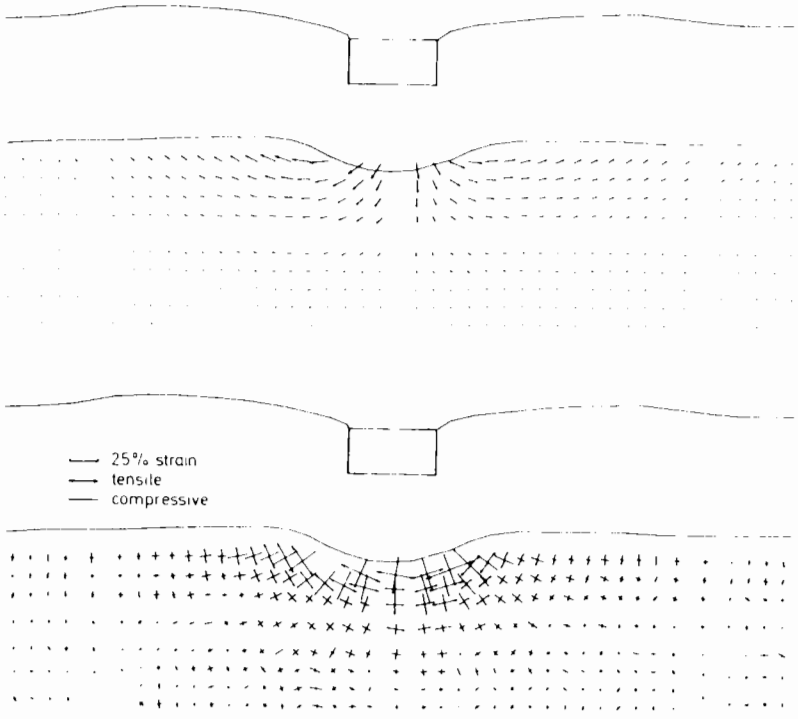

b) H2M (Unreinforced test)

Figure 4.18 Displacement Vector and Strain plots corresponding to 50mm Footing Penetration for tests on Sample H

75mm footings working in tandem. Additionally an earlier set of five clay samples were tested which served to develop testing techniques before the main series above. These earlier tests were conducted using a 40mm width footing onto relatively loose, saturated fill, and before a satisfactory method had been developed for marking the front face of the clay. Pore pressure transducers were embedded into the clay from the surface, rather from ports at the side (Total pressure transducers were not used). Table 4.5 gives a brief summary of the tests that were performed. This early work is not mentioned again.

TABLE 4.5 BRIEF SUMMARY OF AN EARLY SET OF TESTS PERFORMED ON SAMPLES a b c d and e

CENTRAL TESTS

	Strength of Clay (kPa)							
	Unreinforced tests				Reinforced tests			
		6	9	14		6	9	14
Depth of Fill (mm)	50	–	c1M c2M	e1M	50	a1M	–	e2M
	75	–	–	–	75	–	–	–
	100	–	d1M d2M	–	100	–	–	–
	125	–	b1M b2M	–	125	–	–	–

SIDE TESTS

Clay alone	Other side tests	
a1R	a1L a2M a2L	Pinned grid with no overlying fill layer – three rates of penetration
	b1R b1L b2R b2L	125mm Fill layer (Unreinforced)
c1R c2R	c1L c2L	100mm Fill layer (Unreinforced)
	d1R d1L d2R d2L	100mm Fill layer (Unreinforced)
e1R e2R	e1L	50mm Fill layer (Unreinforced)

The chronology of these samples is important to appreciate in that it will explain apparent non-sequiturs, arising from the lettering sequence of samples, since the chronological order is not alphabetical. For example, the triaxial test results from Sample Y are very poor compared to those of Sample X . This is partly explained by the fact that Sample X came 12 months after Sample Y in the programme. Again, Sample G has a full complement of six tests conducted on it, while by Sample A enough confidence had been gained to sacrifice two side tests, one on each layer, in favour of a more complete site investigation (Chapter 5). The chronology of samples was as follows:

a b c d e Y L D B G K H C E J F A X Z M

These twenty samples took 20 months to complete, a steady rate of one sample per month.

4.2 **Subsidiary Test Programme**

4.2.1 Double-Width Footing and a Preliminary Check on Modelling Assumptions

Sample L was a relatively early sample to be tested, coming before the main test programme just described. As such, several items of test procedure differed significantly to that adopted in the run of tests that followed. Therefore caution should be taken in comparing performance between Samples L and E , both of which have the same nominal clay strength and same thickness of fill in tests. The main difference lay in the method of compaction: fill layers on Sample L were compacted less well.

The interest in Sample L lies in the comparison between tests L1M and L2M . The former employed the usual 75mm wide footing, while the latter employed a 150mm footing. The tests were directly comparable in set-up, neither using grid reinforcement. As is seen from Figure 4.5 the loads per unit area on each footing for a given footing penetration are remarkably similar, although towards the end of the test the larger footing starts losing ground to the smaller footing. The relative proximity of the boundaries of the box may have influenced the test with the larger footing. Depending on the coefficient of friction between the sides and base of the box with the clay, the boundaries may have provided weak sliding surfaces, or have provided extra confining action on the system. Whichever is the case it will be assumed for the moment that the effect is small and conclude that a double width footing will carry approximately the same load per unit area as the normal size footing for the same conditions. In fact this is an over-simplistic assumption: the result will depend on the relative strength of the clay and fill, and the ratio of footing width to fill thickness, as will be demonstrated in Chapter 6 . But a preliminary assumption of this kind can enable one to perform a useful check at this stage on the relevance of the modelling theories put forward in Chapter 2 .

The analysis of dimensionless groups in Chapter 2 predicts that a system such as that shown in Figure 4.19a would correctly model that in Figure 4.19b . By reducing the system geometry of Figure 4.19b and the strength of its subgrade by a factor of 2 as in Figure 4.19a , the load per unit area in Figure 4.19a , for a given footing penetration δ/H , should also reduce by the same factor. Putting to good use the simple assumption from the paragraph above, systems in Figures 4.19b and 4.19c carry approximately equivalent loads per unit area for the same value of

δ/H . The system in Figure 4.19c would therefore be expected to also carry roughly twice the load per unit area of the system in Figure 4.19a, for a given value of δ/H . This can be compared with what was observed.

In Figure 4.20 test A1M represents the situation in Figure 4.19a of H = 50mm , C_u = 6.0 (see Table 4.2), and tests J2M and K1M lie either side of Figure 4.19c with H = 100mm and C_u = 8.0 and 14.8 respectively. Footing penetration, δ is normalised with respect to fill thickness, H . The thick line drawn between the results of tests J2M and K1M is an interpolation for the actual conditions that are needed for Figure 4.19c of H = 100mm and C_u = 12.0 , and against this is compared twice the load

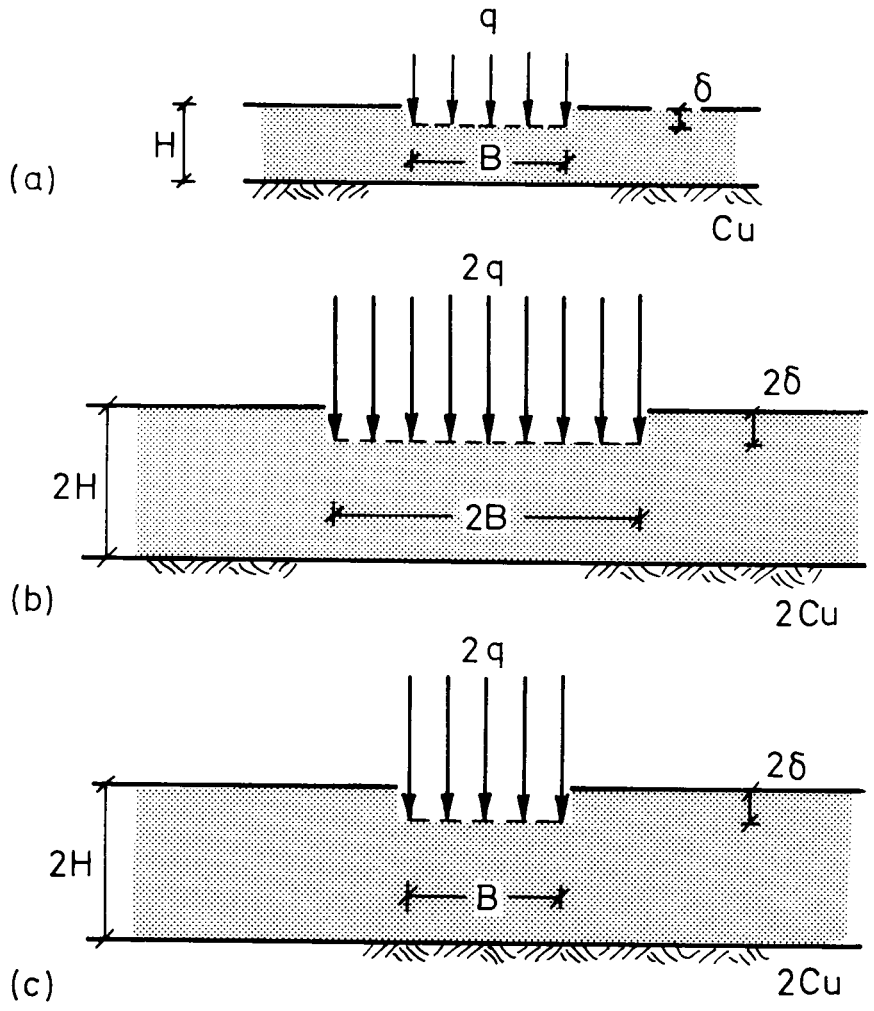

Figure 4.19 Three types of system demonstrating scale effect

per unit area observed for test A1M (broken line). Although there is a discrepancy, the two can be seen to match up reasonably well, lending confidence to the modelling approach of Chapter 2 .

The discrepancy results from the fact that the assumption made between Figures 4.19b and c is over-simplistic, taking no account of the ratio $c_u/\gamma_1 B$ in tests A1M and L2M , as will be examined in Chapter 6 .

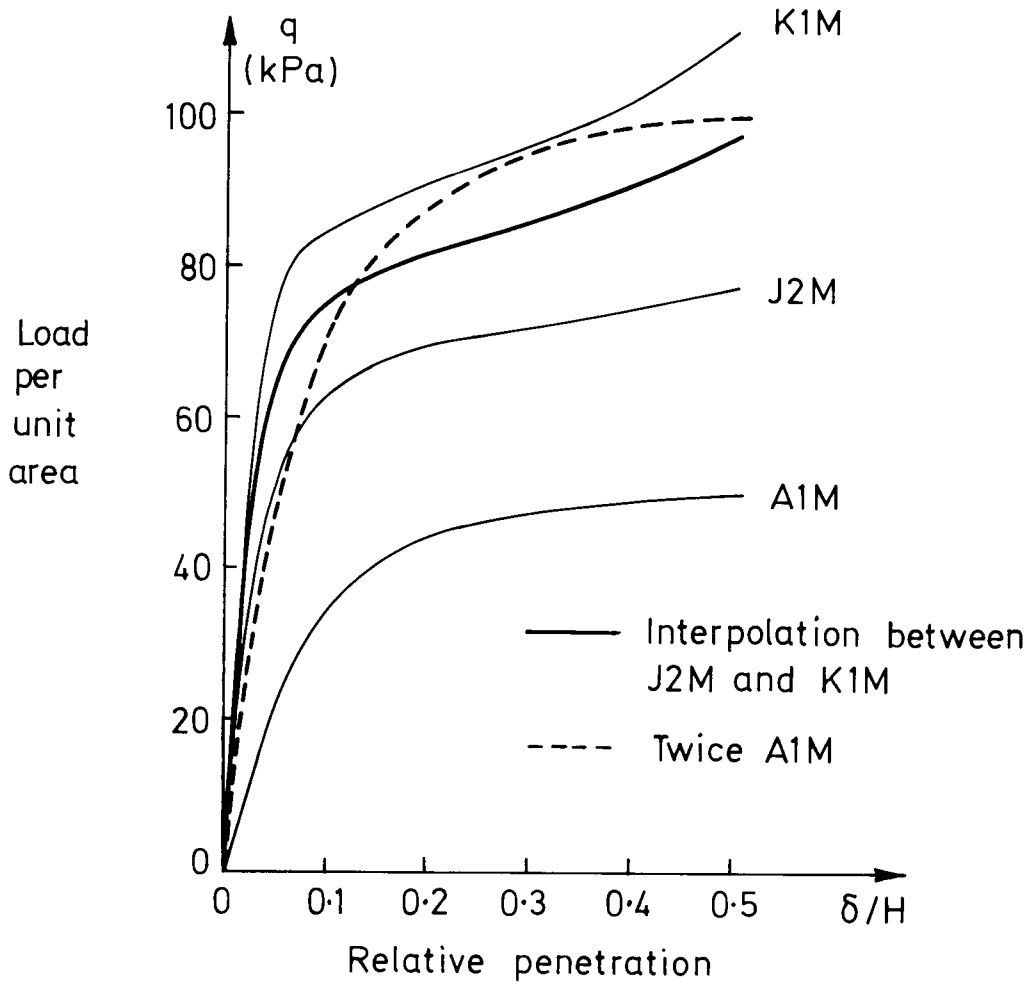

Figure 4.20 Crude check on modelling theories

4.2.2 Dual Footing

All tests so far described have consisted of loading with a single footing since it was felt that the complex behaviour of real traffic loading was initially best modelled in its most simple form. Constant rate of descent, plane strain, monotonic tests under a single footing were considered a good starting point. Once this has been fully explored, further complexity can be added in stages by further researchers.

In Sample M , the last sample to be tested in this project, a preliminary investigation of dual footing loads was made. The double footing consisted of two 75mm footings fixed at 250mm centres, as shown in Figure 4.21 , and tests were otherwise conducted in the normal way (Plate 4.3). Sample M was nominally C_u = 6 kPa , M1M and M2M being reinforced and unreinforced tests respectively on 50mm of compacted fill. Tests on Sample M were direct double-footing equivalents of the single footing tests conducted on Sample A .

In the case of the unreinforced tests, M2M showed an almost identical load carrying capacity per footing to A1M (Figure 4.22). In contrast, for the reinforced tests, M1M showed a greater carrying capacity per footing than A2M , indicating that during double footing tests the grid has more of a beneficial effect than in a single footing test.

Direct comparisons of the before-and-after test profiles for the unreinforced tests M2M and A1M and those for the reinforced tests M1M and A2M (Figures 4.23 and 4.8) raise an important point. By simply superposing two profiles of test A1M displaced by 250mm a very accurate representation for the situation in test M2M can be obtained, as is shown

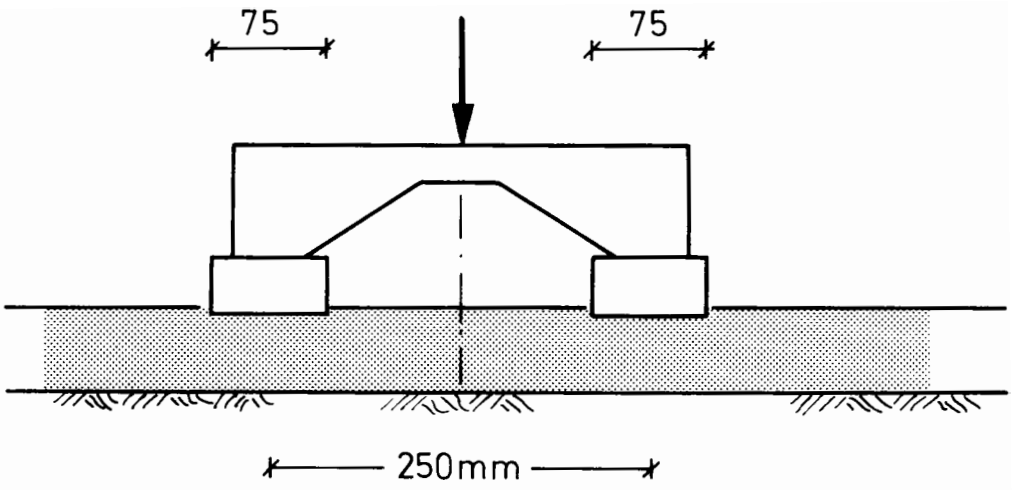

Figure 4.21 Dual Footing

Plate 4.3 Dual Footing test

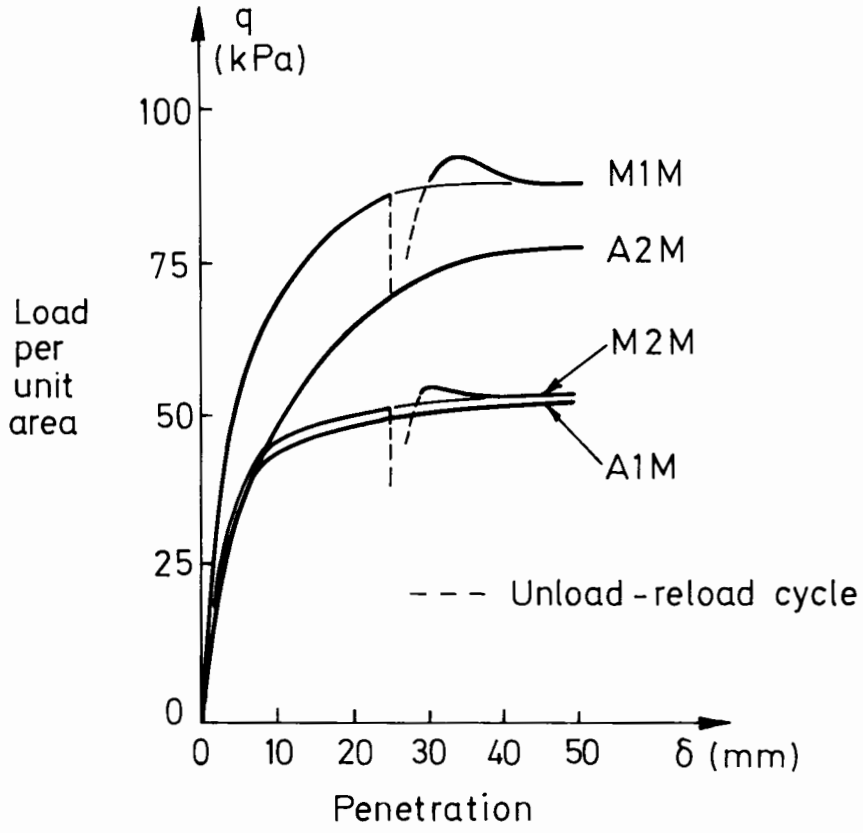

Figure 4.22 Comparison of Load-Penetration curves between tests with single and dual footings (Samples A and M)

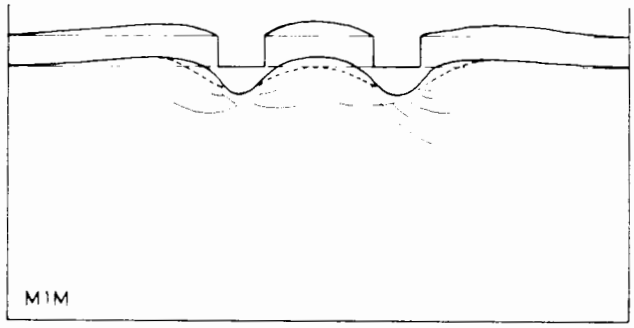

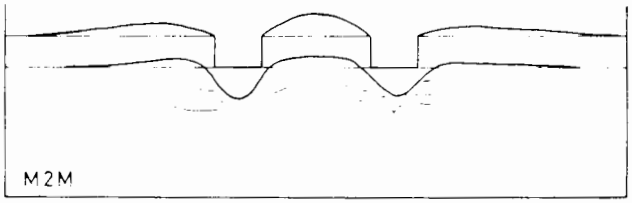

Figure 4.23 Before-and-after profiles for central tests with dual footing for 50mm Footing Penetration (Sample M)

in Figure 4.24a . On the other hand, a similar exercise in superposition using the result from test A2M gives a much less accurate prediction for what happens in test M1M (Figure 4.24b). In the latter case, heave is seen to be less than expected in the area between footings, but greater out to either side. The marker displacement plots for each of these tests are shown in Figure 4.25 (the lines of missing markers representing those obscured from the camera by the metal side frame). A similar result can be produced from these plots. If the clay displacements for two single footings at the appropriate distance apart are vectorially summed for the area between the footings, reasonable agreement is seen for the unreinforced double footing test (Figure 4.25a). Conducting this exercise for the reinforced case (Figure 4.25b) yields less good results, predicting larger displacements between the footings than actually occur. It seems therefore that while the simple unreinforced single footing test can be used to estimate satisfactorily loads and deformations for the unreinforced dual-footing test for this particular footing spacing, the reinforced dual-footing test cannot be 'built' from two single reinforced tests.

The grid serves to restrict severely the upward flow of material between footings, confining heave in the middle section but causing extra heave out to the sides. In these model tests, the grid also cuts quite deeply into the clay in the area between footings, which must reduce its confining action. Quantifying the effect of the grid cutting into the clay is very difficult to do. If it could have been prevented, by perhaps using an underlying layer of fabric (surface vegetation would have a similar effect in the field), still less heave may have resulted between the footings and may even have caused a net downward movement of clay in this area. This being the case, the presence of the grid would

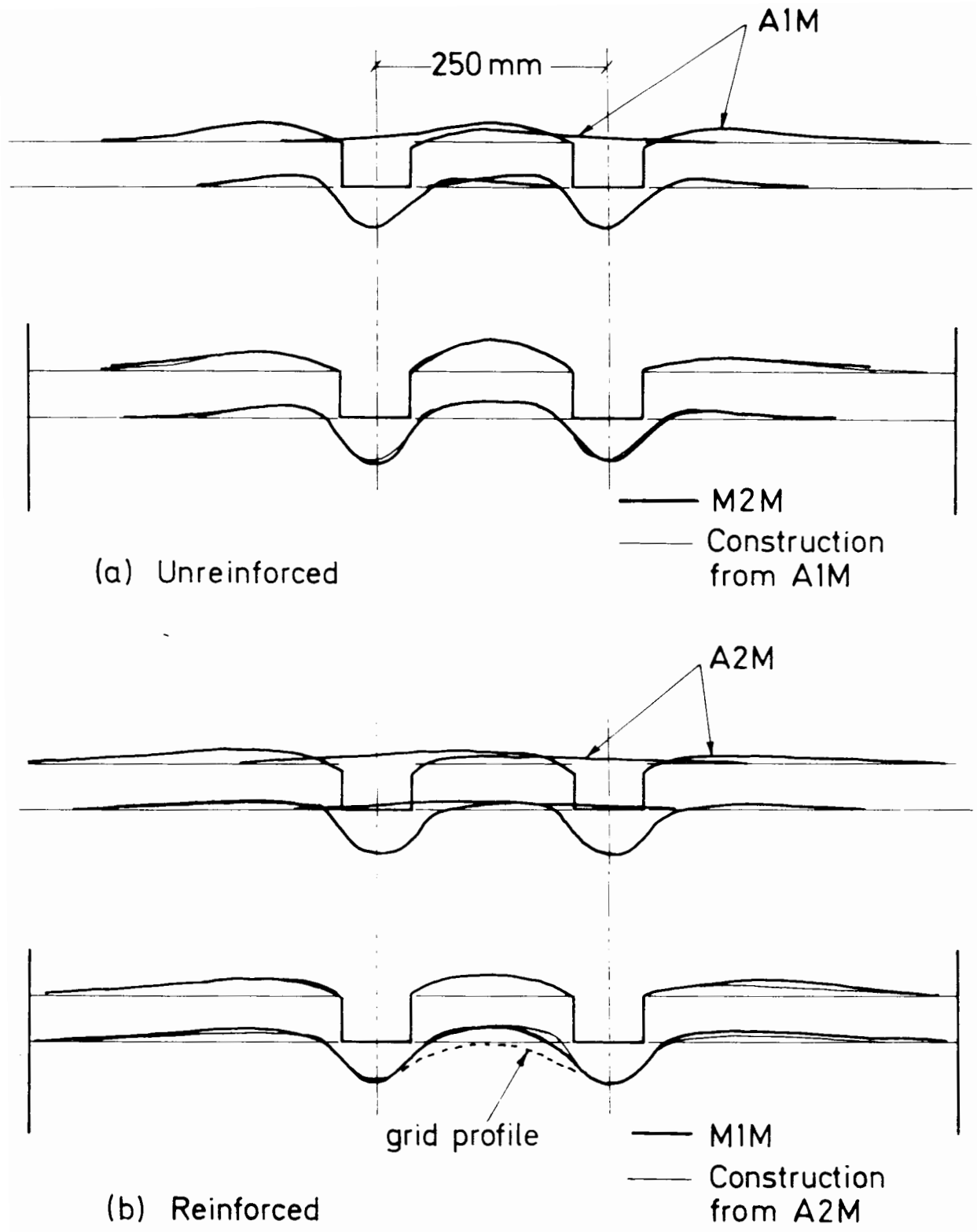

Figure 4.24 Exercise in superposition

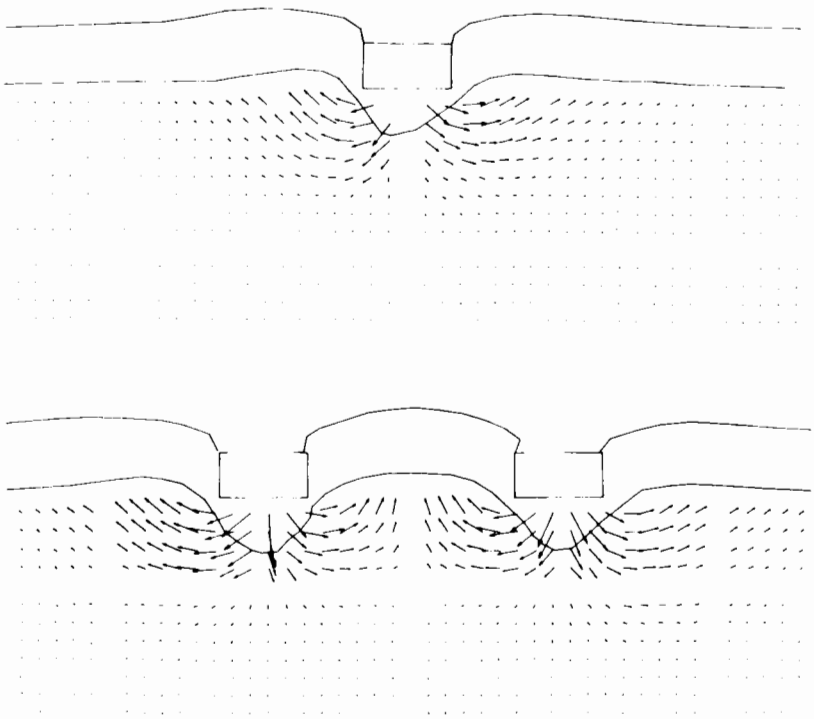

a) Unreinforced test

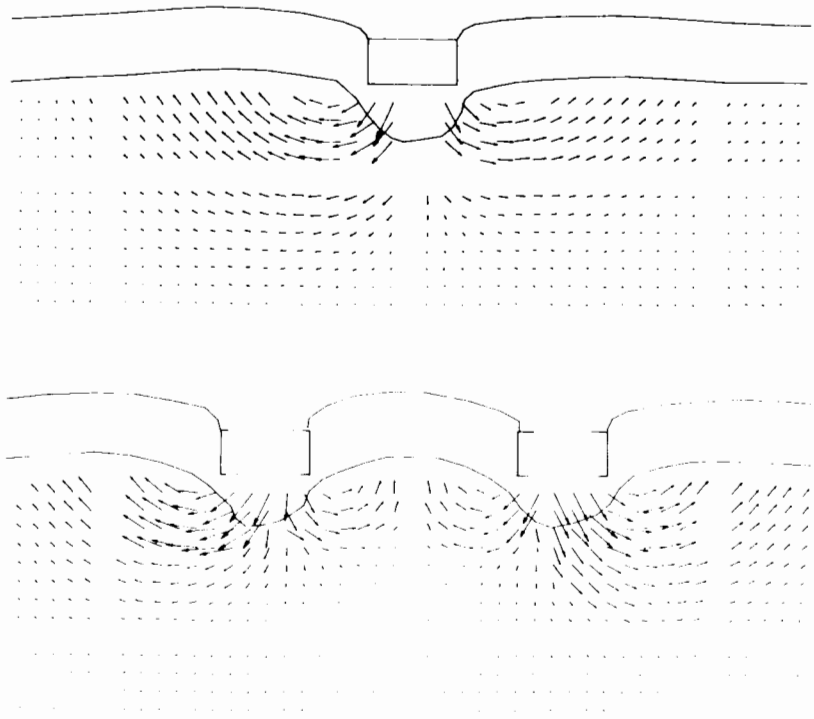

b) Reinforced test

Figure 4.25 Displacement Vector plots corresponding to 50mm Footing Penetration for single and dual footing tests

effectively make the two footings act almost as one, covering the area between them. But whether significant slippage would also then occur at the grid interface, off-setting this effect, is another matter and would clearly depend on the footing width-to-spacing ratio and depth of fill. The depth to which deformations penetrate into the clay is not much more than was observed for the single footing case, going against the concept of an effectively very wide footing, but again this may be attributable to the cutting in of the grid.

The dual-footing tests of Sample M having so far been discussed with a scale factor of 4 in mind in order to make direct comparisons with the tests on Sample A , can alternatively be considered at a scale factor of 8 . The distance of 250mm between footings, being the maximum that could be reasonably accommodated in the test box without significant edge effects, has a full scale equivalent of two single wheels, 150mm wide, 1 metre apart, if a scale factor of 4 is used. If the test is analysed in view of a scale factor of 8 the full scale equivalent becomes a more accurate representation of the typical plant vehicle, with two 150mm wheels either end of a 2 metre axle. The 50mm fill depth corresponds to a road thickness of 400mm, and the clay strength of 6kPa corresponds to a road subgrade strength of approximately 48kPa . Figures 4.23 and 4.25 , however, now correspond to field rut depths of more than 400mm which is clearly excessive: with this alternative way of viewing test results in mind from the start, both tests M1M and M2M were stopped briefly after only 25mm penetration to allow surfaces to be completely surveyed and shear planes in the clay to be recorded, before continuing to the full 50mm penetration. This data is plotted up in Figures 4.26 and 4.27, and applies therefore to a rut depth of just over 200mm if a scale factor of 8 is used.

a) Reinforced

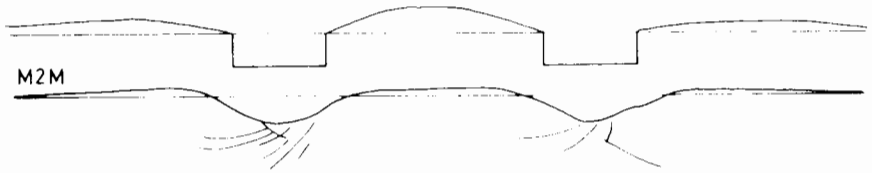

b) Unreinforced

Figure 4.26 Before-and-after profiles for central tests with dual footing after 25mm Footing Penetration (Sample M)

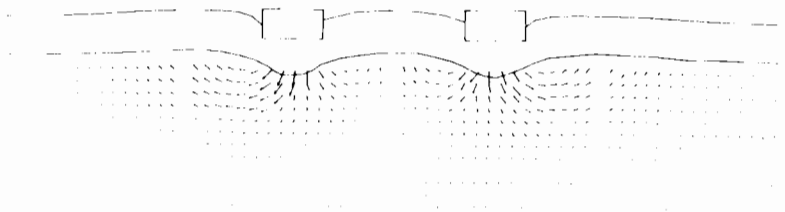

a) Reinforced

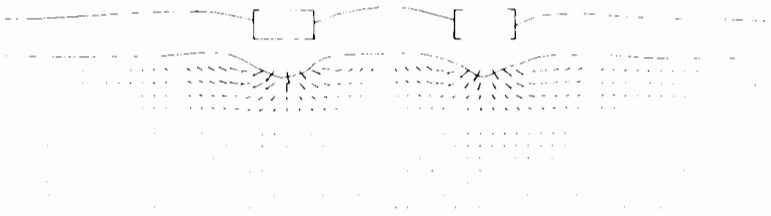

b) Unreinforced

Figure 4.27 Displacement Vector plots for dual footing tests at 25mm Footing Penetration (Sample M)

The modelling is not exact, of course: in the same test the particles of fill material cannot be both 1/8 and 1/4 full size. The rate of footing penetration, the amount of compaction, the size of the grid apertures are also things that will be incorrectly modelled if the test results are to be truly examined at a scale factor of 8 . Nevertheless, the results from these simple tests can provide the researcher with much extra information.

4.2.3 Fill-only Tests

A 'Fill-only' test is where no clay is used, a layer of fill being compacted directly onto the bottom of the test-box instead (Figure 4.28 , Plate 4.4). The bottom of the box effectively provides an infinitely stiff subgrade, whose surface roughness will play an important role.

A series of four such tests were conducted in an otherwise standard way. Besides measuring Load-Penetration data for the footing, photos were taken during tests, surface profiles were surveyed and heave measured. These tests were simpler and faster to do than tests involving a clay subgrade, with the purpose of the series being two-fold:

1. To effectively extend the test programme to its upper limit by doing tests on a 'perfectly' rough, 'infinitely' stiff subgrade.

2. To ascertain the reinforcement effects of a geogrid in isolation of any membrane action, and compare performance with a leading cloth type geotextile for the same situation.

Test 1 consisted of an unreinforced, 100mm thick layer of fill compacted onto a perfectly smooth base, the smooth surface being achieved as follows. The base of the box was thoroughly greased, and inlaid with one

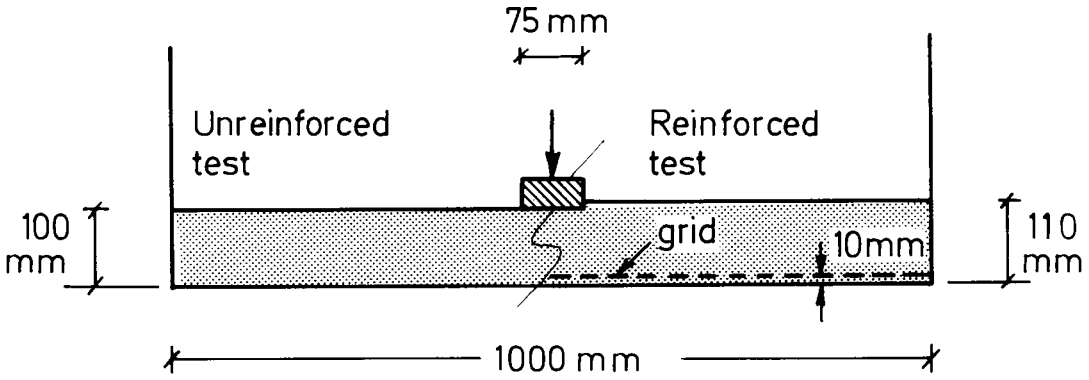

Figure 4.28 Fill-only test set-up

Plate 4.4 Fill-only test in progress

complete sheet of 0.1mm polythene the same size as the base area. This polythene was greased on its top surface. A second piece of the same polythene, the same size, was sliced laterally into 50mm strips (Figure 4.29), then laid out on top of the first sheet, and greased on its top surface. Finally, a third sheet of polythene, again the same size, was similarly cut into 50mm strips, but 25mm out of phase to the second sheet. These were placed across the top of the second sheet and greased also. The layers of this polythene laminate were therefore free to slide freely over one another, and had no continuous longitudinal strength. Compaction was carried out, as for all these tests, at optimum moisture content in 4 lifts of 25mm by the board and hammer process described in Section 3.2.1 .

Test 2 consisted of an unreinforced, 100mm thick layer of fill compacted onto a perfectly rough base. A piece of 1mm thick aluminium sheet was cut to the inside dimensions of the box, rubbed with Emery paper and completely de-greased with Genklene. A layer of Araldite (MY750 cured with HY951) was applied by paintbrush at room temperature to the sheet, and used to stick on one complete layer of the fill material. The larger particles were pressed into place first, and then the smaller

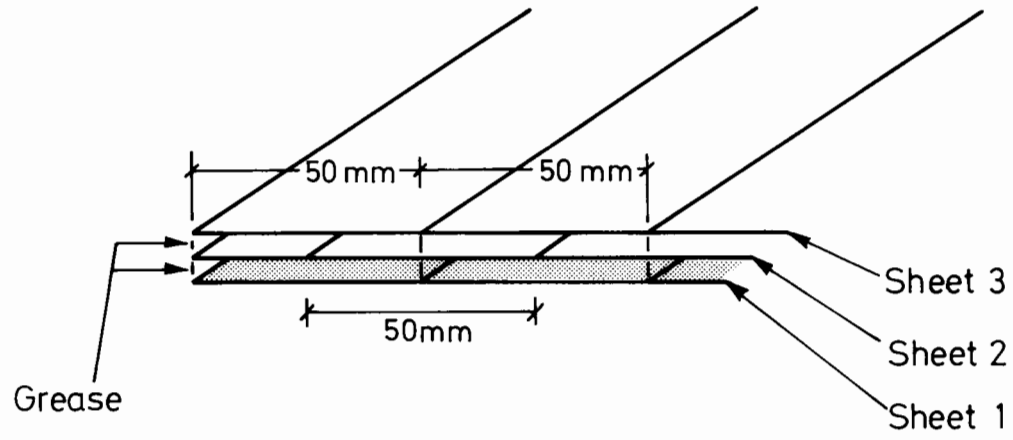

Figure 4.29 Polythene sheet laminates

sand-sized particles sprinkled on afterwards. After it had set, the false bottom was carefully placed into the base of the box and the fill layer compacted on top.

Test 3 consisted of a reinforced, 110mm thick layer of fill compacted onto a perfectly smooth base, this smooth base being prepared in the same way as for Test 1 . The layer of reinforcement, provided by the same mini-grid as used in the main testing programme, was placed on a 10mm bed of the fill material before compacting a 100mm layer on top. In this way the grid had granular material above and below it, which was considered necessary for the interlock mechanism to work.

Test 4 was identical in set-up to Test 3 except that a non-woven geotextile ($140g/m^2$) was used instead of the grid. The object of this test was to see how the reinforcing action of a cloth-type geotextile, arising from soil-fabric-soil friction, would compare to what could be provided by the interlock mechanism of a grid. The geotextile's tensile properties were not scaled down in any way. A comparison of the Force per unit width - Strain characteristic of both materials is shown in Figure 4.30 (see also Section 5.2.2).

The Load Penetration results (Figure 4.31) for these tests are straightforward. The inclusion of a grid at the base of a fill layer compacted on a perfectly smooth surface effectively makes the fill layer behave as if it had been compacted onto a perfectly rough surface. The performance of the geotextile is very similar. The reinforcing action of both materials is indisputable despite the 'infinite' stiffness of the subgrade. This is also shown by the definite differences in surface deformations for the 4 tests, which are shown in Figure 4.32 . The unreinforced system on the smooth base fails by soil sliding outwards

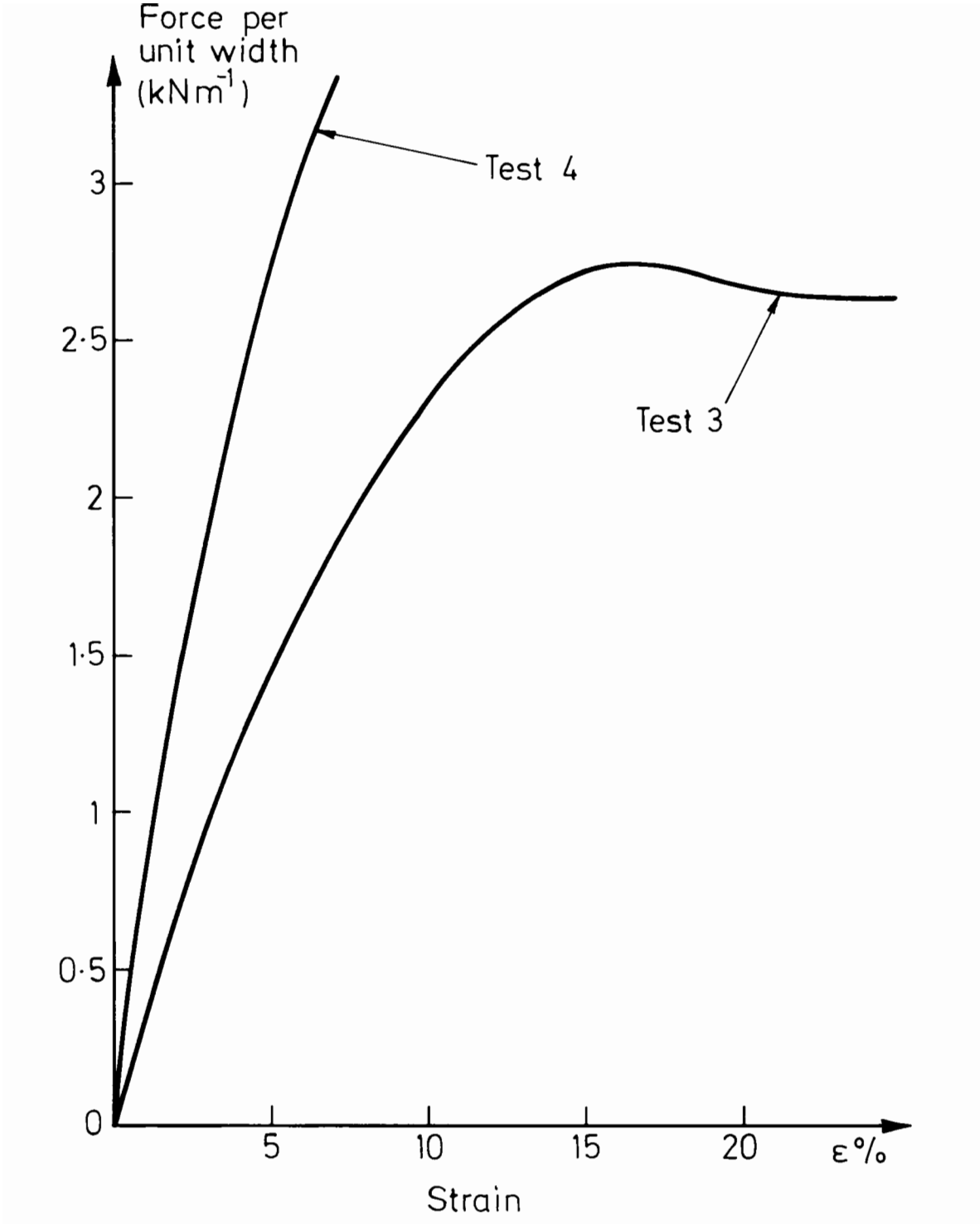

Figure 4.30 Comparison between 2 types of reinforcement used in Fill-only tests

along the base of the box. Wedges of fill are pushed out either side of the loaded footing. But in the reinforced systems, and in the unreinforced system on the rough base, such lateral movement is prevented until much higher loads are reached, and the extent of wedges then forming in the fill in Tests 2 and 3 at least is confined to being much closer to the footing. It is also noted that a marked improvement in performance between Tests 1 and 3 can be seen at a very small amount of

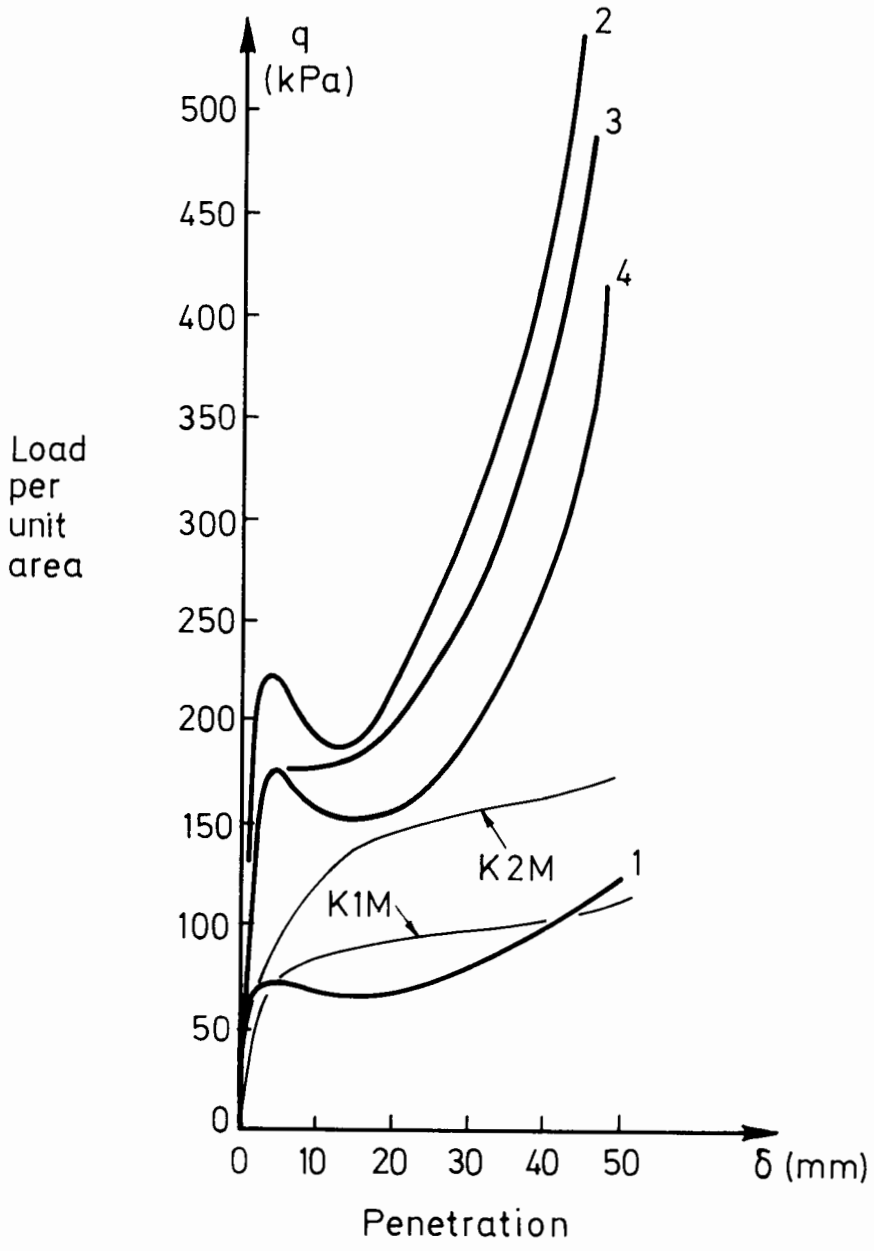

Figure 4.31 Load-Penetration curves for Fill-only tests

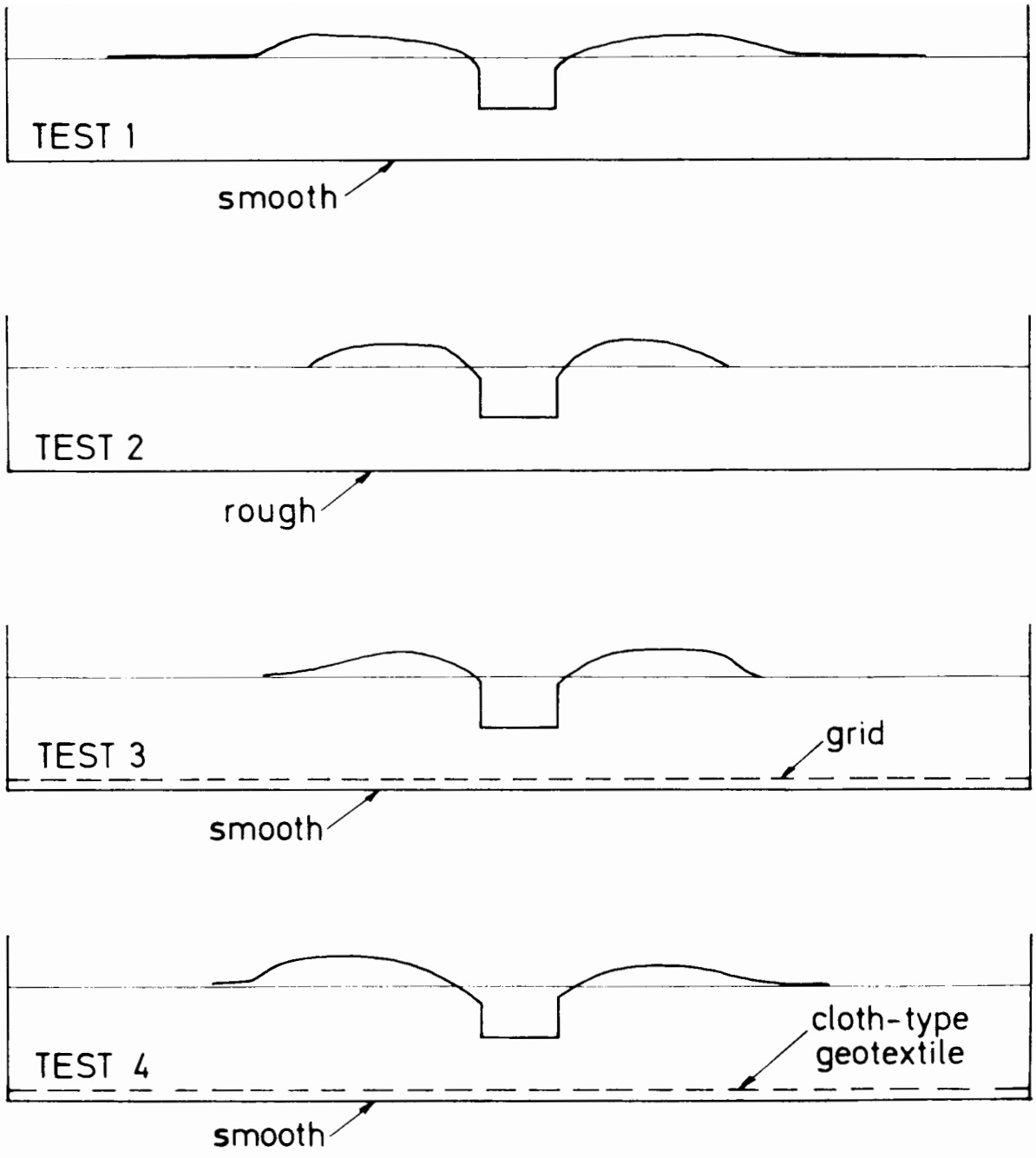

Figure 4.32 Before-and-after profiles for Fill-only tests (50mm Footing Penetration)

footing penetration. Real benefits, therefore, result from reinforcement in this system at relatively small amounts of footing penetration.

The results for tests K2M and K1M are also sketched in on Figure 4.31 for comparison, the former being a reinforced test, conducted on the strongest category of clay with a 100mm thick fill layer. The much stiffer response of the Fill-only tests is immediately apparent. The stiffer response is attributable both directly and indirectly to the infinitely stiff base, the fill layer being probably better compacted on the stiffer base in the first place.

The results of tests K1M and Test 1 are also instructive. After the initial stages of a test, 100mm fill on a solid but very slippery subgrade performs less well than the same thickness of fill on a much weaker clay subgrade. While the solid base is totally impenetrable, the clay surface allows fill particles to embed in it. For slipping to occur at the interface of the latter, the lateral flow of fill material either encounters shearing resistance in the clay, as fill particles try and move with it, or frictional resistance of fill particles as they try to slide over one another, whichever is the lesser of the two in any one region. The upper limit of bearing capacity for unreinforced tests on clay must therefore be represented by an infinitely stiff subgrade that also allows the fill layer particles to embed into it. This is in effect what Test 2 achieves, and thus provides the upper limit for reinforced tests also.

CHAPTER 5

SITE INVESTIGATION AND TESTING OF MATERIALS

5.1 Site Investigation

5.1.1 Introduction

Site investigation is an essential part of any test study, being no less important for reduced scale model tests than for full scale field trials. The more information the researcher can collect concerning subgrade shear strength profiles, water contents and other ground conditions, the more confidence he will have in the interpretation of his test data. The following briefly summarises the extent of information collected from each clay sample in this test study, on the days of testing.

Initially one shear vane test was carried out centrally under each test position, the centre of the shear vane at 55mm below the local clay surface. Details of the Pilcon Shear Vane are given in Chapter 2 , Section 2.4 . The clay block was then trimmed to the uniform height of 407mm for the first main test, the amount of clay removed being significant and calculable from a complete survey of the top surface of the clay conducted the day before. After the main central test had been conducted samples were taken from the fill layer for moisture content determination. The dry density of the fill was calculated from records of the wet weight of fill material used to make up a given layer thickness. After the fill layer had been removed, water content samples

were taken from the clay surface across the complete width of the box as shown in Figure 3.6 . The depth of clay excavated for this was minimal (15 - 20mm) in order not to compromise the subsequent use of the clay block for side tests. Shear vane tests were subsequently taken across the whole clay surface as for the moisture content samples. These, as before, were taken at a mid-vane depth of 55mm below the level of the moisture content trenches. The side tests would have suffered slightly due to this, but the effect would have been small due to the large ratio of footing area to the area affected by the shear vane test. Finally, in later samples, Samples C , E , F , J and A , one side test was cancelled on each layer in favour of further site investigation after the central test. In these samples, well-oiled 38mm diameter sample tubes were inserted to obtain samples for triaxial testing, and shear vane readings were taken at mid-vane depths of both 55mm and 140mm (Figure 5.1).

This represents the limited extent of site investigation work carried out on normal test samples. It unfortunately does not give adequate information about profiles of clay strength and moisture content with depth for the samples, due to it being necessarily collected at the end of a test and not before. The data may demonstrate the extent to which disturbance in the clay occurs due to a particular test, but unless information on the pre-test situation is available no comment can be made. It was essential therefore to have set aside three complete samples X Y and Z , one of each clay strength, entirely for the purpose of site investigation. The results from these three samples will therefore be discussed now before returning to comment on the above data in Section 5.1.8 .

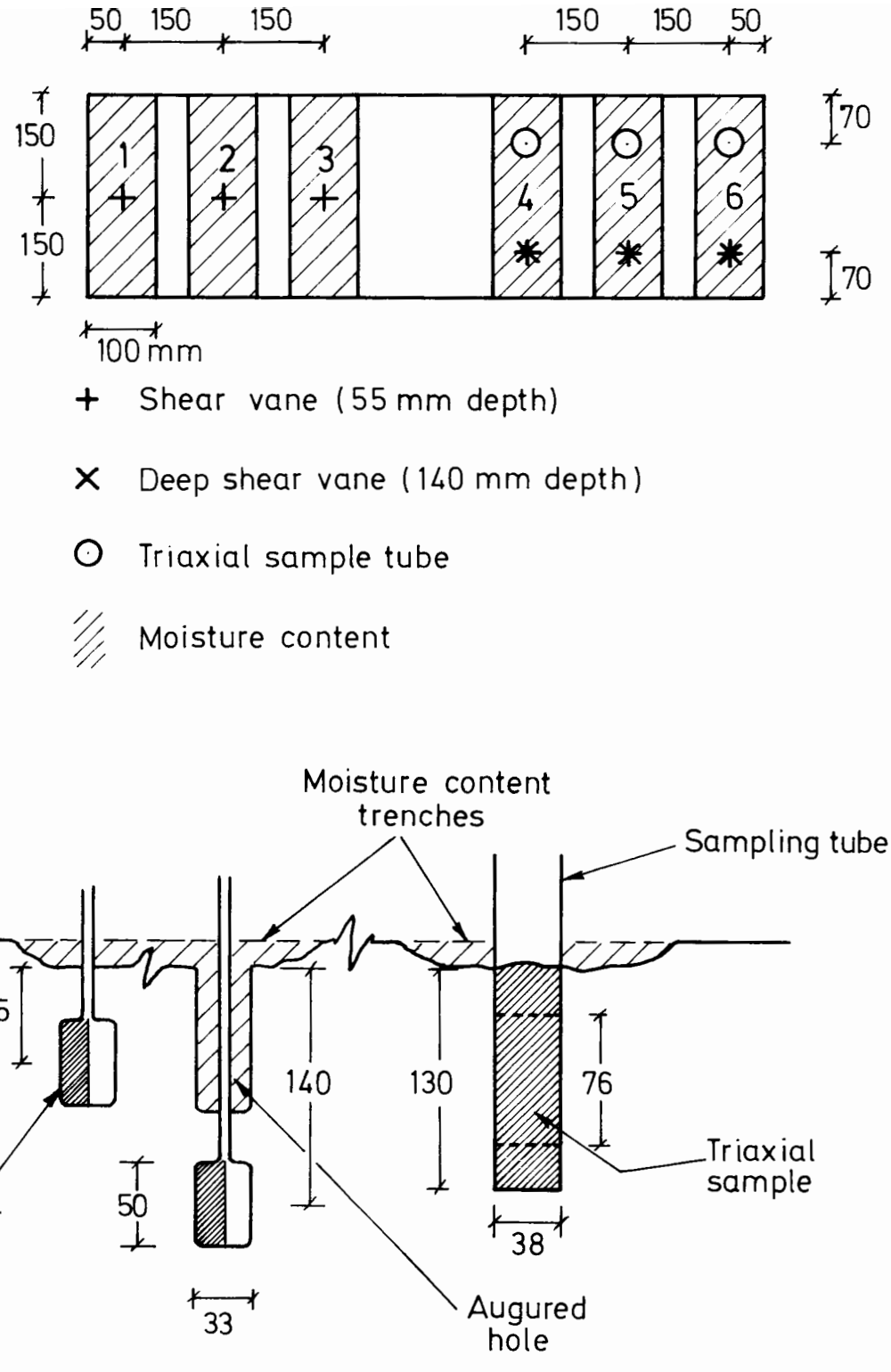

Figure 5.1 Locations of additional Shear Vane readings and Triaxial sampling

5.1.2 Site Investigation Samples

Each of Samples X , Y and Z were prepared in exactly the same manner as other samples of the same nominal clay strength with the same consolidation/swelling time-scales as used for previous samples. On the day before testing the top surface of the clay was surveyed and, on the day of testing, three initial shear vane readings were taken and the clay block levelled at 407mm . Instead of then setting up a footing test as for previous samples the following thorough investigation was made of the sample.

Nine 38mm diameter well-oiled sample tubes (T1 - T9) were pushed 110mm into the clay in the positions indicated in Figure 5.2 to a mid-sample depth of 55mm for direct comparison with the subsequent shear vane readings.

Nine shear vane readings (A1 - J1) were taken in the positions indicated by Figure 5.2 at a mid-vane depth of 55mm below the clay surface. These nine sites were then augured to a depth of 100mm and nine more shear vane readings taken at 155mm , 55mm below the augered depth (A2 - J2). This was repeated twice more for mid-vane depths of 255mm (A3 - J3) and 355mm (A4 - J4). For each reading the mid-vane depth below the bottom of the augered hole was kept at 55mm since this was the depth for which the vane was calibrated.

The front and back face of the test box were then removed, exposing the clay block. A central slice of clay was cut from the block using cheese wire and laid flat on the ground. Twelve samples (M1 - M12) were taken for determination of moisture content. Immediately afterwards, a second slice was cut from one side of the clay block and twelve more samples taken (S1 - S12).

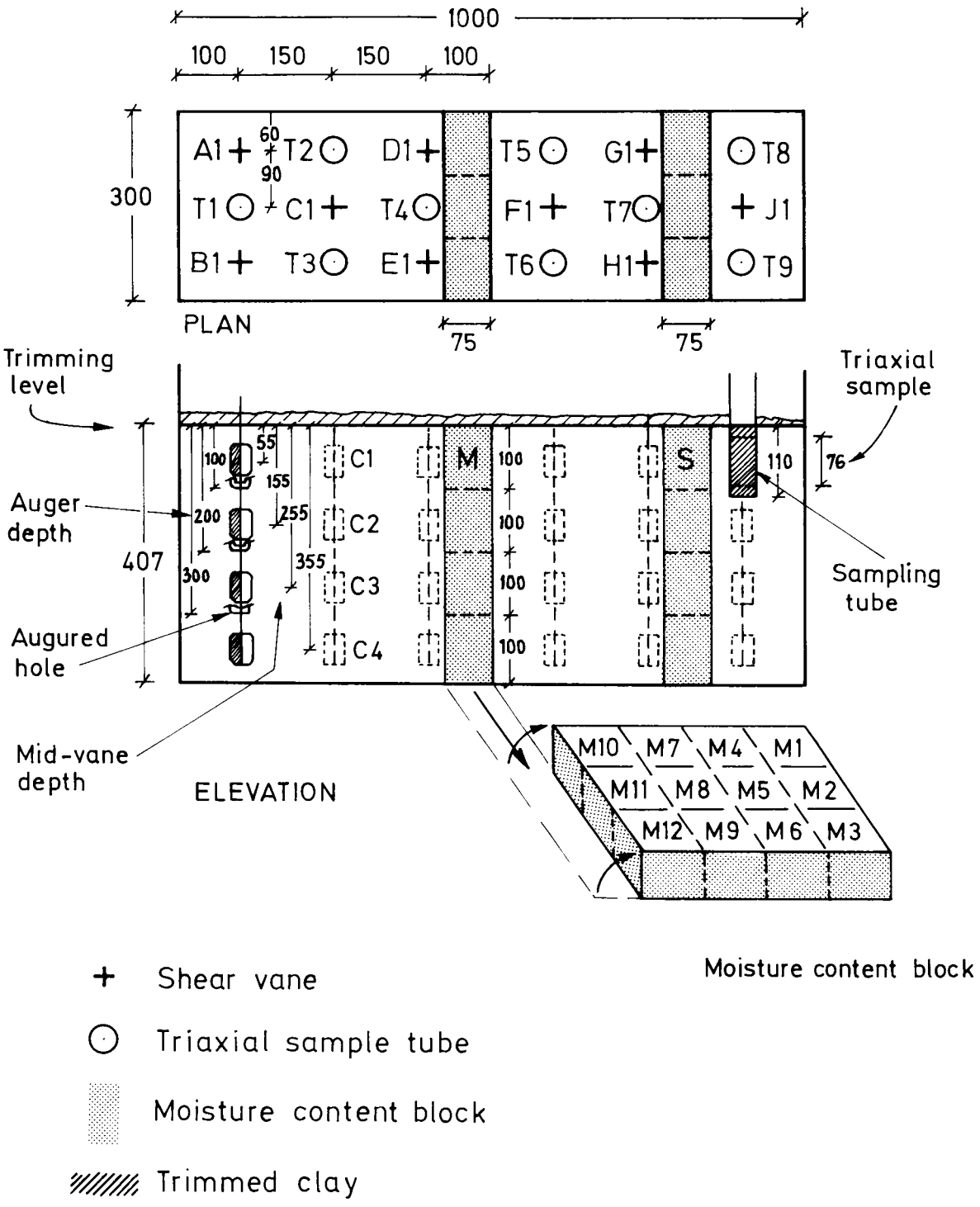

Figure 5.2 Details of 'Site Investigation'

The sample tubes were extracted and waxed up for subsequent Triaxial testing. Samples T4, T5, T6 and T7 were removed in-between the two sets of moisture content readings; the remaining five samples were now extracted. It was considered essential to insert the Triaxial tubes before conducting the shear vane tests in order to sample the clay in virgin condition. In addition the deep holes augured into the clay block for the deep shear vane readings were always kept full of water in order to avoid danger of drainage from the sample tubes. Once the sides of the box were removed, however, drainage would have started to occur. The time interval between this event and the final extraction of the last tube was one hour and this must be borne in mind when looking at triaxial test results (Plate 5.1).

Plate 5.1 'Site Investigation' Sample

5.1.3 Strength and Moisture Content Profiles

The results of the shear vane tests and the moisture content calculations for Samples X , Y and Z are summarised in Figure 5.3 where it can now be clearly seen that the clay strength increases with depth, and that the clay water content correspondingly decreases. Clay samples Y and Z are also shown to be slightly dryer at their sides than at their centre which cannot be entirely due to the fact that the side slice would inevitably have been draining while the central clay slice was being sampled, since for these two Samples the average strength of the clay is also seen to be higher at the side of the box than at the centre. In contrast the weakest clay sample, Sample X , is seen to be wetter at its sides.

A set of index curves (Figure 5.4) for the three types of clay sample were derived from Figure 5.3 . From these curves, individual values of C_u have been assigned to the clay subgrade in each test that take into account the amount of clay which was trimmed before testing took place.

5.1.4 Individual Subgrade Strength Values

Tests conducted on clays of the same nominal strength will not all, unfortunately, have precisely the same subgrade strength profiles for two reasons. Firstly, the final height of the clay block for each sample at the end of consolidation will differ slightly, due to differences in initial water content of the slurry at the start of consolidation and differences in the amount of slurry actually put into the box (it being difficult to judge this exactly). This will present a discrepancy between two samples with identical strength-with-depth profiles, but

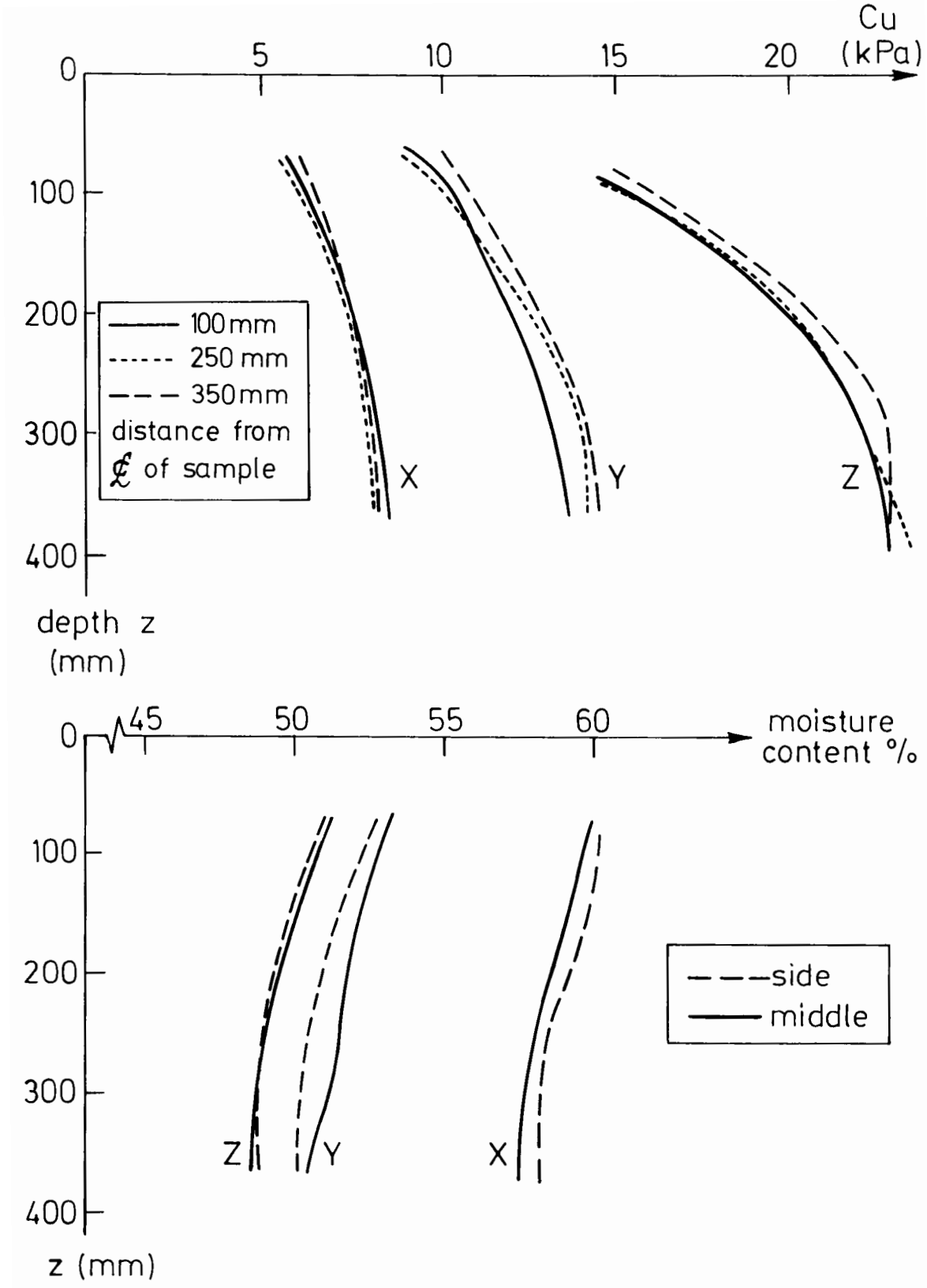

Figure 5.3 Undrained Shear Strength and Moisture content profiles with depth for Clay Samples X , Y and Z (Depth measured from original height of sample before trimming)

which have been trimmed by different amounts. Secondly, due to inaccuracies in setting the gas pressure regulator during the final stage of consolidation and possible variation of side wall resistance acting on the platen between samples, the strength-with-depth profiles for two samples which may have been trimmed by the same amount will still be different. Local differences will also exist within a sample due to appreciable tilting of the platen during consolidation for some samples (see Figures 3.1 - 3.3), and also from differences in the amount of grease placed on the inside faces of the box. In order to take these differences into account it is necessary to allocate a set of individual values of subgrade strength, C_u , to represent the particular subgrade condition for each test.

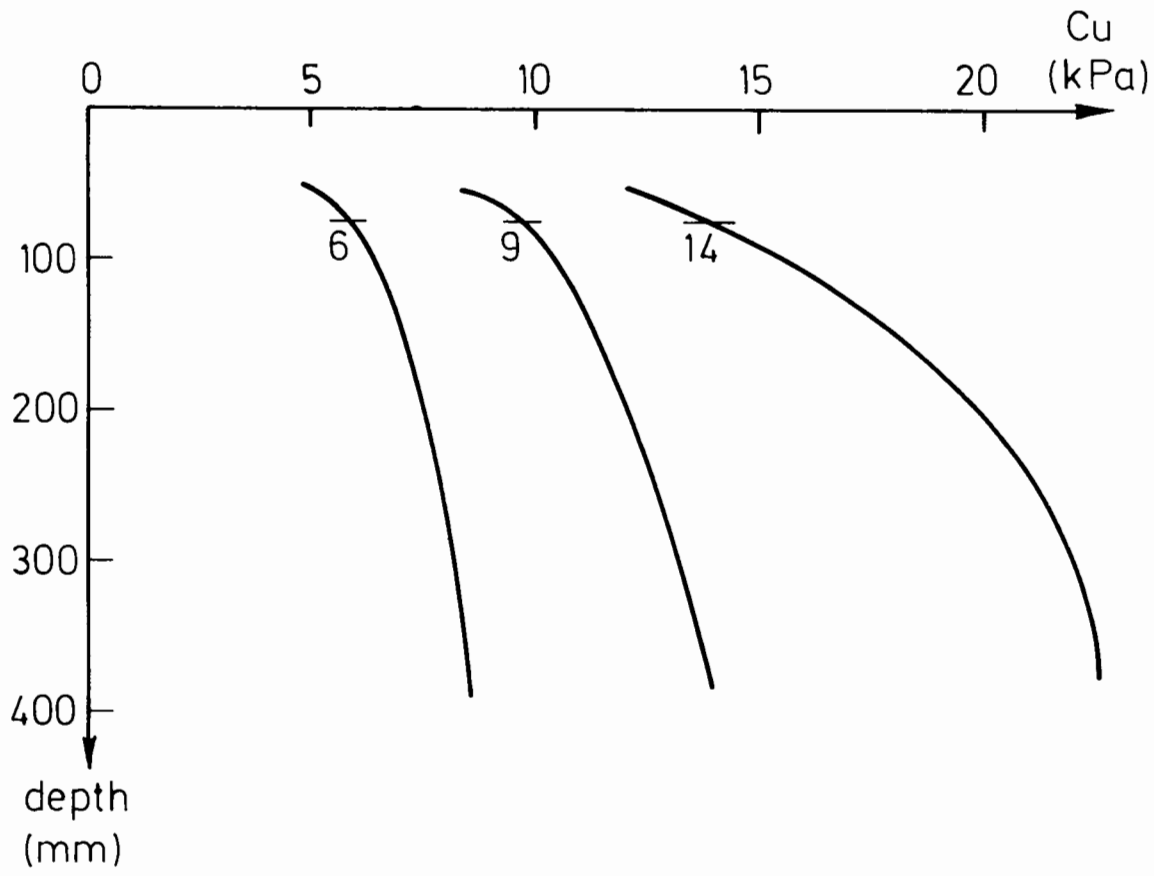

Figure 5.4 Index curves for the three nominal strengths of clay sample (Depth is measured from original height of sample before trimming)

Since the subgrade strength is not constant with depth, its value at a depth of 55mm is chosen since this is the depth at which shear vane readings are taken. The individual values of C_u will enable the comparison of different tests despite variations in their subgrade strengths. The following two stage method was developed for calculating C_u values:

1. The initial shear vane reading taken before trimming of the clay block was used to translate the appropriate index curve in Figure 5.4 horizontally by the amount which the shear vane reading differed from the corresponding index value at 55mm .

2. The amount by which the clay block was trimmed for that test at that location was added to 55mm , and the C_u value corresponding to that depth was read off.

An example can be taken to demonstrate this. Figure 3.4 shows the contour plot for the surface of Sample C . The contours represent the height in mm of the clay surface above the level of 407mm to which it was trimmed the following day for the central test. In order to find the relevant value of C_u for the subgrade-alone test C1L , the following steps are taken. The three initial shear vane readings, taken under each test position the following day immediately before trimming, gave values of 12.9kPa , 12.2kPa and 13.2kPa for test positions L M and R respectively. To the value of 12.9 is therefore added the effect of trimming 44mm of clay initially followed by another 20mm since it is a side test. The total of 64mm represents an additional shear strength of 4.3kPa , read from the right hand curve of Figure 5.4 (Sample C having a nominal strength of 14kPa). The value of 17.2kPa is therefore assigned to test C1L . This is a relatively high value resulting from the

relatively large amount of clay that had to be trimmed for this sample.

It is noted that the scale of Figure 5.4 as presented here is clearly not adequate for the above exercise. The set of individual C_u values presented in Table 4.2 were each derived using a carefully drawn enlargement of the initial stages of each curve, which is not presented here. It is also important to point out that the exercise of assigning values to the Layer 2 tests differed from the above in that a slightly revised set of index curves were used. These profiles represented a less severe increase of strength-with-depth. The corrections for surface trimming were therefore smaller in magnitude.

5.1.5 Triaxial Tests

Triaxial testing fell into two categories. The first type of testing consisted of a quick triaxial compression at a displacement rate of 4.6mm/min , without any kind of cell pressure, and these tests were usually conducted on the same evening that the samples were taken from the clay block. The second type of test was the standard undrained triaxial test; these tests were conducted at 0.1mm/min with a cell pressure of 400kPa and were carried out as soon after the day of extraction as possible. Standard 76mm x 38mm diameter samples were used throughout.

The second type of test represents a truly undrained and well controlled test, but can suffer significantly from changes in condition of the sample during storage. The first type, although a relatively crude test, is more likely to be testing the clay at its in-situ condition. The results for both sets of tests are shown in Figures 5.5 and 5.6a,b respectively. Unfortunately the Type 2 tests on Sample Y

suffered from an initial lack of experience with triaxial testing techniques and are not presented. Nevertheless there is sufficient information to make some important points. The two primary aims with these triaxial tests are firstly, to check the validity of the shear vane readings for determination of undrained shear strength , and secondly to establish the in-situ mean effective pressure in the clay sample at the time of testing since this is of interest for determining overconsolidation ratios.

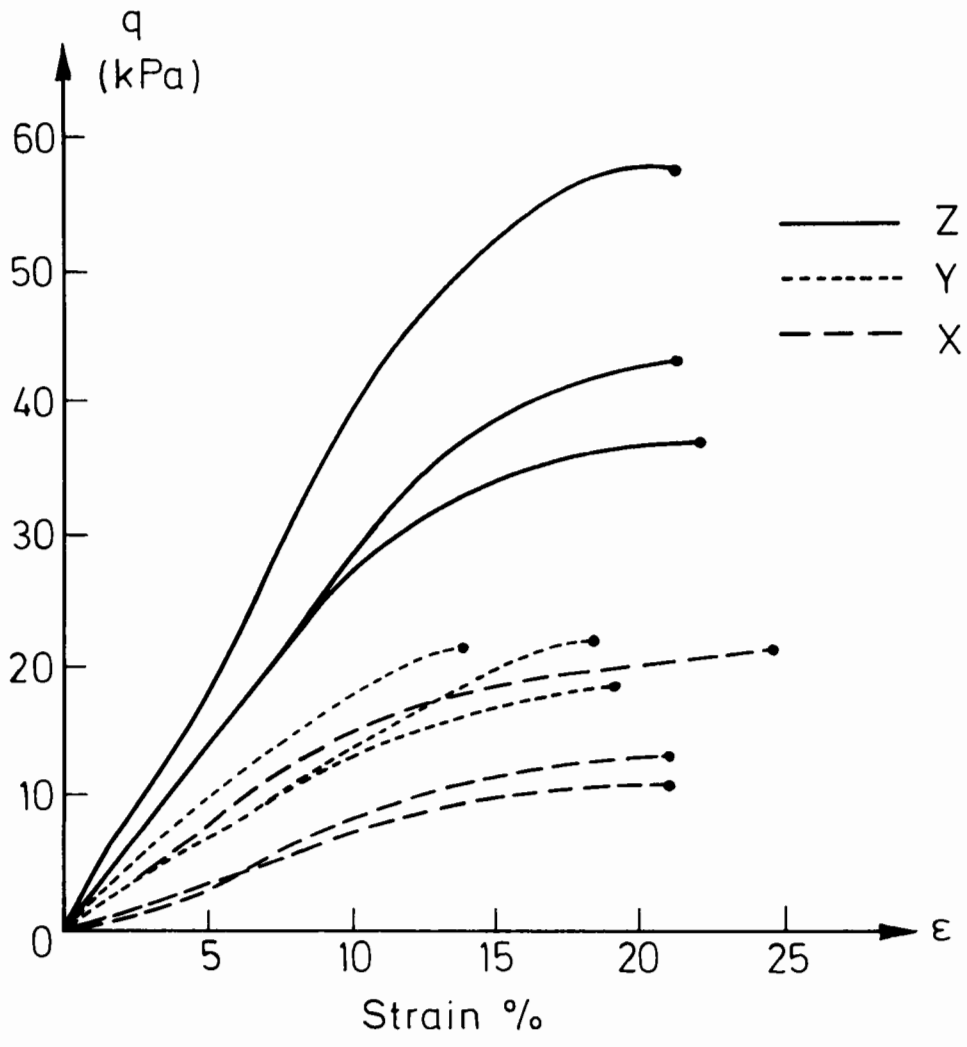

Figure 5.5 Type 1 Quick Undrained Triaxial tests on Samples X , Y and Z (Deviator Stress : Strain)

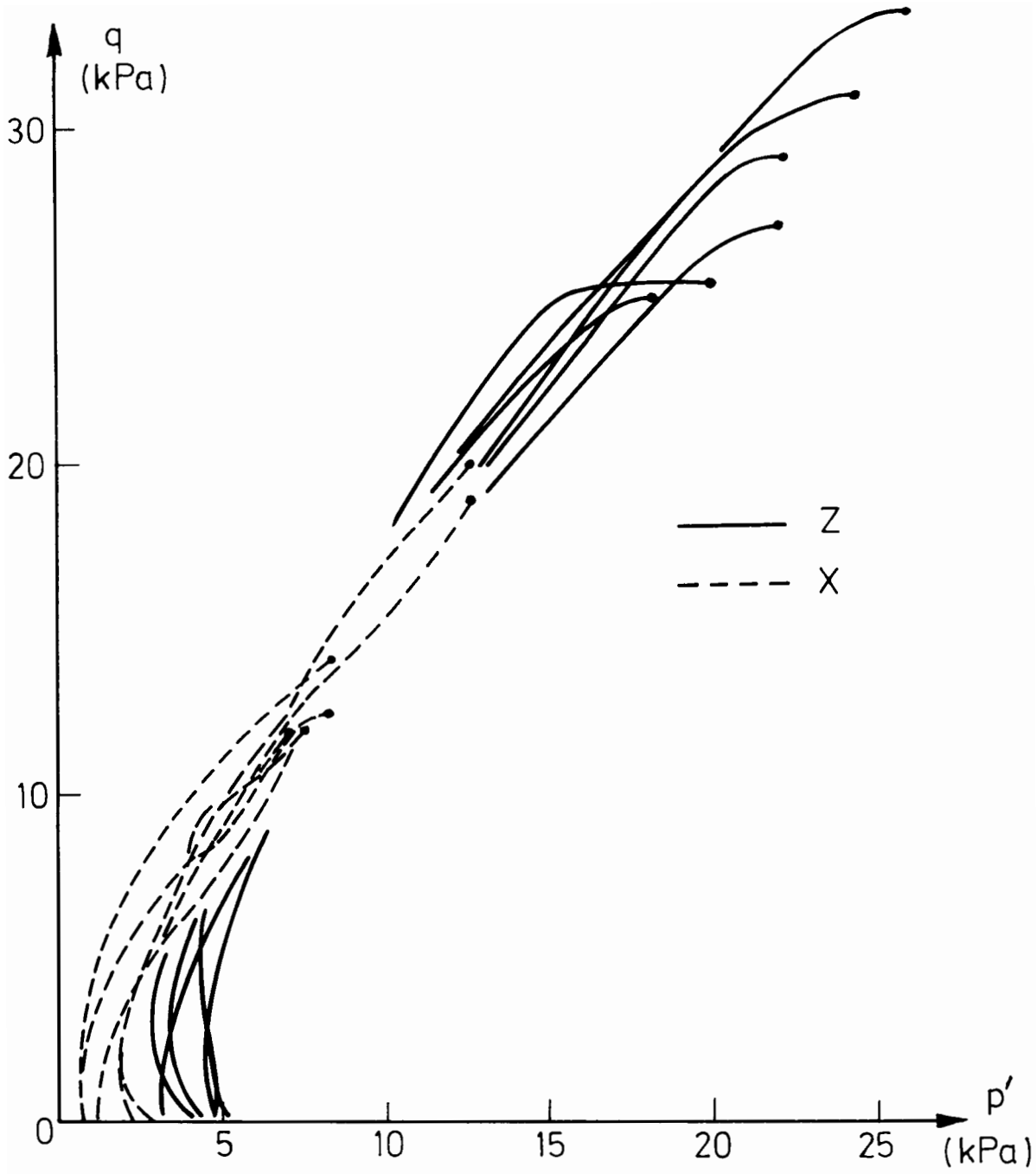

Figure 5.6a Type 2 Undrained Triaxial tests on Samples X and Z

(Deviator Stress : Mean Effective Pressure)

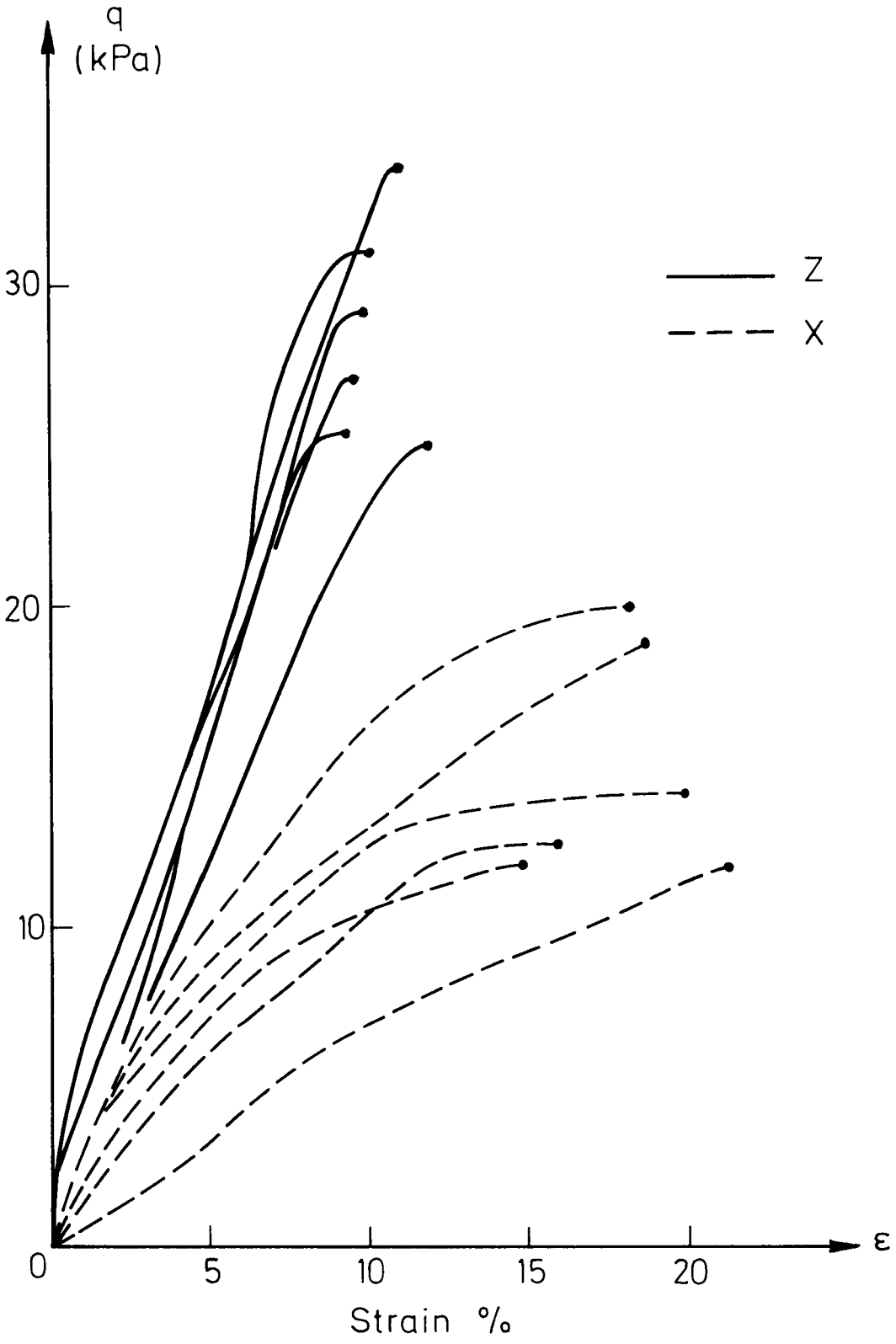

Figure 5.6b Type 2 Undrained Triaxial tests on Samples X and Z

(Deviator Stress : Strain)

5.1.6 Checking Shear Vane Readings

The correlation between the shear vane and triaxial test results is not good, but does not seem to be due to the shear vane results since they show less scatter than the triaxial results. Table 5.1 compares the relevant quantities for Samples X and Z , the figures in (brackets) representing results from Type 1 triaxial tests. A lack of agreement occurs between Types 1 and 2 , especially in Sample Z , and comparing the Type 2 results with shear vane readings show different trends in different Samples. In Sample X the triaxial results give higher values of shear strength than the shear vane, while generally the opposite is seen in Sample Z .

TABLE 5.1 COMPARISON BETWEEN SHEAR VANE READINGS AND TRIAXIAL TEST RESULTS FOR SITE INVESTIGATION SAMPLES X AND Z

Sample X			
SV		TX	
A1	6.5		
		T1	10.0
B1	6.0		
		(T2	10.5)
C1	5.5		
		T3	9.5
D1	6.0		
		(T4	6.5)
E1	5.5		
		T5	6.0
F1	5.5		
		(T6	5.5)
G1	5.5		
		T7	6.5
H1	5.5		
		T8	7.0
J1	5.5		
		T9	6.0

Sample Z			
SV		TX	
A1	16.0		
		T1	17.0
B1	15.0		
		(T2	28.5)
C1	14.5		
		T3	13.5
D1	15.5		
		(T4	21.5)
E1	14.0		
		T5	12.5
F1	15.0		
		(T6	18.5)
G1	14.5		
		T7	12.5
H1	14.5		
		T8	14.5
J1	14.5		
		T9	15.5

Notes
1. Quantities represent values of C_u in kPa (rounded to nearest 0.5kPa)
2. Values of C_u obtained from triaxial tests correspond to the point of maximum deviator stress
3. Figures in (brackets) refer to quick undrained Type 1 triaxial tests
4. Refer to Figure 5.2 for locations A1 - J1 and T1 - 9

Great care was taken in the Type 2 triaxial tests, with the porous stones being deaired thoroughly and the loading shaft well greased. A special differential transducer was used to measure the difference between cell pressure and pore pressure in the sample directly, instead of measuring each on separate transducers which would have introduced extra inaccuracy. The positioning of membranes, 'O-rings' and top caps was executed as carefully as possible, given the weakness of the clay samples. While the Type 1 triaxial test results are not particularly surprising given the coarseness of the test, the Type 2 results are disappointing. It should perhaps be concluded from this that although some researchers will treat the result of hand shear vane tests with scepticism, the alternative of carefully controlled triaxial sampling and testing of clays of this weakness does not necessarily yield more satisfactory results.

If triaxial tests cannot be used reliably to check the shear vane results, an alternative method of doing this must be found. Figure 4.2 shows a plot of the load-penetration results of the 18 footing tests that were conducted on the clay alone. Each set of results has been normalised with respect to the relevant individual shear strength value, C_u, which are all completely based on shear vane readings. The fact that there is a relatively small amount of scatter in this data, and that they tie in well with the classical predictions of elastic and plastic behaviour limits of (πC_u) and $(\pi + 2)C_u$ respectively give considerable confidence in the results obtained by the hand shear vane test.

5.1.7 Overconsolidation Ratio

The calculation of overconsolidation ratio (OCR) necessitates the knowledge of both the maximum previous mean effective pressure and the current mean effective pressure:

$$OCR = p'_{max}/p'$$

The former can be calculated from the maximum vertical load supplied to the sample during consolidation and assuming a value for K_o :

$$p'_{max} = 1/3\ \sigma_v'_{max}(1 + 2K_o)$$

A value of 0.56 was taken for K_o (see Section 5.2.3 below). The current mean effective pressure in the clay at the time of sampling is derived from the triaxial tests (Type 2) conducted on the Site Investigation samples. When setting up a triaxial sample for an unconsolidated undrained test, the initial difference between the cell pressure applied to the sample and the pore pressure resulting in the sample, before any deviator stress is applied, gives this in-situ value of mean effective pressure. It is important in this exercise to have a sufficiently high cell pressure to ensure saturation in the sample, a value of 400 kPa being used here.

For Type 2 triaxial tests conducted on Sample X , an average value of 2kPa was obtained, and a value of 5kPa was obtained for Sample Z . As mentioned earlier this data is not available for Sample Y , but interpolating from the previous two values, a value of 3.5kPa would be appropriate. The values of OCR for each of Samples X Y and Z (at a depth of 55mm from the clay surface) are therefore approximately 30 , 50 and 70 respectively. Taking an average value of water content for each sample from the profiles presented in Figure 5.4 the gradient, κ , of swelling

TABLE 5.2 SHEAR VANE READINGS AFTER EACH CENTRAL TEST

Sample	Unreinforced tests						Reinforced tests					
	1	2	3	4	5	6	1	2	3	4	5	6
A	6.4	5.4	4.8	5.2	5.3	5.8	5.3	5.0	4.5	5.1	5.3	5.3
	(7.7		6.5		6.5)		(6.5		6.5		6.5)	
B	9.2	9.0	8.6	9.1	9.3	8.3	10.2	9.4	8.8	9.1	8.1	9.3
	(9.7		9.6		9.7)		(11.1		9.6		9.7)	
C	13.0	–	11.2	11.3	11.6	12.8	15.4	14.9	11.2	10.8	14.1	15.8
	(13.9		13.7		13.9)		(17.2		16.4		17.4)	
D	5.9	–	5.7	5.1	–	5.1	4.6	–	5.0	4.6	–	4.3
	(7.2		6.2		6.4)		(6.7		6.7		6.0)	
E	8.7	8.6	8.2	8.6	9.3	8.0	9.4	8.2	6.9	8.0	8.1	8.7
	(9.9		9.7		9.6)		(10.5		9.2		9.7)	
F	15.5	13.8	12.5	13.1	12.3	15.3	13.2	13.2	12.1	12.7	11.4	12.3
	(16.6		14.5		14.5)		(14.1		14.0		13.9)	
G	5.9	5.6	5.4	5.4	5.3	5.8	5.0	5.6	5.6	5.7	6.0	5.1
	(7.1		6.5		6.0)		(5.8		6.5		6.1)	
H	9.0	9.1	8.0	8.1	8.6	8.4	9.1	9.1	7.2	7.9	7.5	9.2
	(9.4		9.3		8.8)		(10.5		9.5		9.9)	
J	9.3	8.9	8.1	7.9	9.3	9.1	9.8	8.5	9.7	7.4	9.1	9.8
	(10.3		8.8		9.4)		(10.3		9.4		10.1)	
K	16.9	16.2	16.0	15.5	15.4	15.6	13.6	13.5	13.0	13.8	14.0	14.3
	(17.9		16.0		15.9)		(14.8		14.5		14.6)	

Notes

1. Quantities represent values of C_u in kPa
2. Figures in (brackets) refer to pre-test values of C_u and correspond to sites L M and R shown in Figure 3.4
3. Refer to Figure 3.6 for locations 1 – 6 for Samples B D G H K and to Figure 5.1 for Samples A C E F J

TABLE 5.3 MOISTURE CONTENT SAMPLES AFTER EACH CENTRAL TEST (UNREINPORCED AND REINPORCED TESTS)

Sample	(MC_o)	1	2	3	4	5	6	MC_{av}	σ_{n-1}
A	(60.6)	58.4	55.5	56.7	57.3	57.3	57.5	57.1	1.0
	(60.6)	59.6	58.1	59.2	59.4	59.3	59.4	59.2	0.5
B	(53.8)	54.3	53.6	53.1	52.2	52.7	54.3	53.4	0.9
	(53.9)	53.6	53.1	52.7	53.7	53.6	53.8	53.4	0.4
C	(51.8)	51.9	50.3	49.8	49.8	50.4	51.5	50.6	0.9
	(51.3)	50.6	48.6	48.7	49.0	48.9	50.1	49.3	0.8
D	(60.7)	57.0	-	55.2	55.3	-	58.2	56.4	1.4
	(60.7)	55.6	-	55.8	56.2	-	56.8	56.1	0.5
E	(54.0)	53.8	50.9	50.7	50.8	51.5	51.5	51.5	1.2
	(53.9)	52.3	52.5	52.5	52.2	53.0	53.7	52.7	0.6
F	(51.8)	49.3	48.7	48.5	49.2	49.1	48.6	48.9	0.3
	(51.8)	48.1	49.7	49.2	48.9	48.7	49.2	49.0	0.5
G	(60.7)	57.2	56.5	56.6	55.5	55.9	56.4	56.4	0.6
	(60.6)	58.1	57.0	55.8	54.6	55.3	54.8	55.9	1.4
H	(53.8)	53.7	52.2	52.3	51.6	52.7	53.3	52.6	0.8
	(53.9)	53.2	52.4	52.9	53.2	53.6	53.6	53.2	0.5
J	(53.8)	54.3	51.7	52.0	50.0	51.9	52.0	52.0	1.4
	(53.9)	51.5	51.4	50.6	51.5	51.3	52.8	51.5	0.7
K	(51.4)	47.5	48.0	48.3	48.0	48.1	48.6	48.1	0.4
	(51.8)	50.5	48.8	48.5	48.9	48.7	49.6	49.2	0.8

Notes

1. Top set of readings in each case correspond to the unreinforced test
2. MC_o values in (brackets) are taken from Figure 5.3 and represent an estimate of the average surface moisture content before each test
3. MC_{av} and σ_{n-1} values represent the mean and standard deviation of each set of six readings
4. Refer to Figure 5.1 for locations 1 - 6

water contents (MC_{av} , Table 5.3) are generally much the same for corresponding reinforced and unreinforced tests, , it is apparent that the amount of variation of water content across the six sites (as represented by σ_{n-1} , Table 5.3) is greater for unreinforced tests than for the reinforced tests.

The shear vane readings for some tests indicate greater softening of the subgrade nearer to the footing when compared to pre-test strengths, while others show the opposite, with no obvious relation to the type of test performed. Before-and-after comparisons of shear vane readings for tests on different fill thicknesses show similarly random variations.

TABLE 5.4 COMPARISON BETWEEN SHEAR VANE READINGS AND TRIAXIAL TEST RESULTS FROM POST-TEST SITE INVESTIGATIONS

		SV	TX
A1M	1	6.5	8.0
	2	5.5	7.0
	3	5.0	(5.5)
A2M	1	5.5	6.0
	2	5.0	5.5
	3	4.5	(6.0)
C1M	6	16.0	(25.0)
	5	14.0	(23.5)
	4	11.0	(13.0)
C2M	6	13.0	(14.5)
	5	11.5	(14.5)
	4	11.5	(12.5)

		SV	TX
E1M	1	9.5	(14.0)
	2	8.0	(12.5)
	3	7.0	(9.0)
E2M	1	8.5	(5.0)
	2	8.5	(10.5)
	3	8.0	(9.0)
F1M	1	15.5	13.5
	2	14.0	9.5
	3	12.5	(15.0)
F2M	6	12.5	11.5
	5	11.5	11.0
	4	12.5	(10.0)

		SV	TX
J1M	6	10.0	-
	5	9.0	8.5
	4	7.5	(7.5)
J2M	1	9.5	-
	2	9.0	5.5
	3	8.0	(10.0)

Notes
1. Quantities represent values of C_u in kPa (rounded to nearest 0.5kPa)
2. Figures in (brackets) refer to quick undrained Type 1 triaxial tests
3. Values of C_u obtained from triaxial tests correspond to the point of maximum deviator stress
4. Refer to Figure 5.1 for locations 1 - 6

The Triaxial test results (Type 2 shown here only, Figure 5.7) appear equally 'fuzzy'. It would seem that discrete shear planes in the deformed clay body are the main cause of the variablilty of these results, both in the shear vane readings and for the triaxial samples. If a reading or a sample is taken across an existing shear plane, then the strength for that test will appear low, while a second reading or sample taken from nearby, just missing the shear plane, will appear high. Table 5.4 lists the set of post-test shear vane readings for which corresponding triaxial samples were extracted and Type 1 or Type 2 tests conducted, and Figure 5.1 shows the corresponding locations.

The deep shear vane readings show the extent of softening of the clay which occurs at depth. Figure 5.8 in conjunction with Figure 5.9 show the locations of each shear vane reading in relation to the zone of significant clay movement determined from a typical marker displacement plot. Significant softening is seen to have occurred at Locations 3 and 4 , while very little softening is seen to have occurred at Locations 1 and 6 , outside the zone of 'disturbance'. Appreciable softening is shown to have also occured at Locations 2 and 5 , just outside this zone.

5.2 **Subsidiary Testing Of Main Materials**

5.2.1 The Fill Material

The grading chosen for the fill material was a scaled-down version of the D.O.T Type 1 Specification with particle sizes being reduced by a scale factor of 4 to meet modelling requirements. On a logarithmic Grading Form the full-scale and model specifications retain the same basic shape, being a simple translation of each other (Figure 2.1).

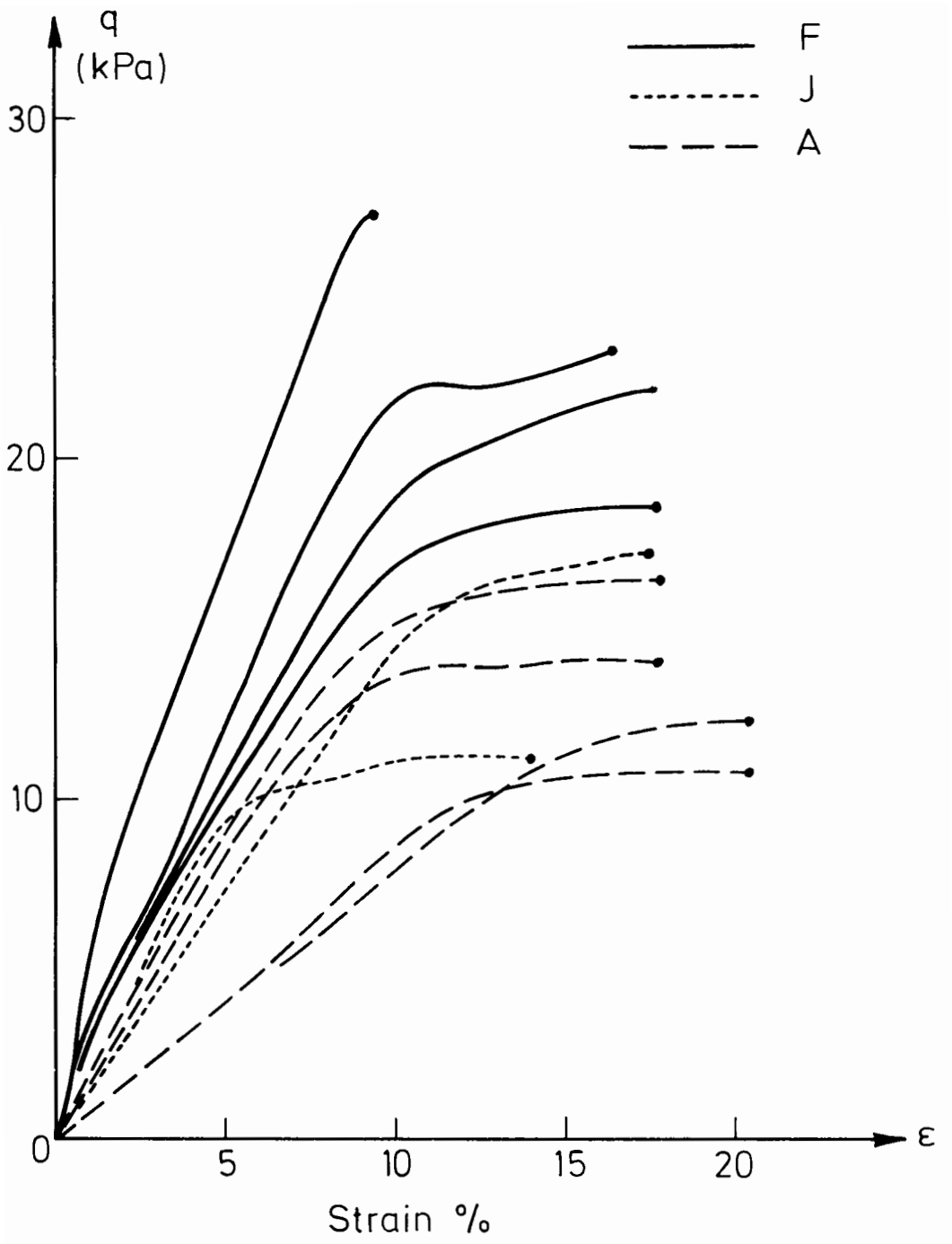

Figure 5.7 Type 2 Undrained Triaxial tests on Samples A , F and J

(Deviator Stress : Strain)

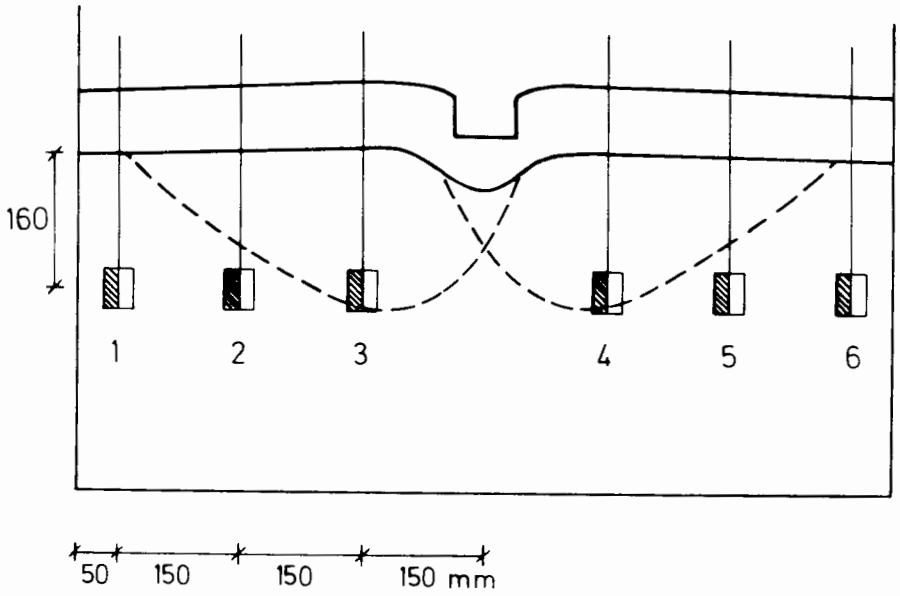

Figure 5.8 Locations of deep Shear Vane tests in relation to a typical zone of deformation

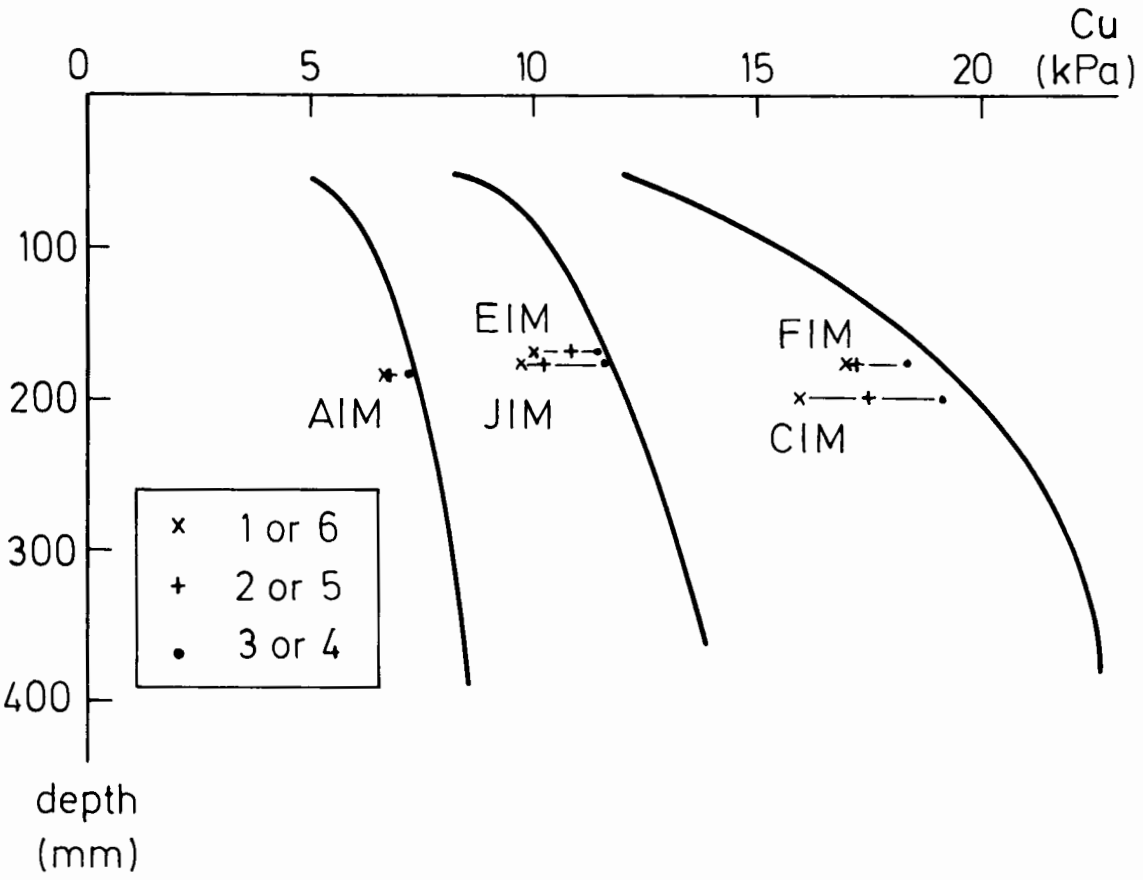

Figure 5.9 Results of deep Shear Vane tests after 1st Layer test on Samples A, C, E, F and J compared against Index Curves (Shear Vane Locations 1-6 shown in Figures 5.1 and 5.8)

During the course of testing sand and gravel were obtained from a single supplier in Cambridgeshire. The sand and gravel were ordered each time in the following sizes: 25/52 sand, 14/25 sand, 7/14 sand, 2 - 4mm gravel, 4 - 8mm gravel and 10 - 15mm gravel. It was found that mixing equal quantities from each category produced a satisfactory, evenly graded fill material which met the required specification. Each shipment of fill was checked several times for grading and the corresponding envelope is shown in Figure 2.1 . The scatter is not large despite the fact that later batches of gravel were noticeably different in the roundedness of particles: the earlier shipments came from a quarry which subsequently closed down and the intermediate gravel of the second type had flat, disc-shaped particles. As a result the densities obtained in the fill layer after compaction were slightly higher in the latter tests - Sample J onwards (see Table 4.3).

An optimum moisture content value of 10% was established for the fill from standard (Proctor) compaction tests. Subsidiary 2-D tests were also done on the fill in a small rectangular box, 250mm by 150mm by 80mm deep (Figure 5.10). A series of simple footing tests were carried out on the fill when dry, when completely saturated and at 10% moisture content. In each case two samples were tested with the 15mm footing; one set up loose, the other well compacted. The results show the extent to which the fill in the latter state, compacted at its optimum moisture content, performed better than the first two.

5.2.2 The Grid

The Force per unit width - Strain index curve for the full scale Tensar SS1 geogrid, tested at the standard strain rate of 2% min^{-1} (McGown, 1982), is shown in Figure 5.11 . The force measured per unit

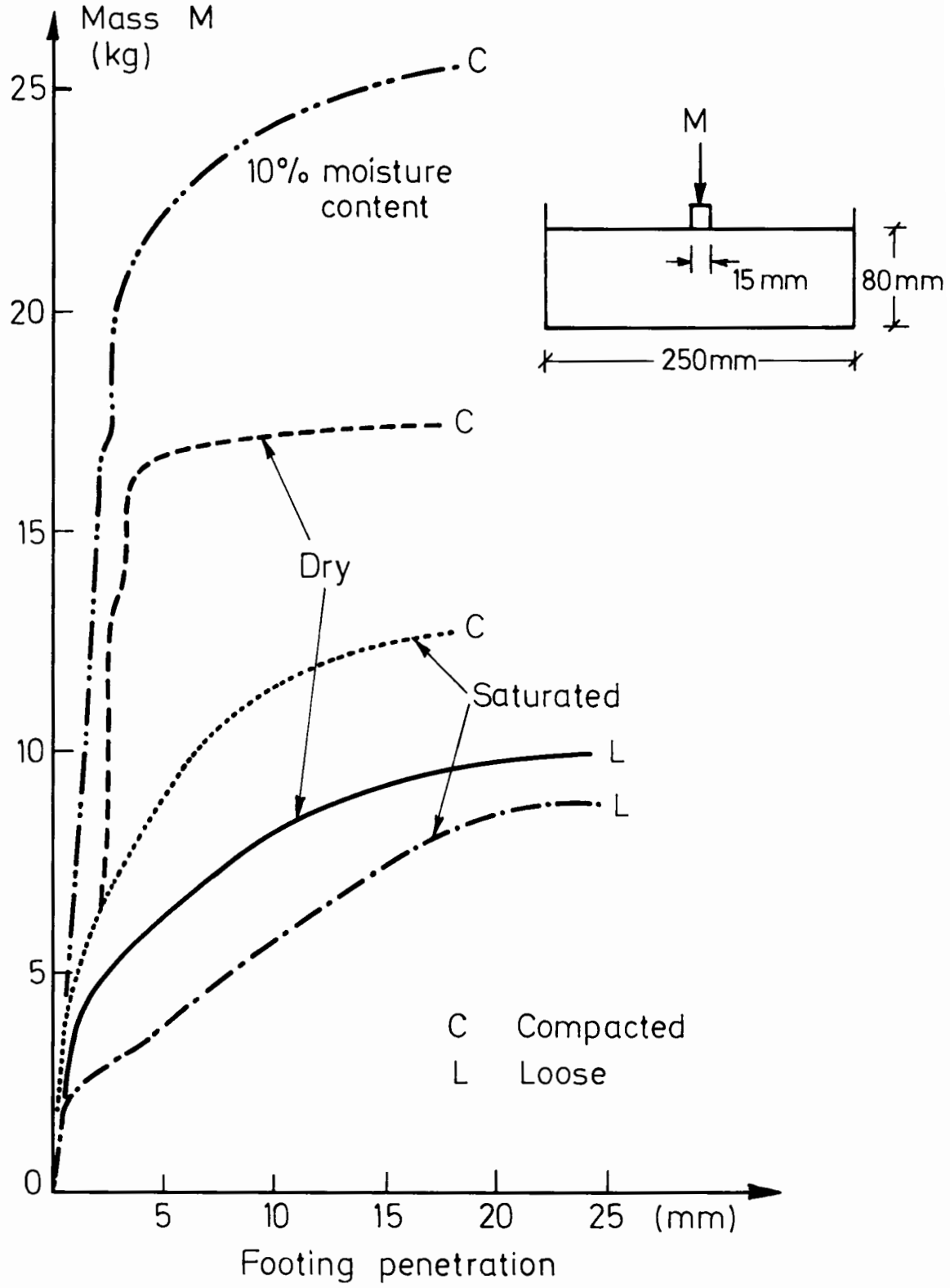

Figure 5.10 Small-scale footing tests demonstrating effect of fill moisture content and compaction

width of the material in kN/m , should be scaled down by a factor of 16 for the model grid according to the dimensionless group $s/C_u B$ (Chapter 2). This is done by rescaling the ordinate axis in Figure 5.11 accordingly. Achieving a grid with both a correctly scaled geometry and a Force per unit width - Strain characteristic matching the curve above proved to be a difficult task, however. Netlon Ltd, who make the full-scale grid from a homopolymer, made the scaled grid from a less stiff copolymer by an otherwise similar stretching process. The resulting grid was not ideal, suffering from the limitations of a small scale laboratory production process, it not being possible to produce a totally uniform specimen. Aperture sizes increased towards the ends of the sample due to the transverse stretching process which had more of an effect at the ends of the sample than at the middle. Figure 5.12 shows the problem in exaggerated form and how samples were cut from each batch of grid to minimise the effect on performance.

More importantly, the Force per unit width - Strain curve for the grid had to meet the necessary modelling requirement. Although many extension tests were carried out, one representative curve is shown for the material on Figure 5.11 for simplicity. The various batches of grid material which were supplied by Netlon Ltd throughout the programme did show some variation in performance but by careful selection of each grid sample this was kept to a minimum. Figure 5.11 shows that when both the full-scale and model materials are tested at the same strain rate of 2% min^{-1} (at 20^{o}C) the model grid is still approximately twice the required stiffness, despite being made from a very weak polymer. The effect of strain rate has not been discussed yet.

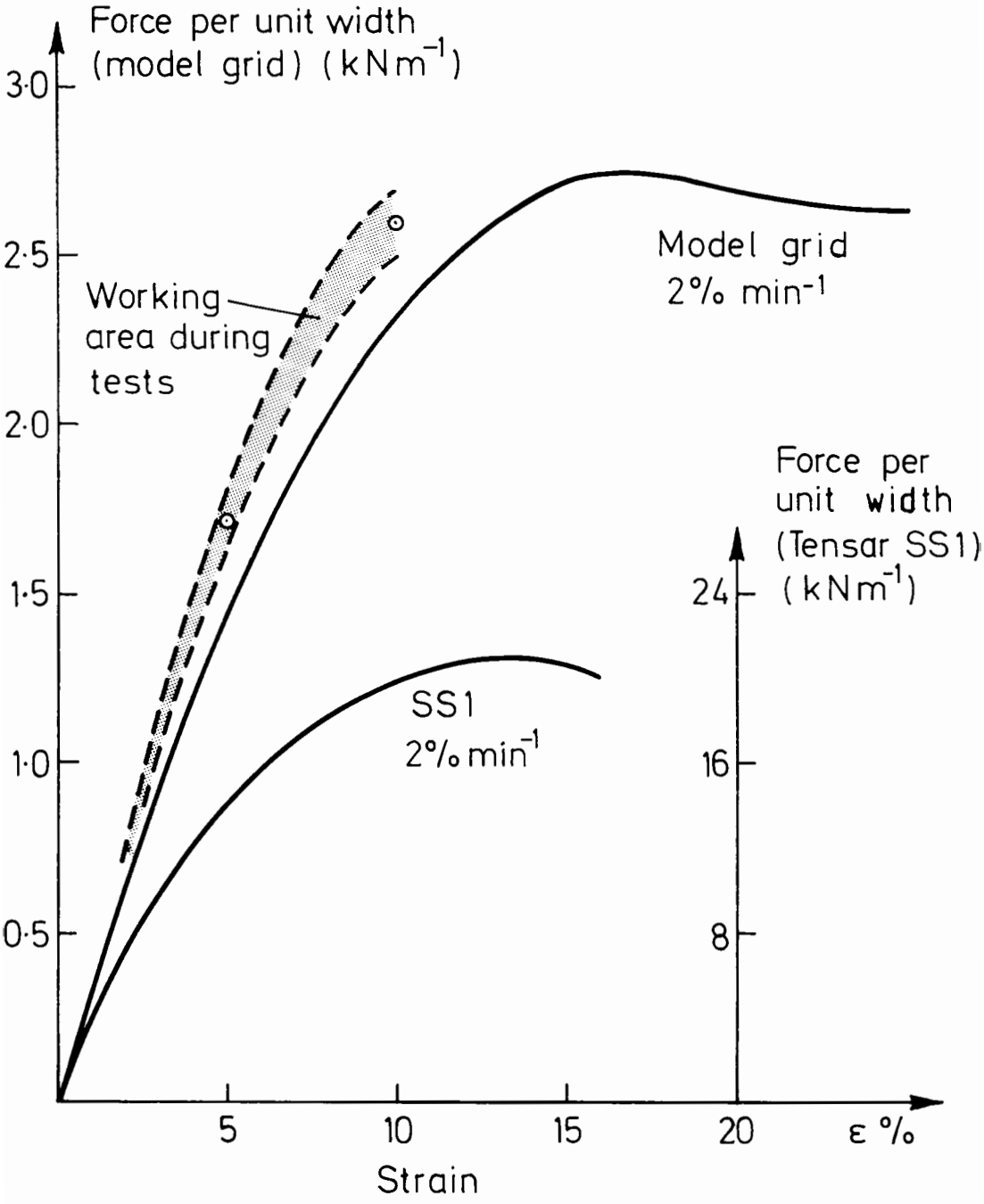

Figure 5.11 Index curves for full-scale and model grid

A polymer material is viscoelastic and has time dependent properties. The faster it is deformed the stiffer it behaves. It was estimated that the average strain rate of the model grid during a test (which took typically 20 seconds) was between 5% and 10% strain min^{-1}, depending on the test (see assumptions in Section 7.2.5). The extent to which the stiffness of the model grid varied with strain rate was investigated and the relevant increase in force per unit width for strain rates of 5% and 10% min^{-1} found to be that shown by the dashed lines in Figure 5.11. Average values for the secant slope of this band at 5% and 10% strain can be measured at 0.34 and 0.26 kNm^{-1}/%. The corresponding full size grid being modelled in these tests is therefore one whose secant slopes are a factor of 16 greater than these values (5.6 and 4.3 kNm^{-1}/% respectively). In Figure 5.13 it is seen that from extrapolation of test data conducted at Strathclyde University (McGown, 1982) these values match those of Tensar SS1 at a strain rate between 6,000 and 10,000 % min^{-1}. An average strain rate of 7.5% min^{-1} for the grid in a

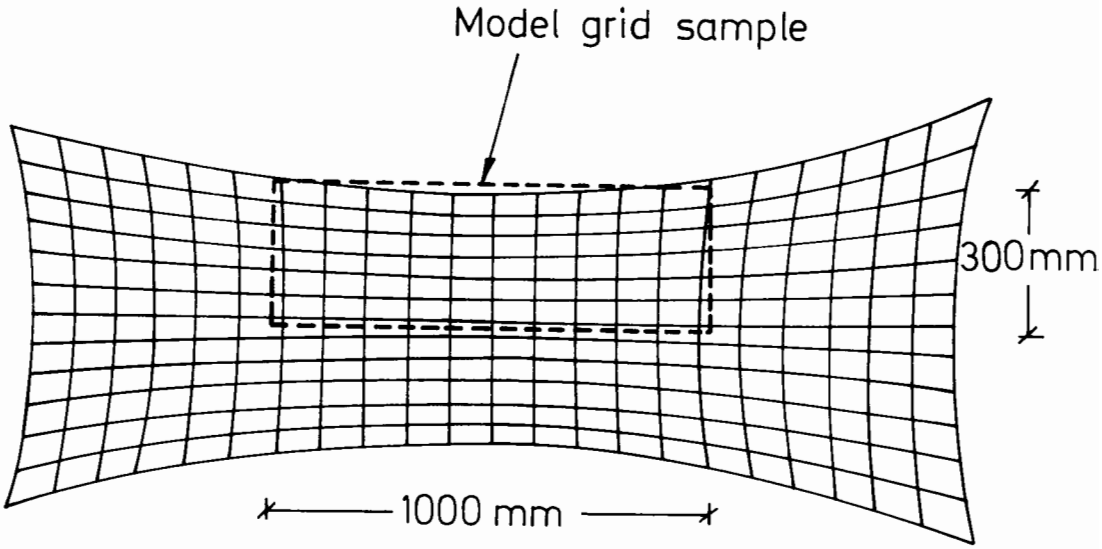

Figure 5.12 Distortions in model grid (Exaggerated)

model test therefore corresponds to the field situation where a full scale Tensar SS1 geogrid is experiencing a strain rate approximately 1,000 times as fast. The loading period for a point beneath a vehicle wheel-load travelling at 30 mph in the field is estimated as being of the order of 1/50th second (cf. 20 seconds in the model test). Thus the factor of 1,000 seems reasonable. It is important to note that the stiffness of the model grid is therefore appropriately scaled for the situation where a single truck causes complete failure of the road system in one pass. It is not appropriate for a long term gradual failure caused by growing rut depth.

All tests on the model grids were conducted at a constant rate of extension in an Instron testing rig, type TT/C . For these tests, samples were typically 14 ribs wide by 16 long, 2 ribs either end being

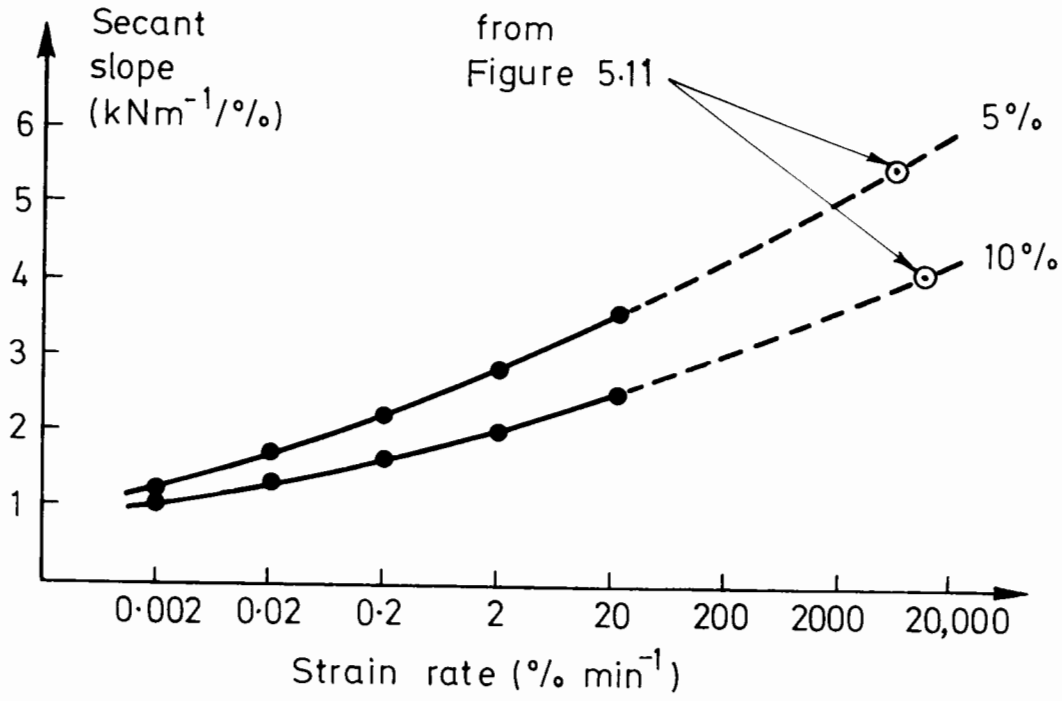

Figure 5.13 Effect of Strain Rate on Secant Slope of Figure 5.11 (at 5% and 10% strain), for Tensar SS1 (after McGown 1982)

cast directly into the clamps on the machine. This was accomplished using the special low melting point alloy, Ostalloy. The gauge length of the sample was measured between the 2nd and 15th ribs, which were embedded in the cast, and averaged 125mm (Plate 5.2), samples always being tested in the primary direction. Before finally choosing the model grid described above, a complete survey of other available grids was carried out. Ten different grids were tested as outlined above using the Ostalloy casts and a 125mm gauge length, the maximum sample width being 110mm. A summary of these tests is presented in Figure 5.14, from which grid 10 was chosen as the most appropriate.

During the main test programme it was considered of great interest to discover what strains the grid was being subjected to. The possibility of attaching strain gauges was discounted for the following reasons:

Plate 5.2 Grid sample with ends cast for extension test

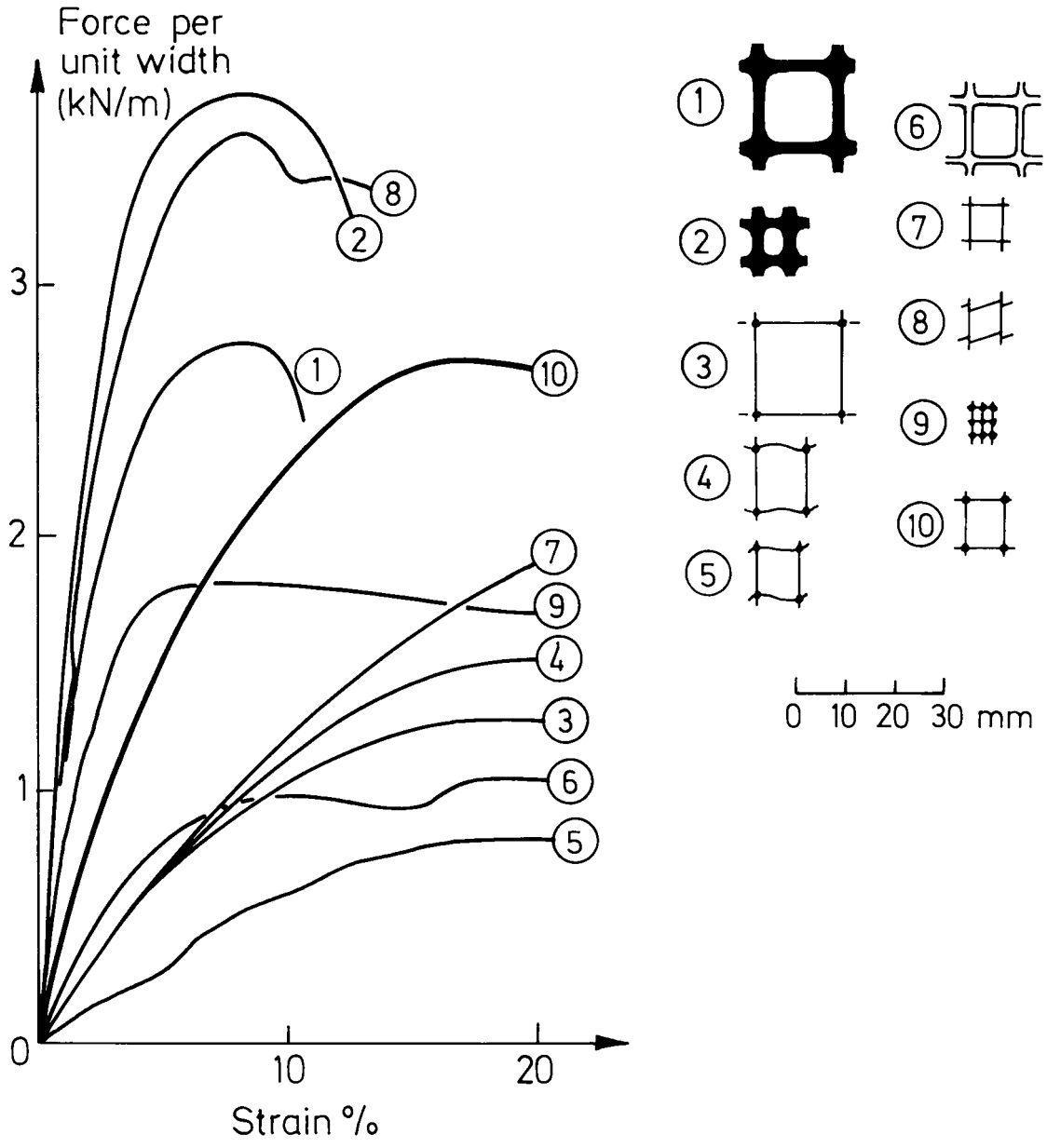

Figure 5.14 Survey of ten types of mini-grid

- relatively large strain magnitudes were involved

- the flimsyness of the grid provided difficulties in attachment

- wires from the device would be pulled out of place during large scale deformations of the system

- the very severe deformation profile of the grid excluded devices of any great length.

Instead, the grid was marked by aralditing 10mm brass washers to every third node along the front edge of the grid. These washers were painted a bright red, and sat vertically against the front perspex face, making them visible to the camera during tests (Plate 5.3). This method had mixed success: many markers became partially or totally obscured by a thin film of clay during the compaction process. Despite this, the exercise was certainly worthwhile and yielded some useful results.

Plate 5.3 Model grid with red markers attached

5.2.3 The Clay

The clay used for the subgrade in this test programme was Speswhite Kaolin, as supplied by the English China Clay Company of St. Austell. Clay powder was mixed with water under vacuum to form a slurry, and then consolidated one dimensionally. At the end of consolidation the sample was allowed to swell under no load for several days, as described in Chapter 2 , to form a very overconsolidated weak clay. This section deals with the Cam Clay parameters associated with the clay.

The consolidation data for clay Samples A-Z are plotted in terms of specific volume, v , and logarithm of mean effective pressure, ln p' , in Figure 5.15 . The points on the virgin 1-D Normal Consolidation Line are taken from the consolidation summaries, such as presented in Figures 3.1 to 3.3 , for when equilibrium was reached at the end of the final increment (Section 4.1.4). In this figure the Normal 1-D Consolidation Line taken from the literature (Steenfelt, Randolph and Wroth, 1981) is shown in bold, corresponding to values of 0.25 for λ and an intercept of 3.58 for N_{1D} at p' = 1kPa . However, values of λ = 0.21 and N_{1D} = 3.30 , as associated with the broken line in Figure 5.15 would seem to fit this data more closely. A value of Ko of 0.56 is assumed.

The value of K_o for 1-D Normal Consolidation can be arrived at theoretically from a comparison between lateral total pressure and the normal applied pressure for times during consolidation when excess pore pressures are zero (see Figures 3.1 - 3.3). There is some scatter between different samples, with values falling in the range 0.5 and 0.6 . The classic expression for K_o during 1-D Normal Consolidation is $1 - \sin\phi'$; taking a value of $\phi' = 26^o$ (Loudon, 1967) gives K_o = 0.56 .

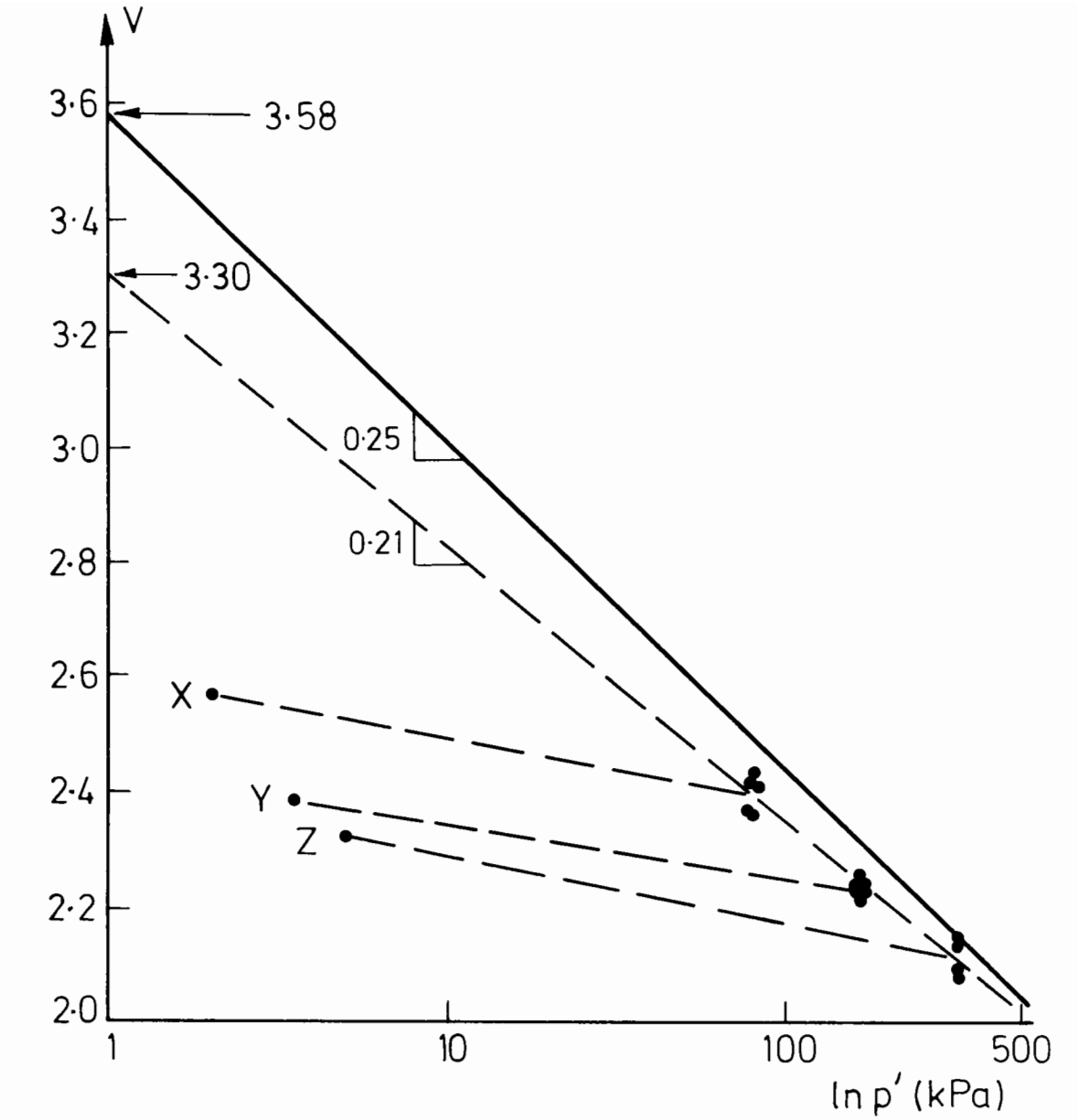

Figure 5.15 Specific Volume plotted against Mean Effective Pressure for end point of consolidation for Samples A-Z

The swelling lines are constructed for the three strengths of sample from detailed knowledge of the sample's average water content and mean effective pressure at the time of testing, as determined by site investigation (Section 5.1.7 above). The coefficient of swelling, κ , is measured approximately at 0.05 .

The coefficient of consolidation, c_v , was calculated for the final increment of load in each of Figures 3.1 - 3.3 . The relevant values for Samples X,J and F , corresponding to vertical stresses of 110kPa , 230kPa and 450kPa respectively, were found to be 11.2 , 13.4 and 13.8 m^2/year .

The gradient of the Critical State Line, M , when plotted on axes of Deviator Stress, q, and Mean Effective Pressure, p' , is a parameter which has little meaning for tests on very overconsolidated clay. Triaxial samples fail due to rupture well before critical state.

CHAPTER 6

ANALYSIS BY DIMENSIONLESS GROUPS

6.1 Dimensionless Groups

6.1.1 Introduction

The usefulness of a model test programme such as this lies in two areas. Firstly by correctly modelling a specific full scale field problem in terms of geometry and strengths of materials, the model test results may be used to predict the performance of that one full scale situation. Secondly, the model tests may be used more generally to try out the effect of a number of variables in several different situations and conduct a parametric study in order to find out which variables are important, and discover what relationships exist between them. This last will be of use in a wide range of field situations since a set of general 'rules' will have been established.

For both ends above the results from this model test study must be presented in non-dimensional form in order to disassociate them from the scale factor of 4 . How to present the data in non-dimensional form requires careful thought. In Chapter 2 it was suggested that the normalised footing load q/C_u depended upon a function of the following variables:

$$\delta/B \ , \ H/B \ , \ \gamma_1 B/C_u \ , \ s/C_u B \ , \ G_2/C_u \ , \ G_1/G_2 \ , \ \gamma_1/\gamma_2 \ , \ \phi'$$

Clearly the footing penetration δ/B and the fill thickness H/B play an

important part, but the role of the last six groups is less obvious. In the case of the last four, very little light is thrown on their importance by the tests conducted here since they are not varied from one test to another:

The ratio of shear modulus to clay strength G_2/C_u is a constant for a given overconsolidation ratio (OCR). Thus in a model where the OCR of the clay subgrade matches that in the field the true relation between G_2 and C_u will be observed. If the OCRs do not match up, but are both large (greater than say 16) the difference in OCR has little effect (Figure 6.1) and an approximately true relation between G_2 and C_u will still be observed. The ratio of unit weights γ_1/γ_2 varies minimally, γ_2 ranging by ±3% between the weak and strong clays. The in-situ magnitude of ϕ', although a difficult parameter to define, is thought not to have varied by much from one test to another, for the reasons outlined in Section 2.2 although compaction will have played a part.

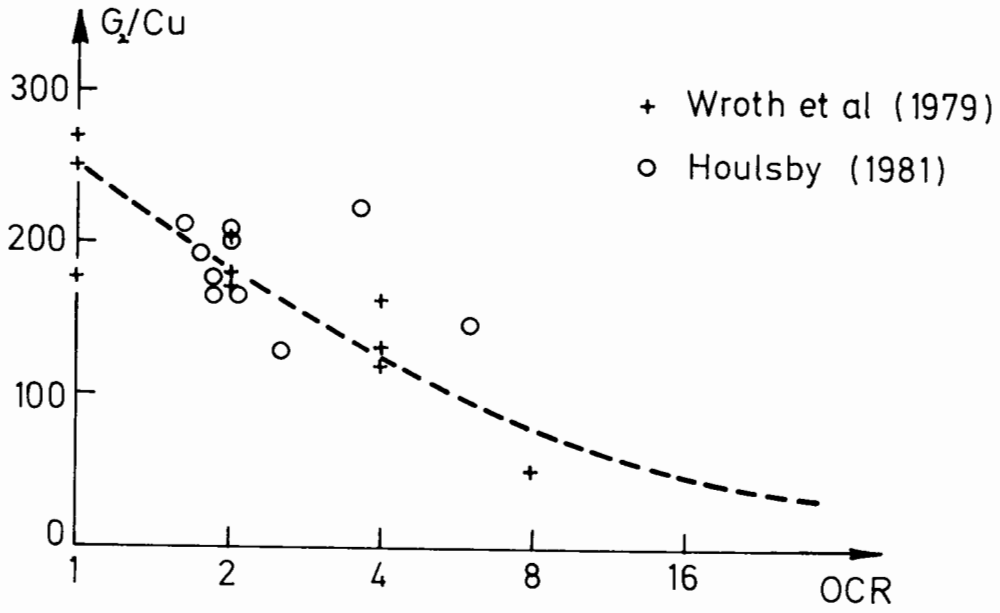

Figure 6.1 Variation of clay Shear Modulus, normalised by C_u, with overconsolidation ratio

Compaction, being more effective on stiffer foundations, is likely to have resulted in slightly higher values of ø' in the thicker fill layers on the stronger clays. Instead of attributing this improvement in performance directly to a change in ø' ,however, this analysis will effectively incorporate it into the improvements in performance attributed to stronger clays and thicker fills. Lastly, the shear modulus of the fill, G_1 ,is also expected to have changed little between tests, any actual changes again resulting from compaction on different foundation stiffnesses. These effects can again be incorporated into the variation of clay strength and fill thickness.

This leaves two remaining variables $\gamma_1 B/C_u$ and $s/C_u B$:

$$q/C_u = f_1(\gamma_1 B/C_u) \qquad \text{.....6.1}$$

$$q/C_u = f_2(s/C_u B)$$

6.1.2 Importance of Fill Thickness

In Figure 6.2a a footing load is shown bearing onto a purely cohesive material. For this situation the ultimate bearing capacity of the footing will be proportional to the undrained shear strength, C_u , of the foundation material.

$$q = A_1 C_u \qquad \text{.....6.2}$$

In Figure 6.2b is shown a second footing load, this time bearing onto a purely frictional material, where the ultimate bearing capacity of the footing can be taken as $1/2\ \gamma_1 B\ N_\gamma$, where B is the width of the footing and N_γ is a function of ø' . For cases where ø' is a constant N_γ also remains a constant, and the ultimate bearing capacity of the footing will be proportional to $\gamma_1 B$:

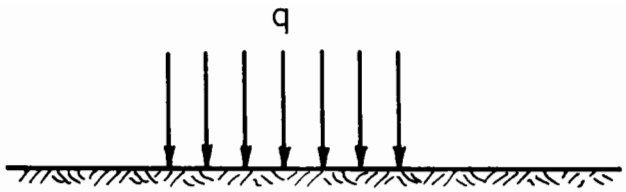

(a) Cohesive

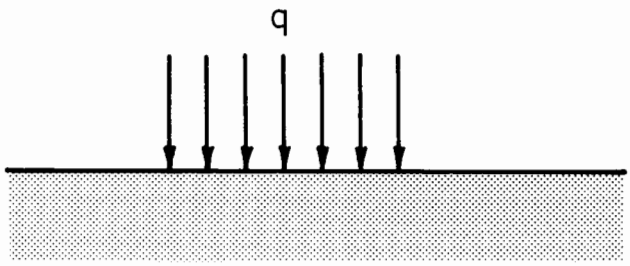

(b) Frictional

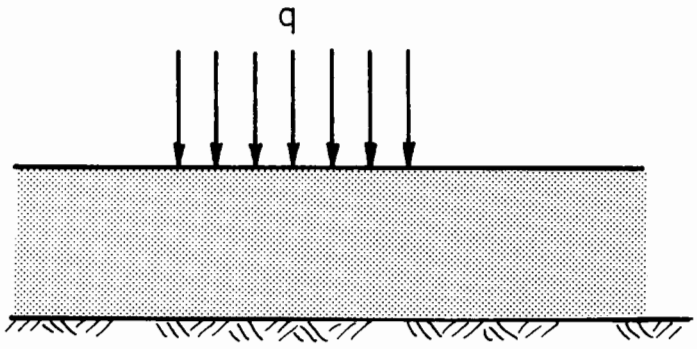

(c) Combination

Figure 6.2 Three types of foundation

$$q = A_2 \gamma_1 B \qquad \text{.....6.3}$$

In the case of Figure 6.2c a third footing load is shown bearing onto a two layer material, the upper layer being purely frictional, and the lower purely cohesive. It seems reasonable to suggest that the ultimate bearing capacity of the footing will now be governed by a combination of Equations 6.2 and 6.3 , the simplest combination being of the type:

$$q = A_3 C_u^m (\gamma_1 B)^n \qquad \text{.....6.4}$$

where n >> m for a very thick fill layer, and m >> n for a very thin fill layer. For dimensional consistency in the equation, if A_3 is dimensionless then the sum of m and n must be unity. Dividing both sides of Equation 6.4 by C_u , the following is arrived at:

$$q/C_u = A_3 (\gamma_1 B/C_u)^n \qquad \text{.....6.5}$$

Thus the ratio $\gamma_1 B/C_u$ is merely a measure of the relative strengths of the two layers in this fill/clay system, where the parameter n is a function of the fill thickness H/B , and possibly the footing penetration δ/B . It would seem appropriate therefore to look at test results in the light of the dimensionless group $q/C_u^m(\gamma_1 B)^{1-m}$, and attempt to find the relationship between between m and H/B .

The dimensionless group $s/C_u B$ of Equation 6.1 must also be considered, however. In the last paragraph it was assumed that A_3 of Equation 6.4 was a constant. Suppose in fact that it is not, and can be rewritten as:

$$A_3 = A_4 (s/C_u B)^k \qquad \text{.....6.6}$$

where A_4 is a constant. Rewriting Equation 6.5 gives:

$$q/C_u = A_4(s/C_uB)^k(\gamma_1 B/C_u)^n \quad \text{.....6.7}$$

A_4 must also be dimensionless, so that $k + m + n = 1$. In which case $q/(s/B)^k C_u^m(\gamma_1 B)^{1-k-m}$ becomes the most relevant dimensionless group for plotting up test results. Information is now needed on how k and m vary with H/B and δ/B.

6.2 **The Test Data Reduced to Dimensionless Form**

The complete set of Load-Penetration data for the central tests from the main testing programme is summarised in one table (Table 6.1). This table gives the footing load measured at each of four footing penetrations in each test, and the relevant individual clay shear strength values for normalising associated with each test. In addition, the equivalent data-set for each of the 'subgrade-alone' side tests is shown in Table 6.2.

6.2.1 Tests With No Fill Layer

The data from Table 6.2 is shown plotted in normalised form in Figure 4.2. In this one figure 18 curves of footing load normalised with respect to a variety of clay strengths, C_u, are represented and for the amount of data the extent of scatter is strikingly small. By drawing a single curve through the middle of the thin band of curves gives further confidence in the data because it agrees well with a classical

TABLE 6.1 LOAD-PENETRATION DATA FOR CENTRAL TESTS

	A1M	A2M	B1M	B2M	C1M	C2M	D1M	D2M	E1M	E2M
C_u	6.0	5.9	8.9	8.8	15.2	12.7	5.6	5.6	8.5	8.2
δ/B										
0.05	29.1	29.2	45.9	35.2	71.7	36.8	41.6	40.1	55.4	35.7
0.1	40.9	41.7	69.6	48.4	98.6	54.3	49.6	53.7	74.1	49.5
0.2	47.3	57.3	86.9	55.6	127.2	71.1	51.2	64.0	94.4	59.6
0.5	50.7	76.4	108.0	67.7	157.6	93.2	54.4	82.7	117.5	68.2
	N	R	R	N	R	N	N	R	R	N

	F1M	F2M	G1M	G2M	H1M	H2M	J1M	J2M	K1M	K2M
C_u	13.3	13.0	5.9	5.8	8.8	8.5	8.8	8.0	14.8	13.5
δ/B										
0.05	41.6	63.8	46.7	49.9	61.5	41.6	60.2	44.8	66.2	81.5
0.1	68.6	87.2	61.1	67.7	82.9	54.5	89.7	58.1	81.3	107.6
0.2	91.6	114.1	66.1	81.0	104.8	63.4	117.1	67.1	87.5	137.2
0.5	103.6	148.0	61.5	96.8	126.2	68.5	135.7	73.4	99.8	157.6
	N	R	N	R	R	N	R	N	N	R

TABLE 6.2 LOAD-PENETRATION DATA FOR CONTROL TESTS ON CLAY ALONE

	A1R	A2R	B2R	C1L	C2L	D2L	E1R	E2R	F1R	F2L
C_u	6.6	6.2	9.4	17.2	13.5	6.1	9.6	8.7	14.4	13.7
δ/B										
0.05	28.3	20.8	31.0	61.1	54.0	24.0	34.5	29.8	52.6	43.0
0.1	38.6	30.0	43.2	86.7	68.5	33.1	48.4	39.0	73.4	63.5
0.2	41.4	34.5	49.9	98.8	84.9	38.6	57.4	45.5	86.3	84.1
0.5	45.0	38.0	59.4	112.3	99.4	44.1	63.8	55.4	101.0	–

	G1R	G2R	H1L	H2L	J1L	J2R	K1R	K2R
C_u	5.9	5.9	10.5	9.0	10.3	9.1	15.7	14.2
δ/B								
0.05	26.8	19.6	35.8	33.7	36.6	28.6	46.2	43.2
0.1	33.4	27.5	51.0	47.9	53.9	42.0	74.1	60.4
0.2	37.8	32.5	61.0	56.2	66.1	51.4	87.3	73.4
0.5	41.1	39.1	71.1	64.0	–	62.8	111.6	90.6

Notes

1. All values of footing load and C_u in kPa
2. δ/B represents the footing penetration, δ , normalised with respect to the footing width, B
3. R refers to a reinforced test; N to an unreinforced test

result: the onset of large plastic deformations can be seen to start at a load of approximately $q/C_u = (\pi + 2)$, while the first departure from purely elastic behaviour starts at approximately $q/C_u = \pi$. Since no particular trend of test data for any one particular strength of clay lying in any one area of the band can be seen, it can be concluded that the small amount of scatter that is seen is random and merely due to experimental error. Either there has been more friction at the sides of the footing in one test, or the individual clay strength used for normalising in another is not truly representative of the clay under that footing due to some inhomogeneity.

6.2.2 Tests with Fill Layer

In Figures 6.3a,b and c the Load-Penetration data for tests on fill thicknesses of 50mm, 75mm and 100mm respectively are plotted, on axes of q/C_u vs δ/B . It will immediately be noted that the 'scatter' of results is much greater than it was in Figure 4.2 . In addition, it can be seen that the 'scatter' of results gets worse with increasing fill thickness. On further inspection it is seen, in reinforced tests and unreinforced tests alike, that the tests on the weaker clays consistently show the greater values of q/C_u for a given footing penetration. The conclusion is that it is not merely random 'scatter' which is being observed in these figures, but that q/C_u is simply not an appropriate group for plotting this data: the data plotted in this form is not independent of clay strength.

In Figure 6.4 the effect of plotting the data in terms of q/C_u^m where $m < 1$ is explored. The actual numbers on the y-axis are irrelevant: it

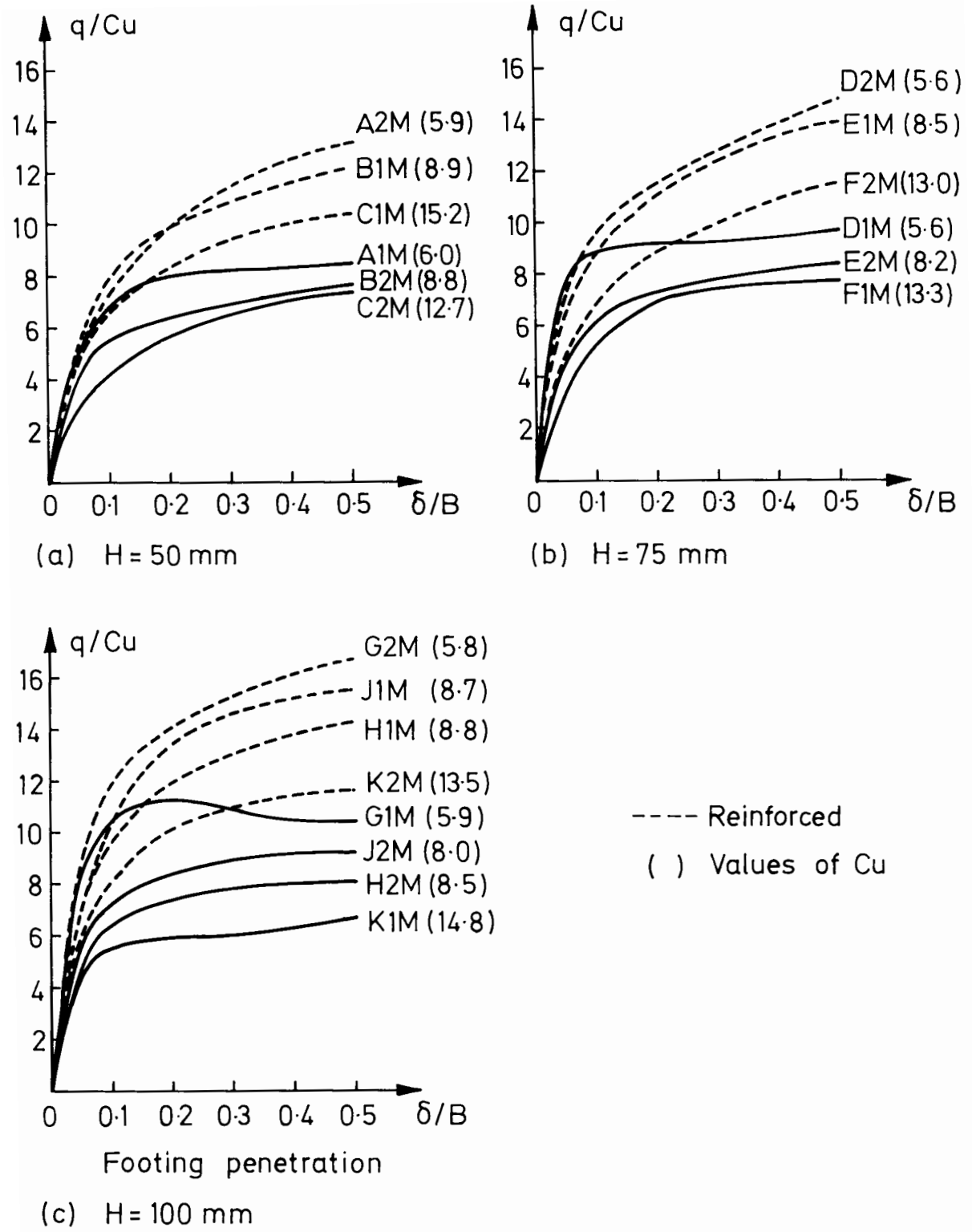

Figure 6.3 Footing Load data, normalised by C_u, plotted against normalised Footing Penetration and grouped according to Fill Thickness

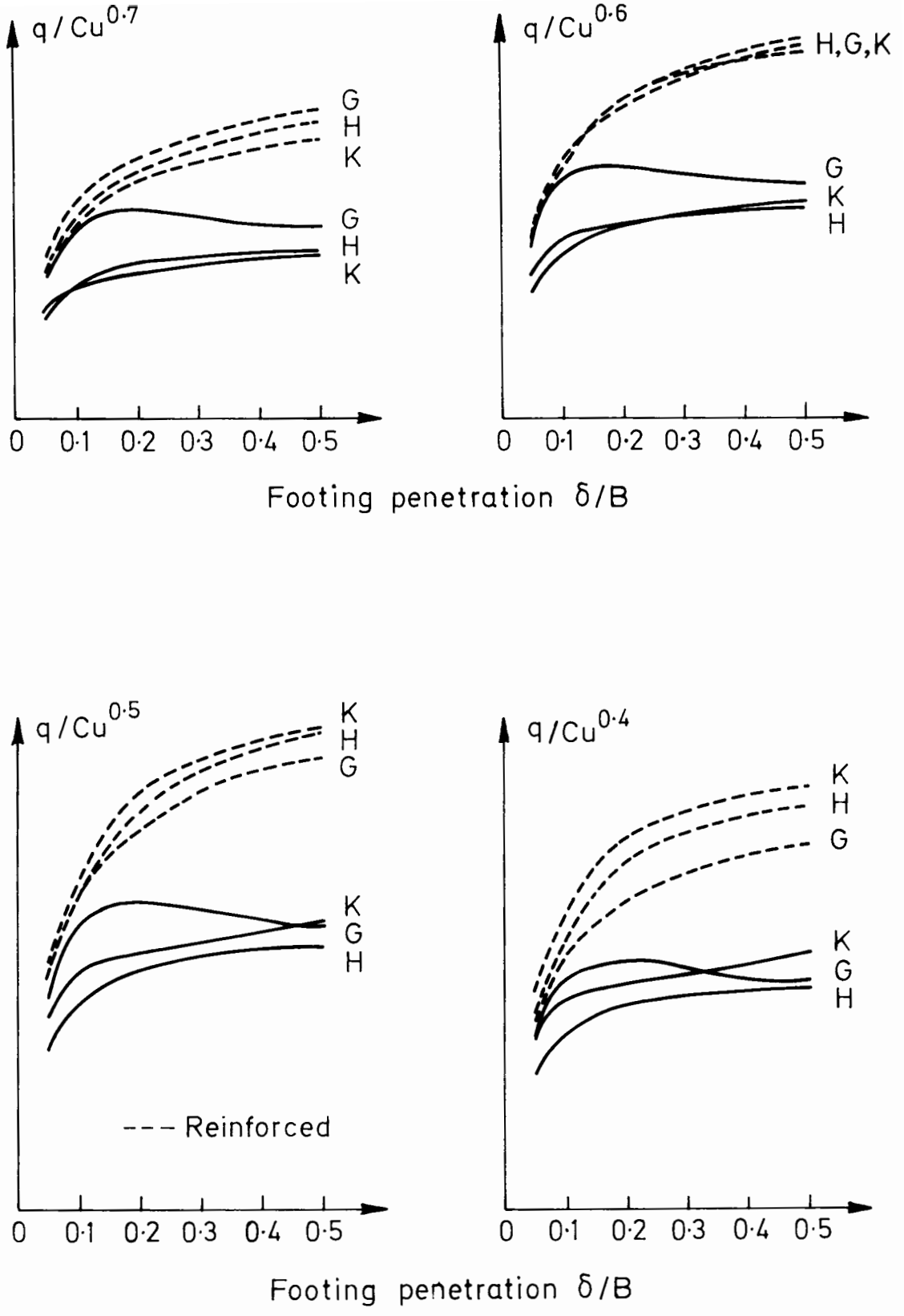

Figure 6.4 Effect of varying the parameter m in the expression q/c_u^m for tests on 100mm fill thickness (Samples G, H and K)

is the focussing or grouping of the test data onto an unique curve which is important. It can be seen by eye perhaps that while a value for m of 0.6 would seem best for reinforced tests on 100mm fill in Figure 6.4 , a value of 0.4 seems more appropriate for the unreinforced tests. When a statistical analysis was conducted on the test data for each fill thickness it was found that the values of m for which the least amount of deviation from a mean were found to be those plotted in Figure 6.5 and that two separate curves emerged: one for reinforced tests and one for unreinforced tests. It would seem therefore that the arguments of Section 6.1 above are on the right track: while q/C_u is the appropriate

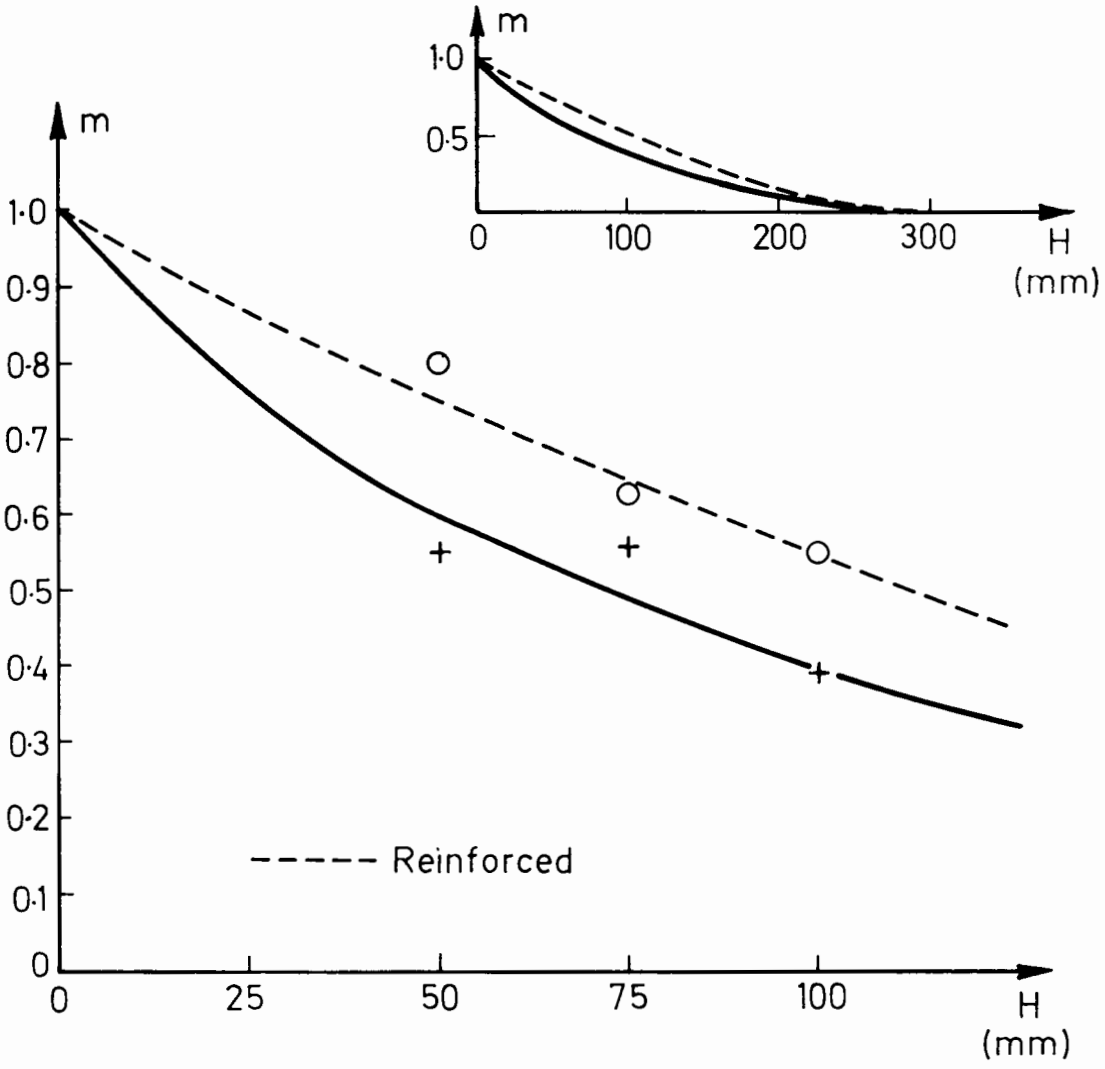

Figure 6.5 Variation of the parameter m with Fill Thickness

ordinate for when no fill layer is used, successively less dependence on C_u should be reflected in the ordinate for tests on increasingly thicker fill layers. It would be expected in addition that m would be a function of the stiffness of the grid.

6.2.3 Reinforced and Unreinforced Test Trends

The downward trend of m with increasing fill thickness for both reinforced and unreinforced tests is a logical one. The influence of clay strength on the bearing capacity of the system would be expected to decrease with increasing fill thickness. Of particular importance, however, is the distinction between reinforced and unreinforced tests. The bearing capacity of a reinforced system is governed more strongly by the strength of the clay for a given fill thickness than the corresponding unreinforced test. This is relevant since it emphasises the greater role of the clay subgrade during a reinforced test. The grid seems to cause more involvement of the clay, which is a result that backs up similar conclusions made from the marker displacement plots in the next chapter. Extending this result to even greater fill depths (see inset, Figure 6.5), the distinction between the two curves is assumed to tail off. Finally there will be a fill depth at which the strength of the clay subgrade will play no part, whether the fill is reinforced or not. This appears to be approximately H = 4B by extrapolation.

Having determined the variation of m with fill thickness H/B , the dimensionless group $q/(s/B)^k C_u^m (\gamma_1 B)^n$ from Section 6.1.2 can now be reconsidered. It has been established that m not only varies with H/B but also with the stiffness of the grid, s , so that the above group might be best simplified by assuming k to be zero, and incorporating

$s/C_u B$ into the value for m . Unfortunately there is no test data to settle this either way, all the reinforced tests being conducted with the one grid stiffness. It seems reasonable to assume that if k is not zero, at least it is small: m is relatively large for small fill thicknesses, and if n can be expected to be equally as large at large fill thicknesses, this leaves a relatively small value for k throughout, since $k + m + n = 1$. Although it is appreciated that grid stiffness is an important factor, small differences in grid stiffness between grids above a certain adequate level of stiffness are probably not significant.

It should be emphasised that it is in-plane, and not bending, stiffnesses which are being discussed. The latter property of the grid used in these tests was very low and no information is offered as to how any significant bending stiffness would have affected results.

6.2.4 3-D Model

The dimensionless group $q/C_u^m(\gamma_1 B)^n$, where $m + n = 1$, is best described with the 3-D picture shown in Figure 6.6 . Curves 1 , 2 and 3 show data for unreinforced tests on three different subgrades, in decreasing order of strength, for a given fill thickness to footing width ratio, H/B (as defined by Plane A), and a given footing penetration. It can be seen that when viewed on Plane C , for which q/C_u is plotted against H/B , the points are 'out of focus', while at the relevant value of m the three curves coincide. Plane B corresponds to a different fill thickness, and contains curves 4 , 5 and 6 . These correspond to unreinforced tests on the same clay subgrade strengths as 1 , 2 and 3 and an identical footing penetration. Again the three points are seen out of focus on Plane C : more out of focus this time because the focus point

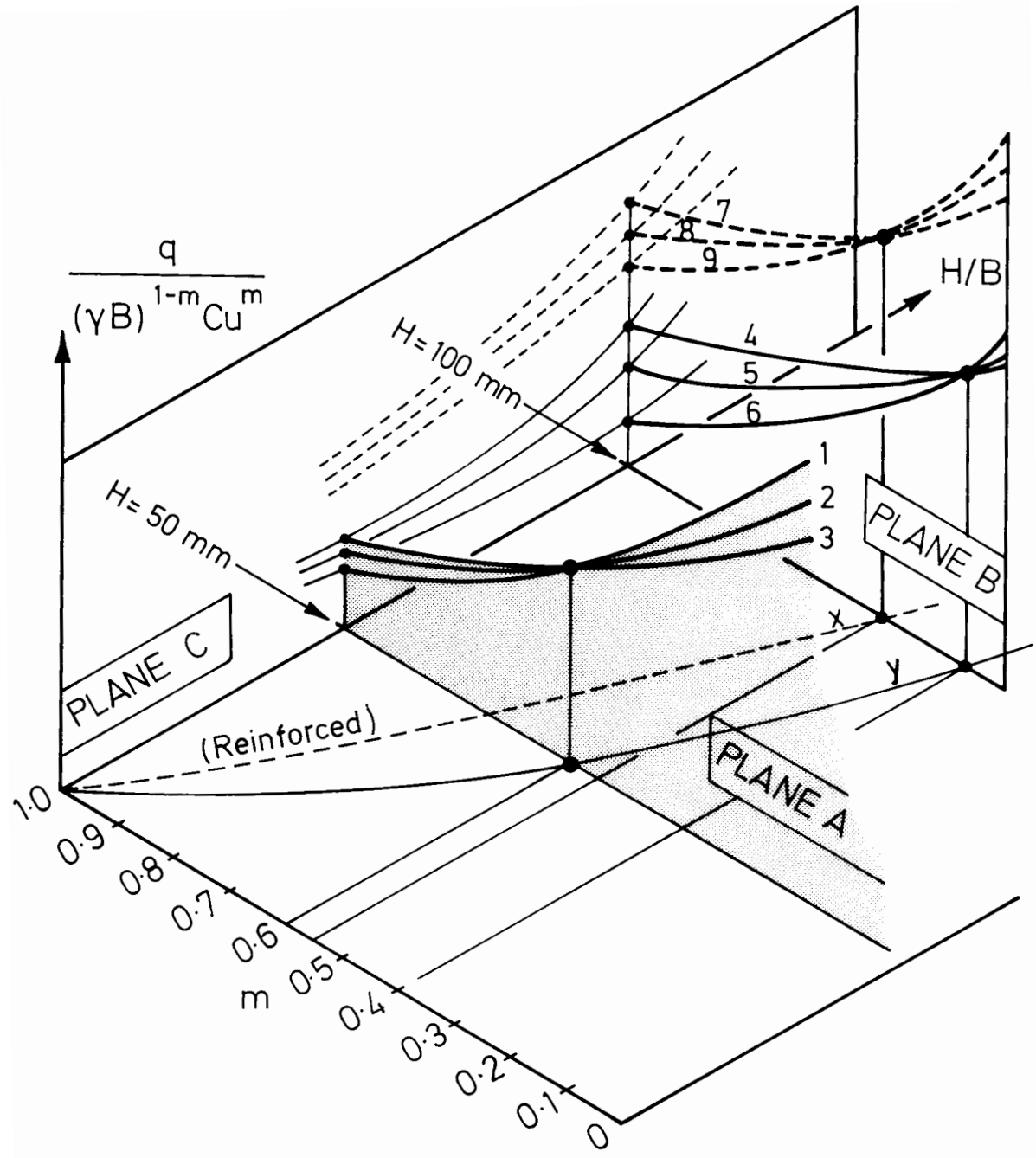

Figure 6.6 Three-dimensional picture

lies further back from C at a smaller value of m . Curves 7 , 8 and 9 on Plane B again represent the same clay strengths and footing penetration as before, but for a reinforced test. This demonstrates how the focus points for reinforced tests lie nearer to Plane C than those for the equivalent unreinforced tests.

This model can be made to fit the test data very closely. By taking the lines of best fit as calculated numerically for values of m = 0.4, 0.5, 0.6 in the unreinforced tests and m = 0.55, 0.65, 0.75 for the reinforced tests on fill thicknesses of 100mm, 75mm and 50mm respectively, the locus of focus points which lie on the two vertical surfaces above curves x and y may be constructed. This is presented in Figure 6.7 which in fact summarises the whole test data-set but is of such a form that does not readily allow quick visual comparison between the performance of reinforced and unreinforced systems. In conjunction with Figure 6.5 it can be used to regenerate every Load-Penetration curve used in its construction, and any number of others besides. Also, for convenience in Figure 6.7 , $\gamma_1 B$ has been taken as unity, so that the number scale on the ordinate is false. For each value of $\gamma_1 B$ chosen, not only will a corresponding change in the scale be necessary, but also a change in the shape of the curves themselves, due to the changing power of $\gamma_1 B$ across the page.

Thus, despite the correctness and completeness of Figure 6.7 , it is an inconvenient and a rather meaningless manner in which to present data. Instead, the information is represented in a simpler and more visually communicative way in Figures 6.8a b and c . These figures each represent a view of Plane C (of Figure 6.6), and therefore show q/C_u vs H/B . The strength of the clay subgrade is not now irrelevant,

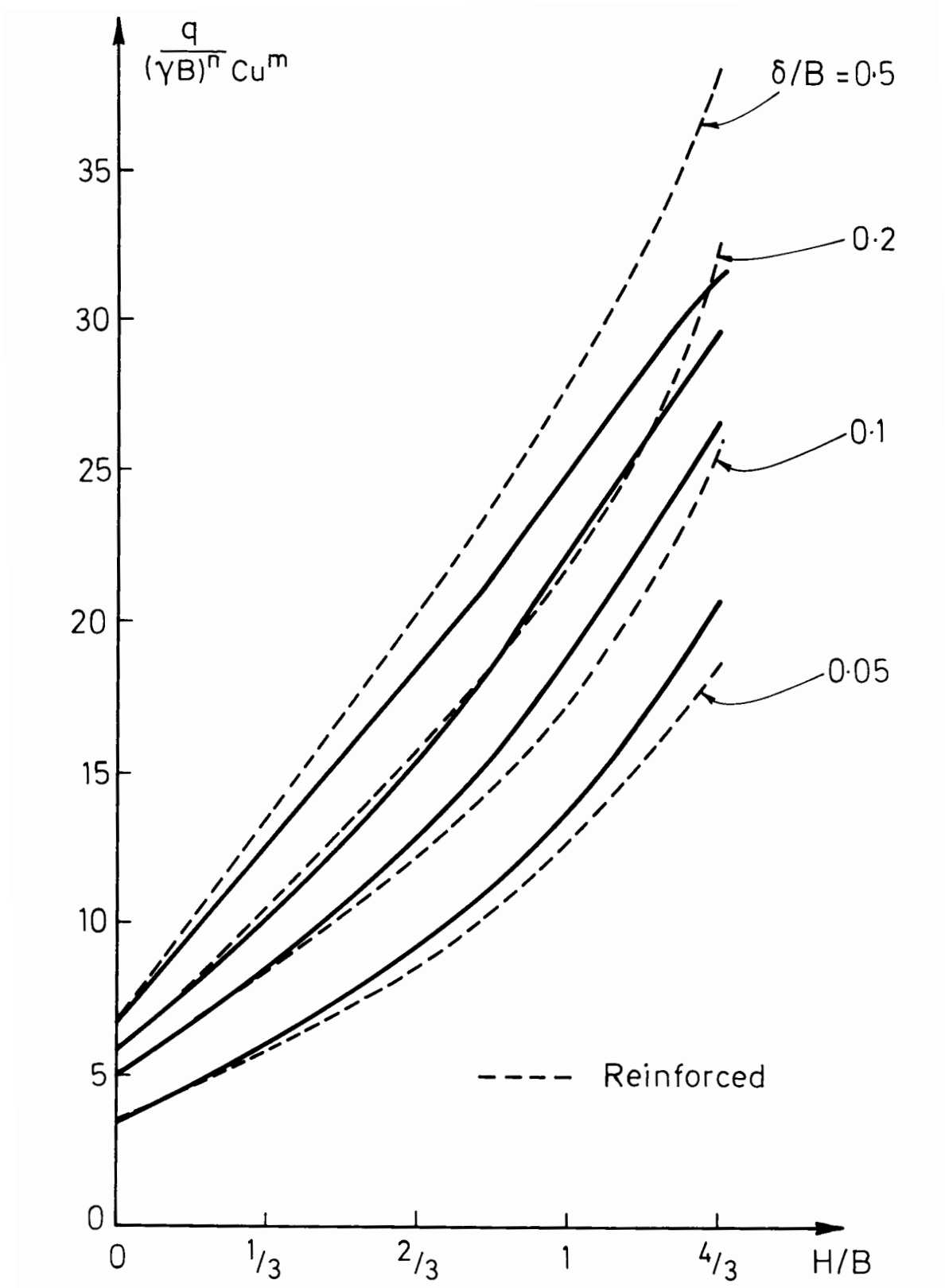

Figure 6.7 Summary of data set in non-dimensional form, normalised Footing Load versus normalised Fill Thickness (γB taken as unity)

and so separate curves are drawn for each subgrade strength $C_u/\gamma_1 B$. Several points arise from these plots:

- the reinforced and unreinforced tests are assumed to behave identically when there is no fill layer, due to lack of any restraint on the grid without a fill layer

- the depth of fill at which adequate restraint for the grid is provided by the fill layer would seem to be approximately 1/2B . For fill layers thicker than this the benefit of the grid appears to remain constant

- the benefit of the grid shows no signs of declining with increasing fill thickness over the range of thicknesses tested, throwing no further light on the limit of H/B = 4 suggested by the 'm' plot of Figure 6.5

- in unreinforced tests, the improvement of bearing capacity provided by increasing fill layer thickness shows different trends over the three ranges of clay strength tested. While for the weakest clay additional fill thickness always improves performance, in the case of the strongest clay a thin fill layer actually decreases bearing capacity slightly before going on to improve it.

The value of γ_1 was measured at 19.0 kN/m^3 , giving $\gamma_1 B$ a value of 1.43kPa . Strictly Figures 6.8a, b and c correspond respectively therefore to values of 4.2 , 6.3 and 9.8 for $C_u/\gamma_1 B$. To qualify this, the nominal values of C_u adopted throughout this chapter correspond to the strength of the clay as measured at a depth of 55mm , the depth to the centre of the shear vane. Normalising this figure with respect

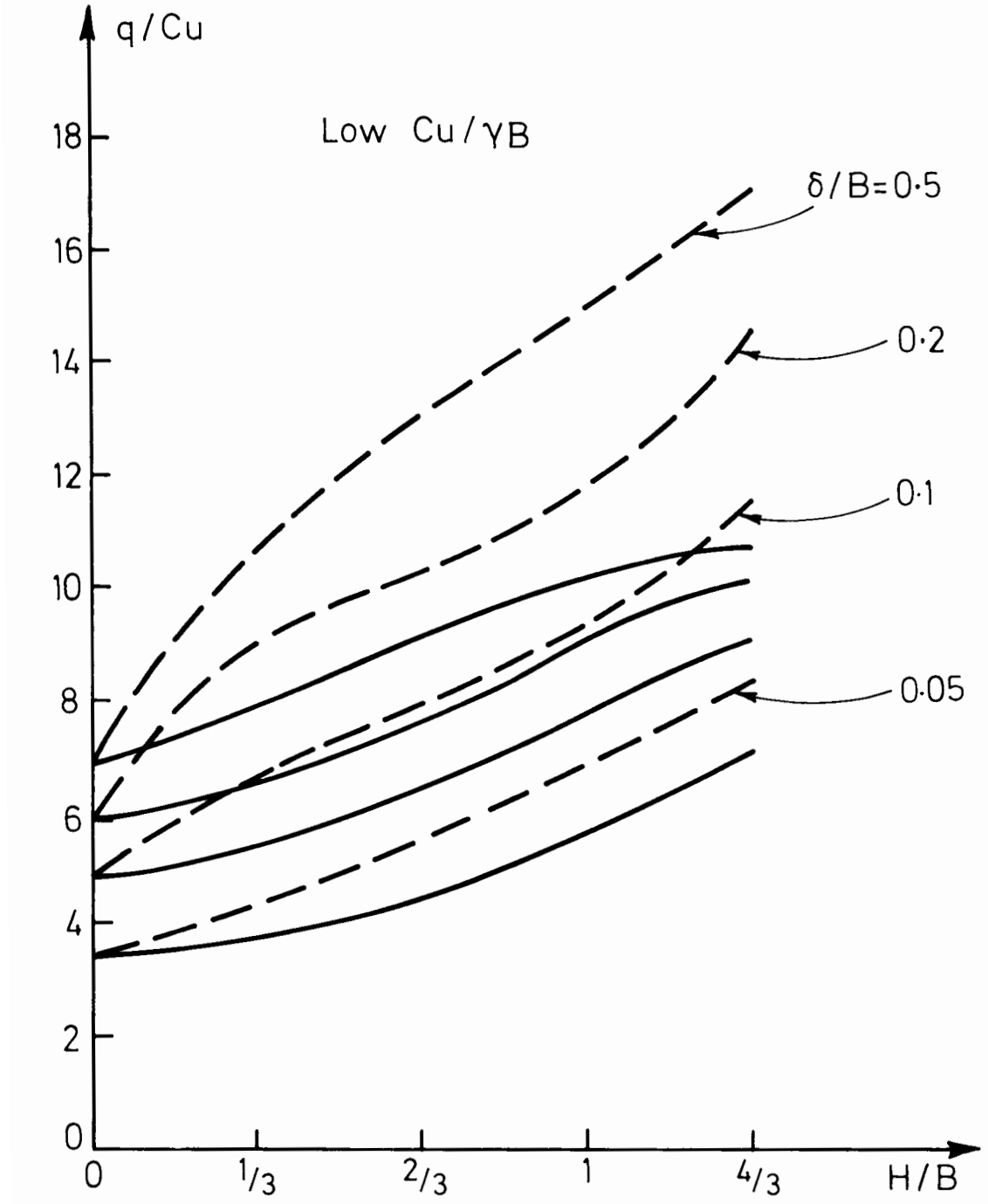

Figure 6.8a Summary of data for tests on clay of nominal strength C_u = 6kPa, normalised Footing Load versus normalised Fill Thickness (γB taken as unity)

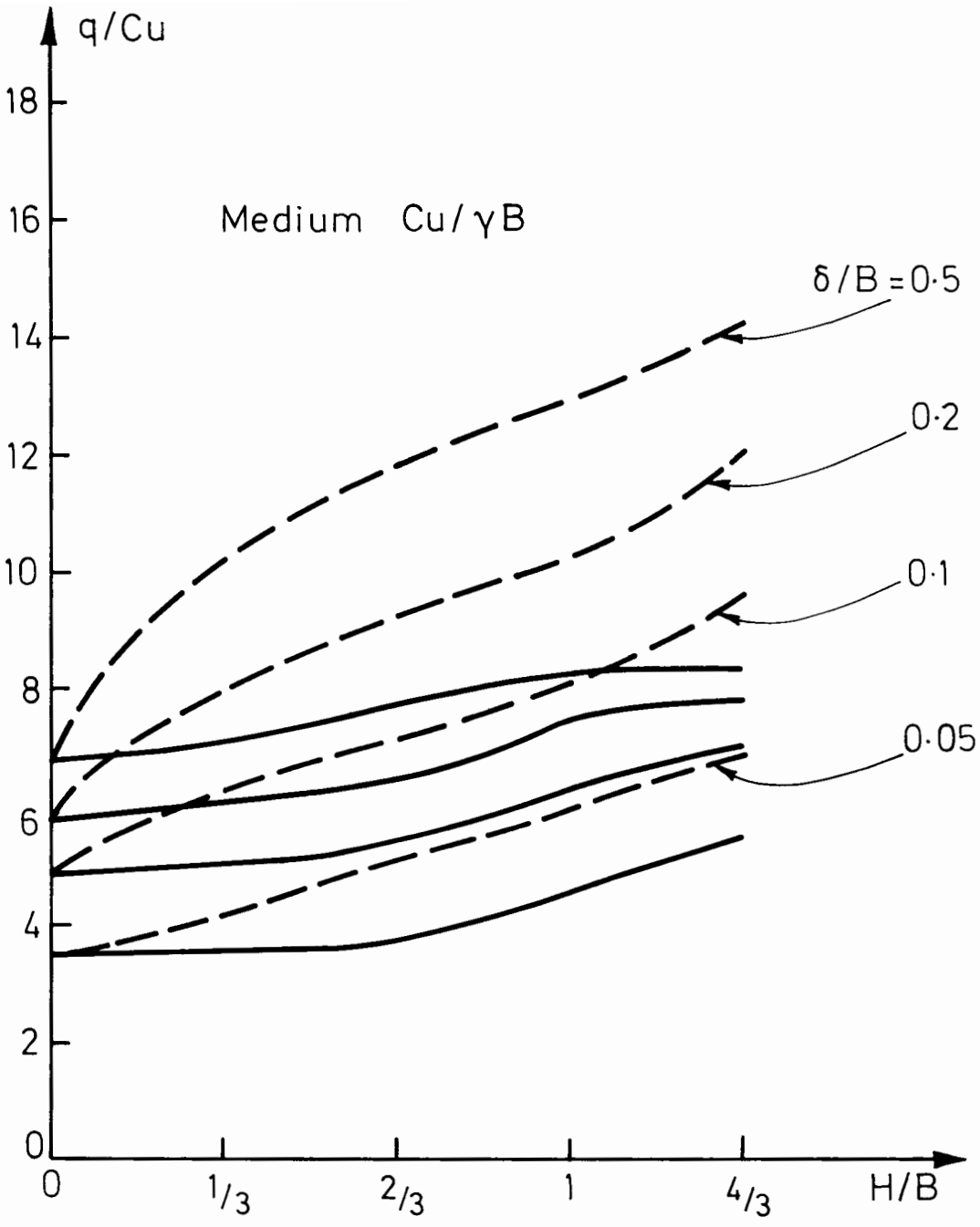

Figure 6.8b Summary of data for tests on clay of nominal strength C_u = 9kPa, normalised Footing Load versus normalised Fill Thickness (γB taken as unity)

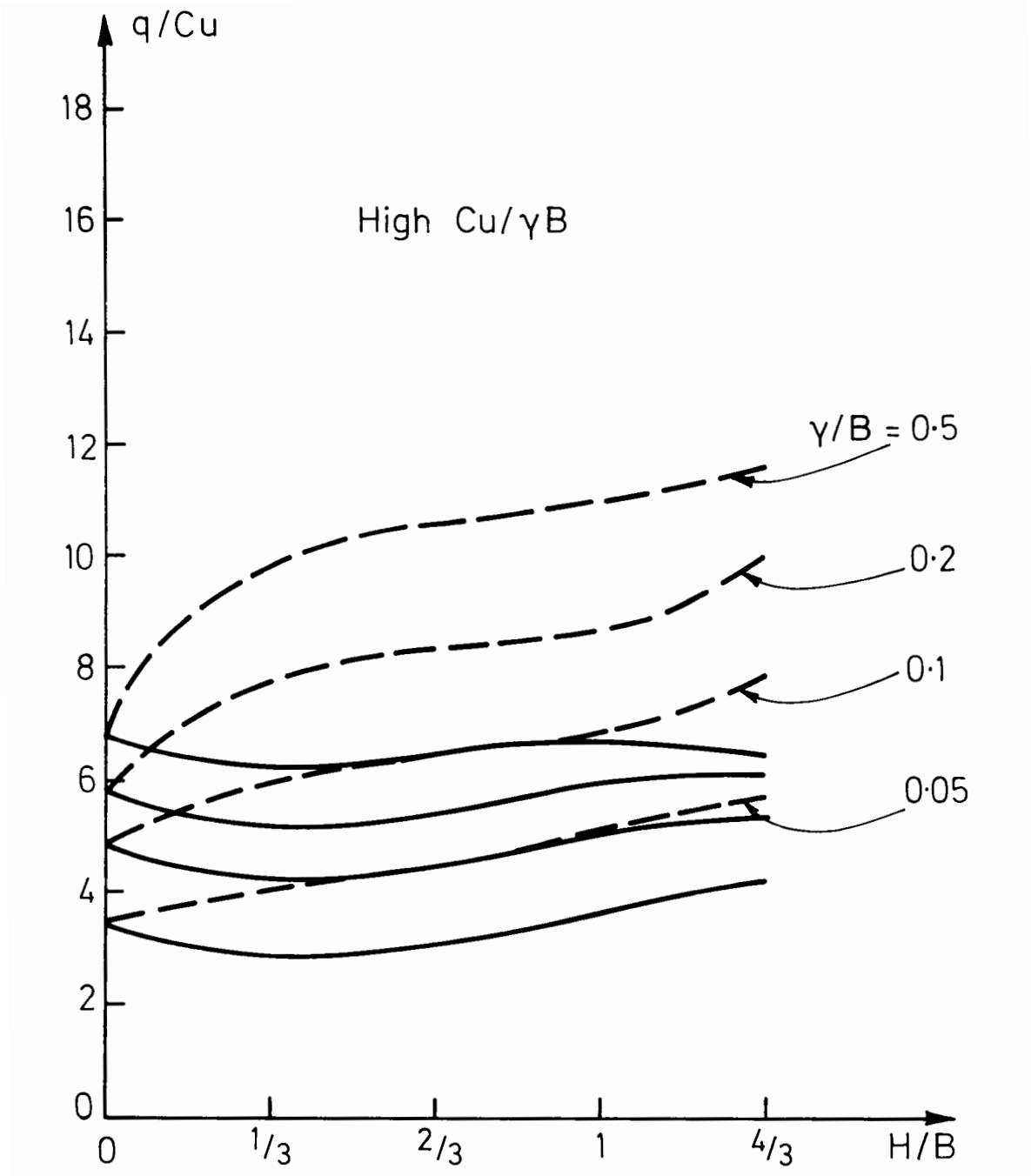

Figure 6.8c Summary of data for tests on clay of nominal strength c_u = 14kPa, normalised Footing Load versus normalised Fill Thickness (γB taken as unity)

to footing width gives a value of 0.73 . At full scale, therefore, corresponding subgrade shear strengths must also be estimated for the same depth. Secondly, due account must be taken of the differences in the shear strength with depth profiles used in these tests (Figure 5.4) and those measured for any particular field location: surface crust effects and vegetation will certainly cause complications. There are also many other areas in which difficulty will be met in trying to relate test results directly to a full scale field situation, not least in the matter of compaction. For this reason Figures 6.8a,b,c are simply labelled respectively 'low', 'medium' and 'high' $C_u/\gamma B$ instead.

The model makes a valuable contribution as a method of identifying the interactive relationships between the main variables. It also provides a body of data from a relatively well controlled situation, against which any numerical analysis may be rigorously checked and calibrated for its development.

CHAPTER 7

MARKER MOVEMENTS IN THE CLAY

7.1 Introduction

7.1.1 The Camera

The clay face was covered with a 15mm square grid of lead shot markers, diameter 1mm , as described earlier (Section 3.1.4). The movement of these markers during each main test was recorded by a series of slides taken with an OM1 camera mounted on a tripod, using power drive. The number of exposures per test varied from 8 to 20 . A 135mm lens was used for the close-up pictures taken during a test, while a 50mm lens was used for more general wider-angled pictures before and after each test. The film used was Kodak Ektachrome ASA 400 .

7.1.2 The BITPAD

A specially modified De Vere 203 type enlarger was used to project the slide vertically down onto a flat table. Bolted to the table was a 300mm by 300mm Summagraphics BITPAD digitising board, onto which the image of the slide was focused (Plate 7.1). The BITPAD cursor, consisting of a 20mm diameter viewing window inscribed with two fine crosshairs, and four buttons, can be moved to any point on the surface of the pad. Pressing any one of these buttons immediately returns the X-Y coordinates of the intersection of the crosshairs, in mm ±0.1mm , to the monitoring device, in this case a 380Z micro computer, IEEE-linked.

Plate 7.1 BITPAD and enlarger

These coordinates were recorded onto floppy disk together with a flag denoting which button had been used, according to a simple control program written in BASIC (Houlsby 1984). The careful digitising of a large number of individual markers (600 plus) with each point being measured twice, necessarily took a long time (approximately 45 minutes per slide). Commercial photographic enlargers are not designed for such long exposures and modifications to the cooling system around the bulb were necessary to prevent over-heating. An enlarger was found to be more suitable than a simple slide projector, since it was imperative for the image to remain perfectly still during this time. The enlarger-BITPAD table was surrounded by a heavy curtain to exclude any other light.

7.1.3 Reference Points

In order to make true comparisons between successive slides in a test, corrections must be made to each set of marker coordinates to take account of the variations in scale and position at which each slide was digitised on the BITPAD . Account must also be taken of local distortions introduced into each slide due to processing and projecting inconsistencies. There is in addition a global distortion introduced to each set of slides arising from the camera not being perfectly normal to the front face of the box, the extent of which will be different in each test.

For this purpose a grid of stationary reference points were stuck onto the front face of the test-box. The coordinates of these points, measured accurately, provided the necessary reference frame against which all distortions could be corrected for and all true marker movement could be measured.

7.1.4 Procedure

The procedure for measuring each slide consisted of first digitising the reference points. The upper and lower profiles of the fill layer were then recorded , followed by the outline of the footing itself which, by suitable use of flags, were subsequently treated as continuous line segments instead of discrete points.

The positions of the markers themselves were digitised in sections. This was always done in a specific order, labelling any missing markers which may have disappeared from view behind the metal support frame or which had become obscured by excessive clay movement. This whole

exercise was repeated.

The session was terminated by re-measuring the set of reference points. After each slide had been digitised, the data files were transferred from the floppy disks on the micro-computer to the larger departmental VAX system computer where this data was processed.

7.1.5 Computation

The data files were briefly processed by a FORTRAN program (Houlsby 1984) where the user was required to assign a number to each recorded point, the program automatically recognizing any doubly or multi-recorded points. These processed data files were then run in a much larger FORTRAN program (Houlsby 1984) to compute the true position of each point in each slide at full scale using the reference point coordinates to correct for translation, rotation and scale effects from the digitizing process and for distortional effects from within the picture itself. The program was able to present plots of marker movement between two slides by simply drawing a line vector from the old to the new marker positions. It could also compute and plot the principal strain magnitudes and directions at the centre of each area enclosed by data points. Naturally any continuous profiles digitised such as the top and bottom surfaces of the fill and the outline of the footing could be included in these plots.

The errors arising in this process depended mainly on the following:

- the accuracy with which the operator placed the crosshairs of the cursor on each point

- the accuracy to which the BITPAD returned the coordinates of the crosshairs

- any movements of the projected image itself during the measuring process

- the accuracy with which the reference point coordinates were measured at full scale

- the accuracy to which the reference elements were able to take account of the photographic distortions in the picture

The small errors introduced through refraction in the 25mm thick perspex face of the test box, and refraction in the 1mm thick viewfinder on the cursor are included under general 'photographic distortions'.

In order to appreciate the extent of these errors, two slides were taken of the same set of points and measured up independently. When run on the plotting program the results for displacements and strains were as shown in Figures 7.1 and 7.2 respectively. Figure 7.1 is encouraging showing no discernible movement at any point, while Figure 7.2 shows that there is a certain background level of spurious 'noise' which must be taken into account when looking at plots of strain. In Figure 7.1 the metal side frame has been superimposed on the plot to demonstrate the extent to which it obscures markers from the camera. The blank lines which occur across each plot of marker displacements is simply a result of this. These discontinuities are not so noticeable, however, in the case of the strain plots since values of strain are simply computed for elements of larger size in these regions.

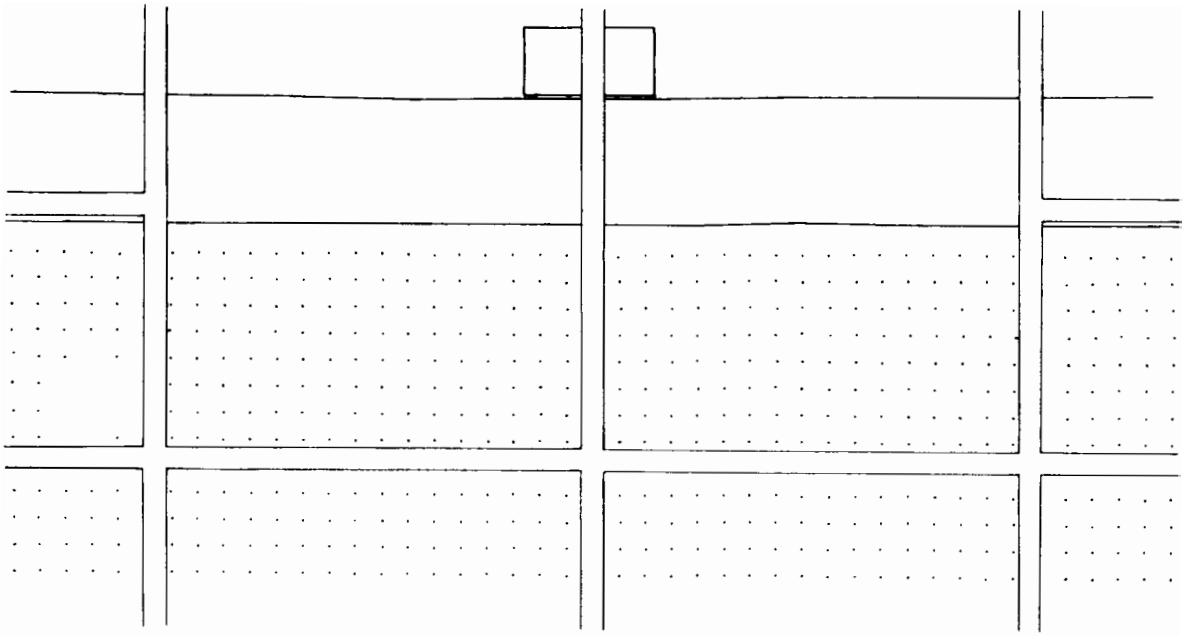

Figure 7.1 Displacement Vector plot - a test for errors

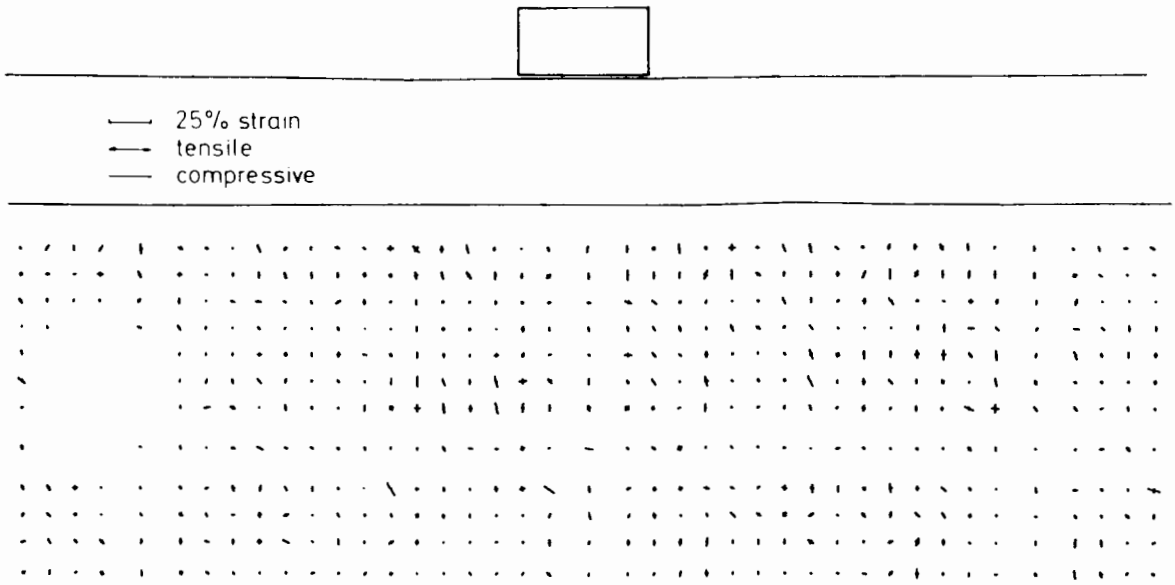

Figure 7.2 Strain plot - a test for errors

7.2 **Discussion of Results**

7.2.1 General

Displacement Vector and Strain plots are presented for mid-test and end of test points for tests J1M (a reinforced test) and J2M (an unreinforced test) in Figures 7.3 and 7.4 , these results being selected as a typical example of the trends seen in other tests. The general characteristics of a reinforced and an unreinforced test can be seen clearly from those plots. The marker displacements in the reinforced test are larger in magnitude and extend deeper into the clay body than the corresponding displacements in an unreinforced test for the same footing penetration. A relatively tight radius of curvature of flow is seen in the reinforced test compared to the rather longer radius of curvature and shallower failure in the unreinforced test. The presence of a grid therefore restrains lateral flow of foundation material, and in so doing sends deformations much deeper into the clay. In Figures 7.3 and 7.4 the principal compressive strains are seen to form radially, with the corresponding principal tensile strains (as marked with arrow heads) developing circumferentially. The plots of strain back up the displacement vector plots by showing much larger zones of deformation in a reinforced test than in an unreinforced test, for a given amount of footing penetration. In addition the individual magnitudes of the principal tensile strains, ϵ_1 , and compressive strains, ϵ_3 , are seen to be very similar indicating that the volumetric strains, ϵ_v , are minimal throughout the sample

$$\epsilon_v = \epsilon_1 + \epsilon_3$$

This is a good check on whether the clay is behaving in an undrained

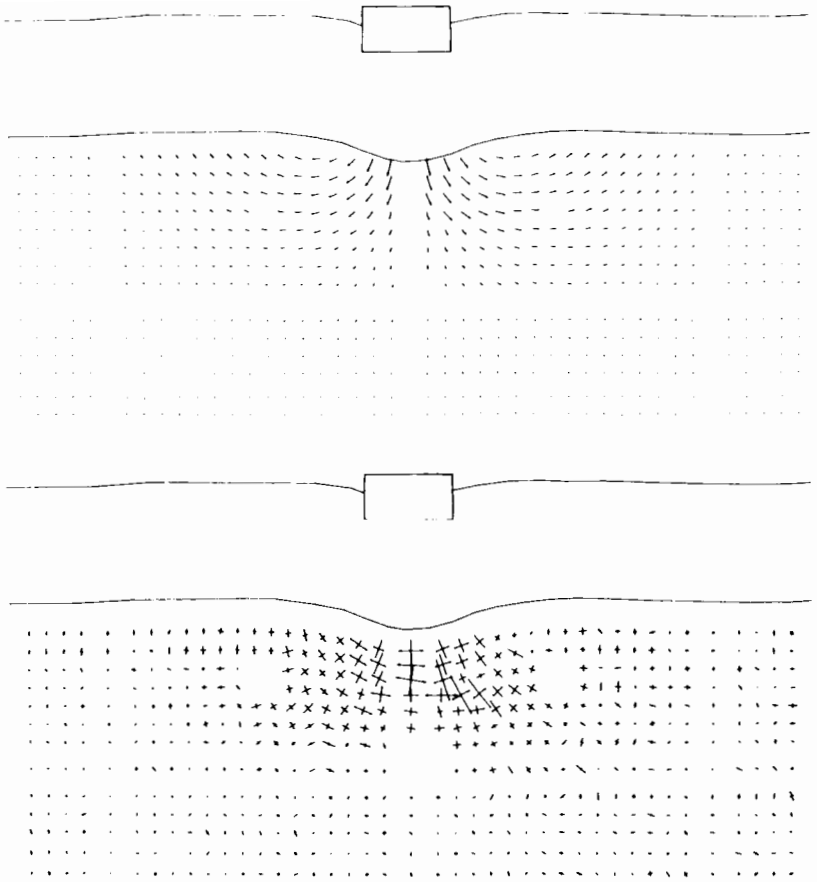

a) J1M (Reinforced test)

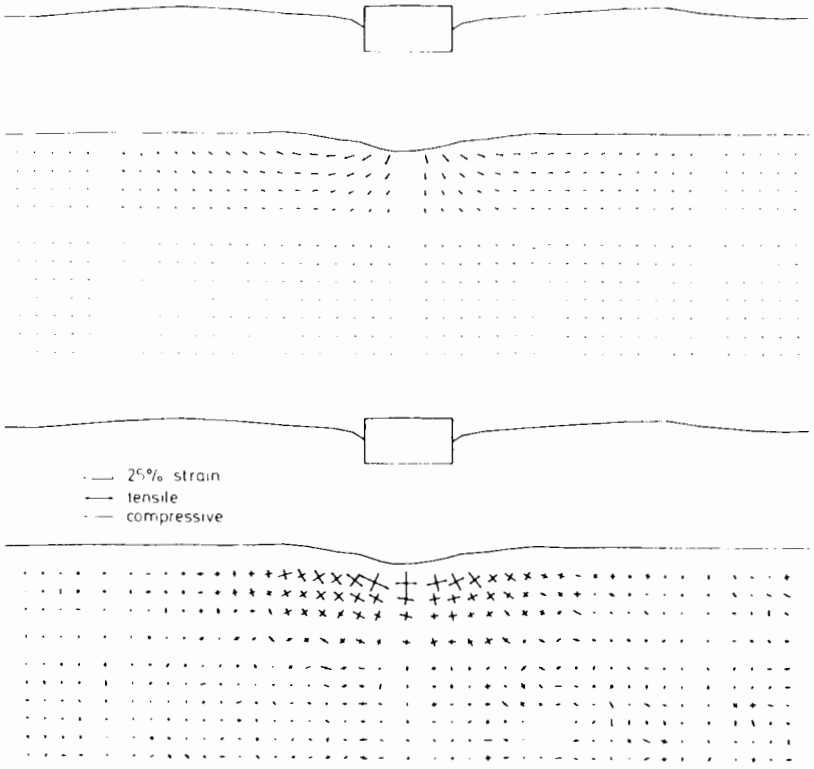

b) J2M (Unreinforced test)

Figure 7.3 Displacement Vector and Strain plots corresponding to 25mm Footing Penetration for tests on Sample J

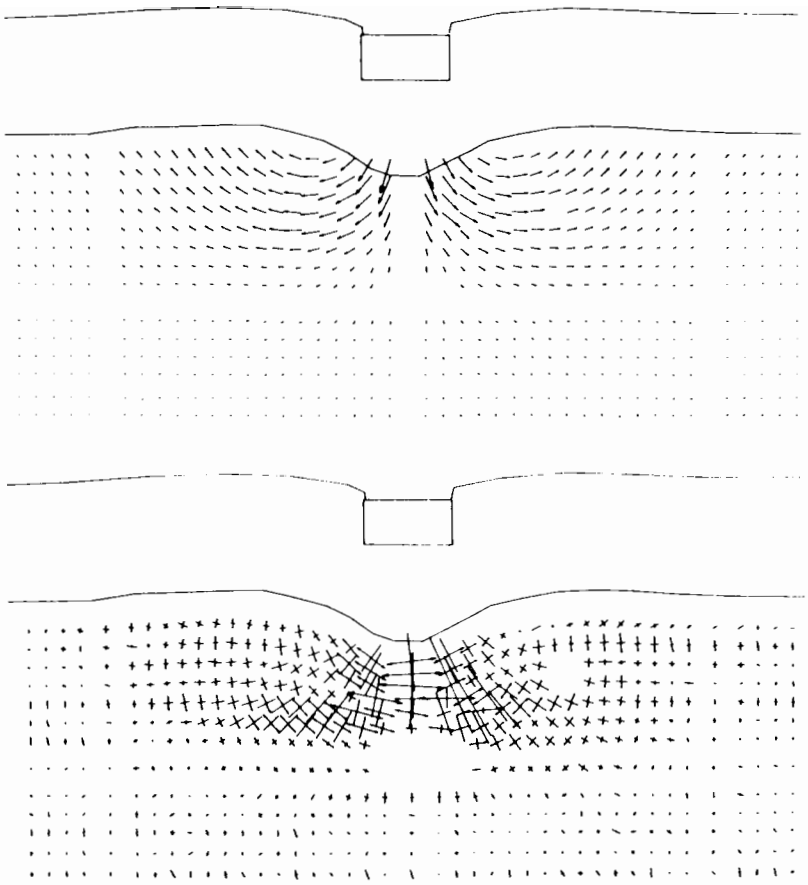

a) J1M (Reinforced test)

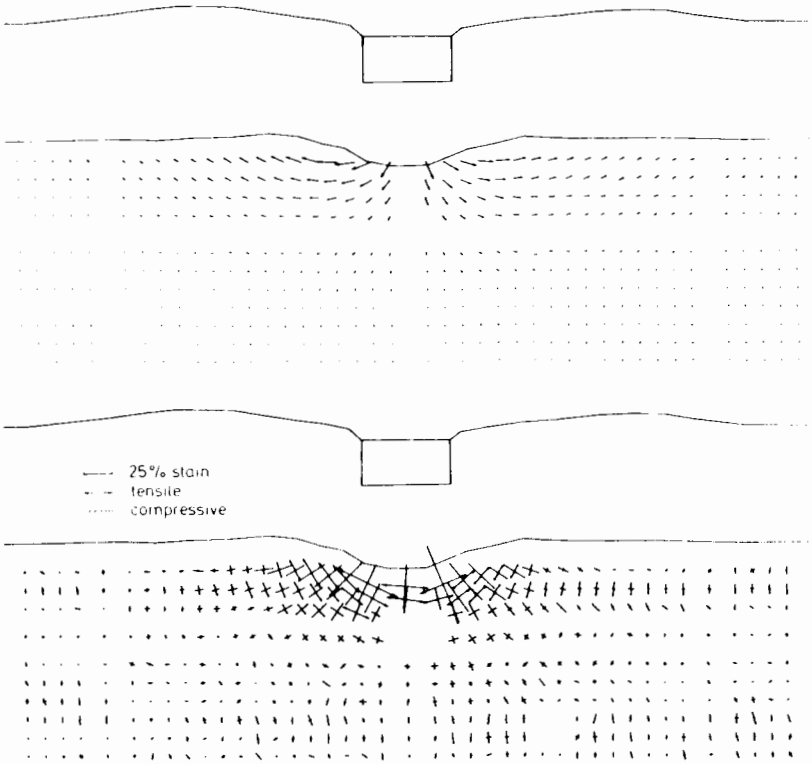

b) J2M (Unreinforced test)

Figure 7.4 Displacement Vector and Strain plots corresponding to 50mm Footing Penetration for tests on Sample J

manner, since for truly undrained conditions ϵ_v must be zero. It is a good indication of the validity of using the undrained shear strength parameter, C_u , in this study.

In Figures 7.3 and 7.4 any gaps in the strain plots arise from markers having disappeared from view in one or both of the frames being measured. The loss of a single marker (for example Figure 7.5) brings about a disproportionately large loss of strain information due to the simple quadrilateral data elements chosen for these plots. In future work the choice of triangular data elements would minimise this loss.

7.2.2 Concept of Footing Roughness

Surface roughness does not affect the bearing capacity of a footing loaded to failure on a cohesive perfectly plastic material: whether rough or smooth, the footing will fail at a net surface load of $(\pi + 2)C_u B$, where B is the width of the footing. But the deformations that develop in the foundation can vary significantly, as shown in Figure 7.6 .

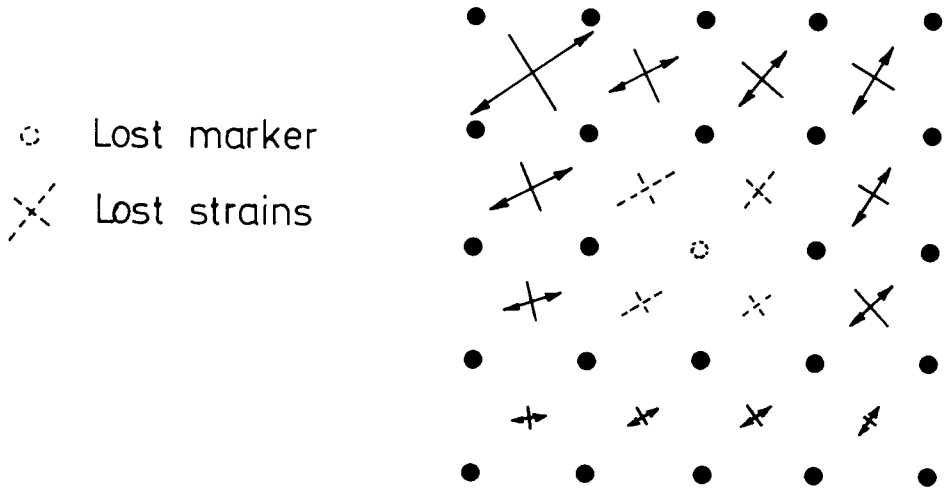

Figure 7.5 Effect of a lost marker on a Strain plot

The rough footing is constrained to the mechanism shown in Figure 7.6a , while for the smooth footing any mechanism a),b) or c) may result. There will be a tendency towards c) for materials with any appreciable increase of strength with depth. Conversely there will be a tendency towards Figure a) for materials which work-harden significantly, due to the lower magnitude of displacements and hence the lower levels of strain associated with this mechanism. For the model tests, where both the above effects play a part, some mechanism such as shown in b) is most likely. It can be concluded, therefore, that deeper deformations into the subgrade body do not necessarily indicate a greater surface load being applied. It is noted, however, that for the test with a rough footing, the zone of deformation will extend into clay of greater strength if the clay strength does increase with depth.

In an unreinforced test the wedge of fill bearing onto the clay surface beneath the footing is effectively acting as a smooth footing, because the fill particles on the clay surface move laterally with the clay. Since there is no relative movement between fill material and clay, the clay 'sees' an effectively smooth footing. Conversely, in the reinforced test, where the lateral movement of fill material at the clay surface is prevented by the grid, this wedge of fill can only behave as a rough footing.

7.2.3 Load Distribution

The effect of the fill layer can be considered simply as a means by which load is transferred from the real footing at the fill surface onto the clay surface. The clay sees a more generally distributed load as a result, and so can be considered loaded by an imaginary footing of

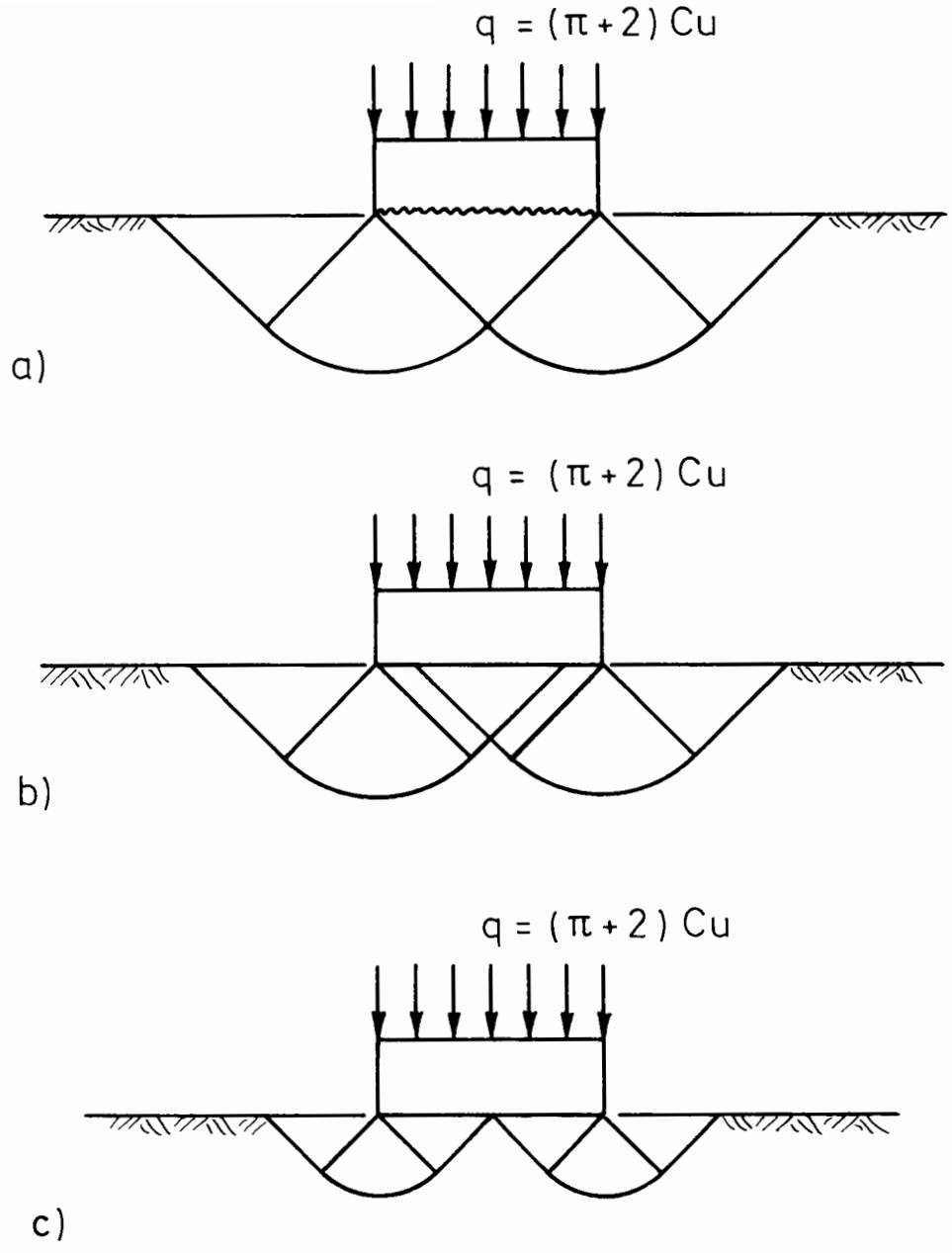

Figure 7.6 Failure mechanisms associated with footings of different surface roughness

greater width B' than the real footing width B (Figure 7.7a). This is certainly not a new concept, being often assumed for convenience and forming the basis of many design codes. The subject of debate at present lies in the value chosen for B' .

The distance B' is often taken to be the distance L_1 shown in Figure 7.7b which is a length referred to the clay profile at the beginning of the test. It may also be taken as the distance between the points of inflexion, L_2 . But the points between which B' should be measured are the points about which rotation is seen to occur in the clay (Figure 7.7c). That is, to one side of the point clay is seen to be descending while on the other it is seen rising. If two photos are taken quickly together at any point during the test and the clay surface profile is traced from one and superimposed on the other, the points of intersection of the two profiles will show the instantaneous points of rotation for that particular stage of the test, the 'stationary' points. It would be desirable to perform some sort of upper bound calculation based on mechanisms such as shown in Figures 7.6a,b and c using this definition of B' in order to try and estimate the load being carried by the system at a particular instant of the test. If reasonably close agreement can be achieved between the actual footing loads at any point in a test and the loads that are deduced from a particular failure mechanism, this will give confidence as to the relevance of that particular mechanism.

It is important to look at marker movements incrementally, however. To demonstrate this the marker movements during test J1M are shown first in Figure 7.8 , in toto, from the beginning of the test to 50mm footing penetration, and then again in Figures 7.9a,b c and d , in four equal increments during the test. Each increment corresponds approximately to

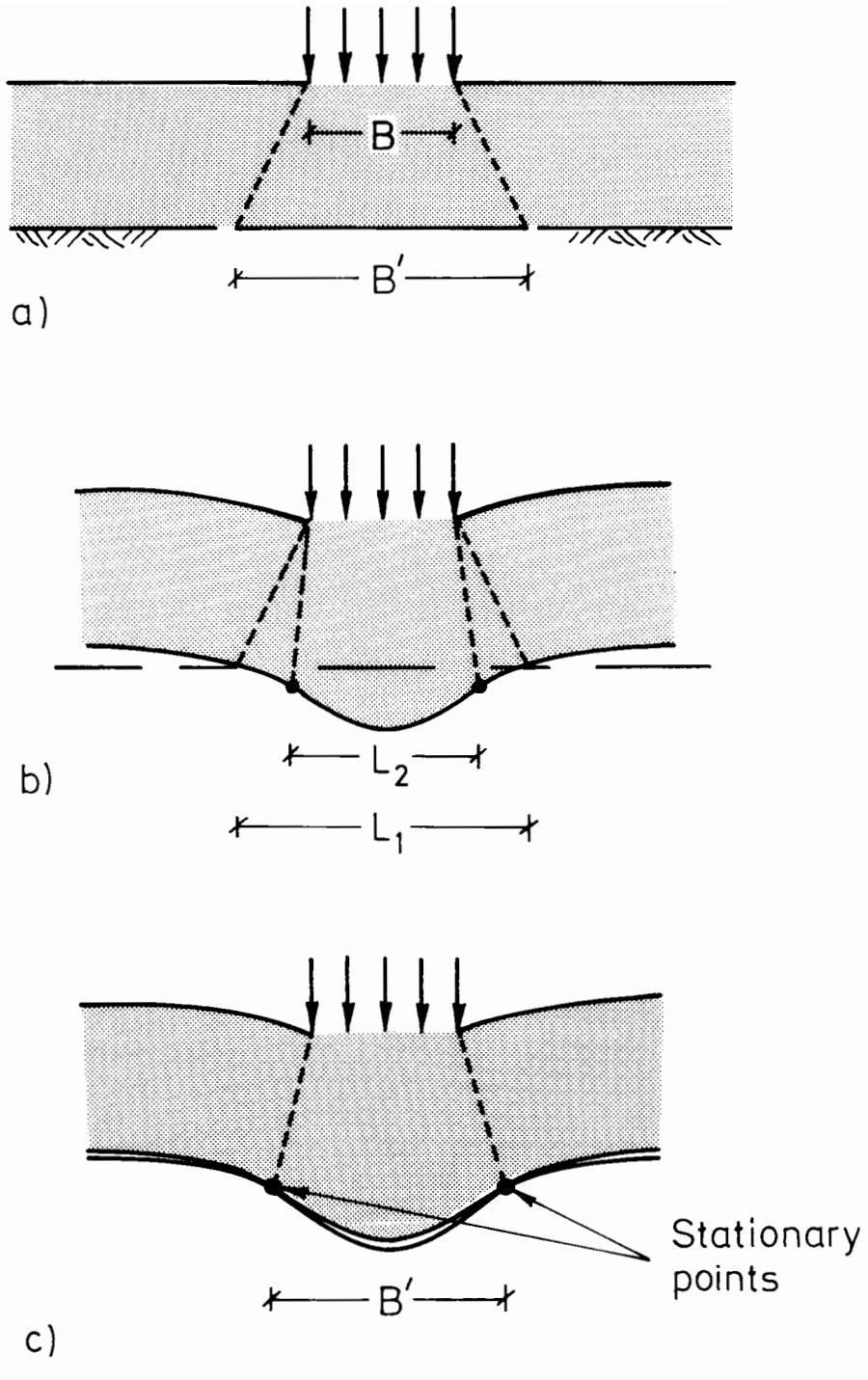

Figure 7.7 Three different definitions of Load-distribution in the fill layer

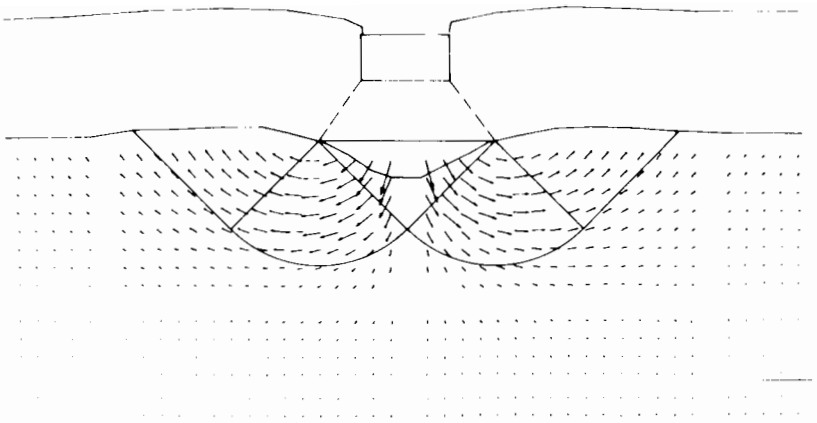

Figure 7.8 Displacement Vector plot corresponding to 50mm Footing Penetration for the reinforced test J1M (Single Increment)

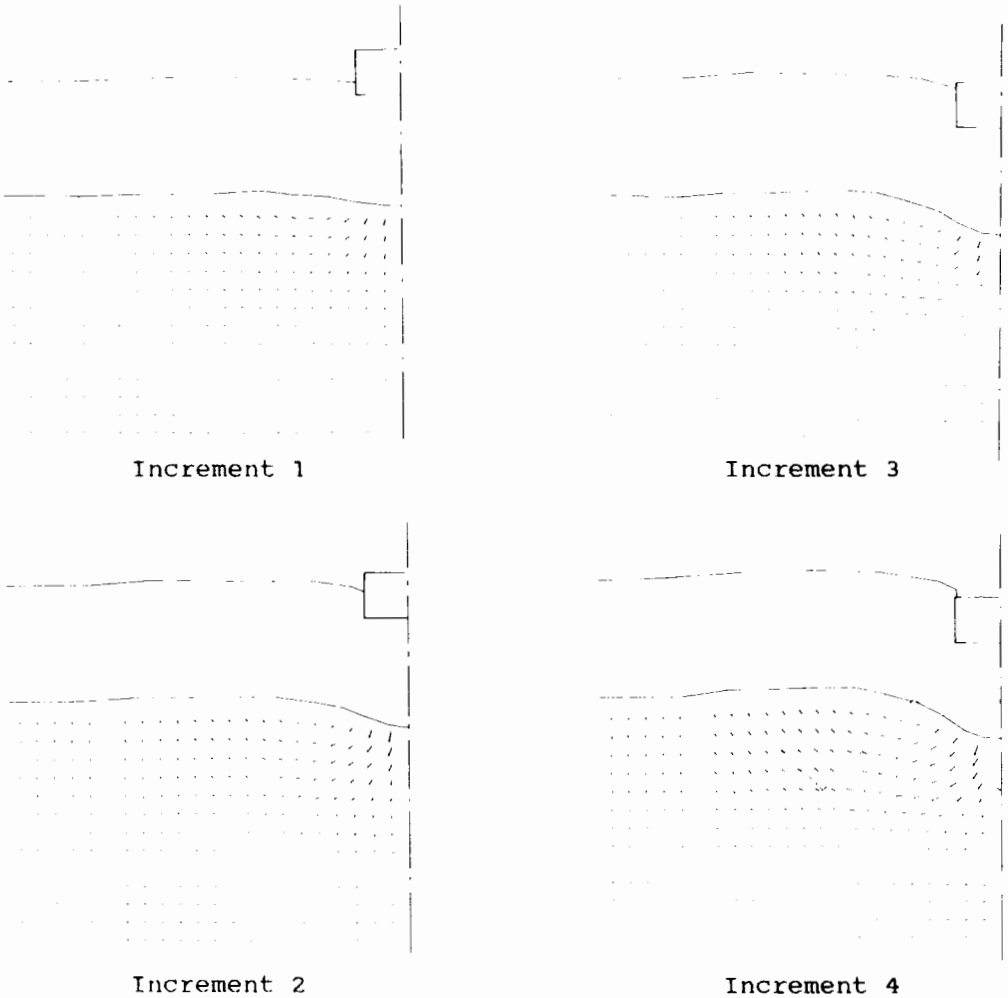

Figure 7.9 Displacement Vector plots corresponding to 12.5mm, 25mm, 37.5mm and 50mm Footing Penetration for the reinforced test J1M (Four Increments)

an additional 12mm footing penetration. For the last increment the relevant upper bound mechanism has been superimposed on the marker movements. It can be seen that while the mechanism in this figure seems plausible, in Figure 7.8 it seems rather less plausible.

It is also important to look at the development of strain incrementally. The strains accumulated during the whole 50mm of footing penetration during test J1M have already been shown in Figure 7.4 . Splitting this test up into 4 approximately equal increments as before, the strain resulting from each increment separate into those shown in Figure 7.10a,b,c and d . From these it is immediately possible to follow the development and gradual deepening of a significant slip-plane throughout the test. The presence of this slip-plane is confirmed from the post-test inspection of the clay shown in Figure 4.10 . Secondly, from this incremental study, it is noticed that the pattern of strains begins to resemble those predicted by classical analysis, as shown in Figure 7.11 . Figure 7.11a represents Prandtl's upper bound failure mechanism for a footing on frictionless soil superimposed onto the usual grid of markers used in these tests. An arbitrary downward displacement of the central block was imposed on the system, together with an arbitrary angle of load distribution through the fill layer, so that the displacement of each marker could be digitised from the plot on the DITPAD. It was found from this exercise that the principle strains associated with these displacements are those plotted in Figure 7.11b .

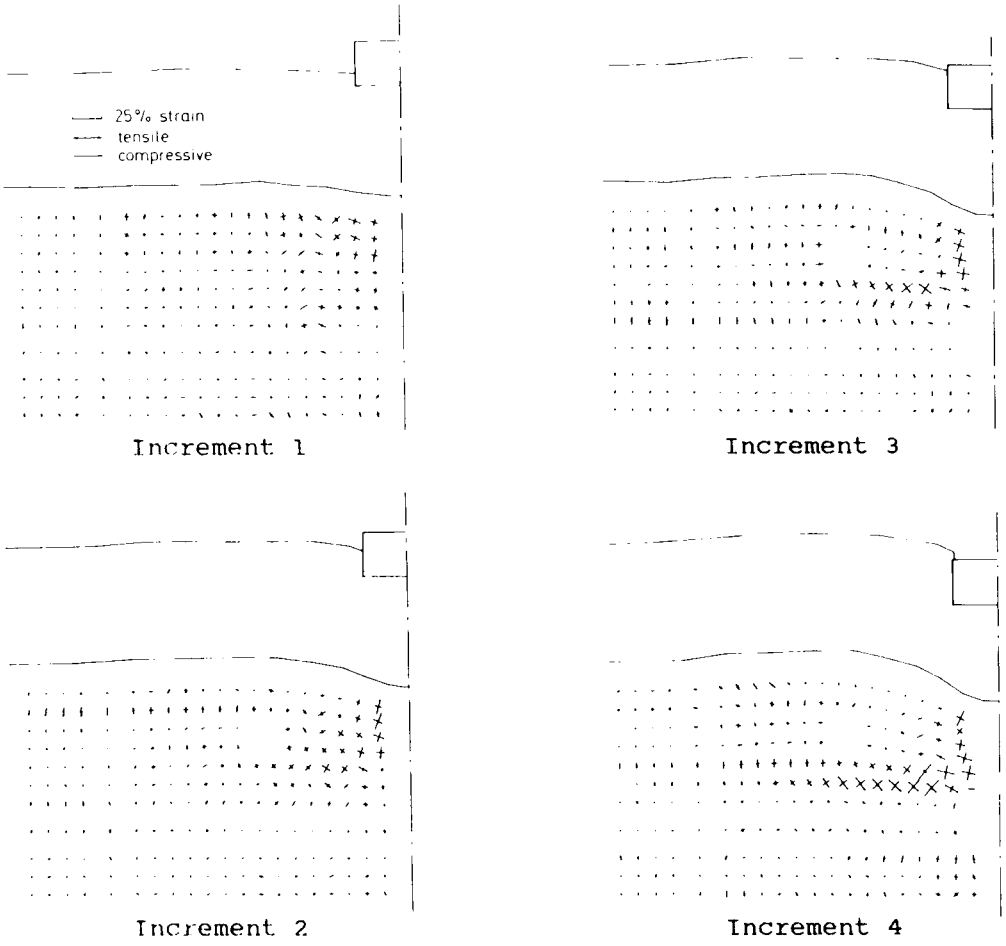

Figure 7.10 Strain plots corresponding to 12.5mm, 25mm, 37.5mm and 50mm Footing Penetration for the reinforced test J1M

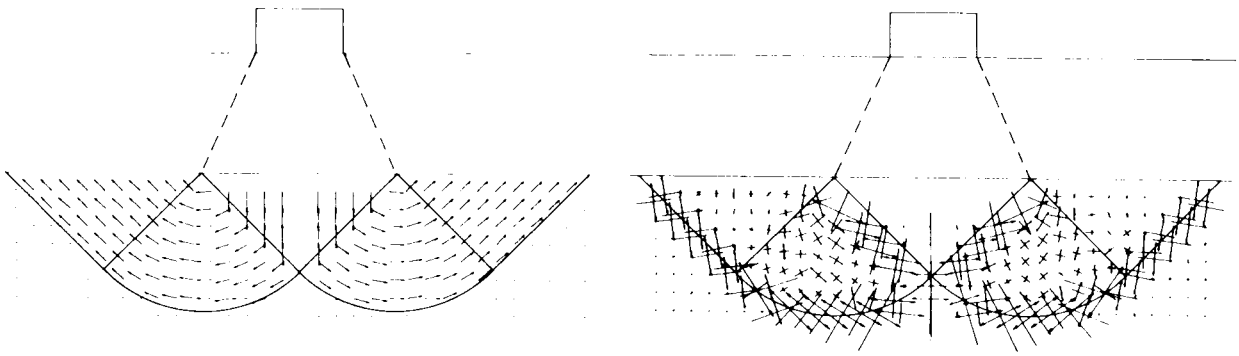

Figure 7.11 Displacement Vector and Strain plots corresponding to an idealised failure mechanism

7.2.4 Membrane Effect of Grid

A grid, having only a minimal bending stiffness, cannot contribute any significant vertical load carrying capacity until it starts to deform. As the grid profile is deformed further and further from its original horizontal position so a greater component of its in-plane tension acts vertically. The effect of this membrane action is to relieve the clay of some of the applied load directly beneath the footing, and to increase the pressure on the clay out to the sides. The magnitude of this membrane force at any point on the grid will depend upon the local slope-angle of the grid profile and the strain in the grid at that point.

Several simplifying assumptions concerning the deflected shape of the grid (eg parabolas, circular arcs), and the strain profile along the grid (eg that it is constant) have been made by researchers in the past. In this research it was found that the deflected shape of the grid cannot reasonably be predicted by such assumptions. Secondly in this research it was found very difficult to shed any light on the strains occuring in the grid. Attempts were made: a set of markers were glued onto the nodes along the front edge of the grid (described in Section 5.2.2) and traced during a test.. Some of the markers became obscured by the clay during compaction of the fill, and others became obscured during the test by deforming clay. The marker movements which could be traced are shown for three tests in Figure 7.12 . The movements of these markers on the front edge of the grid may not truly represent the movement of the grid away from the edge however. In many cases only a small portion of the markers were visible so that the centre of the marker had to be estimated. Taking this into account, little information concerning the

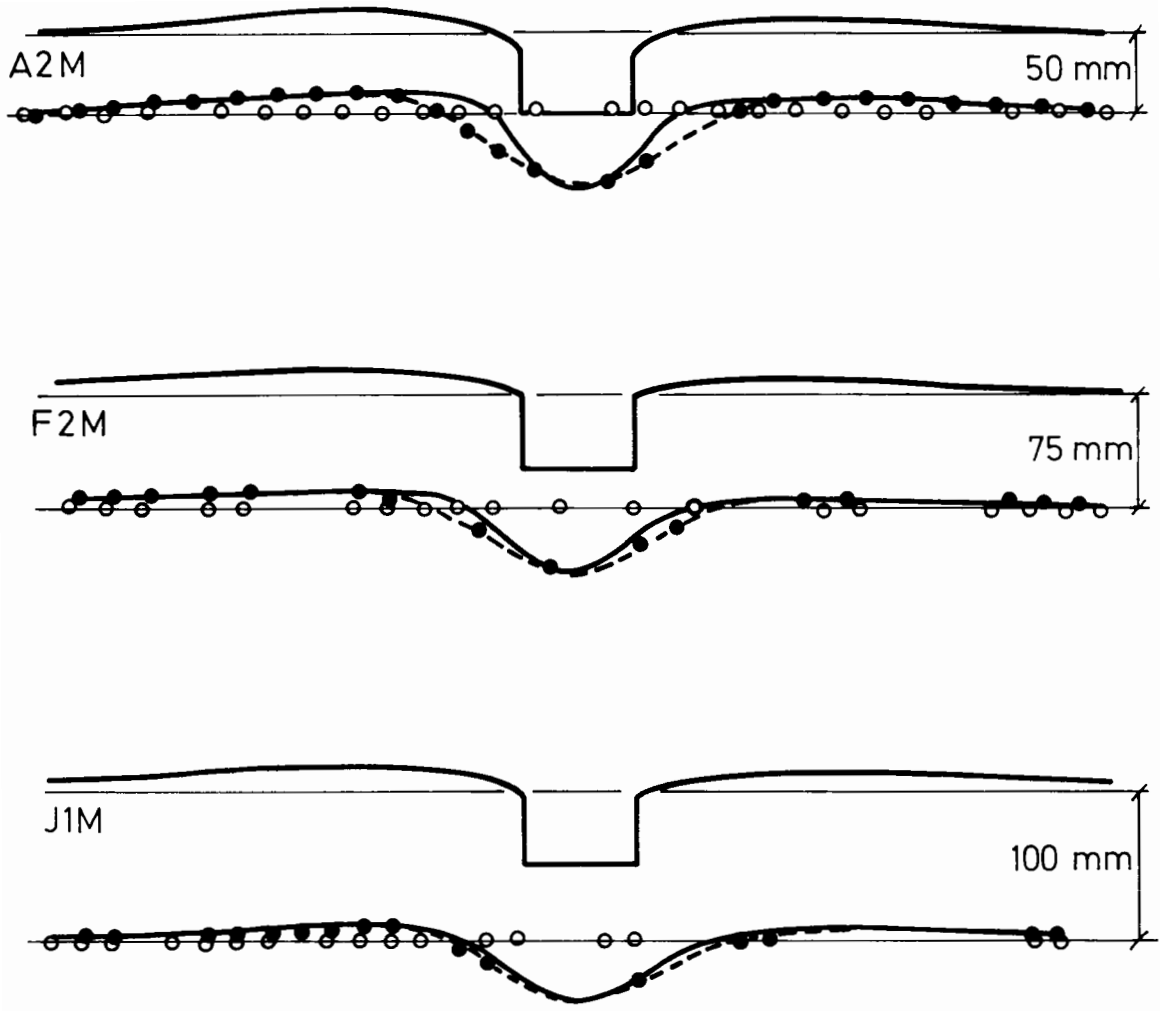

Figure 7.12 Displacements of grid markers for three tests

true strain profile in the grid can be gathered. Since the strain profile of the grid is therefore not known in detail, reasonable assumptions about the magnitude of the membrane forces must be made based on other pieces of information. Two useful points that may be used are as follows:

1. The grid was observed to begin slipping at its ends well before the end of each test when a 50mm or 75mm fill layer was used, and just at the end of the test for a fill layer of 100mm.

2. On recovery of each piece of grid at the end of a test, no measurable permanent elongation of the grid was seen to have occurred.

The first piece of information indicates that, once the grid starts to slip at its ends, the horizontal component of the tension in the grid at the stationary points will be approximately the same in all tests using the same depth of fill. The second indicates that the maximum tension in the grid does not exceed the elastic limit of the material. Let it be assumed that the horizontal component of the grid's tension at the stationary points for a test using a 100mm fill depth reaches a limiting value of, say, F and that the corresponding values for fill depths of 75mm and 50mm are therefore 0.75F and 0.5F respectively. The slope angle, ψ , of the grid profile at the stationary points D and E on Figure 7.13 can be measured. The tension, T , in the grid at the stationary points for a 100mm fill test is given by F secψ . The effect of the grid's membrane force between D and E is therefore equivalent to the vertical component of T which is F tanψ (and hence 0.75F tanψ , 0.5F tanψ for H = 75, 50mm).

7.2.5 The Reinforced Test

The following two assumptions are made: that the surface load per unit width , Q (= qB) is distributed onto the grid surface only over the area D-E and not beyond, so that, ignoring overburden effects,

$$Q = Q' = \int_{-B'/2}^{+B'/2} q' \, dx \qquad \text{.....7.1}$$

and secondly that this load is uniformly distributed, making q' a constant so that

$$qB = q'B' \qquad \text{.....7.2}$$

The membrane force will act to reduce the load onto the clay between these two points. The total load per unit width carried by the clay between D-E is Q'' , where

$$Q'' = \int_{-B'/2}^{+B'/2} q'' \, dx \qquad \text{.....7.3}$$

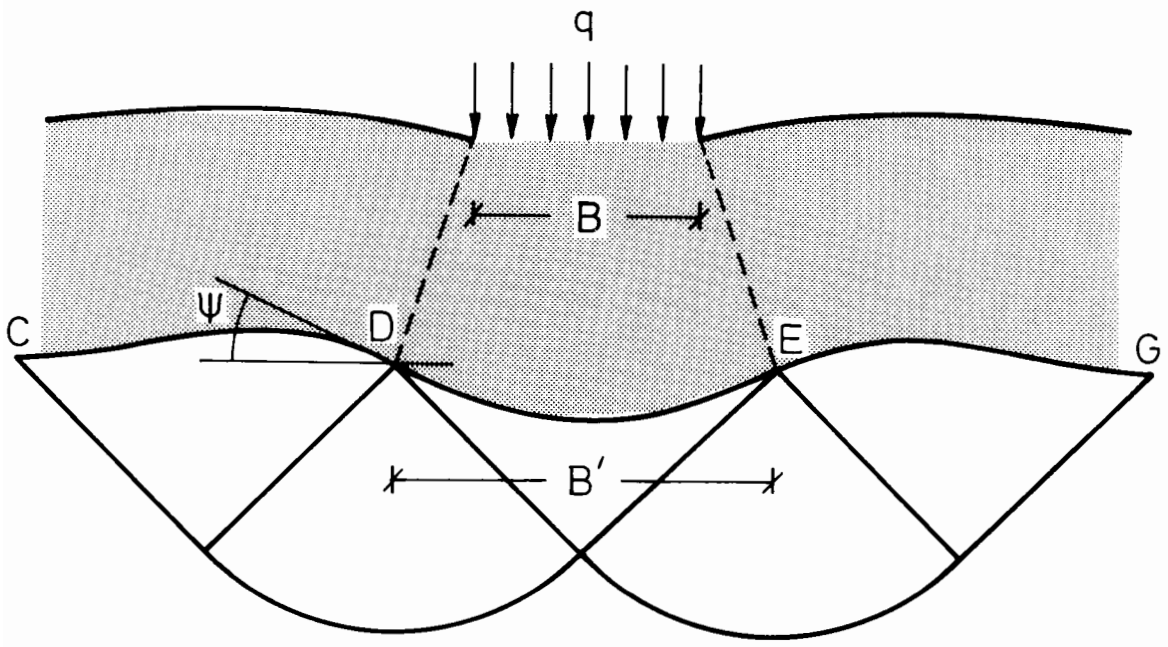

Figure 7.13 Failure mechanism for a reinforced test

If it is assumed that q'' is also uniform across D-E , then

$$q''B' = q'B' - M \qquad \text{.....7.4}$$

where M is the vertical component of the total membrane force per unit width acting between the stationary points D , E which has already been shown to be $2T\sin\psi$.

In addition the grid exerts a membrane force onto the heaved portion of clay beyond the points D , E and this must also be taken into account. The slope angle of the grid profile is ψ at one end of this heaved section and nearly zero at the far end. The effective overburden pressure between points CD and EG (Figure 7.13) is therefore increased by approximately $(T\sin\psi)/B'$. Since it is the magnitude of the differential pressure acting on sections DE and CD, EG which determines failure then the effect of this additional membrane force can simply be incorporated by increasing the magnitude of M to $3T\sin\psi$. Equations 7.2 and 7.4 can be rewritten as

$$q = q'' B'/B + (3T\sin\psi)/B \qquad \text{.....7.5}$$

Substituting $(\pi + 2)C_u$ for the critical value of q'' , and $F\sec\psi$, $0.75F\sec\psi$ or $0.5F\sec\psi$ for T according to the value of the fill thickness H , the surface pressure on the footing, q , may be estimated at any stage of a test for which B' and ψ can be measured. This may be readily done from plots such as in Figure 7.9 , which represent sufficiently small increments of footing penetration for the measurement of B'.

Observed values of B' and ψ , at both mid- and end-of-test points, are listed for all reinforced tests in Tables 7.1 and 7.2 . Table 7.3 compares the predicted and measured footing pressures for each of these

TABLE 7.1 VALUES OF B' (REINFORCED AND UNREINFORCED TESTS)

			Reinforced			Unreinforced		
			Nominal Clay Strength (kPa)					
			6	9	14	6	9	14
25mm Footing Penetration	H=	50mm	124	110	108	105	105	97
		75mm	134	132	137	110	129	129
		100mm	163	153	142	139	139	130
50mm Footing Penetration	H=	50mm	126	116	113	89	-	87
		75mm	132	132	137	90	110	108
		100mm	158	147	145	126	126	113

Notes
1. Values of B' measured between Stationary Points from Displacement Vector plots
2. All lengths in mm

TABLE 7.2 VALUES OF ψ (REINFORCED TESTS)

			Nominal Clay Strength (kPa)		
			6	9	14
25mm Footing Penetration	H=	50mm	20	27	22
		75mm	15	15	13
		100mm	11	11	9
50mm Footing Penetration	H=	50mm	33	31	33
		75mm	23	29	21
		100mm	19	22	15

Notes
1. ψ is the slope angle of the grid profile at the Stationary Points, as measured from the Displacement Vector plots
2. Angles are in degrees

cases for F = 2kN/m and the individual test values of C_u taken from Table 4.2 . The contributions from the clay and from the grid membrane force are shown separately and the sum of these estimations seem reasonable. Although the value of F is arbitrary, the value of 2kN/m represents an upper limit in order that the strains in the grid remain elastic (Figure 5.11). The estimations consistently fall short of the measured data, but this may be attributed to two effects. Figure 4.2 indicates that at 25mm footing penetration the bearing capacity of the clay may be underestimated by between 5% and 35% by the conventional $5.14C_u$, and by even more than this at 50mm footing penetration. Secondly, in practice the grid is not horizontal at points C and G (Figure 7.13) suggesting a factor of greater than 3 being appropriate in Equation 7.5 . It is therefore concluded that this assumed mechanism of failure in a reinforced test models reasonably both the observed clay deformation patterns and the measured failure loads.

TABLE 7.3 COMPARISON BETWEEN PREDICTED AND MEASURED LOADS (REINFORCED TESTS)

		Predicted			Measured		
		Nominal Clay Strength (kPa)					
		6	9	14	6	9	14
25mm	50mm	49+14	67+20	112+17	68	100	146
Footing H=	75mm	51+16	76+16	121+14	79	104	132
Penetration	100mm	64+16	92+16	130+13	88	115	147
50mm	50mm	50+26	70+24	117+26	82	115	163
Footing H=	75mm	50+26	76+33	121+23	90	123	157
Penetration	100mm	62+28	89+32	133+22	101	133	162

Notes
1. Predicted Loads separately sum contributions from the clay and from the grid respectively
2. All values in kPa

7.2.6 The Unreinforced Test

The unreinforced test data was initially examined in the same way as the reinforced test data. There is of course no membrane force to take into account, so that $q'' = q'$, and therefore that

$$q = q'B'/B \qquad \text{.....7.6}$$

where $q' = (\pi + 2)C_u$. While this did not seem unreasonable for the tests on the weakest clays, it proved to overestimate the observed loads on the stronger clays and thicker fill depths by up to 40% .

Figures 7.14 and 7.15 perhaps show why this is so. While the assumed failure mechanism fits the flow of material on the weaker clay (Figure 7.14) quite well, the mechanism is clearly inappropriate for the stronger clay (Figure 7.15) where a much shallower failure mechanism occurs. A more thorough investigation of the general mechanism of failure in an unreinforced test must clearly be made.

7.2.7 The Effect of Shear Stress in an Unreinforced Test

The fill material beneath the footing is not constrained laterally in unreinforced tests as it is in reinforced tests. A free lateral flow of fill material along the fill/clay interface takes place which sets up an outward acting shear stress on the clay across the loaded area. This shear stress acting on the clay can greatly reduce its bearing capacity.

Consider the simple footing in Figure 7.16 which is subjected to a normal stress q and a lateral stress τ . The correct upper bound failure mechanism is shown in the diagram, plastic failure occurring for a weightless soil when

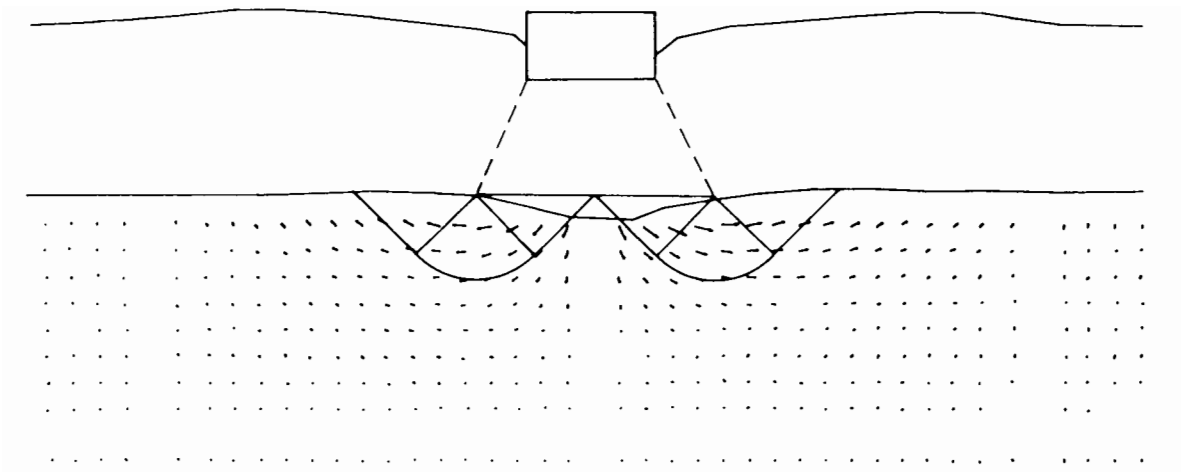

Figure 7.14 Displacement Vector plot for the unreinforced test G1M (25mm Footing Penetration)

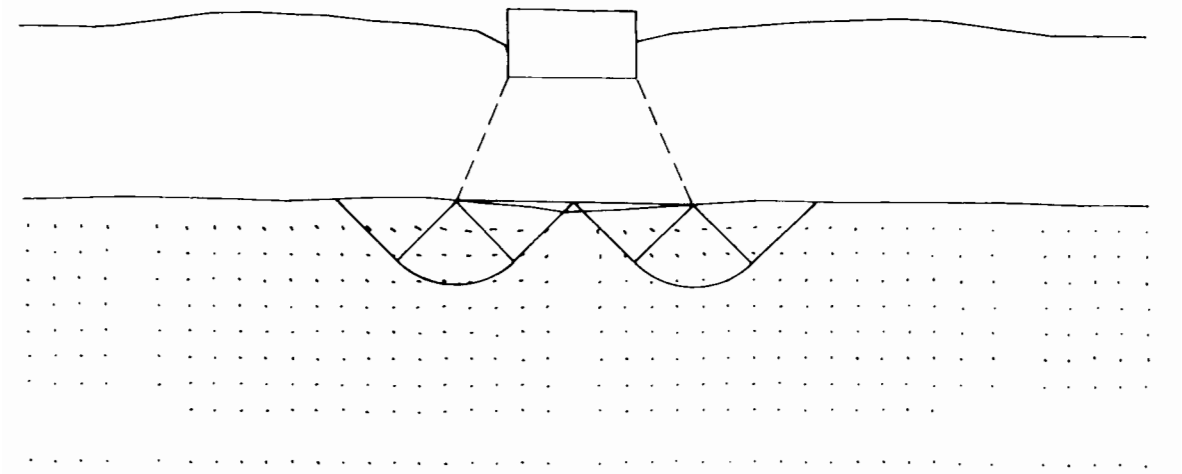

Figure 7.15 Displacement Vector plot for the unreinforced test K1M (25mm Footing Penetration)

$$q = (\pi/2 + 2\beta + 1 + \sin 2\beta) \quad \text{.....7.7}$$

where $\tau = C_u \cos 2\beta$. It will be seen that for no shear force, then $\beta = 45^{\circ}$ and the bearing capacity becomes $(\pi + 2)C_u$; while for $\tau = C_u$, the bearing capacity halves. It is proposed that this effect accounts for the reduced bearing capacity of unreinforced tests on the stronger clays giving rise to shallower and flatter flow vectors. The effect is emphasised as the fill thickness increases because the lateral flow of fill material becomes a greater factor.

The movements in the fill and clay layers are therefore interrelated: if a flow of fill exists across the surface of the clay, giving rise to outward shear as well as normal stresses, the bearing capacity of the clay will be reduced. If the normal stresses at any particular point exceed that bearing capacity, then plastic deformation will occur locally in the clay. This will alter the flow pattern of the fill reducing its lateral movement. This in turn increases the clays bearing capacity, and causes further lateral flow to develop. In the

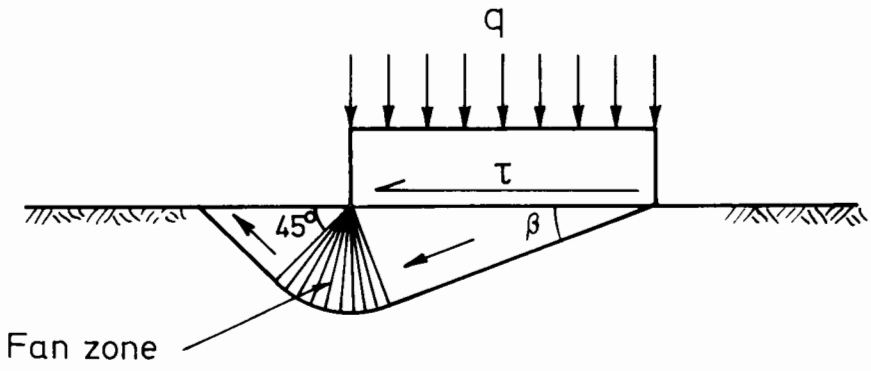

Figure 7.16 Failure mechanism associated with footing subjected to normal and lateral loading

case of a relatively strong clay (small values of $\gamma_1 B/C_u$), more lateral flow will develop in the fill layer than for a relatively weak clay (high values of $\gamma_1 B/C_u$).

Shear stresses on the clay surface increase from zero at the centre of the loaded area where there is no lateral fill movement to a maximum in the vicinity of the stationary points, and then die away to zero beyond this sketched approximately in Figure 7.17 . In the region between the stationary points the combination of normal stress and shear stress is critical (ie exceeding the bearing capacity of the subgrade) and yielding takes place. A simplification of the situation is presented in Figure 7.18 . A central portion of clay, width 2b , is assumed to experience no shear stresses and therefore has a bearing capacity factor of $(\pi + 2)$; the two outside portions, width a , experiencing a uniform shear stress τ have a bearing capacity factor given by $(\pi/2 + 2\beta + 1 + \sin 2\beta)$.

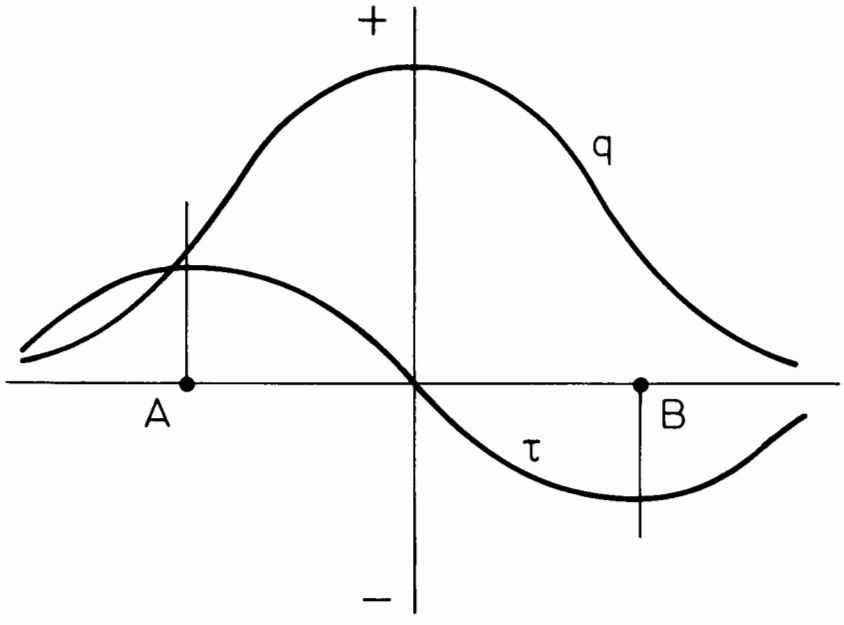

Figure 7.17 Approximate profiles of normal stress, q and shear stress, τ acting on clay surface during an unreinforced test

The shaded areas are fan zones in which infinitely thin radial slices of soil slide relatively to each other. The total load per unit width carried by the clay (ignoring overburden) can therefore be estimated as

$$2a(\pi/2 + 2\beta + 1 + \sin 2\beta)C_u + 2b(\pi + 2)C_u \quad \ldots\ldots\ldots 7.8$$

As a and τ decrease to zero so the failure mechanism shown in Figure 7.18 will be seen to approach the type shown in Figures 7.6a,b and c . There are many 'families' of mechanisms of the type shown in Figure 7.18 : q is both a function of β and of a/b . The aim is to deduce which family best models an unreinforced test by analyzing the marker displacement plots. It is not possible from the plots, however, to measure either a or b . So for the sake of convenience in taking measurements from the marker plots it will be assumed, for the stronger clays only, that a/b is always such that the continuation of line CD passes through point B .

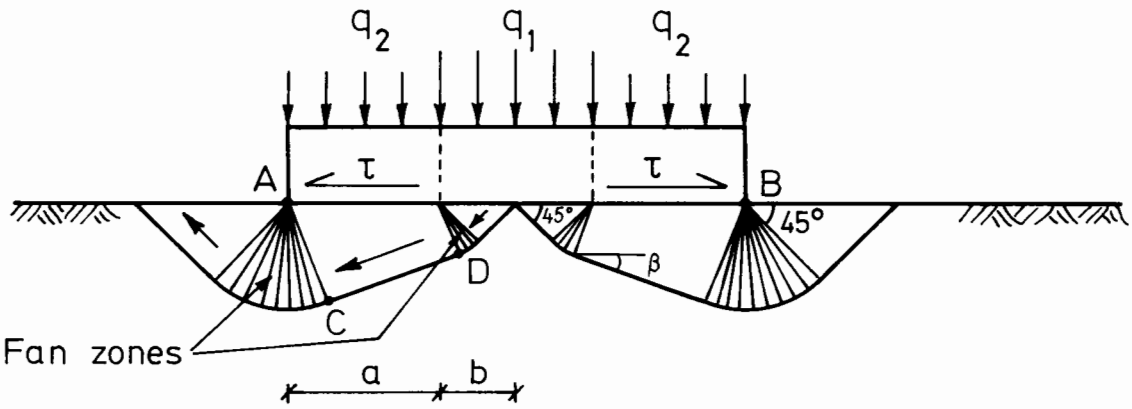

$$q_1 = 5.14\ C_u$$

$$q_2 = N\ C_u \qquad \text{where } N = f(\beta)$$

$$q_{av} = (aq_2 + bq_1)/(a + b)$$

Figure 7.18 Assumed loading acting on clay surface in an unreinforced test, with associated upper bound failure mechanism

For tests on the very weak clay, it has already been determined that minimal lateral flow develops and that mechanisms approaching that shown in Figure 7.6b are more appropriate.

This is a particularly useful constraint in that β is given simply by $\sin^{-1}$ d/B' (Figure 7.19), and both d and B' can be measured with confidence. For this 'family' of mechanisms there is a unique value of q for a particular value of β, given by the curve in Figure 7.20 . Tables 7.1 and 7.4 list the values of B' and β , both mid-test and at the end of the test, for all unreinforced tests. Table 7.5 compares the predicted and measured footing pressures for each of these cases and the estimations look reasonable.

No account of overburden has been taken in this analysis. Underestimations of bearing capacity would therefore be expected as a result, and the underestimation would also be expected to be more noticeable at later stages in the test when there is clearly a greater

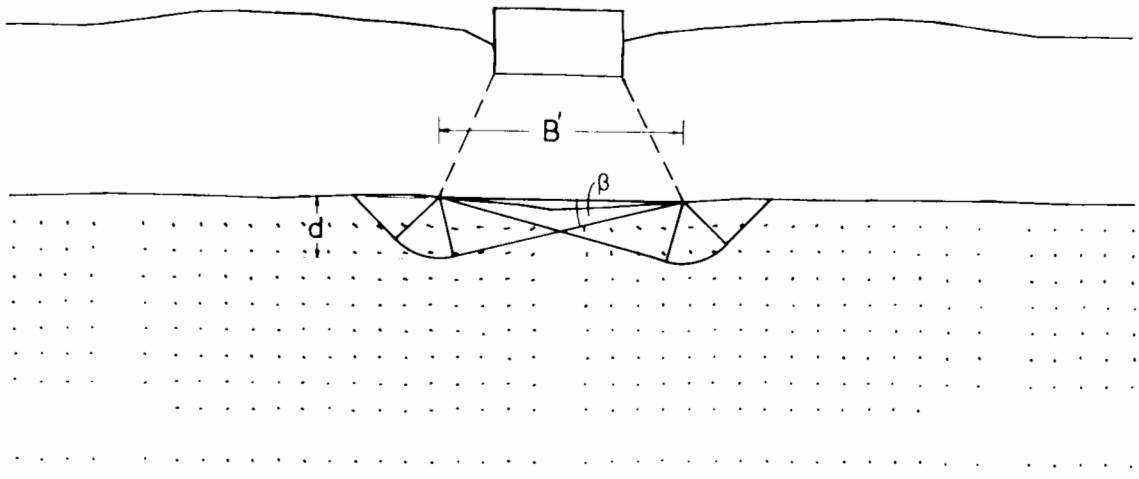

Figure 7.19 Displacement Vector plot for the unreinforced test K1M (25mm Footing Penetration)

TABLE 7.4 VALUES OF β (UNREINFORCED TESTS)

		Nominal Clay Strength (kPa)		
		6	9	14
25mm Footing Penetration	H= 50mm	40	32	28
	H= 75mm	40	19	16
	H= 100mm	35	15	8
50mm Footing Penetration	H= 50mm	45	-	39
	H= 75mm	45	34	32
	H= 100mm	40	26	20

Notes

1. β is a direct measure of the shear stress acting across the clay surface, and is defined by $\sin^{-1}$ d/B' in Figure 7.19
2. Angles are in degrees

TABLE 7.5 COMPARISON BETWEEN PREDICTED AND MEASURED LOADS (UNREINFORCED TESTS)

		Predicted			Measured		
		Nominal Clay Strength (kPa)					
		6	9	14	6	9	14
25mm Footing Penetration	H= 50mm	42	61	78	48	64	84
	H= 75mm	42	59	91	52	65	100
	H= 100mm	53	63	86	64	67	93
50mm Footing Penetration	H= 50mm	36	-	75	52	-	97
	H= 75mm	35	60	93	57	70	105
	H= 100mm	50	67	96	59	69	106

Note

All values in kPa

overburden acting on the heaved portions with respect to material directly under the footing. The general trends of the quantities listed in Tables 7.1 and 7.4 are discussed below:

B'

In both reinforced and unreinforced tests values of B' are clearly greater for tests conducted on thicker layers, with values of B' for reinforced tests slightly greater again than those for unreinforced tests. This lends support to the angle-of-spread concept whereby surface load is spread by the fill layer onto the subgrade by an angle α_1 for unreinforced tests and a slightly greater angle α_2 for reinforced tests. Values of α_1 and α_2 may be deduced from Figure 7.21 which is a plot of how the length B' varies during a test. But caution should be taken in adopting such an angle-of-spread model, for the reasons outlined earlier in this section. The bearing capacity factor for the clay subgrade is a

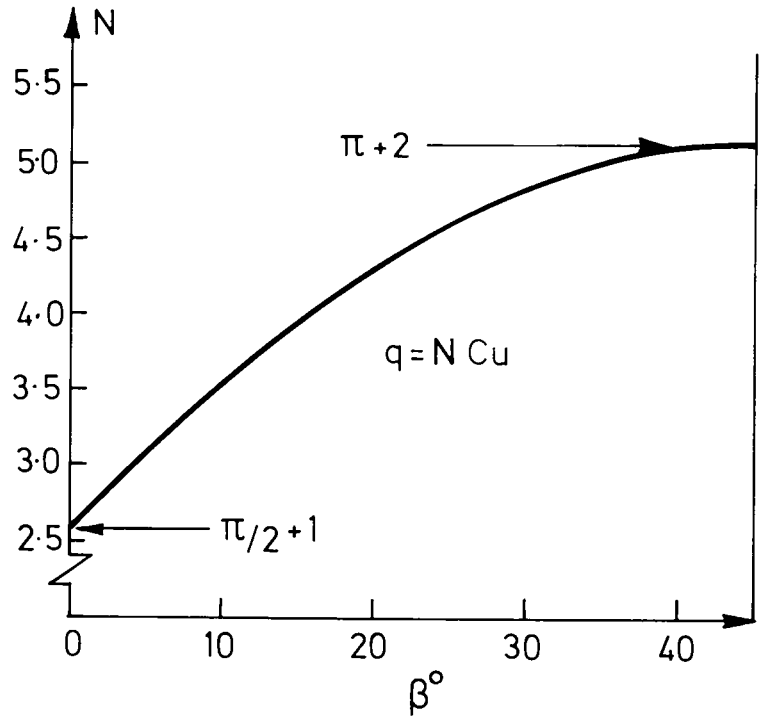

Figure 7.20 Variation of Bearing Capacity Factor, N with the angle β

variable which depends on the shear stresses set up by lateral flow of fill material, and can lie anywhere between (π + 2) and (π/2 + 1).

From Figure 7.21 it can also be seen that during a reinforced test B' stays fairly constant, while for an unreinforced test it decreases. The curves in this plot are averaged from the results from all three clay strengths. There is a slight trend for the value of B' to increase as clay strength decreases for the reinforced tests but not for the unreinforced tests. A better angle of load distribution might have been expected for a fill layer on the stronger clay, but the fact that a stronger clay encourages greater lateral flow of fill across its surface would seem to give rise to a narrower band of critical stresses acting below the footing.

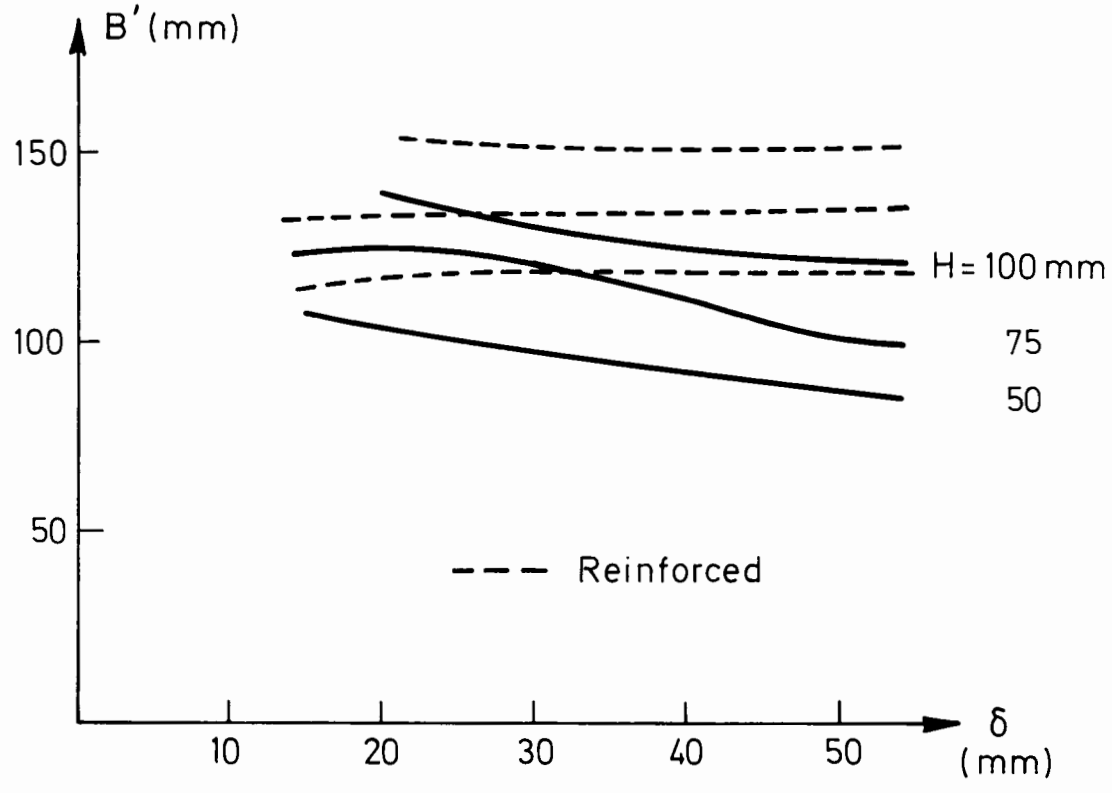

Figure 7.21 Variation of the length B' during reinforced and unreinforced tests on fill thicknesses of 50mm, 75mm and 100mm

β

β is a direct measure of the shear stress acting across the clay surface. Two consistent trends in β are seen from Table 7.4 . Firstly that β increases during a test. This confirms an expected result: the extent of lateral flow decreases as the test progresses, and once an appreciable trough begins to form the fill material becomes confined. Secondly, β is seen to decrease with increasing clay strength. This indicates that the extent of lateral flow of fill material and hence the magnitude of shear stresses imposed on the clay surface increase with increasing clay strength. The range over which β varies with clay strength for a particular fill thickness is greatest for the thickest fill.

7.2.8 Lateral Flow of Fill Material on Very Strong Clays

The lateral flow of fill material is a more marked phenomenon in tests on stronger clays. In Test 1 , Chapter 4 , on an infinitely stiff (but perfectly smooth) subgrade it was observed that the bearing capacity of the system was less than that found in test K1M on a weaker clay subgrade. Although the former situation combined the worst of two effects (a very strong subgrade, with a very weak interface layer acting as a slip surface) the same effect is being seen, albeit to a much lesser extent, in the range of clay strengths tested here (from the values of β in Table 7.5). Figures 7.14 and 7.15 for tests G1M and K1M have already been compared and it has been seen that for the test on the strongest clay, much more lateral flow seemed to be occurring. Both tests were conducted on a thick layer of fill. If tests A1M and C2M are compared (Figures 7.22 and 7.23) the former on a weak clay, the latter on a strong clay and both on a thin layer of fill, it will be seen that the

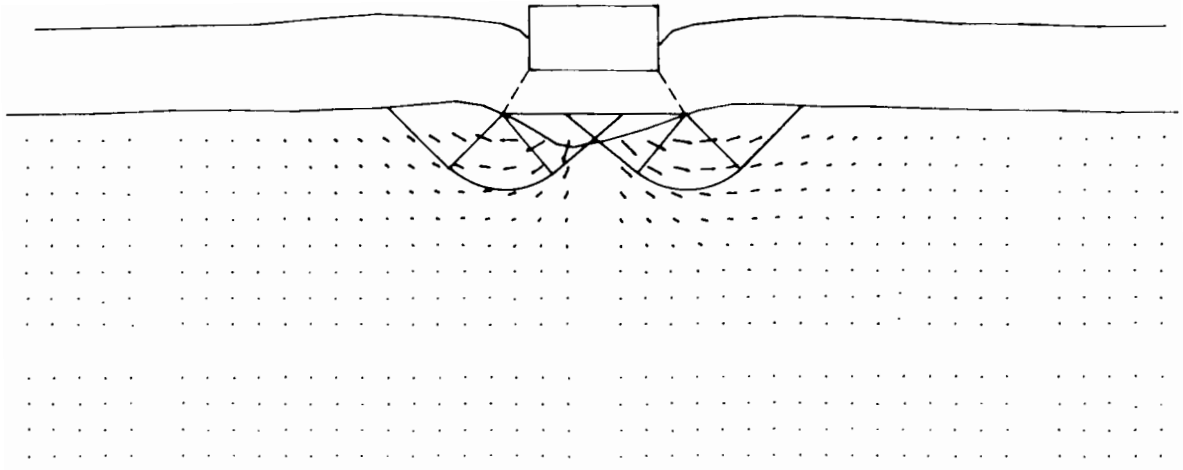

Figure 7.22 Displacement Vector plot for the unreinforced test A1M (25mm Footing Penetration)

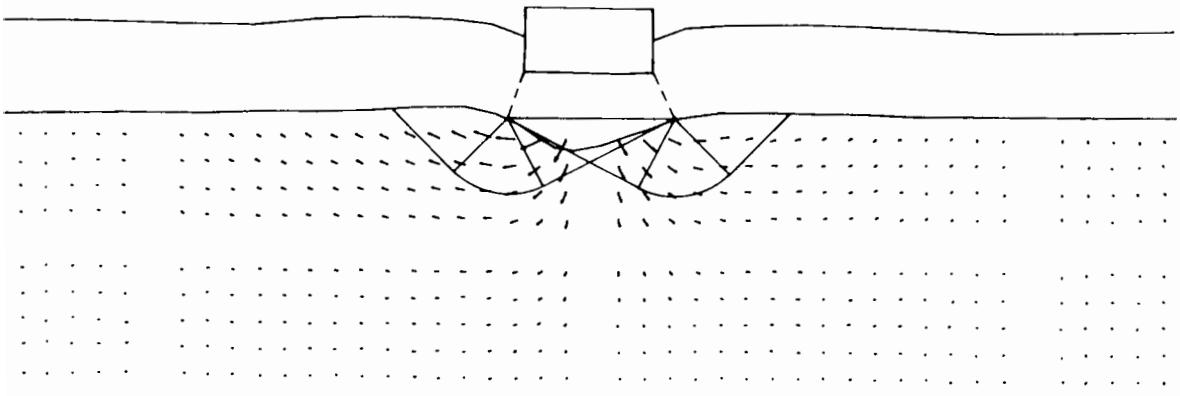

Figure 7.23 Displacement Vector plot for the unreinforced test C2M (25mm Footing Penetration)

differences are less striking. The much thinner fill layer does not allow such a great extent of lateral flow to develop in C2M . It is therefore concluded that there is less lateral flow of fill material across the surface of weak clays than of strong clays, and that this effect is emphasised at larger fill depths (for the range of fill thicknesses and clay strengths investigated).

This observation perhaps explains the trends established by non-dimensional analysis, summarised at the end of the last chapter. If unreinforced tests on a weak clay mobilise a high clay bearing capacity factor and vice versa for a strong clay, and if this effect is emphasised at greater fill thicknesses, then it matters less and less what actual strength the subgrade has as the fill thickness increases. Thus the natural decay of m , shown in the reinforced tests, is accelerated in the unreinforced tests. This is precisely the effect which the plot in Figure 6.5 shows.

7.3 **Additional Factors**

7.3.1 Elastic Deformations in the Clay

The clay subgrade is unfortunately not perfectly plastic. The deformations predicted by the failure mechanisms proposed in this chapter will only be seen in a material which is rigid/perfectly plastic. As such, a smaller set of elastic deformations in the surrounding material are seen superimposed on the plastic deformation pattern. Since the material is not perfectly elastic either, it has almost zero rebound, so that even after the footing load is removed a confusing sum of plastic and 'elastic' strains is still seen, where the word 'elastic' is used to describe the small but irrecoverable strains seen in the clay before the

onset of yield.

The effect of this is to give the viewer a misleading impression of the relevant plastic deformation mechanism by causing a less clear cut boundary between failing and non-failing clay.

7.3.2 Equivalent Load Comparisons

Before leaving the subject of marker movements in the clay, it should be stressed again that, in many instances above, comparisons have been made between the deformation patterns in reinforced and unreinforced tests for a given footing penetration. It is important to appreciate at the same time, therefore, that in this kind of comparison at a given footing penetration the loads being carried in the reinforced test are substantially larger than those in the unreinforced test. It is worthwhile comparing the two types of test when they are carrying the same load. Figure 7.24 shows a reinforced test (J1M) and an unreinforced test (J2M) both under the same footing load of 77kPa . While the unreinforced fill layer has suffered large displacements with clear lateral failures involving loss of fill from below the footing, the reinforced fill, with only about 1/10th the footing penetration, shows no real signs of distress.

7.3.3 Justification of Layer 2 Tests

Throughout this analysis equal weighting has been given to both Layer 1 and Layer 2 tests when comparing results. The validity of the assumption that the sets of tests are comparable depends on whether the disturbances caused by the Layer 1 tests significantly affect the clay in the lower half of the box. If the 'limit of disturbance' from a

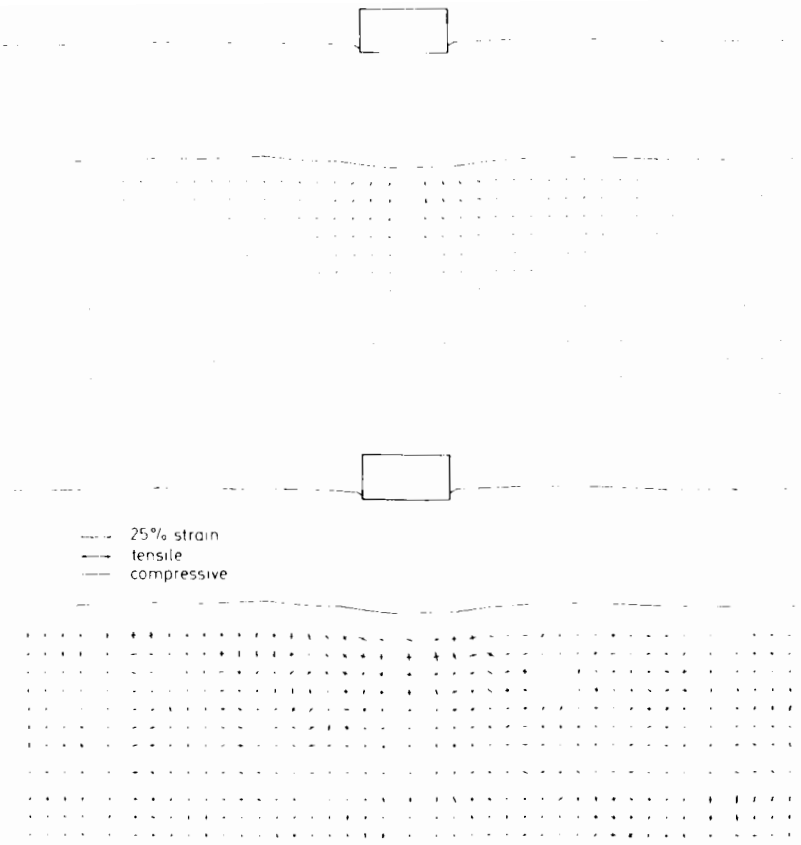

a) J1M (Reinforced test)

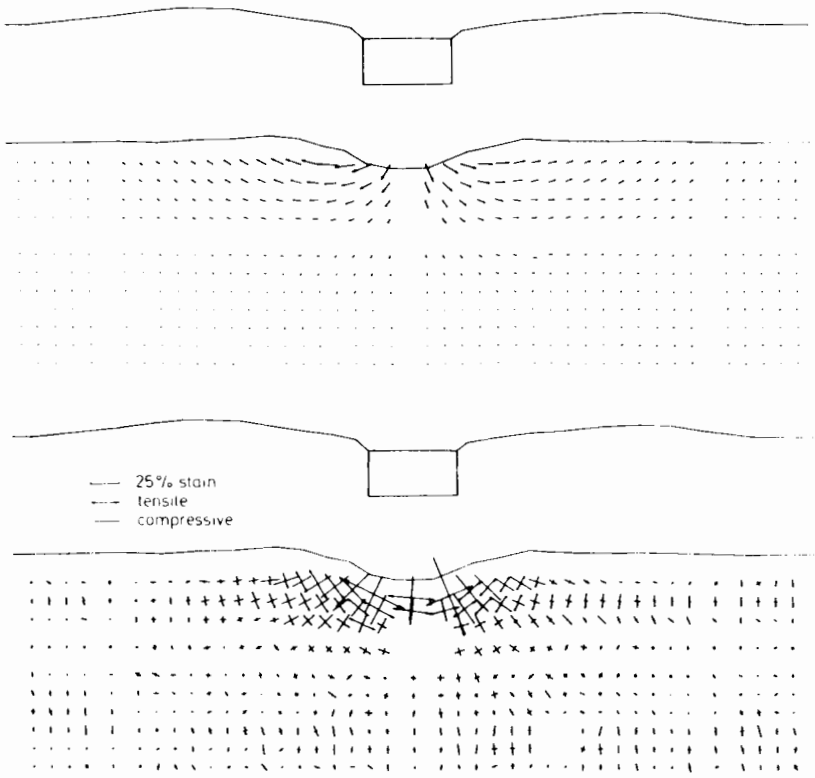

b) J2M (Unreinforced test)

Figure 7.24 Displacement Vector and Strain plots corresponding to 77kPa Footing Pressure for tests on Sample J

particular test is defined as being the depth at which discernible marker movement in the clay ceases, then the most critical case will be for a reinforced test conducted on the strongest clay, with the greatest fill thickness. In fact this particular test (K2M) was a Layer 2 test making J1M the most critical case. Looking at Figure 7.8 the limit of disturbance can be seen to lie comfortably above the Layer 2 level. In addition the basic shape of mechanisms are not seen to change between Layer 1 and Layer 2 tests. This would also indicate that the greater proximity of the boundary in the latter tests is not significant.

CHAPTER 8

CONCLUDING REMARKS AND AREAS FOR FURTHER RESEARCH

8.1 Conclusions

8.1.1 The Testing Technique

The testing technique whereby a single rig was used for both the consolidation and the testing of each sample was found to be very manageable. The problems associated with a rectangular test box subjected to high internal pressure did not prove to be significant during consolidation. The two perspex sides of the test box did not distort excessively, being given sufficient support at their centre points by the special reaction frame.

The concept of having an all-gas system on the high pressure side of the rams, and an all-oil system on the low pressure side proved to be satisfactory. The pneumatic consolidation method was economic while the hydraulic method of test control proved reliable.

8.1.2 Test Results

The general differences between reinforced and unreinforced tests emerged clearly.

The Load-Penetration results from the test programme (Figure 4.1) demonstrate the very marked increase that the inclusion of a grid can provide to the load carrying capacity of a system. In addition, the reinforced systems on the two stronger categories of clay were shown to be noticeably stiffer from the very start of the test.

For a reinforced test the zone of deformations could be generally seen to extend deeply into the clay. There was little loss of fill material from immediately beneath the footing, and the surface heave profile was seen to be generally smooth.

The unreinforced test with the same fill thickness and clay strength, at the same footing penetration (but a much smaller load) generally showed a relatively shallow zone of deformations in the clay. Within the fill, the depth of aggregate beneath the footing by the end of the test was much smaller than at the beginning of the test. The reduction in thickness was due to lateral flow of material from beneath the footing resulting in wedge-type failures in the fill layer either side of the footing. By the end of the test these formed clearly visible outcrops in the surface of the fill. These observations were backed up by observation made from Video film taken during tests.

The pore pressure and total pressure data were useful during the consolidation process as a check on the rate at which increments of load could be applied and for giving an indication when equilibrium was reached. During tests, on the other hand, the pore pressure and total pressure responses showed some inconsistent behaviour but the following emerged: the general magnitude of the pore pressure responses was greatly increased by the presence of a grid, while that of the total pressure transducers appeared unaffected.

8.1.3 Photographic Data

The method by which slides were taken of the movements of a grid of small markers in the clay during each test, and by which these slides were subsequently measured up on the BITPAD system, worked well, yielding vital extra information about failure mechanisms. Each slide took approximately 40 minutes to measure up. With 20 minutes of subsequent work on the computer, marker displacement plots or the corresponding plots of principal strain in the clay body could be produced for any stage of a test.

These plots allowed a detailed comparison between unreinforced and reinforced tests to be made. In both types of test it was found that the effect of the fill layer was to distribute load onto the clay. The clay can then be considered to behave as if loaded at its surface by a footing of increased width. This would seem to be the case even at excessive amounts of footing penetration. During a reinforced test this footing should be considered rough, constraining the clay to deform according to the classical mechanism associated with rough footings on cohesive material as in Figure 7.6a . During an unreinforced test the footing should be considered to act in the composite manner shown in Figure 7.18. The outer parts of the footing are assumed to combine a normal force with an outward directed shear force at the clay surface, while the central part is assumed to be perfectly smooth and loading the clay normally. The shear stresses arise as a result of lateral flow of fill material across the surface of the clay, an effect which is not seen in reinforced tests.

In the reinforced test a bearing capacity factor of 5.14 is appropriate for determining the contribution of the clay. In an unreinforced test a reduced bearing capacity factor should be used, depending on the magnitude of the shear stresses imposed on the clay and the length over which they act. The magnitude of this reduced bearing capacity factor lies in the range 2.57 to 5.14 . In situations where the lateral flow of fill material across the surface of the clay is marked (for strong clays and thick fills) the bearing capacity factor will lie at the lower end of the range. For tests on very weak clays and thin fill depths, where flow of fill material will be predominantly downward, a bearing capacity factor at the higher end of the range will be seen.

8.1.4 Load Estimation from Marker Plots

By applying the above concepts of bearing capacity factor to the analysis of reinforced and unreinforced tests, reasonable agreement is seen between actual footing loads and the predicted loads based on measurements taken from the plots of marker movement. In the case of the reinforced test, the membrane effect of the grid is accounted for by a simple construction based on the slope-angle of the grid profile at the 'stationary points'. These are the points which define the width over which the clay is being loaded, and about which the clay material is seen to be rotating at that particular instant of the test.

The simple concept of a constant load spread angle through the fill layer, often adopted by engineers for convenience, could be used more effectively in the light of the above concept of variable bearing capacity factors: a design method which proposes 5.14 as a bearing capacity factor for an unreinforced system will almost always be unsafe, while one that always adopts a value of, say, 3.14 will often be

over-conservative. The latter design method would also, therefore, often overestimate the benefits of including a grid.

8.1.5 Non-Dimensional Analysis

The most appropriate method of reducing both reinforced and unreinforced test data to dimensionless form has been found to be according to the dimensionless group

$$q / C_u^m (\gamma_1 B)^{1-m}$$

The value of m was shown to decrease from unity for an infinitely thin fill layer to zero for an infinitely thick fill layer. The rate of change of m with fill thickness was found to be greater for unreinforced tests than for reinforced tests, giving rise to a higher value of m in a reinforced test for a given fill thickness. This reflects the greater part that the clay subgrade plays in the failure mechanism associated with a reinforced test. The group demonstrates for both tests the decreasing relevance of the shear strength of the clay with increasing fill layer thickness.

8.1.6 Dual Footing Loads

The set of tests conducted on the last sample (Sample M) gave a useful insight into how the results from these single footing tests might be used to predict the performance of dual footings under the same conditions. A comparison between tests on Sample M and Sample A showed that while the dual footing loads on the unreinforced system were the same as seen in the single footing test, in the case of the reinforced test some extra bearing capacity was seen. This would seem to result from the confining action of the grid between the two footings. The grid

acts to combine the two footings into a single large one - an effect which in this test on a thin fill layer and a weak clay was perhaps only seen partially. With a thicker fill layer this effect would become more pronounced, a stiffer grid or a smaller footing spacing also having the same effect.

8.2 **Areas for Further Research**

8.2.1 Introduction

The approach adopted in these tests has necessarily been a very simple one. Monotonic, constant rate of penetration, plane-strain footing tests at reduced scale have given a basic understanding of the way in which unreinforced and reinforced subbase-subgrade systems behave. These model tests, however, are still a far cry from the field situation where complications of long term non-uniform traffic loading become important. In any next stage of this type of modelling the following steps might be taken to close the gap between laboratory testing techniques and the true field situation.

8.2.2 Cyclic Loading and Scale Effects

An obvious next step after monotonic testing is to conduct cyclic load tests. But if such tests are also performed at reduced scale additional modelling complications will arise in addition to those encountered in this research programme. The tests will naturally consist of a set number of load applications, and will therefore be load-controlled by nature. In this programme it was an important factor that the tests were controlled by constant rate of penetration, not by load, and that by choosing an appropriate rate of penetration, the strain

rate and therefore the correct stiffness of the grid could be modelled. This degree of freedom will not exist in cyclic tests and so much more care will need to be taken in producing a model grid with correctly scaled properties: the appropriate rate of creep in the grid will also need to be correctly modelled.

A second important factor in cyclic loading will be the rate at which pore pressures dissipate in the clay. At reduced scale, drainage paths become shorter and dissipation times become faster by the scale factor squared.

Thirdly, though less importantly, significant drying out of the fill layer may occur over the long periods of time associated with cyclic tests.

8.2.3 Additional Steps

It would be desirable to move from single footing loads to dual footing loads, and from 2-D footing tests to more realistic 3-D plate tests. In the case of the latter the very useful technique of photographing marker movements in the clay could still perhaps be employed by conducting tests on a semi-cylindrical specimen with a semi-circular plate.

It would also be desirable to have more information on the effect of the properties of the grid itself. While doing tests on different types of grid with different aperture sizes and different stiffnesses, tests should also be conducted with other geotextiles, and a clear relation between the types of reinforcement established.

The cutting in of the grid observed in some tests in this programme may simply have been a result of the large deformations imposed on the system over a relatively short time, but this effect should be looked out for in any further testing. It may be that grids should be used in conjunction with an underlying layer of fabric on particularly soft subgrades.

Lastly, a satisfactory method of measuring strains in the model grid needs to be developed.

REFERENCES

Andersson, O. (1977), "The use of plastic fabric for pavement protection during frost break", Proc. Int. Conf. on the use of fabrics in Geotechnics, ENPC, Paris, pp 143-151.

Atkinson, J.H. and Bransby, P.L. (1978), The mechanics of soils - an introduction to critical state soil mechanics, McGraw-Hill Book Company, London.

Bakker, J.G. (1977), "Mechanical behaviour of membranes in road foundations", Proc. Int. Conf. on the use of fabrics in Geotechnics, ENPC, Paris, pp 139-142.

Barenberg, E.J. Dowland, J.H. and Hales, J.H. (1975), "Evaluation of soil-aggregate systems with Mirafi fabrics", The Highway Research Lab. University of Illinois, UILU-ENG-75-2020.

Barker, J.A. (1981), Dictionary of soil mechanics and foundation engineering, Construction Press, Harlow, Essex.

Barksdale, R. Robnett, Q.L. and Lai, J. (1982), "Experimental and theoretical behaviour of geotextile reinforced aggregate soil systems", Proc. 2nd Int. Conf. on Geotextiles, IFAI, Las Vegas, pp 375-380.

Barvashov, V.A. et al (1977), "Deformations of soil foundations reinforced with prestressed synthetic fabric", Proc. Int. Conf. on the use of fabrics in Geotechnics, ENPC, Paris, pp 67-70.

Bassett, R.H. (1979), "The use of physical models in design", Proc. VIIth ECSMFE, Brighton, Vol. 5, pp 253-270.

Bell, J.R. Greenway, D.R. and Vischer, W. (1977), "Construction and analysis of a fabric reinforced low embankment on muskeg", Proc. Int. Conf. on the use of fabrics in Geotechnics, ENPC, Paris, pp 71-76.

Bender, D.A. and Barenberg, E.J. (1978), "Design and behaviour of SFA systems", Transportation Research Record 671, TRB, Washington.

Binquet, J. and Lee, K.L. (1975), "Bearing capacity of strip footings on reinforced earth slabs", University of California, UCLA-ENG-7538.

Bishop, A.W. and Henkel, D.J. (1962) The measurement of soil properties in the Triaxial Test - 2nd edition, Edward Arnold Publishers Ltd., London.

Bjerrum, L. and Lo, K.Y. (1963), "Effect of aging on the shear strength properties of a normally consolidated clay", Geotechnique, Vol. 13, pp 147-157.

Bourdeau, P.L. Harr, M.E. and Holtz, R.D. (1982), "Soil fabric interaction - an analytical model", Proc. 2nd Int. Conf. on Geotextiles, IFAI, Las Vegas, pp 387-392.

Brantman, B.P. et al (1977), "Experiments on the use of synthetic non-woven materials for road surfaces", Proc. Int. Conf. on the use of fabrics in Geotechnics, ENPC, Paris, pp 35-40.

British Standard 1377 (1975), Methods of test for soils for civil engineering purposes, London, British Standards Institute.

Brown, S.F. Jones, C.P.D. and Brodrick, B.V. (1982), "Use of non-woven fabrics in permanent road pavements", Proc. Instn. Civ. Engrs., Part 2, 1982, 73, Sept, pp 541-563.

Butterfield, R. Harkness, R.M. and Andrawes, K.Z. (1970), "A stereo photogrammetric technique for measuring displacement fields", Geotechnique, Vol 20, No 3, pp 308-314.

Denver, H. Christensen, N.H. Hansen, B. and Steenfelt, J.S. (1983), "Reinforcement of cohesionless soil by PVC-grid", Proc. VIIIth ECSMFE, FGS, Helsinki, pp 481-489.

Department of Transport (1976), "Specification for road and bridge works", HMSO.

Freeman, T. (1982), Private communication.

Giroud, J.P. and Noiray, L. (1981), "Geotextile-reinforced unpaved road design", Jnl. Geotech. Eng. Div., ASCE, Vol 107, No GT9, pp 1233-1254.

Giroud, J.P. Ah-line, C. and Bonaparte, R. (1984), "Design of unpaved roads and trafficked areas with geogrids", Symp. Polymer Grid Reinf., ICE, London.

Gourc, J-P. (1982), Thesis (in French), L'Universite de Grenoble.

Gourc, J-P. Matichard, Y. et al (1982), "Bearing capacity of a sand - soft subgrade system with geotextile", (French), Proc. 2nd Int. Conf. on Geotextiles, IFAI, Las Vegas, pp 411-416.

Gourc, J-P. Perrier, H. et al (1982), "Cyclic loading of a two layer soil system reinforced by geotextile", (French), Proc. 2nd Int. Conf. on Geotextiles, IFAI, Las Vegas, pp 399-404.

Gourc, J-P. Perrier, H. and Riondy, G. (1983), "Unsurfaced roads on soft subgrade: mechanism of geotextile reinforcement", Proc. VIIIth ECSMFE, FGS, Helsinki, pp 495-498.

Gue, S.S. (1984), D.Phil Thesis, University of Oxford.

Hanna, A.M. and Meyerhof, G.G. (1980), "Design charts for ultimate bearing capacity of foundations on sand overlaying soft clay", Can. Geotech. Jrnl, Vol 17, pp 300-303.

Hoare, D. J. (1978), "Permeable synthetic fabric membranes: 1", and "2", Ground Engineering, Jul. and Nov. 1978, Vol 11, Nos 5 (pp 33-36) and 8 (pp 25-31).

Hoare, D.J. (1983), "Geotextiles in the UK", Ground Engineering, Nov. 1983, Vol 16, No 8, pp 30-38.

Houlsby, G.T. (1981), Ph.D Thesis, University of Cambridge.

Houlsby, G.T. (1984), "A program for calculating displacement and strain from a photograph of marker points", OUEL Report No. 1519/84, Dept. Eng. Science, University of Oxford.

Ingold, T.S. and Crowcroft, P. (1984), "The notion of geotextiles as separators in roads", Ground Engineering, Jan. 1984, Vol 17, No 1, pp 27-34.

Jarrett, P.M. Lee, R.A. and Ridell, D.V.B. (1977), "The use of fabrics in road pavements constructed on peat", Proc. Int. Conf. on the use of fabrics in Geotechnics, ENPC, Paris, pp 19-22.

Jessberger, H.L. (1977), "Load-bearing behaviour of a gravel subbase - nonwoven fabric - soft subgrade system", Proc. Int. Conf. on the use of fabrics in Geotechnics, ENPC, Paris, pp 9-14.

Jewell, R.A. (1980), Ph.D thesis, University of Cambridge.

Kenter, C.J. and Sellmeijer, J.B. (1983), "Increase in bearing capacity due to the application of Geolon fabric below a granular base of a road", Delft Soil Mechanics Lab., Report No DSML CO 254920/20.

Kinney, T.C. and Barenberg, E.J. (1982), "The strengthening effect of geotextiles on soil-geotextile-aggregate systems", Proc. 2nd Int. Conf. on Geotextiles, IFAI, Las Vegas, pp 347-352.

Kinney, T.C. (1982), "Small scale load tests on a soil-geotextile-aggregate system", Proc. 2nd Int. Conf. on Geotextiles, IFAI, Las Vegas, pp 405-410.

Kinney, T.C. (1979), Ph.D Thesis, University of Illinois.

Kinney, T.C. and Barenberg, E.J. (1979), "The mechanisms by which fabrics stabilize aggregate layers on soft subgrades", US Army Engineers WES, Vicksburg, WES MP-GL-79-5.

Koerner, R.M. and Welsh, J.P. (1980), Construction and geotechnical engineering using synthetic fabrics, John Wiley and Sons, New York.

Kraft, L.M. and Helfrich, S.C. (1983), "Bearing capacity of shallow footing, sand over clay", Can. Geotech. Jrnl, Vol 20, pp 182-185.

Lai, J.S. and Robnett, Q.L. (1981), "Design and use of geotextiles in road construction", Proc. 3rd Conf. Road Eng. Assoc. of Asia and Australasia, Vol 1, pp 699-718.

Loudon, P.A. (1967), Ph.D Thesis, University of Cambridge.

Maagdenburg, A.C. (1977), "Fabrics below sand embankments over weak soils, their technical specifications and their application in a test area", Proc. Int. Conf. on the use of fabrics in Geotechnics, ENPC, Paris, pp 77-82.

Mair, R.J. (1979), Ph.D Thesis, University of Cambridge.

McGown, A. (1982), "Progress Report : 1st December 1982", Internal Report to the SERC/Netlon Co-operative Award Steering Committee.

McGown, A. and Andrawes, K.Z. (1977), "The influence of non-woven fabric inclusions on the stress strain behaviour of a soil mass", Proc. Int. Conf. on the use of fabrics in Geotechnics, ENPC, Paris, pp 161-166.

McGown, A. and Ozelton, M.W. (1982), "Fabric membrane in flexible pavement construction over soils of low bearing strength", Civil Eng. Publ. Wks. Rev, London, No 798, pp 25-29.

Michelin Tyre Plc (1982), Earthmover tyres for vehicles used on construction sites, roadworks and in mines, Printed in France.

Michelin Tyre Plc (1982), Technical Data : March 1982, printed by Waterlow Ltd., Dunstable.

Milligan, G.W.E. (1981), "The use of mesh products to improve the performance of granular fill on soft ground", OUEL Report No 1346/81, Dept. Eng. Science, Oxford University.

Milligan, G.W.E. (1982), "Some tests on the relative effectiveness of grid reinforcements for granular soils", OUEL Report No 1441/82, Dept. Eng. Science, Oxford University.

Morel, G. Quibel, A. Puiatti, D. and Puig, J. (1977), "The use of fabrics under a subbase upon a low bearing capacity subgrade", (French), Proc. Int. Conf. on the use of fabrics in Geotechnics, ENPC, Paris, pp 29-34.

Netlon Ltd. (1982), The design inclusion of polymer grids into foundations and pavement structures, Civil Eng. Dept. Publication.

Nieuwenhuis, J.D. (1977), "Membranes and the bearing capacity of road bases", Proc. Int. Conf. on the use of fabrics in Geotechnics, ENPC, Paris, pp 3-8.

Petrik, P.M. (1977), "Development of stresses in reinforcement and subgrade of a reinforced soil slab", Proc. Int. Conf. on the use of fabrics in Geotechnics, ENPC, Paris, pp 151-154.

Potter, J.F. and Currer, E.W.H. (1981), "The effect of a fabric membrane on the structural behaviour of a granular road pavement", TRRL, Crowthorne, Lab. Report 996.

Potter, J.F. Mayhew, H.C. and Mayo, A.P. (1969), "Instrumentation of the full-scale experiment on A1 trunk road at Conington, Huntingdonshire", Road Research Lab., Crowthorne, RRL Report LR 296.

Ramalho-Ortigao, J.A. and Palmeira, E.M. (1982), "Geotextile performance at an access road on soft ground near Rio de Janeiro", Proc. 2nd Int. Conf. on Geotextiles, IFAI, Las Vegas, pp 353-358.

Rankilor, P.R. (1981), Membranes in ground engineering, John Wiley and Sons, New York.

Raumann, G. (1982), "Geotextiles in unpaved roads: design considerations", Proc. 2nd Int. Conf. on Geotextiles, IFAI, Las Vegas, pp 417-422.

Rigo, J.M. and Perfetti, J. (1980), "New approach to the measurement of the tensile strength of non-woven geotextiles", (French), Bull. Liaison Lab, P. et Ch, Paris, No 107, pp 83-92.

Robnett, Q.L. and Lai, J.S. (1982), "Effect of fabric properties on the performance and design of AFS systems", Proc. 2nd Int. Conf. on Geotextiles, IFAI, Las Vegas, pp 381-386.

Robnett, Q.L. and Lai, J.S. (1982), "Fabric reinforced aggregate roads - an overview", Presented at 61st Annual Meeting of the Transportation Research Board, Washington.

Ruddock, E.C. (1977), "Fabrics and meshes in roads and other pavements - a state of the art review", ISSN : 0305-1781, CIRIA.

Ruddock, E.C. Potter, J.F. and McAvoy, A.R. (1982), "Report on the construction and performance of a full-scale experimental road at Sandleheath, Hants", Project Record 245, CIRIA.

Rush, K.J. (1974), M.Sc Thesis, University of Cambridge.

Sarsby, R.W. and Marshall, C. (1983), "A method for determining the interactive behaviour of polymer grids and granular soils", Internal Report No BCS/G1/2A, Bolton Institute of Higher Education.

Schwab, E.F. Pregl, O. and Broms, B.B. (1977), "Deformation behaviour of reinforced sand at model tests measured by the X-Ray technique", Proc. Int. Conf. on the use of fabrics in Geotechnics, ENPC, Paris, pp 105-112.

Scott, C.R. (1974), An introduction to soil mechanics and foundations, Applied Science Publishers Ltd, Barking, Essex.

Scott Wilson Kirkpatrick and Partners (1975), "Stafford inner relief road : Report on earthworks trials", Ref. GM/EGS/70091.

Sellmeijer, J.B. Kenter, C.J. and Van den Berg, C. (1982) "Calculation method for a fabric reinforced road", Proc. 2nd Int. Conf. on Geotextiles, IFAI, Las Vegas, pp 393-398.

SERC (1982), A discussion document on good supervisory practice, SERC(SD/SPD), Polaris House, Swindon.

Sørlie, A. (1977), "The effect of fabrics on pavement strength - plate bearing tests in the laboratory", Proc. Int. Conf. on the use of fabrics in Geotechnics, ENPC, Paris, pp 15-18. p15, Paris

Sowers, G.F. Collins, S.A. and Miller, D.G. (1982), "Mechanism of geotextile - aggregate support in low cost roads", Proc. 2nd Int. Conf. on Geotextiles, IFAI, Las Vegas, pp 341-346.

Steenfelt, J.S. (1979), "Scale effect on bearing capacity factor", DGI, Copenhagen, Bulletin No 33.